Inaugural dissertation
for
obtaining the doctoral degree
of the
Combined Faculty of Mathematics, Engineering and Natural Sciences
of the
Ruprecht - Karls - University
Heidelberg

Presented by
M.Sc. Yonggang Ren
born in Shaanxi, China
Oral examination:_____

Studies of *Jmjd6* in embryogenesis and ISL1 phosphorylation in cardiac development

Referees:
Prof.Dr. Thomas Wieland
Prof.Dr. Gergana Dobreva

Summary

The controls of early lineage cells and cardiac progenitor cells specification, migration, and differentiation by a regulatory network consisting of multiple transcription factors and signaling molecules are important during early lineages formation and heart development. Beyond the genetic level, regulation of those transcription factors and signaling molecules on the epigenetic level is also essential. Histone modification is one of the most important and well-studied epigenetic regulations. Modification such as methylation at different amino acid residues on histone allows modified histone to regulate gene expression repressively or actively. Bivalent domain consisting of both repressive mark trimethylation at lysine 27 residue of histone protein 3 (H3K27me3) and active trimethylation at lysine 4 residue of histone protein 3 (H3K4me3) on key developmental gene allows tight regulation of gene expression and quick response of a cell to extracellular stimulation. Many key developmental genes are marked by bivalent domain and thus are poised for later lineage-specific activation or repression.

Jumonji domain-containing protein 6 (*Jmjd6*) plays an essential role in mouse embryogenesis; however, the detailed mechanism is poorly understood. Here I found that *Jmjd6* ablation results in imbalanced germ layer formation in which mesoderm and endoderm lineages are impaired, and ectoderm is favored. Similarly, at later stages, during the commitment and differentiation of progenitor cells to different populations, *Jmjd6* plays a key role by regulating chromatin state at lineage-specific regulators. Mechanically, I found less active histone marker H3K4me3 and more repressive histone marker H3K27me3 accumulation, leading to the downregulation of many essential genes for lineage specification and cardiac morphogenesis genes. Using proteomic analysis, I found that JMJD6 interacts with many spliceosome components. Consistent with the protein studies, alternative splicing analysis revealed that *Jmjd6* regulates splicing variety on chromatin modification and RNA splicing genes. I focused that the *Prmt6* methyltransferase is alternatively spliced to significantly increased PRMT6 protein level. As a methyltransferase for asymmetric dimethylation at arginine 2 residue of histone protein 3 (H3R2me2a), upregulated PRMT6 protein results in increased H3R2me2a and decreased H3K4me3 modification on early lineage

specification and heart morphogenesis genes. Polycomb repressive complex 1 (PRC1) and Polycomb repressive complex 2 (PRC2) are the critical players for depositing repressive histone marks Ubiquitination at lysine 119 residue of histone protein 2A (H2AK119ub) and H3K27me3, respectively. *Cbx7*, a member of the PRC1 complex, is increased in mesodermal and cardiac progenitor cells differentiated from *Jmjd6* knockout mouse embryonic stem cells (mESCs). Increased CBX7 protein leads to higher H2AK119ub, which recruits the PRC2 complex. Ezh2 from the PRC2 complex methylates lysine residue at histone 3 to form H3K27me3. The imbalance of bivalent chromatin marks causes the downregulation of early lineage specification and cardiac morphogenesis gene expression. This study highlights the essential roles of *Jmjd6* in early cell lineage choice and heart development by maintaining bivalent chromatin marks balance at the promoter.

The transcription factor Isl1 marks the second heart field (SHF) cardiac progenitor cell population and is crucial for cardiac lineage differentiation and heart development. In addition, the expression of Isl1 is tightly regulated to express in second heart field progenitor cells during cardiogenesis. Post-translational modifications of proteins significantly alter their physical and chemical properties, including their folding, stability, activity and function. This study shows that p38α could phosphate Isl1 at S269 and protect it from degradation. Manipulating p38 activity can largely affect the Isl1 protein level in cardiac progenitor cells. Inhibiting p38 activity with an inhibitor or knocking down p38α impairs cardiac progenitor cells and cardiomyocyte marker gene expression, which leads to impaired cardiogenesis. Moreover, Inhibition of p38 in zebrafish or mouse embryos affects heart morphogenesis and function in vivo. In summary, the phosphorylation of Isl1 at S269 by p38α plays a key role in its protein stability and cardiogenesis.

Zusammenfassung

Die Kontrolle der Spezifizierung, Migration und Differenzierung von Zellen früher Abstammungslinien und kardialer Vorläuferzellen durch ein regulatorisches Netzwerk, das aus mehreren Transkriptionsfaktoren und Signalmolekülen besteht, ist während der Bildung früher Abstammungslinien und der Herzentwicklung wichtig. Über die genetische Ebene hinaus ist auch die Regulation dieser Transkriptionsfaktoren und Signalmoleküle auf epigenetischer Ebene essentiell. Histonmodifikationen sind eine der wichtigsten und am besten untersuchten epigenetischen Regualtionsmechanismen. Modifikationen, wie die Methylierung verschiedener Aminosäureresten an Histonen, ermöglichen es die Genexpression repressiv oder aktiv zu regulieren. Die bivalente Domäne, die sowohl die repressive Modifizierung Trimethylierung am Lysinrest 27 des Histonproteins 3 (H3K27me3) als auch die aktiven Trimethylierung am Lysinrest 4 des Histonproteins 3 (H3K4me3)-Modifizierung aufweist, ermöglicht eine strenge Regulierung der Genexpression und eine schnelle Reaktion der Zelle auf extrazelluläre Stimulation. Viele wichtige Entwicklungsgene sind durch eine bivalente Domäne gekennzeichnet und stehen daher für eine spätere abstammungsspezifische Aktivierung oder Repression bereit.

Das die Jumonji-Domäne enthaltende Protein 6 (*Jmjd6*) spielt eine wesentliche Rolle bei der Embryogenese der Maus. Der detaillierte Mechanismus hierbei ist jedoch bisher kaum verstanden. Im Zuge dieser Arbeit fand ich heraus, dass die Abaltion von *Jmjd6* zu einer unausgeglichenen Keimschichtbildung führt, bei der Mesoderm- und Endoderm-Linien beeinträchtigt werden und die Ektodermbildung bevorzugt wird. In ähnlicher Weise spielt *Jmjd6* in späteren Stadien eine Schlüsselrolle. Durch die Regulierung des Chroamtinzustandes an linienspezifischen Regulatoren bereinflusst *Jmjd6* die Differenzierung von kardialen Vorläuferzellen. Auf epigentischer Ebene beobachtete ich eine Reduzierung des aktiven Histonmarker H3K4me3 und eine Akkumulation des repressiven Histonmarkers H3K27me3 an vielen essentiellen Genen der Abstammungsspezifikation und der kardiale Morphogenesegene, was zur Herunterregulierung dieser Gene führte. Mithilfe von Proteomik-analysen zeigte ich, dass JMJD6 mit vielen Spleißosomenkomponenten interagiert. In Übereinstimmung

mit diesen Proteinstudien ergab eine alternative Splicing-Analyse, dass *Jmjd6* die Splicing-Vielfalt verschiedener chroamtin-modifizierender Proteine und RNA-Splicing-Gene reguliert. Ich konzentrierte meine Arbeit darauf, dass die *Prmt6*-Methyltransferase alternativ zu einem signifikant erhöhten PRMT6-Proteinspiegel gespleißt wird. Als Methyltransferase für die asymmetrische Dimethylierung am Arginin 2-Rest des Histonproteins 3 (H3R2me2a), führt das hochregulierte PRMT6-Protein zu einer erhöhten H3R2me2a- und einer verringerten H3K4me3-Modifikation bei frühen Linienspezifikations- und Herzmorphogenesegenen. Der Polycomb-Repressionskomplex 1 (PRC1) und Polycomb-Repressionskomplex 2 (PRC2) sind die entscheidenden Akteure für die Regulierung der repressiven Histonmarkierungen Ubiquitinierung am Lysinrest 119 des Histonproteins 2A (H2AK119ub) bzw. H3K27me3. *Cbx7*, ein Mitglied des PRC1-Komplexes, ist in mesodermalen und kardialen Vorläuferzellen, die aus embryonalen *Jmjd6*-Knockout-Maus-Stammzellen (mESCs) differenziert sind, erhöht exprimiert. Erhöhtes CBX7-Protein führt zu einem erhöheren H2AK119ub Level, welches widerrum den PRC2-Komplex rekrutiert. Ezh2, eine Untereinheit des PRC2-Komplexes, methyliert den Lysinrest 27 an Histon 3, um H3K27me3 zu bilden. Das entstandene Ungleichgewicht zwischen H3K27me3 und H3K4me3 an Genen der frühen Abstammungsspezifikation- und der kardialen Morphogenese verursacht die Herunterregulierung deren Genexpression. Diese Studie unterstreicht die wesentliche Rolle von *Jmjd6* bei der Festlegung der frühen Zelllinie während der Entwicklung und der Herzentwicklung, indem es das Gleichgewicht zwischen repressiven und aktiven Histonmodifikationen an bivalenen Domänen am Promotor aufrechterhält.

Der Transkriptionsfaktor *Isl1* markiert die kardiale Vorläuferzellpopulation des zweiten Herzfelds (SHF) und ist entscheidend für die Differenzierung der kardialen Abstammungslinie und die Entwicklung des Herzens. Darüber hinaus ist die Expression von *Isl1* streng reguliert und die Expression ist während der Kardiogenese auf Vorläuferzellen des zweiten Herzfelds beschränkt. Posttranslationale Modifikationen von Proteinen verändern signifikant ihre physikalischen und chemischen Eigenschaften, einschließlich ihrer Faltung, Stabilität, Aktivität und Funktion. Ich zeige, dass *p38α Isl1* an S269 phosphoryliert und somit *Isl1* vor der Degradierung schützen

kann. Die Manipulation der p38-Aktivität kann den *Isl1*-Proteinspiegel in kardialen Vorläuferzellen stark beeinflussen. Die Hemmung der *p38*-Aktivität mit einem Inhibitor oder der Abbau von *p38α* beeinträchtigt die Expression von kardialen Vorläuferzellen und Kardiomyozyten-Markergenen, was zu einer beeinträchtigten Kardiogenese führt. Darüber hinaus beeinflusst die Hemmung von *p38* in Zebrafisch- oder Mausembryos die Herzmorphogenese und -funktion in vivo. Zusammenfassend spielt die Phosphorylierung von *Isl1* an S269 durch *p38α* eine Schlüsselrolle bei seiner Proteinstabilität und während Kardiogenese.

Content

List of figures

Chapter2.1 Introduction

List of tables

Chapter 1. *Jmjd6* regulates early lineage choices and cardiogenesis by maintaining the bivalent domain balance

1. 1 Introduction

1.1.1 Early lineage specification in the mouse embryo

1.1.1.1 The timeline of early lineage specification

By a succession of cleavage divisions, the zygote generates a blastocyst consisting of three cell types: the trophectoderm (TE), the inner cell mass (ICM), and the primitive endoderm (PrE). After the blastocyst is implanted in the uterus at embryonic day 4 (E4.0), ICM gives rise to a pluripotent epithelial layer (the epiblast) from which embryonic and other extraembryonic tissues are derived. At E5.5, the TE mediates the implantation and then gives rise to the extraembryonic ectoderm (ExE) and the ectoplacental cone. The PrE gives rise to parietal endoderm and visceral endoderm (VE). Then the parietal endoderm migrates from the surface of the ICM and directly contacts the maternal tissue. The VE remains in contact with the embryo and gives rise to the endoderm of the visceral yolk sac. The epiblast cell remains pluripotent and gives rise to a primitive streak in the later stage. Between implantation and gastrulation, the proximal-distal (PD) axis is set up to provide spatial information for the early embryo. This process relies on secreted growth factors of the TGFβ family, such as nodal and bone morphogenetic protein (BMP), the Wnt family, and the FGF family. At E6.0, the millstone event of embryogenesis—gastrulation starts. During the early gastrulation stage, epiblast undergoes epithelial-to-mesenchymal transition (EMT) to form the first mesenchymal population called primitive streak. Germ layer formation begins once the primitive streak is established at the proximal posterior pole of the epiblast. Establishing the anteroposterior (AP) axis is essential for restricting the location of the primitive streak and proper induction of the germ layers.

To establish the AP axis, the rapid and directed migration of the distal VE to the prospective anterior side of the embryo at E6.0 is critical. Three germ layers, ectoderm, mesoderm, and definitive endoderm, are generated during the gastrulation. All fetal tissues will develop from those three germ layers (Figure 1.1.1).

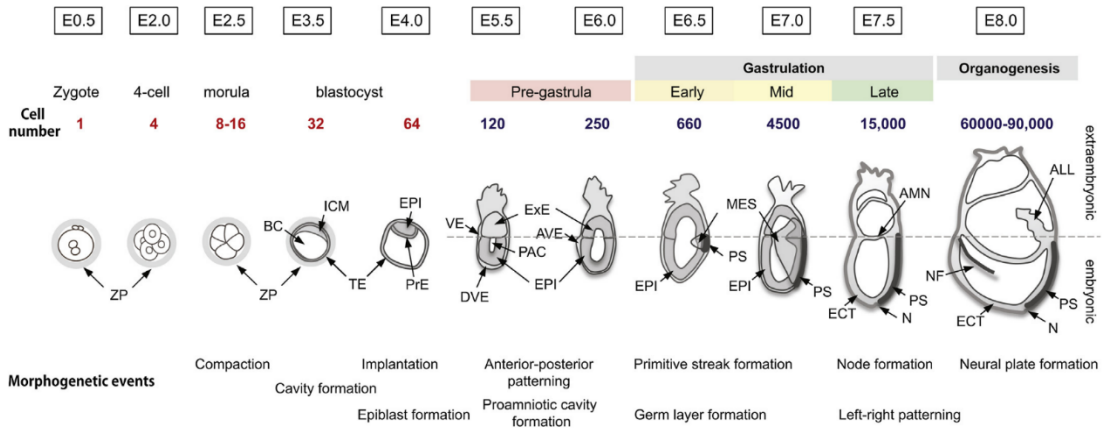

Figure 1.1.1. Timeline of early embryogenesis. Schematic representative of characteristic anatomical features of mouse embryos (E0.5- E8.5). ALL: allantois, AMN: amnion, AVE: anterior visceral endoderm, BC: blastocyst cavity, DVE: distal visceral endoderm, ECT: ectoderm, EPI: epiblast, ExE: extraembryonic ectoderm, ICM: inner cell mass, MES: mesoderm, N: node, NF: neural fold, PAC: proamniotic cavity, PrE: primitive endoderm, PS: primitive streak, TE: trophectoderm, VE: visceral endoderm, ZP: zona pellucida. (modified from (Kojima, Tam et al. 2014))

1.1.1.2 Genes in early cell lineage allocation

After four cleavage divisions of the zygote, the morula embryo is formed. Asymmetrical cell divisions at the morula stage generate two distinct subpopulations: ICM and TE at E3.5. Those two cell populations form the blastocyst. Two transcriptional factors, octamere-binding transcription factor 3/4 (*Oct3/4*) and caudal-type homeobox protein 2 (*Cdx2*), mediate this binary cell fate decision. *Oct3/4*and *Cdx2* are initially both expressed in all cells of the morula. While in the later stage, a mutually exclusive expression pattern is established (Figure 1.1.2A). The highly expressed *Cdx2* in the TE lineage is essential for its expansion. TEA-domain family member 4 (*Tead4*) is another transcription factor essential for the TE lineage's

specification. *Tead4*-deficient embryos fail to induce *Cdx2* expression, and all cells adopt an ICM fate (Yagi, Kohn et al. 2007).

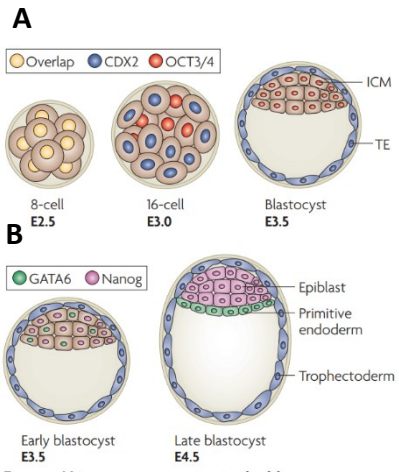

Figure 1.1.2. Lineage segregation in the blastocyst. (A) *Cdx2* and *Oct3/4* expressions are overlapped at eight blastomeres but mutually excluded in the later stages. **(B)** *Gata6* and *Nanog* are mutually excluded in the early blastocyst. *Gata6* positive cells give rise to primitive endoderm, and *Nanog* positive cells give rise to the epiblast. (modified from (Arnold and Robertson 2009))

Over the next few hours after establishing the blastocyst, the outmost layers of ICM cells give rise to the PrE. The rest of the cells give rise to epiblast. Until E4.5, the late blastocyst is established. Before the formation of PE and epiblast, there were already two distinct subpopulations in ICM marked by GATA-binding factor 6 (*Gata6*) and *Nanog*. *Gata6* expressed ICM cells are committed to PE, while *Naong* expressed ICM cells give rise to epiblast (Figure 1.1.2B). Forced expression of *Gata6* in cultured ES cells is sufficient to induce PE lineage. The pluripotency of epiblast is maintained by Naong and Sal-like 4 (*Sall4*). The suppression of WNT signaling, which promotes differentiation, is also required to maintain pluripotency. In the absence of wingless-related MMTV integration site 3 (*Wnt3*), the epiblast continues to express the pluripotency marker *Pou5f1 (Kemler, Hierholzer et al. 2004)*.

Between implantation and gastrulation, the proximal-distal (P-D) axis and the anterior-posterior (A-P) axis are established. The three cell populations at this stage, ExE, VE, and epiblast, are communicated by secreted growth factors of the TGFβ family, including nodal and BMP, the Wnt family, and the FGF family. The regionalized gene-expression pattern in the epiblast, the ExE, and the VE tissue is then built by this communication. The first sign of this tissue regionalization is the different marker genes expressed along the P-D axis. Then, the radial symmetry is broken, and marker

genes indicating anterior and posterior tissue are expressed soon afterward. Nodal signals are essential for inducing P-D patterning in the epiblast (Figure 1.1.3A). *Nodal* expressed in the epiblast activates its intercellular effector *Smad2* in the VE. Furthermore, phosphorylated SMAD2 complexes are essential for forming the distal VE (DVE), which attenuate nodal signaling in the adjacent epiblast to contribute to forming a P-D gradient of nodal signaling (Figure 1.1.3B). In DVE, Forkhead box A2 (*Foxa2*) and the LIM homeobox protein 1 (*Lhx1*), together with *Smad2*, govern the production of extracellular antagonists of Wnt and nodal signaling, including Dickkopf homologue (*Dkk1*), cerberus-like protein 1 (*Cer1*), and the left-right determination factor 1 (*Lefty1*).

At E6.0, the A-P axis is established by the migration of the DVE to the prospective anterior side of the embryo. The movements of DVE to form the anterior VE (AVE) repositions the source of nodal and Wnt antagonists and breaks the radial symmetry of the embryo (Figure 1.1.3C). The migration of DVE is affected mainly by nodal signaling. Reduced *Nodal* transcription prevents DVE migration(Norris and Robertson 1999). The DVE remains distal in the embryos that lack the nodal co-receptor teratocarcinoma-derived growth factor precursor (*Tdgf1*).

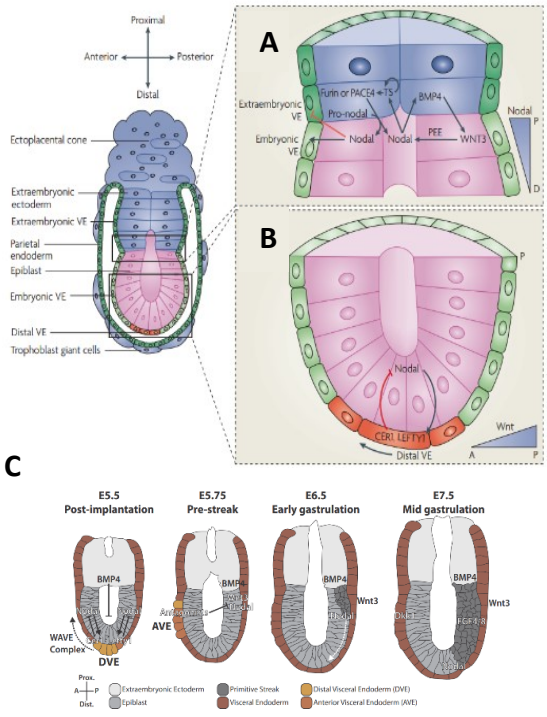

Figure 1.1.3. Establishment of the proximo-distal and anterior-posterior axis. (A) In the embryonic day 5.5 (E5.5) embryo, a gradient of nodal signaling levels preconfigures the proximal-distal axis. Two independent feedback loops enhance the strength of nodal signaling at the proximal epiblast. One is the positive feedback loop between secreted proprotein-convertases furin (also known as PCSK3) and SPC4 (also known as PCSK6 and PACE4) from extraembryonic ectoderm and nodal from the epiblast. Another is the positive feedback loop of BMP4 from extraembryonic ectoderm and WNT3 and nodal from the epiblast. **(B)** DVE is formed at the distal tip of the pre-gastrula embryo and starts to express extracellular nodal and Wnt-signalling inhibitors DKK1, CER1, and LEFTY1, which attenuate nodal signaling in the adjacent epiblast. **(C)** DVE migrates to the anterior side to form the anterior VE (AVE). Secretion of nodal and Wnt antagonist set up the gradient of WNT and Nodal signaling to set up the A-P axis. (modified from (Arnold and Robertson 2009, Bardot and Hadjantonakis 2020))

At the beginning of gastrulation, epiblast cells start to converge towards the posterior proximal pole of the embryo to form the primitive streak (Figure 1.1.4). The initiation of the primitive streak formation is induced by the high levels of nodal-SMAD2 and SMAD3 signals. Loss of both nodal antagonists CER1 and LEFTY1 leads to the formation of multiple streaks or enlarged primitive streak regions(Perea-Gomez, Vella et al. 2002). One hallmark of the primitive streak is that those cells undergo epithelial-to-mesenchymal transition, which is regulated by multiple signaling pathways, including Wnt, BMP, and FGF. Mutations in genes encoding FGF signaling pathway members such as *Fgf4*, *Fgf8*, or *Fgfr1* lead to an inability to complete EMT, and cells fail to migrate away from the primitive streak(Ciruna, Schwartz et al. 1997, Ciruna and Rossant 2001). Loss of *Bmp4* or the receptors *Alk2*, *Alk3*, or *Bmpr2* results in arrest during gastrulation, due to defects in AVE specification and primitive streak formation(Mishina, Suzuki et al. 1995, Winnier, Blessing et al. 1995, Mishina, Crombie et al. 1999, Beppu, Kawabata et al. 2000). Transcription factors *Eomes* and *Snail1*, which target and repress E-cadherin, are essential for induction of EMT. Loss of *Snai1* leads to accumulation of mesoderm in the primitive streak(Carver, Jiang et al. 2001). A switch from *Sox2* to *Snai1* expression in the primitive streak epiblast is necessary for mesoderm migration (Acloque, Ocaña et al. 2011). Mutants that lack or misexpress *Eomes* do not specify definitive endoderm or cardiac mesoderm(Arnold, Huang et al. 2008, Costello, Pimeisl et al. 2011). *Tbx6* and *T* mark the mesoderm-producing posterior of the primitive streak during gastrulation. In the absence of *T*, posterior

mesoderm is specified but fails to exit the primitive streak (Rashbass, Cooke et al. 1991). The expression of *T* is restricted by *Mixl1*. And the loss of *Mixl1* affects the movement of the definitive endoderm.

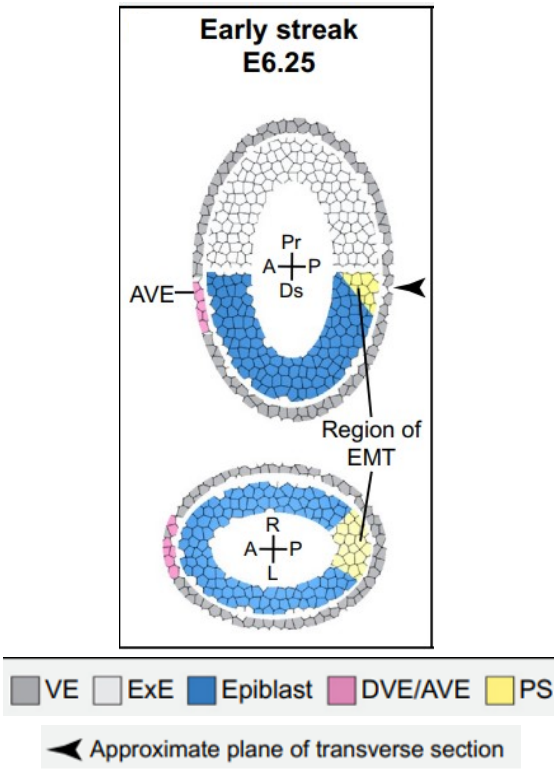

Figure 1.1.4. Schematic representation of the formation of the primitive streak. At E6.25, epiblast in the posterior proximal pole undergoes an epithelial-mesenchymal transition (EMT) in a region known as the primitive streak. Pr, proximal; Ds, distal; A, anterior; P, posterior. (modified from (Morgani and Hadjantonakis 2020))

During the next 36 hours after initiation of the primitive streak, it elongates and extends to the distal tip of the embryo. At the same time, ectoderm, endoderm, and distinct mesodermal cell lineages become allocated (Figure 1.1.5). BMP signaling, which is required for mesodermal formation in vivo, is critical for choosing ectodermal and mesodermal fates. *Bmp4* loss of function embryos fail to gastrulae and form no mesoderm(Winnier, Blessing et al. 1995). *Bmpr1* and *Bmpr2b* deficient embryos show reduced epiblast proliferation and no formation of mesoderm (Wilson, Rashbass et al. 1993, Mishina, Suzuki et al. 1995). *Chordin* and *Noggin*, the BMP antagonists, promote differentiation of ectodermal lineages. Another key player in the specifications of

mesoderm is *Wnt3a*. WNT3A signaling induces epiblast cells to adopt a paraxial mesodermal rather than a neuroectodermal fate(Yoshikawa, Fujimori et al. 1997). FGF pathway was shown to interact with the WNT signaling pathway to induce mesoderm formation. For instance, *Fgfr1* is required for the expression of *T* and *Tbx6* (Ciruna and Rossant 2001). *Smad2* deficient ES cells cannot contribute to the definitive endoderm lineages, which indicates Smad-mediated TGFβ is required to initiate definitive endoderm lineage(Tremblay, Hoodless et al. 2000). *Sox17* and *Mixl1* are needed for the differentiation but not for the formation of the definitive endoderm(Hart, Hartley et al. 2002, Kanai-Azuma, Kanai et al. 2002).

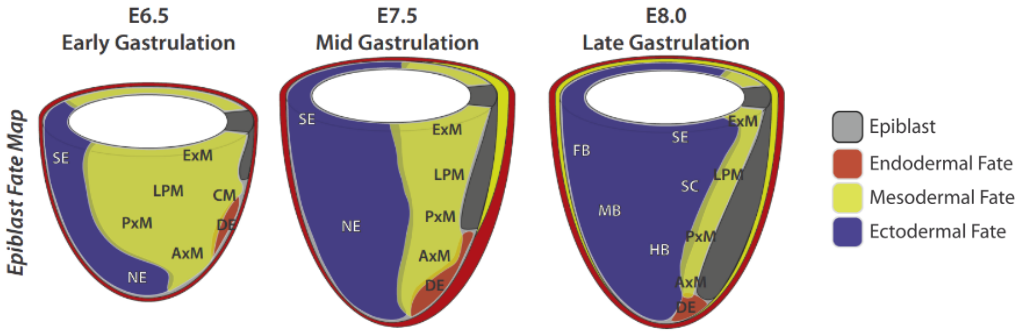

Figure 1.1.5. Epiblast cell fate decision during gastrulation. Prior to the commitment to particular fates, the relative positions of epiblast cells to the primitive streak are highly predictive. DE, definitive endoderm; CM, cardiac mesoderm; ExM, extraembryonic mesoderm; LPM, lateral plate mesoderm; PxM, paraxial mesoderm, AxM, axial mesoderm; SE, surface ectoderm; SC, spinal cord; NE, neurectoderm; FB, forebrain; MB, midbrain; HB, hindbrain. (modified from (Bardot and Hadjantonakis 2020))

1.1.2 General epigenetic regulation

The eukaryotic DNA is wrapped around histone octamers which consist of H2A, H2B, H3, and H4. The DNA itself and histone proteins can be modified. Epigenetic modifications of the genome, such as DNA methylation and histone modifications, have been reported to play an essential role in embryogenesis. Unlike genetic variation, global epigenetic variation is dynamic and reversible. The post-transcriptionally modification of histone often happens at the N-terminal tail. These

covalent modifications can be phosphorylation, ubiquitination, acetylation, and methylation (Figure 1.1.6). The mass spectrometry of calf histones reveals 13 modification sites in histone H2A, 12 modification sites in histone H2B, 21 modification sites in histone H3, and 14 modification sites in histone H4. Some lysine residue can either be methylated or acetylated, and there are three different possibilities for each methylated site (mono, di, or tri). Therefore, there are enormous combinations of possible histone modifications.

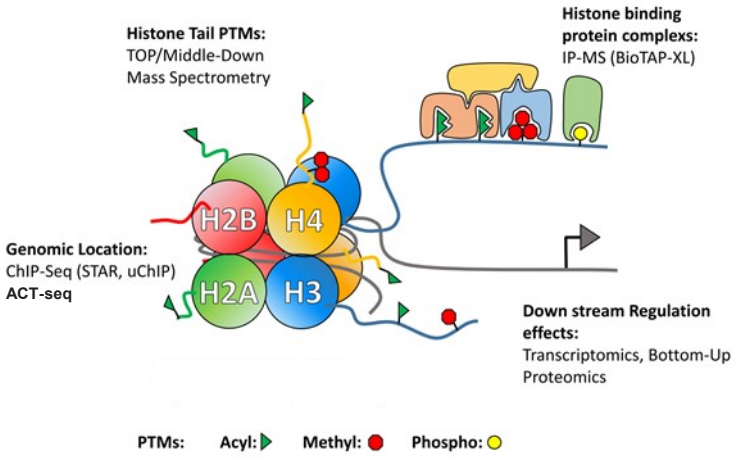

Figure 1.1.6. Histone modification code. A schematic representation of different histone modification codes and methods used for histone tail PTMS studies. ChIP-seq and ACT-seq are used for identifying the genomic location of histone modifications. TOP/Middle-Down mass spectrometry is used for detecting histone tail PTMs. IP-MS can be used for detecting histone binding protein complexes. The downstream regulation effects from different histone tail PTMs can be checked by transcriptomics analysis. (modified from (Holt, Wang et al. 2017))

1.1.2.1 Histone modification code

The histone methylation has been detected on arginine, lysine, and histidine residues. Unlike acetylation and phosphorylation, methylation does not change the overall charge of the histone. The most well-studied histone methylations are methylation on lysine and arginine residues. H3K4, H3K9, H3K27, H3K36, H3K79, and H4K20 are the main characterized sites of histone lysine methylation. Active genes in euchromatin are often associated with the methylation of H3K4, H3K36, and H3k79, while the

methylation of H3K9, H3K27, and H4K20 is associated with genes in heterochromatic regions. H3R2, H3R8, H3R17, H3R26, and H4R3 are the main sites of arginine methylation. One essential way histone arginine methylation regulates gene expression is by cross-talk with other histone modifications. For instance, H4R3 methylation stimulates H4 acetylation by p300; however, the acetylation of H4 inhibits H4R3 methylation (Lee, Koh et al. 2002). Another well-characterized cross-talk is between H3R2me2a and H3K4me3. Studies from different groups have shown that H3R2me2a and H3K4me3 are mutually exclusive(Guccione, Bassi et al. 2007, Kirmizis, Santos-Rosa et al. 2007, Bouchard, Sahu et al. 2018)

Histones are acetylated on multiple lysine residues. The most well-studied acetylations are those on the N-terminal tails of histones such as H3K9, H3K14, H4K5, H4K8, H4K12, and H4K16. Histone acetylations are often associated with active state chromatin, such as during DNA replication and transcription. Histones are highly positive charge due to the lysines and arginines residue. This positive charge allows histone to bind to negatively charged DNA tightly. Acetylation neutralizes the lysine's positive charge, which can weaken the interaction of histones with DNA to make the chromatin more open. In addition, histone acetylation has at least two other functions. First, they can recruit proteins with centrin domains, such as bromodomains, to open chromatin. For instance, the bromodomain of *Swi2*/*Snf2* is required to retain the SWI/SNF remodeling complex on the acetylated nucleosome. Second, the acetylation of histones has been proven to inhibit the binding of chromatin-associated proteins to chromatin. It has been shown that H3K4ac reduces the affinity of spChp1 to the methylated H3K9.

Histone phosphorylation sites are found in multiple amino acid residues of all four histone proteins. Those sites can be divided into two categories, one is involved in transcription regulation, and another is involved in chromatin condensation.

1.2.2.2 Bivalent domain

In mouse embryonic stem cells, H3K4me3 and H3K27me3 can both present at the

promoter of essential developmental genes. Bernstein et al. used the term 'bivalent domains' to describe the conflicting combination of H3K4me3 and H3K27me3 in the same chromatin regions in mouse embryonic stem cells (mESCs) (Bernstein, Mikkelsen et al. 2006). Around 2700 genes were marked both with active and repressive chromatin marks termed as posied status for activation or repression in pluripotent cells. As the differentiation of mESCs, this posied status is resolved by losing H3K27me3 at active genes or losing H3K4me3 at silenced genes(Bernstein, Mikkelsen et al. 2006).

In addition, bivalent promoters are not exclusive to mESCs. The presence of bivalent promoters was also reported in neuron progenitor cells (NPCs) and mouse embryonic fibroblasts (MEFs) (Mikkelsen, Ku et al. 2007). Further, Mohn et al. showed that even though ~660 bivalent domains were dissolved during the differentiation of mESC into neural progenitors, ~550 genes gained H3K27me3 and formed novel bivalent domains in neural progenitors (Mohn, Weber et al. 2008). Instead of simple 'on' or 'off', the bivalent promoter is considered a poised state that can be tightly regulated to gain a fine tun of gene expression. One raising hypothesis is that bivalency is a mechanism commonly used by cells for tight regulation of tissue-specific gene expression.

1.1.2.3 PcG (Polycomb group) proteins

PcG proteins mainly form two complexes: the PRC1 and the PRC2 complex. PRC2 complex contains four core components: *Ezh2*/*Ezh1*, *Eed*, *Suz12*, and *RbAp46*/*48*. The SET domain-containing methyltransferase EZH2 or EZH1 catalyzes the di- and trimethylation of lysine 27 on histone H3 as the catalytic subunit in PRC2. *Ezh1* is mainly expressed in adult tissue, whereas *Ezh2* is often expressed during embryogenesis(Laible, Wolf et al. 1997, Margueron, Li et al. 2008).

Through association with subunits that can modulate its enzymatic activities or chromatin target sites, PRC2 achieved functional diversity(Li, Margueron et al. 2010, Pasini, Cloos et al. 2010, Ciferri, Lander et al. 2012). Proteomics study in human cells

revealed two alternative core complexes of PRC2 (Figure 1.1.7). PRC2.1 is defined by binding one of the three Polycomb-like homologs (PCLs): PHF1, PHF19, or MTF2, which are mutually exclusive. PRC2.2 complex includes the zinc-finger proteins AEBP2 and JARID2, which enhance enzymatic activity and regulate chromatin binding of the PRC2 complex.

In mESCs, a large number of genes are targeted by PRC2. Those genes targeted by PRC2 encode various regulators for development(Boyer, Plath et al. 2006, Bracken, Dietrich et al. 2006, Lee, Jenner et al. 2006). Given the more open and flexible chromatin organization of ES cells, the occupation of H3k27me3 on those developmental genes is important for their repression in mESCs. At the same time, H3K4me3 histone marks, often associated with active transcription, are found in most, if not all, PRC2 targeted genes in mESCs and form the bivalent domain(Zhao, Han et al. 2007, Mohn, Weber et al. 2008).

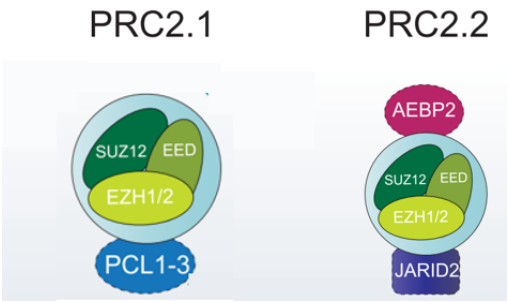

Figure 1.1.7. Schematic representation of core components in PRC2 complexes. The presence of PCL1-3 defines PRC2.1 complex, and PRC2.2 complex is defined by the presence of AEBP2 or JARIAD2. (modified from (Healy, Mucha et al. 2019))

The core of the PRC1 complex contains several members: Cbx(CBX2, CBX4, CBX6, CBX7, or CBX8); Ring1A or Ring1B; PHC(PHC1, PHC2, or PHC3); PCGF(PCGF1, PCGF2, PCGF3, PCGF4, PCGF5, or PCGF6); RYBP and YAF2(Gao, Zhang et al. 2012, Luis, Morey et al. 2012). The canonical PRC1 (cPRC1) is characterized by the presence of one chromobox protein (CBX2, CBX4, CBX6, CBX7, or CBX8) which recognizes H3K27me3 and a Polyhomeotic (Ph) homologous protein (PHC1-PHC3). On the other side, non-canonical PRC1 (ncPRC1) possesses the zinc-finger domain and YY1-binding protein

(RYBP) or its paralog, YAF2, which associates with PCGF1, PCGF3/5, or PCGF6 to form ncPRC1.1, ncPRC.3/PRC1.5, or ncPRC1.6 respectively (Figure 1.1.8).

The canonical view of PRC1 function in gene repression is through the sequential cooperation with PCR2. In this model, PRC2 first deposits the H3K27me3 histone mark, which is recognized by the Cbx subunit of PRC1 and attracts the PRC1 complex to chromatin. The Ring1 subunit of PRC1 ubiquitinates histone H2A at lysine 119 (H2AK19ub), which is thought to contribute to transcriptional repression by restraining RNA pol II from elongation(Simon and Kingston 2009). Contrasting to the canonical model, non-canonical is recruited to the chromatin independently of PRC2 and H3K27me3(Morey, Pascual et al. 2012, Tavares, Dimitrova et al. 2012).

In ES cells, Polycomb complexes contribute to the repression of lineage specification gene expression; however, they appear to be required to repress pluripotency genes during the differentiation. For instance, *Cbx7* represses *Cbx2*, *Cbx4*, and *Cbx8* to prevent premature differentiation in ES cells, while *Cbx7* and the pluripotency genes are repressed in a PRC1/PCR2-dependent manner to enable lineage specification during the differentiation (Morey, Pascual et al. 2012). *Cbx7* is the predominant CBX protein and a direct target of the pluripotency factor *Oct4*, *Nanog*, and *Sox2* in ES cells (O'Loghlen, Muñoz-Cabello et al. 2012). It is highly expressed in mESCs and gradually decreases during development. Virtually all genes bound by PRC2 and decorated with H3K27me3 are also bound by *Cbx7* and *Ring1B*(Morey, Pascual et al. 2012, O'Loghlen, Muñoz-Cabello et al. 2012, Tavares, Dimitrova et al. 2012). *Cbx7*-depleted ES cells spontaneously express ectoderm and mesoderm markers in culture conditions favoring self-renewal(Morey, Aloia et al. 2013). During the development, CBX7 is replaced by other CBX proteins such as CBX2 and CBX4 to mediate fate choices along the three germ layers.

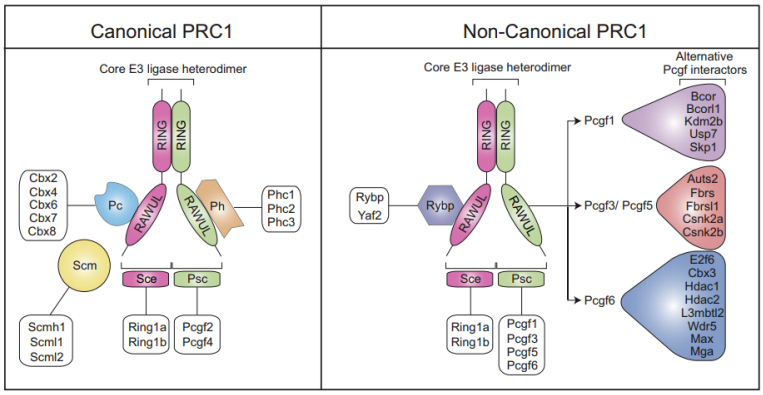

Figure 1.1.8. Schematic representation of core components in PRC1 complexes. Canonical PRC1 complex contains CBX proteins that recognize H3K27me3. The non-canonical PRC1 complex contains RYBP. (modified from (Conway and Bracken 2017))

1.1.2.4 TrxG (Trithorax group) protein

Similar to PcG proteins, TrxG proteins were first identified in *Drosophila* as regulators of homeotic genes (*Hox* genes). As conserved chromatin regulators, TrxG proteins can be divided into three classes based on their molecular function, the MLL (also known as ALL-1 and HRX) complex, ATP-dependent chromatin-remodeling complexes like the BRM/BAF complex, and a supercomplex that directly bind specific DNA sequence which is comprised of some histone modifiers and chromatin remodelers.

1.1.2.4.1 MLL complex

The MLL complex trimethylates lysine 4 of histone H3(Milne, Briggs et al. 2002). Yeast SET domain-containing 1 (*Set1*) was the first histone methyltransferase that was discovered to catalyze mono-, di- and trimethylation of H3K4. Six mammalian homologs of Set1 were found, *Set1A*, *Set1B*, *Mll1*, *Mll2*, *Mll3*, and *Mll4*. SET1A and SET1B form the COMPASS (complex proteins associated with Set1) complex with the unique WB repeat-containing 82(WDR82) subunit. It was suggested that Set containing COMPASS complex are involved in global gene activation. MLL1-4 forms the COMPASS-like complex. *Mll1* is required to resolve small subset mammalian genes, including HOX genes(Wu, Wang et al. 2008). *Mll2* is responsible for H3K4me3 at the bivalent promoters in mESCs. *Mll3* and *Mll4*- containing complexes are essential for

the methylation of H3K4 at retinoic acid target genes but not for HOX genes (Figure 1.1.9). In vitro enzyme studies with Set1 and MLL complex suggest that the Set1 complex is a more robust H3K4 trimethylase than the MLL complexes(Wu, Wang et al. 2008).

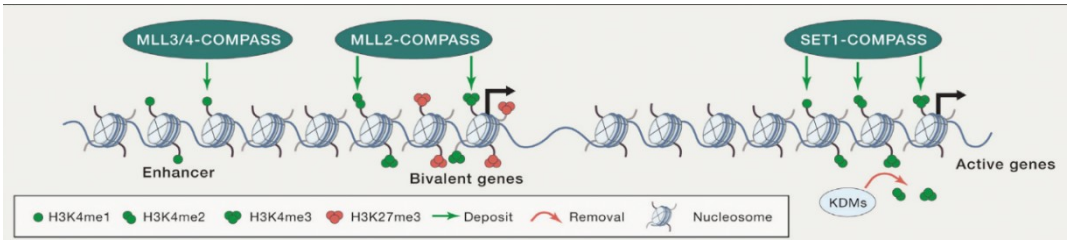

Figure 1.1.9. Schematic representation of functional diversity of MLL complexes. SET1- COMPASS is responsible for mono-, di-, and trimethylation on H3K4 at active promoters. COMPASS complexes containing MLL3/KMT2C and MLL4/KMT2D lead to the deposition of H3K4me1 at enhancers. MLL2/COMPASS performs the deposition of methyl marks on H3K4 at bivalent regions. (modified from (Schuettengruber, Bourbon et al. 2017))

1.1.2.4.2 ATP-dependent chromatin remodeling complexes

ATP-dependent chromatin-remodeling complexes open up chromatin by inducing nucleosome sliding or eviction or by mediating chromatin looping. There are three ATP-dependent chromatin-remodeling complexes which are SWItch/sucrose nonfermentable (SWI/SNF), imitation switch (ISWI), and chromodomain helicase DNA-binding (CHD) complex.

SWI/SNF subfamily was the first chromatin-remodeling complex discovered in yeast (Winston and Carlson 1992). Brahma (BRM) is a bromodomain-containing protein in *D. melanogaster*, homologous to yeast SWI/SNF. The mammalian homologous are *Brm* and Brahma-related gene 1 (*Brg1*) from TrxG proteins. *Brm* and *Brg1* are the core component as the ATPase, and only one is present in a BAF complex. Except for the catalytic subunit *Brg1* or *Brm*, each SWI/SNF complex contain a single ARID (AT-rich interacting domain) containing subunit. The SWI/SNF complex can be subdivided into BAF and PBAF complexes based on the catalytic and ARID subunits. In the BAF complex,

the ARID subunit is either BAF250a or BAF250b (also known as ARID1a and ARID1b), and the catalytic subunit is *Brg1* or BRM. Whereas the PBAF complex, whose catalytic subunit is exclusively Brg1, contains BAF200(also known as ARID2) in the complex.

The CHD family is defined by the presence of chromodomains and can be divided into three subfamilies according to the component of different CHD proteins. CHD1 and CHD2 form the first subfamily, which binds H3K4me3 via their chromodomains and plays a vital role in the development and ES cell maintenance(Gaspar-Maia, Alajem et al. 2009). The second subfamily contains CHD3 and CHD4 and is part of the Mi2-NuRD (Mi2-nucleosome remodeling and deacetylase) complex. This subfamily couples chromatin remodeling and histone deacetylation to mediate repressive functions involved in transcriptional regulation and cell fate determination(Unhavaithaya, Shin et al. 2002). CHD6, CHD7 and CHD8 make up the third complex, which counteracts PcG-dependent silencing and activates transcription(Srinivasan, Dorighi et al. 2008).

1.1.3 Alternative splicing

1.1.3.1 General introduction of alternative splicing

For higher eukaryotic organisms, alternative splicing (AS) is one of the most extensively used mechanisms, contributing to the greater macromolecular and cellular complexity. By alternative splicing, the exons of the primary transcripts (pre-mRNAs) can be spliced in different combinations to produce structurally and functionally distinct mRNA and protein variants (Figure 1.1.10). In mice, most genes undergo alternative splicing to generate multiple mRNAs that encode different proteins. More than 30% of human genes have multiple first exons generated by alternative splicing, up to 70% of genes have multiple polyadenylation sites, and more than 90% of genes undergo alternative splicing (Wang, Sandberg et al. 2008). The alternative splicing can be grouped into different types (Figure 1.1.10)(Blencowe 2006). The most common type of AS involves cassette-type alternative exons that are

skipped or included in the final message RNA. At least one-third of known AS events belong to this type. Another common AS events use 5’ or 3’ splice sites within exon sequences, introducing subtle changes into coding sequence as little as a single condon. Around one quarter of the known AS events belong to this eype.

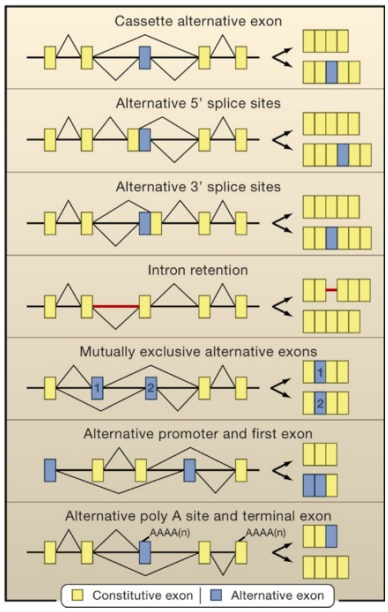

Figure 1.1.10. Differentiate types of alternative splicing events. Types of AS generateing functionally distinct transcripts are illustrated. Blue boxes indicate alternative exons. (modified from (Blencowe 2006))

1.1.3.2 Components and formation of Spliceosome

The pre-mRNA splicing is carried out by spliceosome, a large RNA-protein complex composed of five small nuclear ribonucleoproteins (snRNPs), including U1, U2, U4/U6, and U5, and numerous accessory proteins. There is a GU at the 5’ end and AG at the 3’ end for a typical eukaryotic intron. In between, near the 3’ splice site, there is a branch-point sequence (BPS) and a series of pyrimidines, known as the polypyrimidine tract (Py tract). During the spliceosome assembly onto each intron, U1 snRNP binds to the 5’ splice site. Splicing factor 1 (SF1) binds to BPS as a branch-point binding protein. The 65kDa subunit of the dimeric U2 auxiliary factor (U2AF) binds to the Py tract. In some cases, the 35KD subunit of U2AF binds to AG at the intron/exon junction. Then, the earliest defined complex, the so-called E complex, is formed. After recruitment of the U2 snRNP, which binds to the branch point, the A complex is formed. The remaining three snRNPs (U4, U5, and U6) are recruited to form the B complex, and the C complex that catalyzes the chemical steps of splicing is formed after a

rearrangement. During the rearrangement, U6 snRNA is brought to contact with the 5' splice site, and the U1 and U4 snRNPs are lost. (Figure 1.1.11).

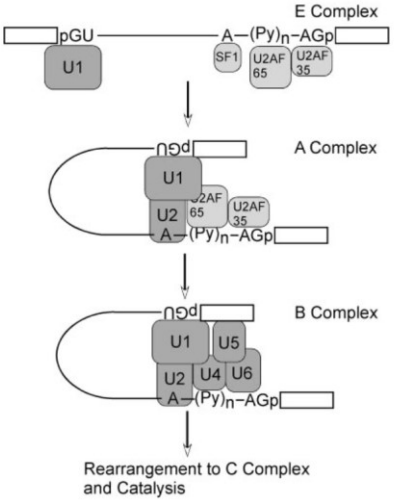

Figure 1.1.11. Schematic representation of the process of spliceosome formation. E complex is formed by the binding of U1 snRNP, SF1, U2AF65/U2AF35 to the pre-mRNA. The recruiment of U2 snRNP to the E complex leads to A complex. By the recruitment of U4, U5 and U6 snRNPs to the A complex, the B complex is formed which will be rearranged to C complex. BPS, branch-point sequence; (Py)n, polypyrimidine tract. (modified from (Black 2003))

1.1.4 Jumonji domain-containing protein 6

Jumonji domain-containing protein 6 (*Jmjd6*) is a member of a large family of metalloenzymes containing the Jmjc domain. This family comprises ferrous iron (Fe^{2+})- and 2-oxoglutarate(2OG)-dependent dioxygenases reported to hydroxylate and demethylate protein and nucleic acid substrates (Chang, Chen et al. 2007, Webby, Wolf et al. 2009, Mantri, Loik et al. 2011, Liu, Ma et al. 2013, Unoki, Masuda et al. 2013, Poulard, Rambaud et al. 2014, Wang, He et al. 2014, Gao, Xiao et al. 2015). Most (likely >95%) 2-OG oxygenases catalyze two-electron oxidations by the conversion of 2-OG and O2 to succinate and carbon dioxide with Fe^{2+} as a cofactor (Figure 1.1.12). Hydroxylation is the most common 2OG-dependent oxygenase catalyzed reaction. (Hausinger 2004, Walport, Hopkinson et al. 2012).

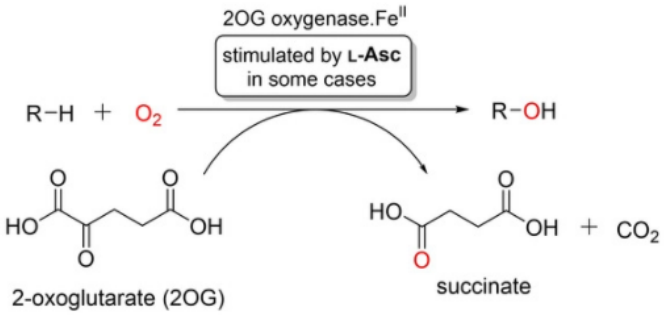

Figure 1.1.12. Schematic representant of the 2-OG-catalyzed oxidation reaction. The binding of 2OG and substrate to Fe(II) of the oxygenase provides a vacant coordination site for O2. Oxidative decarboxylation of 2OG forms succinate, CO2, and hydroxylated substrate. (modified from (Khan, Schofield et al. 2020)).

1.1.4.1 Jmjc subfamily of 2-OG dependent oxygenases

There are ~60-70 human 2-OG and Fe2+ dependent oxygenases with diverse functions, including collagen biosynthesis, lipid metabolism, hypoxia sensing, DNA damage repair, and epigenetic regulation (Islam, Leissing et al. 2018). The JmjC oxygenases are a subfamily of 2OG oxygenases in which most of the members have been assigned as histone lysine demethylases due to their wide roles in protein hydroxylation. However, for the members with only JmjC domains like *Jmjd6*, MINA53 (also known as RIOX2 or JMJD10), NO66 (also known as RIOX1 or JMJD9), and Jmjd5 is controversial whether they have demethylation function or not (Figure 1.1.13).

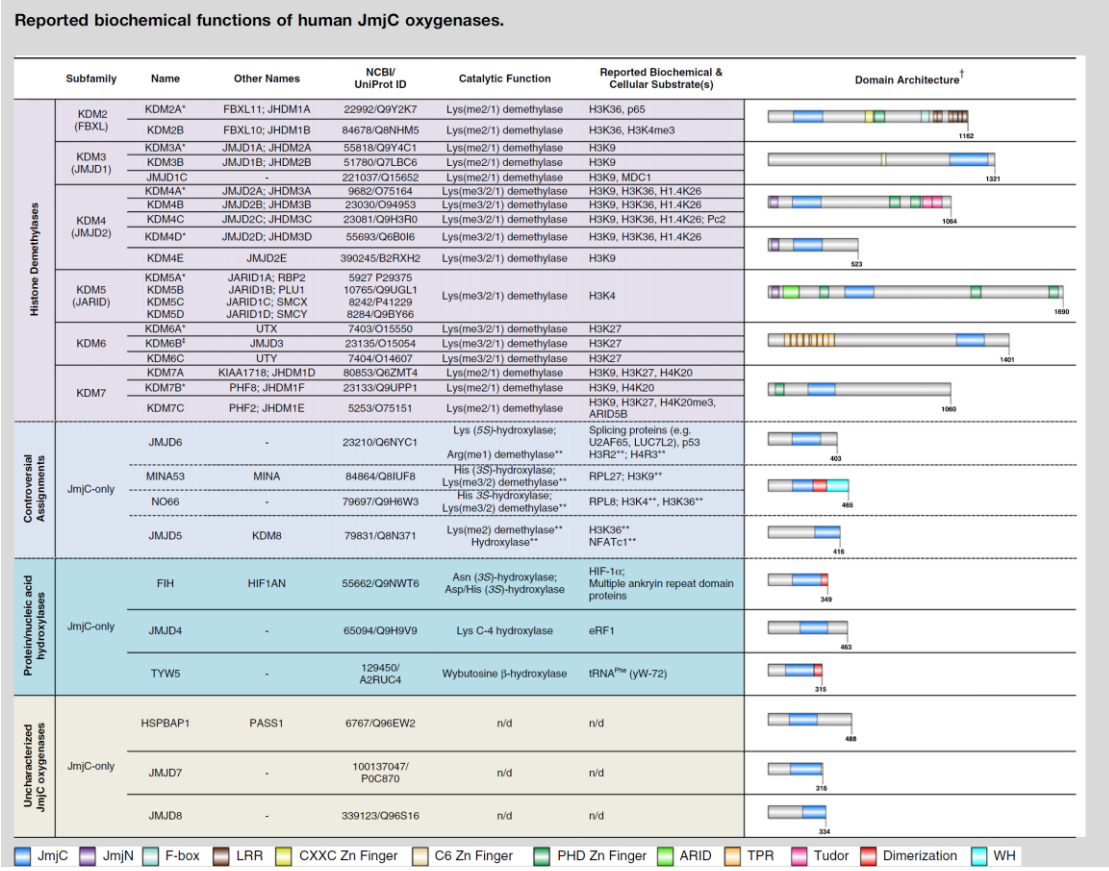

Figure 1.1.13. Reported human JmjC oxygenases. Summary of reported JmjC oxygenases with demethylases, oxygenases, or both functions assigned. Catalytic functions, reported biochemical or cellular substrate, and domain architecture for each protein are shown. *Subfamily domain architecture representation is based on this enzyme. ** Controversial functional assignments. (modified from (Markolovic et al. 2016))

The phylogenetic relationship amongst the 33 human JMJD proteins showed that those JmjC-only members are evolutionarily separated from other members (Figure 1.1.14) (Oh, Shin et al. 2019). The molecular weight for those JmjC-only members is smaller than 100 kDa, while other JMJD proteins are bigger than 100 kDa except for JMJD2D, JMJD2E, and JMJD2F. Those JMJD proteins with bigger molecular weight have been reported to demethylate histone residues except JARID2, JMJD2D, and JMJD2F (Oh, Shin et al. 2019). Those JMJD proteins are assigned as histone lysine demethylases (KDMs). Most JmjC KDMs are 2-3 times longer than JmjC hydroxylases because they have extra domains that bind to histone protein and nucleic acid, whereas JmjC hydroxylases only have one JmjC domain (Figure 1.1.13). For instance,

the plant homeodomain (PHD) domain on the N-terminal of KDM7B interact strongly with H3K4me3. Whereas JmjC hydroxylases seem to lack those domains, they have other domains/regions such as dimerization, which could be involved in substrate binding. While the oligomerization of JmjC KDM is not well characterized. Forming dimer or oligomer is essential for the enzyme activity of Jmjc hydroxylases. The dimerization domain of the JmjC nucleic acid hydroxylase, tRNA wybutosine-synthesizing protein 5 (TYW5), plays a role in tRNA binding. A hydrophobic region in the dimerization domain of factor inhibiting HIF-1α (FIH) promotes the binding of HIFα, which is a substruct of FIH.

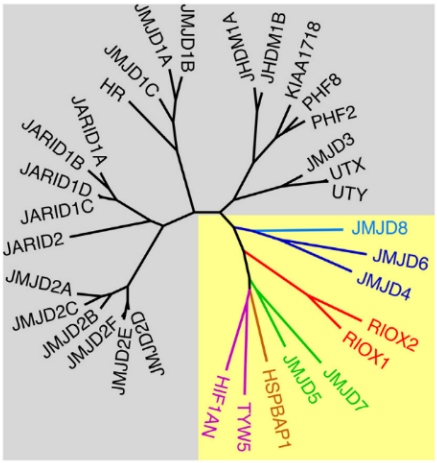

Figure 1.1.14. The phylogenetic relationship amongst the 33 human JMJD proteins. The yellow background highlights the evolutionarily separated small JMJD proteins. All other proteins marked in black color that have a calculated molecular weight over 100 kDa (except for JMJD2D-F) have been reported to demethylate histone lysine residues (except for JARID2 and JMJD2F). (Oh, Shin et al. 2019)

1.1.4.2 introduction to the history and protein structure of JMJD6

Jmjd6 was initially discovered as a phosphatidylserine receptor (PSR or Ptdsr) expressed on the cell membrane of macrophages and was involved in phagocytosis of apoptotic cells two decades ago (Fadok, Bratton et al. 2000). However, a later study showed that *Jmjd6* has essential functions during embryogenesis but not in apoptotic cell removal(Böse, Gruber et al. 2004, Mitchell, Cvetanovic et al. 2006). Cikala et al. cloned *Jmjd6* homologous genes in Hydra and found the protein contained a central jumonji C (JmjdC) domain and predicted that it would function as Fe^{2+} and 2-OG dependent dioxygenase (Cikala, Alexandrova et al. 2004). Later, *Jmjd6* was found in the cell nucleus, and this nuclear localization is mediated by five independent nuclear localization signals, each of which alone is sufficient to target GFP in the cell

nucleus(Cui, Qin et al. 2004). Overexpression *Jmjd6*-GFP-Flag plasmid in Madin-Darby Canine Kidney (MDCK), PC3, 293T, HeLa, and NIT 3T3cells showed that the fusion protein is localized in the nucleus(Cui, Qin et al. 2004). Similarly, *Jmjd6* localizes to the nucleus in Hydra. Overexpression HA-*Jmjd6* or *Jmjd6*-V5 tagged construct in 3T3 cells showed that the fusion protein localized in nuclear(Mitchell, Cvetanovic et al. 2006). Besides its nuclear localization, *Jmjd6* was also found in the cytoplasm in MEF cells(Hahn, Wegener et al. 2010).

From yeast to mammals, *Jmjd6* is conserved (Hahn, Bose et al. 2008). The double-stranded β-helix fold (DSBH) formed in the central Jmjc domain is shared by all known 2OG-dependent dioxygenases (Clissold and Ponting 2001, Loenarz and Schofield 2008). The DSBH constitutes eight anti-parallel β-strands forming the major and minor β-sheets and forms a barrel-like structure functioning as the catalytic center. The Fe^{2+} binding site is located at the open end of the barrel (Figure 1.1.15). Crystallographic studies have revealed that DSHB is present in *Jmjd6* (Hong, Zang et al. 2010, Mantri, Krojer et al. 2010, Islam, McDonough et al. 2019). Three amino acids, H187, D189, and H273, as the binding site for Fe^{2+}, are essential for the enzymatic activity of *Jmjd6*.

Compared to the typical JmjC KDMs like UTX and *Jmjd3*, *Jmjd6* is much smaller, only one-third or half the length, and lacks a domain for histone binding. *JMJD6* forms a stable oligomer in vivo and in vitro, which is not well characterized in JmjC KDMs but is common in JmjC hydroxylase-like factors like FIH and TYW5. The comparison of protein structures between *Jmjd6* and other 2OG oxygenases, including histone lysine demethylases (KDMs), supported a hydroxylase rather than a demethylase activity for *Jmjd6* (Mantri, Krojer et al. 2010, Markolovic, Leissing et al. 2016).

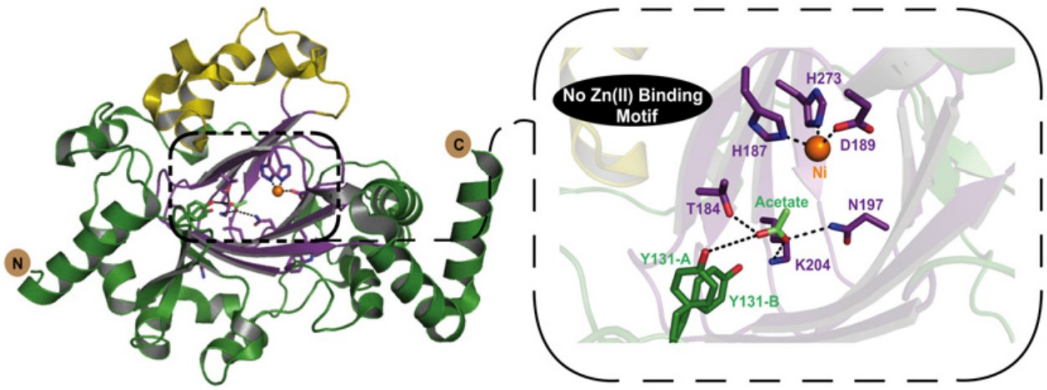

Figure 1.1.15. Protein structure of *Jmjd6.* Anti-parallel β-strands form a barrel-like structure as the catalytic center (left). Enlarge catalytic center of JMJD6 (right). (modified from (Bottger, Islam et al. 2015))

1.1.4.3 Expression of *Jmjd6*

In *Xenopus*, *Jmjd6* is highly expressed from four-cell to gastrula embryos (Zhang, Gao et al. 2015). During mouse embryo development, *Jmjd6* is expressed throughout development. As early as E1.0 to E4.5, *Jmjd6* starts to express in the mouse embryos (Guo, Huss et al. 2010). Analysis of the Ptdsr-β-geo gene trap reporter mouse line, *Jmjd6* is expressed in developing neural tube, somites, heart, gut, and branchial arches from E9.5 to E10.5 with higher expression in limb bud and eye(Böse, Gruber et al. 2004). During the cardiac genesis, *Jmjd6* expression can be detected through the heart in E10.5, but in E11.5, *Jmjd6* showed an increased expression in the myocardial wall and decreased expression in trabeculation(Schneider, Böse et al. 2004). In adult mice, *Jmjd6* is expressed in most tissues with a prominent expression level in the heart, testis, thymus, kidney, liver, and skin (Böse, Gruber et al. 2004).

1.1.4.4 *Jmjd6* knockout mice

Three knock-out mice have been generated by different groups (Figure 1.1.16 B, C and D) (Li, Sarkisian et al. 2003, Böse, Gruber et al. 2004, Kunisaki, Masuko et al. 2004). Due to the close position of *Jmjd6* and *Mettl23* in the genome (Figure 1.1.6A). The *Jmjd6* knockout mouse generated by Li et al. and Kunisaki et al. were double knockouts of *Jmjd6* and *Mettl23*. All three different *Jmjd6* homozygous mutants are lethal, but

the heterozygous mutants are healthy and fertile.

Li et al. showed that breeding the *Jmjd6* heterozygous mice results in relatively standard Mendelian ratios of the litters in embryonic stages E15.5 and E17.5 but no viable mice at postnatal day8. The viable *Jmjd6* homozygous mutant is unable to breathe and shows cyanotic skin color, and dies within hours. They showed the dead cells accumulated in the lung and brain, which caused abnormal organ development. They also found that ~15% of *Jmjd6* deficient embryos showed severe brain malformation(Li, Sarkisian et al. 2003).

Kunisaki et al. showed that *Jmjd6* deficient pups are born alive but die within 24 hours. Homozygous mutants are present at a roughly Mendelian ratio at various embryonic stages. *Jmjd6*-/- embryos are normal until E12.5, but in E15.5, *Jmjd6* -/- embryos are small and pale compared to *Jmjd6* +/-(Kunisaki, Masuko et al. 2004). Both studies by Li et al. and Kunisaki et al. showed that the failure of apoptotic cells uptake is the reason for organ development problems, including lung development and erythropoiesis and T lymphopoiesis in *Jmjd6*-/- mouse embryos(Li, Sarkisian et al. 2003, Kunisaki, Masuko et al. 2004). Two *Jmjd6* knockout mouse models described above are both *Jmjd6* and *Mettl23* double knockout.

The *Jmjd6* knockout mouse generated by Böse et al. does not impair the *Mettl23* gene. By analyzing 1,031 between E9.5 to E18.5 embryos from interbreeding of heterozygous mutants, 198 (19.2%) *Jmjd6* -/- embryos were harvested indicating a low rate of embryonic lethality in utero. *Jmjd6* -/- embryos are viable and of normal size from E9.5 to E12.5. However, at E13.5 and after that, most *Jmjd6* -/- embryos show morphological abnormalities. In detail, the terminal differentiation of the kidney, intestine, liver, and lung are delayed during embryogenesis. However, with this model, *Jmjd6* was not found to be essential for apoptotic cell removal (Böse, Gruber et al. 2004).

The *Jmjd6* knockout mouse used in this study was generated by the European conditional mouse mutagenesis program (EUCOMM) project. *Mettl23* was not affected in this *Jmjd6* knockout mouse (Figure 1.1.16E).

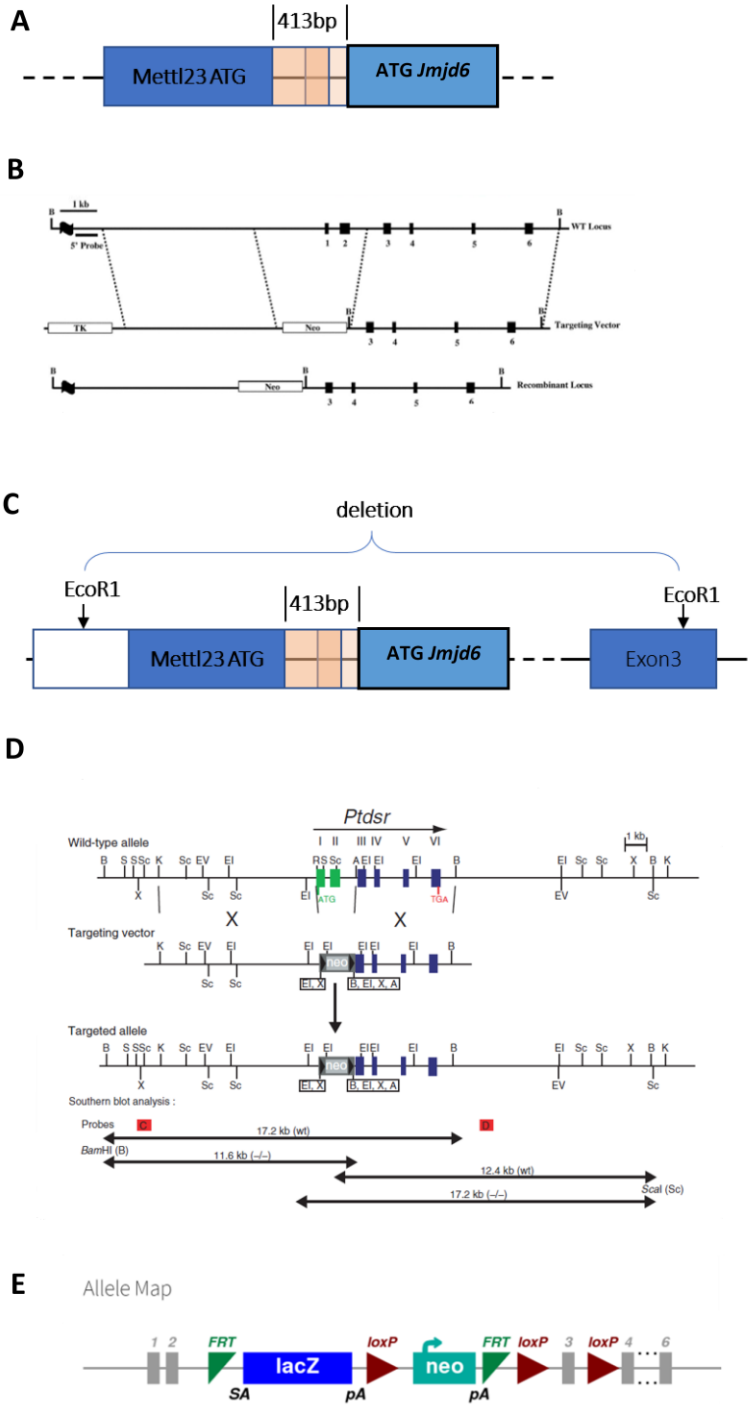

Figure 1.1.16. Chromosomal regions of *Jmjd6* and the *Jmjd6* Knockout mouse models. **(A)** *Jmjd6* and its neighboring gene *Mettl23* overlap in 5'UTR; there is a 413bp gap between the two genes' start code (ATG). **(B)** *Jmjd6* knockout mouse model used by Li et al., double knock out of *Jmjd6* and *Mettl23*. The Deletion region includes exon1 and exon2 from *Jmjd6* and part from *Mettl23*. **(C)** *Jmjd6* knockout mouse model used by Kunisaki et al., double knock out of *Jmjd6* and *Mettl23*. The Deletion region includes exon1, exon2, and exon3 from *Jmjd6* and part from *Mettl23*. **(D)** *Jmjd6* knockout mouse model used by Böse et al., deletion region include exon1 and exon2 from *Jmjd6*. **(E)** *Jmjd6* knockout mouse model used in this thesis.

1.1.4.5 *Jmjd6* works as a hydroxylase/demethylase

Cikala et al. cloned the homologous of *Jmjd6* in Hydra and predicted its hydroxylation function from the conserved JmjC domain in the *Jmjd6* protein sequence (Cikala, Alexandrova et al. 2004). A few years later, *Jmjd6* was shown to interact with and hydroxylate alternative splicing factor U2AF65 (Webby, Wolf et al. 2009). By hydroxylating alternative splicing factors such as U2AF65 and LUC7L2, *Jmjd6* is involved in gene alternative splicing (Webby, Wolf et al. 2009, Boeckel, Guarani et al. 2011, Heim, Grimm et al. 2014, Yi, Shen et al. 2016). More and more studies afterward support the hydroxylation function for *Jmjd6* with different subtracts such as p53, LUC7L2, histone H3/H4, and itself (Han, Li et al. 2012, Mantri, Webby et al. 2012, Unoki, Masuda et al. 2013, Wang, He et al. 2014). MS-based in vitro assay further confirmed the hydroxylation function of *Jmjd6* on those substrates (Unoki, Masuda et al. 2013, Islam, McDonough et al. 2019). Moreover, Islam et al. showed *Jmjd6* hydroxylate Luc7L3, LUC7L1, RBM39, Acinus S, and SRSF11 in vitro with an MS-based assay (Islam, McDonough et al. 2019). Interestingly, *Jmjd6* could also hydroxylate its N terminal tail, which is vital for its oligomerization (Han, Li et al. 2012). From both in vivo and in vitro experiments, it is now widely accepted that *Jmjd6* could hydroxylate wide substrates.

An initial study showing *Jmjd6* work as a demethylase was reported by Chang et al. based on in vitro assay (Chang, Chen et al. 2007). Recombinant *Jmjd6* protein was incubated with bulk histones and synthetic histone tail peptides with various methylated lysine and arginine sites. They showed reductions in H3R2me2 and H4R3me2 levels by western blot. After purifying the resulting peptide from the in vitro assay with the anti-H4R3me1 antibody, they show 14 daltons mass shift of the synthetic 30–amino acid peptide contained in H4R3me2 to the left, which indicates loss of one methyl group. On the other hand, Liu et al. showed that *Jmjd6* demethylates H4R3me2a, H4R3me2s, and H4R3me1 by incubation of recombinant *Jmjd6* with synthetic histone peptide but not other methylated arginine or lysine residues including H3R2me2 (Liu, Ma et al. 2013). In HEK293 cell, *Jmjd6* was shown to bind at distal regions (intergenic and intragenic regions) and highly correlated with the Brd4 binding site. By interacting with Brd4, *Jmjd6* mediates the demethylation of

H4R3me2s and 7SK snRNA which promotes the pause release at target genes by ensuring the dismissal of the 7SK snRNA/HEXIM inhibitory complex. However, many independent groups could not repeat *Jmjd6* arginine demethylation activity on H3 and H4 histone peptides in MS-based assay (Webby, Wolf et al. 2009, Han, Li et al. 2012, Unoki, Masuda et al. 2013, Islam, McDonough et al. 2019). In addition, Chang et al. also detect a strong 16 and 32 daltons mass shift of this demethylated peptide to the right side, caused by hydroxylation on lysine residue at K5 and K8 (Chang, Chen et al. 2007). The hydroxylation of *Jmjd6* on histone is also confirmed by other groups (Han, Li et al. 2012, Unoki, Masuda et al. 2013, Islam, McDonough et al. 2019). There are also works by *Jmjd6* gain or loss of function that did not support *Jmjd6* as a histone demethylase. *Jmjd6* silencing in endothelial cells did not change the arginine methylation of H4R3me2s (Boeckel, Guarani et al. 2011). Loss or overexpression of *Jmjd6* in MEF or HEK293T cells did not cause changes in H3K4, H3K9, H3K27, H3K36, and H4K20 histone methylation (Hahn, Wegener et al. 2010).

Besides histones, *Jmjd6* was also shown to demethylate other substrates like HSP70, estrogen receptor α (ERα), and RNA helicase A (Lawrence, Conderino et al. 2014, Poulard, Rambaud et al. 2014, Gao, Xiao et al. 2015). However, Islam et al. could only find +16-Da instead -14-Da shift after incubation peptide with *Jmjd6* protein, corresponding to hydroxylation instead of demethylation(Islam, McDonough et al. 2019). Thus, the assignment of the demethylation function of *Jmjd6* is controversial for now.

1.1.4.6 Function beyond hydroxylase/demethylase

Besides the function as hydroxylase/demethylase, JMJD6 can also bind to ssRNA and protein involved in alternative splicing and regulates alternative splicing (Hong, Zang et al. 2010, Boeckel, Guarani et al. 2011, Heim, Grimm et al. 2014, Yi, Shen et al. 2016). For instance, during angiogenesis, Boeckel et al. demonstrated that silencing of *Jmjd6* impairs angiogenic functions of endothelial cells by modulating the splicing of the VEGF-receptor 1 (Flt1) (Boeckel, Guarani et al. 2011). Yi et al. reported that *Jmjd6* and U2AF65 regulate alternative splicing regardless of the enzymatic activity of *Jmjd6* (Yi,

Shen et al. 2016). Moreover, *Jmjd6* was also shown to regulate remote promoter-enhancer interaction to release RNA polymerase II. In this regulation, *Jmjd6* erases H4R3me2s, which is read by 7SK snRNA, on anti-pause enhancers after being recruited by Brd4. Demethylation of 7SK snRNA also ensures the dismissal of the 7SK snRNA/HEXIM inhibitory complex (Liu, Ma et al. 2013).

1.1.5 Protein arginine N-methyltransferase

Arginine methylation is a common post-translational modification. There are three types of methylarginine: ω-N^G-monomethylarginine (MMA), ω-N^G , N^G -asymmetric dimethylarginine(ADMA) and ω-N^G ,N^G -symmetric dimethylarginine(SDMA). A family with nine protein arginine N-methyltransferases (PRMTs) are responsible for arginine methylation. PRMTs transfer a methyl group from S-adenosylmethionine (AdoMet) to guanidino nitrogen of arginine resulting in S-adenosylhomocysteine (AdoHcy) and methylarginine. The nine PRMTs can be divided into three types, type I and type II PRMTs catalyze the production of an MMA intermediate. The type I PRMTs (PRMT1,2,3,4,6 and 8) further catalyze the formation of ADMA, while type II PRMTs (PRMT5 and 7) catalyze the formation of SDMA. PRMT7 belongs as well to type III as it only monomethylates specific substrates.

1.1.5.1 *Prmt6*

Prmt6 was identified as a histone methyltransferase in 2002 as a novel member of the PRMT family (Frankel, Yadav et al. 2002). In 2007, two independent groups showed that *Prmt6* is the major H3R2 methyltransferase in vivo or in vitro (Guccione, Bassi et al. 2007, Hyllus, Stein et al. 2007). Overexpression of *Prmt6* in MCF7 resulted in the elevated level of H3R2me2a. While knocking down *Prmt6* with siRNA in HEK293T resulted in a reduced level of H3R2me2a(Hyllus, Stein et al. 2007). In addition, *Prmt6* was also shown to methylate R29 at H2A(Waldmann, Izzo et al. 2011). H3R2me2a was found to be associated with the repression of transcription as it counteracts the formation of H3K4me3. In MCF7 cells stably overexpressing *PRMT6*, H3K4me3 was

decreased. On the contrary, the H3K4me3 level was elevated in the *PRMT6* knockdown cells. Future analysis showed that R2 methylation at H3 abolished the interaction of H3 with WDR5, which is the methyltransferase for H3K4me3(Hyllus, Stein et al. 2007). ChIP analysis of WDR5 and ASH2 in HL60 cells showed their negative correlation with H3R2me2a but positive correlation with H3K4me3(Guccione, Bassi et al. 2007). In budding yeast, H3R2me2a is enriched throughout all heterochromatic loci and inactive euchromatic genes and is mutually exclusive with the trimethylation of H3K4(Kirmizis, Santos-Rosa et al. 2007). A new study showed *PRMT6*-dependent H3R2 methylation results in a different outcome to gene expression depending on its building either at the promoter or the distal enhance regions (enhancer). In the promoter region, loss of H3R2me2a leads to elevated KMT2A binding and H3K4me3 deposition which result in increased target gene transcription. At the enhancer region, loss of H3R2me2a leads to reduced KMT2D binding and lower H3K4me1/H3K27ac which result in decreased transcription of associated genes (Bouchard, Sahu et al. 2018).

1.2 Objective

During the initial stages of embryogenesis, the coordinated regulation of diverse transcriptional programs is crucial and must be tightly regulated. Gastrulation is the first millstone during the development, which leads to the formation of the three germ layers. Deficient gastrulation leads to multiple organ development defects. The heart is the first organ formed in the early embryo. Sophisticated and tightly regulated transcription networks in cardiac progenitor cells are needed to form a functional heart. *Jmjd6* is expressed at all stages and in nearly all the organs, including the embryonic heart. Loss of function of *Jmjd6* results in perinatal lethality and multiple organ defects, including the heart during embryogenesis (Böse, Gruber et al. 2004). Various studies showed that *Jmjd6* has essential functions during embryogenesis (Böse, Gruber et al. 2004, Mitchell, Cvetanovic et al. 2006). However, the precise molecular mechanism remains largely unexplored. This work aims to 1) explore the effect of *Jmjd6* depletion in early developmental cell fate choices and cardiogenesis and 2) explore the underlying molecular mechanism.

1.3 Result

1.3.1 Loss of *Jmjd6* in mouse embryonic stem cells leads to impaired germ layer lineage choice

1.3.1.1 Generation of *Jmjd6* knockout mESC line

In order to study the role of *Jmjd6* during development, E14-Nxk2.5-EmGFP mouse embryonic stem cells (mESCs)(Wu, Fujiwara et al. 2006) were used, and *Jmjd6* knockout (*Jmjd6* KO) mESCs were generated with CRISPR/Cas9. Two guide RNAs (gRNAs) were used to delete the genomic region from exon1 to exon6 of *Jmjd6*. A forward primer together with two reverse primers were used to identify WT and *Jmjd6* KO clones (Figure 1.3.1A). In total, 46 clones were picked and genotyped. 19 (41.3%) clones showed a WT and KO band, and 20 (43.4%) clones showed only a KO band by PCR (Figure 1.3.1B). Three knockout clones were chosen to validate *Jmjd6* mRNA and protein expression. By qPCR and western blot, *Jmjd6* mRNA and protein are naturally absent compared with WT mESCs (Figure 1.3.1C and D).

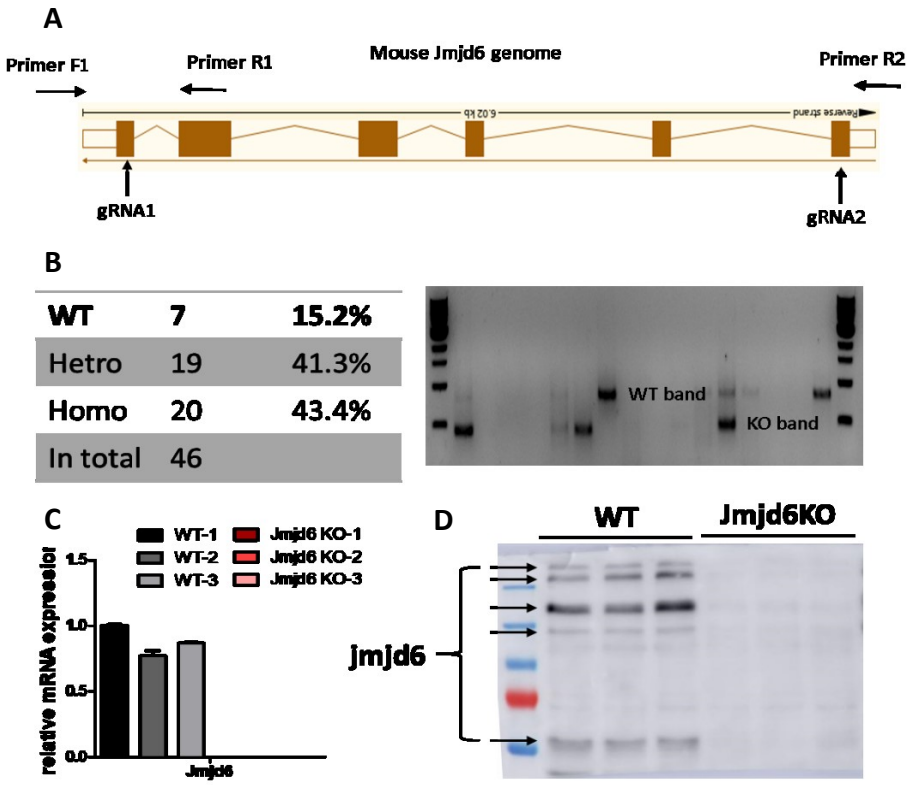

Figure 1.3.1. Generation of *Jmjd6* knock-out mESC line. (A) Two gRNAs were used to delete exon1 to exon6 of *Jmjd6*; primer F1 and R1 were used to amplify the WT band, and primer F1 and R2 were used to amplify the KO band. **(B)** Screen *Jmjd6* KO line with PCR. **(C)** Relative mRNA expression of *Jmjd6* in WT and *Jmjd6* KO mESC lines (n=4). **(D)** Western blot shows the protein expression of *JMJD6* in WT and *Jmjd6* KO mESC lines.

1.3.1.2 Loss of *Jmjd6* leads to upregulation of ectoderm gene expression and downregulation of endoderm and mesoderm gene expression

To evaluate *Jmjd6* function in embryonic differentiation, handing drop method was utilized. mESCs were hanged on the Petri dish lid with a concentration of 33,000/ml. Cultured mESCs in the drop will form complex embryoid bodies (EBs) with endoderm, mesoderm, and ectoderm germ layers. With further differentiation, EBs can develop to the progenitor stage at day 5, including cardiac progenitor cells (CPC), and finally, the beating EBs with cardiomyocyte at day 9 (Doetschman, Eistetter et al. 1985, Wobus, Wallukat et al. 1991, Maltsev, Rohwedel et al. 1993). By taking advantage of the E14-Nkx2.5-eGFP mESC line, the cardiac progenitor cells could be sorted by GFP signal with FACS (Figure 1.3.2A).

Gastrulation, a critical step in development, gives rise to mesoderm, endoderm, and ectoderm. To evaluate *Jmjd6* function in gastrulation, I first analyzed gene expression of different germ layers in D4 EBs derived from WT and *Jmjd6* KO mESCs using RT-qPCR. Mesodermal markers such as *Cer1*, *Brachyury*, *Eomes*, *Foxa2*, *Mesp1,* and *Mesp2* were strongly decreased. Endoderm maker genes like *Gata4*, *Gata6, and Sox17* were also downregulated. However, ectoderm marker genes like *Sox1*, *Pax2*, *Pax6,* and *Gbx2* were strongly upregulated (Figure 1.3.2B). The immunostaining of pluripotency marker *Oct4* showed no difference between control and *Jmjd6* KO mESCs (Figure 1.3.2C), indicating loss of *Jmjd6* impairs gastrulation during the differentiation but not the pluripotency at early stages. To sum up, *Jmjd6* ablation in mESCs results in increased expression of ectodermal genes and decreased expression of endodermal and mesodermal genes.

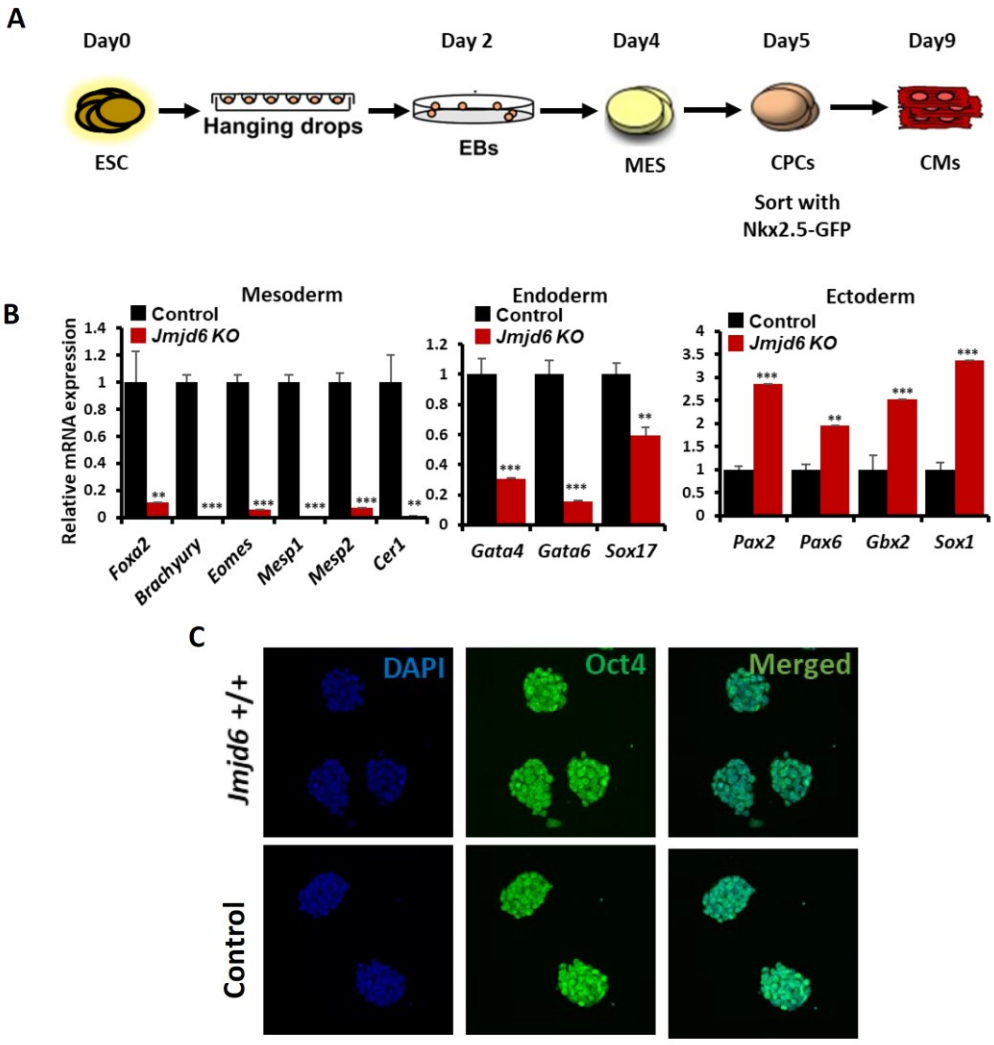

Figure 1.3.2. Loss of *Jmjd6* leads to impaired germ layers marker gene but not stem cell pluripotency gene expression. (A) Schematic representation of hanging drop differentiation. **(B)** Relative mRNA expression of marker genes for mesoderm, endoderm, and ectoderm in D4 EBs derived from control and *Jmjd6* KO mESCs (n=4). **(C)** Immunostaining for pluripotency marker Oct4 and DAPI (nuclei) in control and *Jmjd6* KO mESCs.

To systematically evaluate the function of *Jmjd6* on germ layer lineage choices, D0, D2, D3, and D4 EBs derived from control and *Jmjd6* KO mESCs were harvested and sent for RNA-sequencing. Compare analysis revealed that the most dramatic dysregulation of genes happened in D4 EBs, in which 927 genes were downregulated, and 919 genes were upregulated (Figure 1.3.3A). Gene ontology (GO) analysis was then performed for downregulation and upregulation genes in *Jmjd6* KO D4 EBs. The top GO terms of downregulation genes are highly enriched for pattern specification process,

gastrulation, and cell fate commitment (Figure 1.3.3B). In comparison, the GO terms of upregulated genes were linked to synapse organization and axonogenesis, essential processes in neuron development (Figure 1.3.3C). Genes set enrichment analysis (GSEA) of GO term gastrulation showed that depletion of *Jmjd6* impairs gastrulation as differentiation develops (Figure 1.3.3D, E and F). The GO terms enriched in both downregulated and upregulated genes imply imbalanced gastrulation in *Jmjd6* KO cells, suggesting *Jmjd6* plays a crucial role in early lineage choice during embryogenesis.

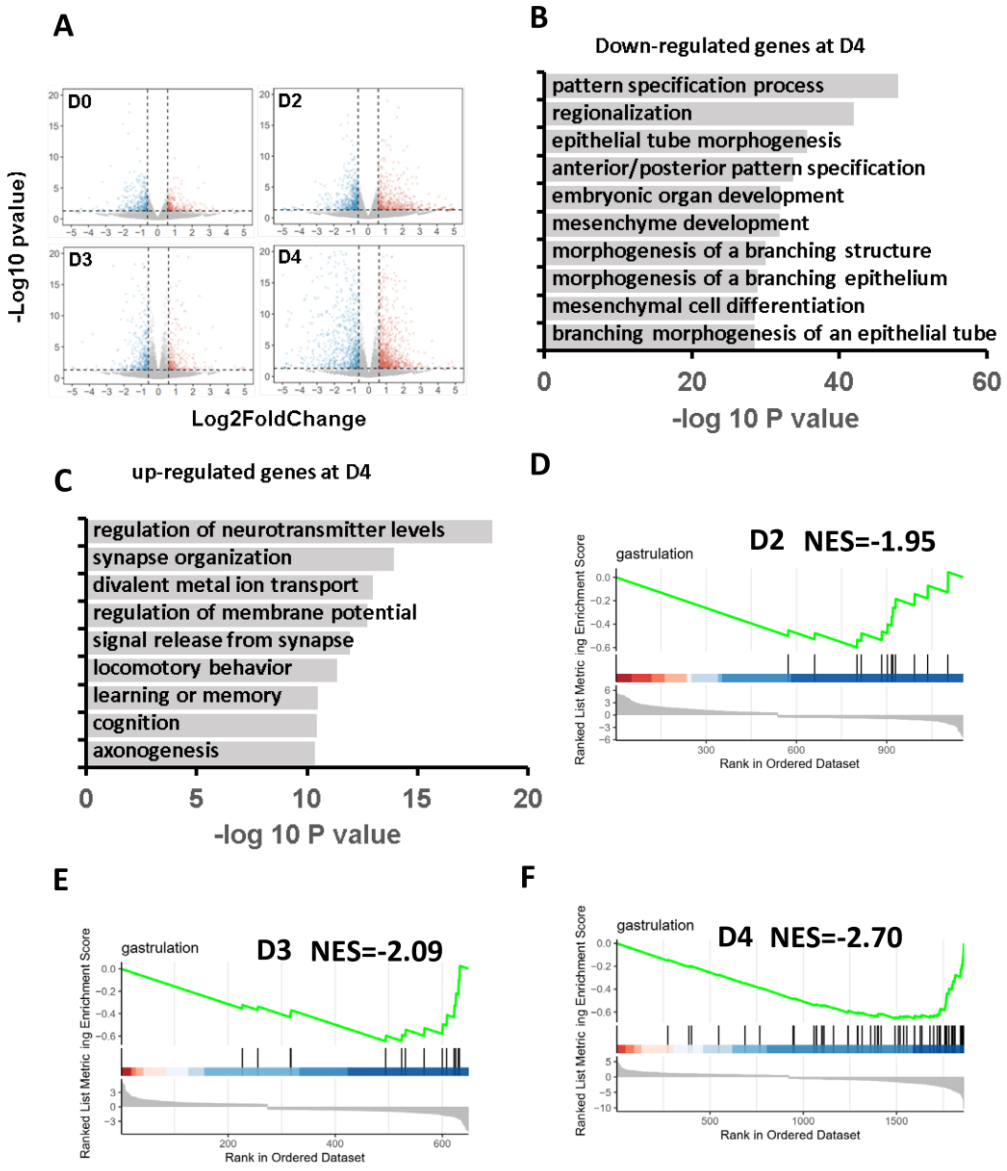

Figure 1.3.3. RNA-sequencing reveals imbalanced early lineage gene expression upon *Jmjd6* knockout. (A) Volcano plot of RNA-Seq data of D0, D2, D3 and D4 EBs derived from control and *Jmjd6* KO mESC (n=2) (fold change > 1.5; log2 fold change <

-0.58, > 0.58; p-value < 0.05). **(B and C)** Representative GO terms for downregulated genes **(B)** and upregulated genes **(C)** of D4 EBs derived from control and *Jmjd6* KO mESC. **(D, E and F)** GSEA plots of GO term gastrulation at D2 EBs **(D)**, D3 EBs **(E)** and D4 EBs **(F)**.

To analyze the transcriptome dynamics during mESCs differentiation, I performed cluster analysis with genes showing dysregulation (Log2FC < -0.58 or Log2FC > 0.58) in at least one stage. The dysregulated genes from all four days were clustered by K-MEAN clustering into six clusters with a custom script in R (Figure 1.3.4A). Among all clusters, cluster 5 drew my attention as it showed consistent downregulation from D2 to D4. Along with the differentiation, this downregulation in cluster 5 became more and more significant. In D4 EBs, those genes showed the most significant downregulation (Figure 1.3.4A). To understand the biological meaning of those clusters, I performed a GO analysis. Interestingly, GO terms of cluster 5 genes were mainly enriched to the pattern specification process, and cell fate commitment, similar to the top GO terms of downregulation genes in D4 (Figure 1.3.4B). Conversely, cluster 4 showed similar upregulation to the analysis in D4, which was enriched in GO terms like synapse organization which is highly relevant to neuron differentiation (Figure 1.3.5B). In summary, cluster analysis supported our RT-qPCR data showing that *Jmjd6* regulates early lineage choice. Without *Jmjd6*, mESCs differentiate more to ectoderm lineage but not to the mesoderm or endoderm lineage. The imbalanced germ layer formation may explain the multiple organ development defects in *Jmjd6*KO embryos, such as the deformed head and impaired heart, which derives from the mesoderm germ layer.

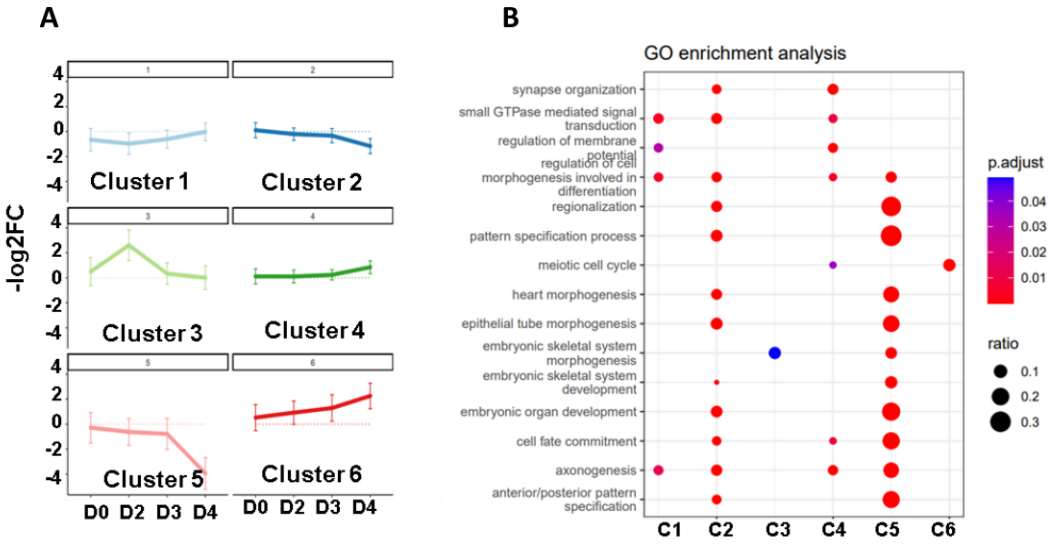

Figure 1.3.4. *Jmjd6* regulates early lineage choice. (A) K-MEAN clusters of dysregulated genes in D0, D2, D3, and D4 EBs. **(B)** Dot-plot of GO terms enriched in clusters from 1.3.4A.

Single-cell sequencing has been used for identifying the sub-population during embryonic development in a high resolution. Recently, Mittnenzweig et al. reported a single-cell time-resolved model for mouse gastrulation by performing single-cell RNA-seq using embryos spanning from E6.5 to E8.1 (Mittnenzweig, Mayshar et al. 2021). They identified 29 different cell populations during the gastrulation (Figure 1.3.5A). By comparing the relative gene expression among all 29 populations, the top 100 relative highly expressed marker genes for each population were identified. The fold change of those genes in D4 EBs derived from control and *Jmjd6* KO mESCs was plotted (Figure 1.3.5B). Epiblast, the earliest cell cluster during gastrulation, will further develop into the definitive ectoderm and the primitive streak (PS), giving rise to mesoderm and endoderm lineages. *Jmjd6* knockout EBs showed upregulated expression of the epiblast, primitive streak, rostral neural plate, definitive ectoderm, and caudal neural plate marker gene. The last four populations all belong to the ectoderm. Except for the surface ectoderm, which showed both upregulation and downregulation of marker genes expression, marker genes of all sub-populations of ectoderm are upregulated (Figure 1.3.5B). However, marker genes expression of the endoderm and mesoderm subpopulation, including caudal mesoderm, paraxial mesoderm, cardiac mesoderm, rostral mesoderm, late nascent mesoderm, late intermediate mesoderm,

early nascent mesoderm, visceral endoderm, and definitive endoderm, were downregulated upon *Jmjd6* knockout (Figure 1.3.5B). In summary, *Jmjd6* knockout promoted ectoderm formation but impaired the mesoderm and endoderm formation.

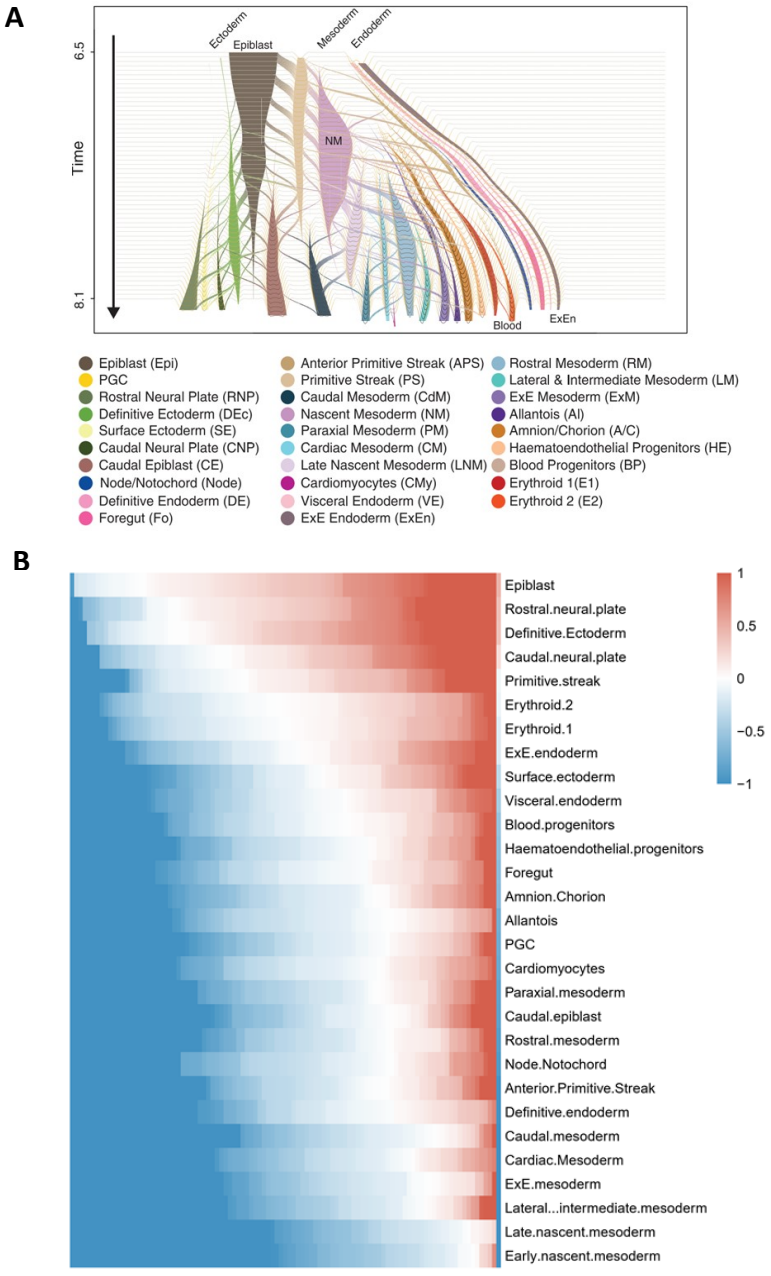

Figure 1.3.5. *Jmjd6* knockout leads to dysregulated gene expression in subpopulations during the gastrulation. (A) Complete flow model showing all cell types and major predicted transitions during gastrulation (Mittnenzweig, Mayshar et al. 2021). **(B)**, Maker genes expression of different subpopulations upon *Jmjd6* knockout in D4 EBs.

1.3.2 Loss of *Jmjd6* in mouse embryonic stem cells leads to the imbalance of H3K27me3 and H3K4me3 at the bivalent promoter of gastrulation genes

1.3.2.1 Downregulated gastrulation genes upon *Jmjd6* knockout are marked by the bivalent domain

Many genes that play an essential role in development are marked by bivalent domains, which contain active and repressive histone modifications like H3K4me3 and H3K27me3 on their promoter region (Bernstein, Mikkelsen et al. 2006, Zhao, Han et al. 2007, Blanco, González-Ramírez et al. 2020). As many dysregulated genes upon *Jmjd6* knockout are developmental genes, which encouraged me to look into whether those dysregulated genes are markered by bivalent domains or not. I took the published H3K4me3 and H3K27me3 ChIP-seq data at different stages of cardiomyocyte differentiation (Wamstad, Alexander et al. 2012). After calling peaks from H3K4me3 and H3K27me3 ChIP-seq data at different stages, I identified 5050, 4704, and 4687 genes marked by both H3K4me3 and H3K27me3 in ESC, MES, and CPC. To assess the percentage of bivalent genes in each cluster (Figure 1.3.4A), I overlapped genes from each cluster and bivalent genes at the MES stage. The bivalent domain marks about 50% of genes in cluster 4 and cluster 5, while only around 20% of genes are marked by the bivalent domain in other clusters (Figure 1.3.6). The analysis highlighted the significance of the bivalent domain on gene expression for genes in clusters 4 and 5, which encouraged me to study the bivalent domain dynamics during mESCs differentiation.

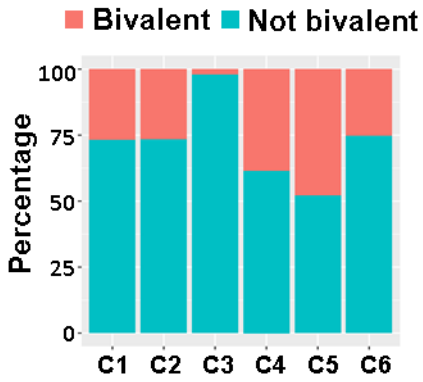

Figure 1.3.6. Percentage of the bivalent gene in each cluster. Bivalent genes at the MES stage were overlapped with genes in each cluster from 1.3.4A.

1.3.3.2 Both active and repressive histone markers on the promoter region of gastrulation genes are dysregulated in MES

To gain insights into the bivalent domain dynamics in the early lineage choice, chromatin from D0, D2, D3, and D4 EBs derived from control and *Jmjd6* KO mESCs were collected for ChIP-seq of H3K4me3 and H3K27me3 (Figure 1.3.7A, Figure 1.3.8A). The TSS profile plot of H3K27me3 ChIP-seq of all four days showed no or very subtle changes genome-wide (Figure 1.3.7B). Then I plot the TSS profile plot of H3K27me3 ChIP-seq for all 6 clusters from Figure 1.3.4A. Interestingly, the average H3K27me3 enrichment for cluster 5 genes is significantly higher in *Jmjd6* KO cells than WT cells at D4 but not in earlier stages (Figure 1.3.7C). Consistent with the higher H3K27me3 accumulation, the gene of cluster 5 is significantly lower expressed in *Jmjd6* knockout cells (Figure 1.3.4A). In contrast, H3K27me3 enrichment for other clusters has no apparent change. Given that genes in cluster 5 are all relevant to early lineage choice, those data indicate that loss of *Jmjd6* leads to higher H3K27me3 accumulation at the bivalent domain of early lineage choice genes, which contributes to the imbalanced gastrulation.

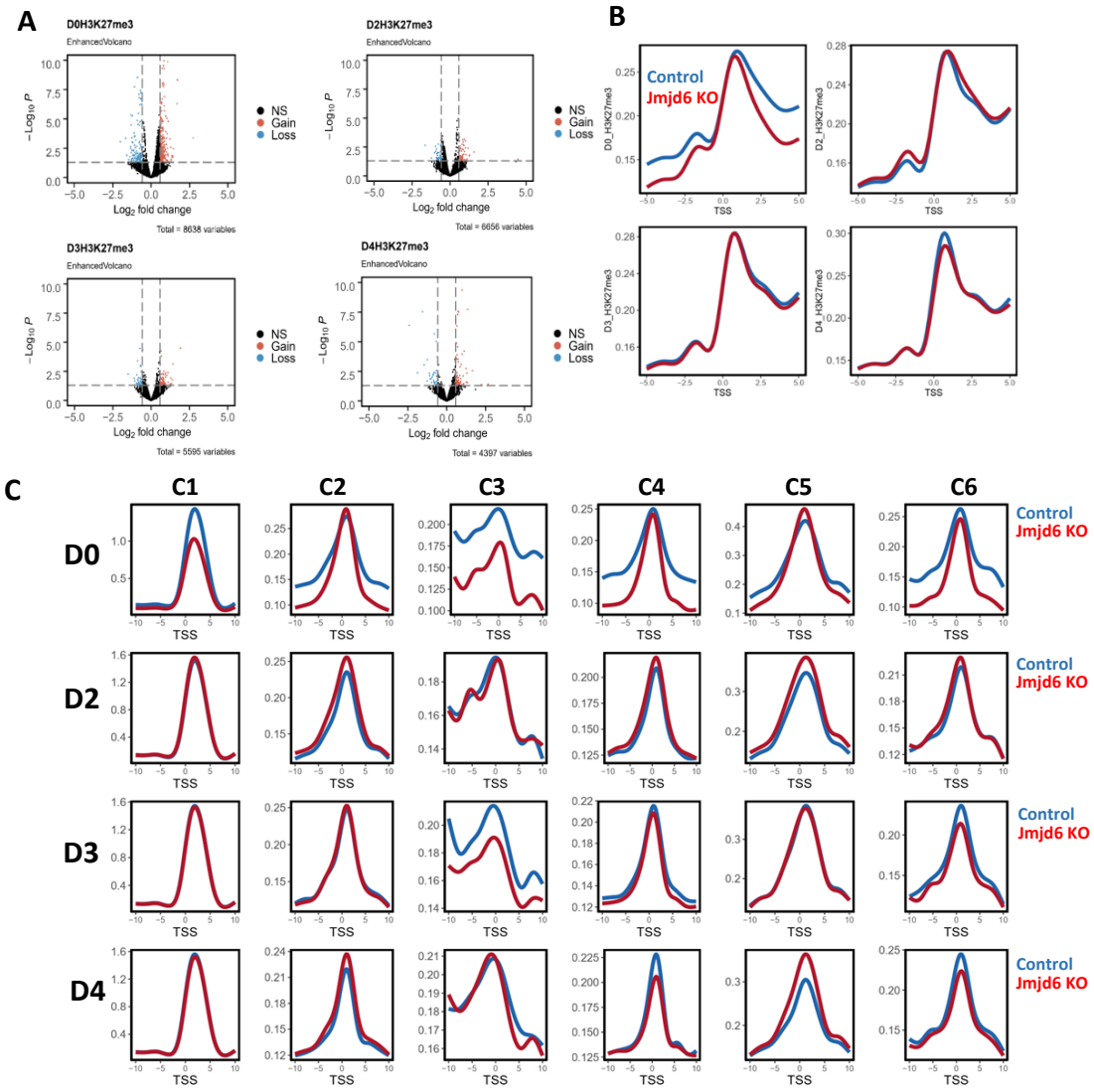

Figure 1.3.7. Loss of *Jmjd6* leads to increased H3K27me3 at gene cluster related to gastrulation. (A) Volcano plot of H3K27me3 ChIP-seq from D0 to D4 (n=2). **(B)** TSS profile plot of H3K27me3 genome-wide from D0 to D4. **(C)** TSS profile plot of H3K27me3 for each cluster from D0 to D4.

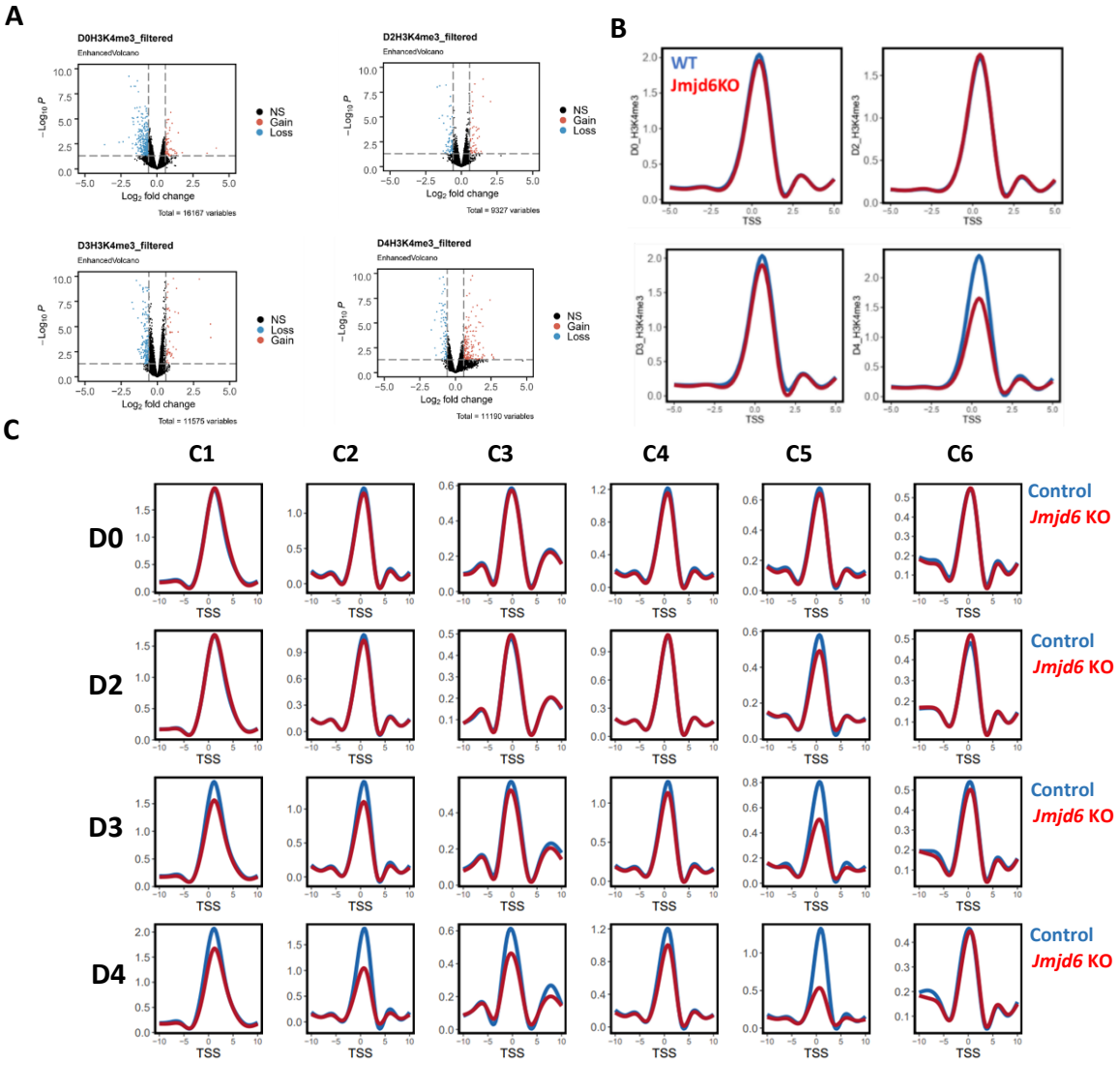

Figure 1.3.8. Loss of *Jmjd6* leads to decreased H3K4me3 at gene cluster related to gastrulation. (A) Volcano plot of H3K4me3 ChIP-seq from D0 to D4 (n=2). **(B)** TSS profile plot of H3K4me3 genome-wide from D0 to D4. **(C)** TSS profile plot of H3K4me3 for each cluster from D0 to D4.

I then performed H3K4me3 ChIP-seq for D0 to D4 EBs derived from WT and *Jmjd6* KO mESCs (Figure 1.3.8A). Surprisingly, the TSS profile plot of H3K4me3 ChIP-seq of genome-wide shows significant downregulation of H3K4me3 accumulation at D4 but not in D0, D2, or D3 genome-wide. (Figure 1.3.8B).

I then performed the TSS profile plot of H3K4me3 ChIP for all 6 clusters I obtained

from RNA-seq data. Remarkably, the average H3K4cme3 enrichment for cluster 5 was significantly lower in *Jmjd6* KO cells compared to WT cells at D4, whereas cluster 2, for example, did not show any change (Figure 1.3.8C). Those data indicate that loss of *Jmjd6* leads to lower H3K4me3 at the bivalent domain of early lineage choice genes, which contributes to the downregulation of these genes.

In summary, loss of *Jmjd6* leads to the most dysregulated genes at D4 instead of early days of differentiation, indicating that *Jmjd6* may play a more critical role in early lineage choice decision rather than embryonic stem cell self-renewal or pluripotency maintenance. By clustering the dysregulated genes in all stages, I observed the dynamic change of these dysregulated genes. Among all the clusters, I found that cluster 5 is linked to gastrulation, cell fate commitment, and mesoderm development which are all processes relevant to the early lineage choice decision. Notably, genes in cluster 5 are significantly downregulated in D4 EBs derived from *Jmjd6* KO mESCs when lineage specification genes should be induced to a high expression level. By analyzing the genome-wide profile of H3K4me3 and H3K27me3 binding at promotes for cluster 5 genes, I showed the higher H3K27me3 and the lower H3K4me3 accumulation in the TSS region. Some examples of downregulated gastrulation genes with dysregulated bivalent domain resolution upon *Jmjd6* knockout are shown (Figure 1.3.9). In line with the increased repressive histone modification and decreased active histone modification, genes in cluster 5 were dramatically downregulated in D4 EBs derived from *Jmjd6* KO mESCs. In conclusion, *Jmjd6* plays a vital role in early lineage choices by balancing the bivalent domain.

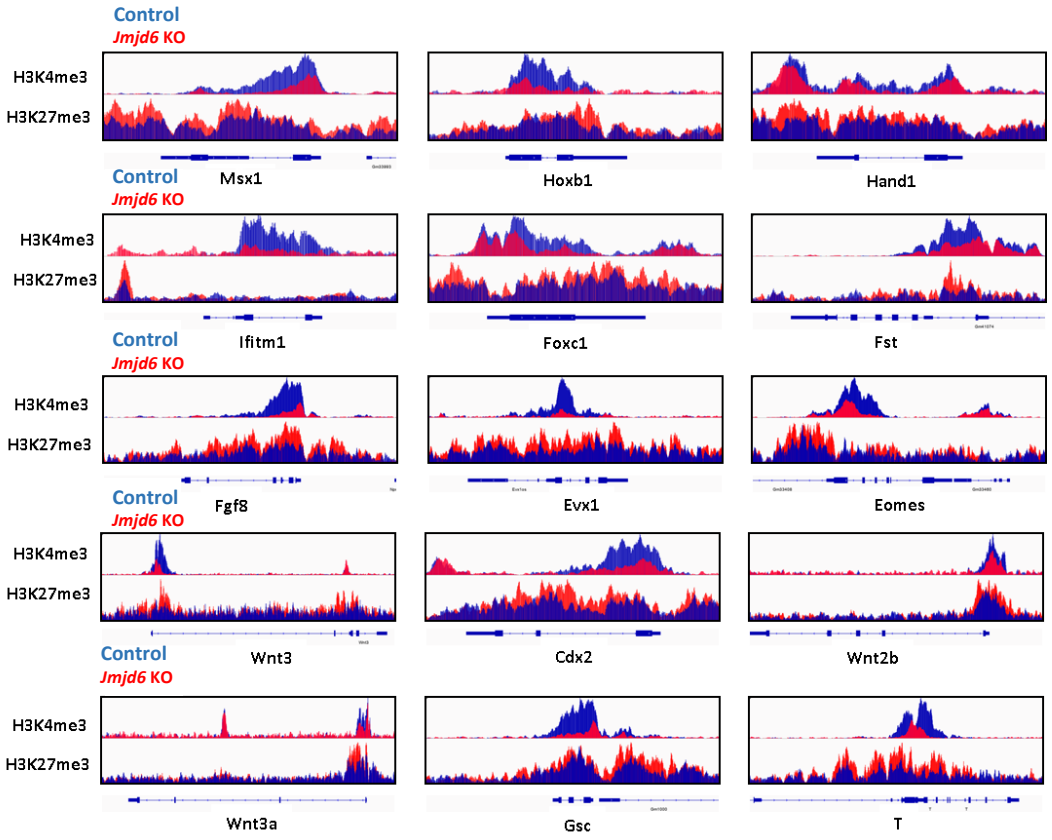

Figure 1.3.9. Examples of genes in cluster 5 with dysregulated bivalent domain in *Jmjd6* KO MES cells, showing genome tracks of H3K4me3 and H3K27me3 ChIP-Seq.

1.3.3 Loss of *Jmjd6* blocks cardiac progenitor cell differentiation

1.3.3.1 Loss of *Jmjd6* leads to downregulation of many heart developmental genes in CPCs

To study the role of *Jmjd6* in later stages during development, I first analyzed its role in cardiovascular differentiation. During hanging drop differentiation, mesodermal marker genes peaked at D4, and cardiac progenitor cell (CPC) markers peaked at D5. From D8, functional cardiomyocytes start to form, making the EBs beat. As I have shown that *Jmjd6* knockout impaired mesoderm marker gene expression, I then checked whether the cell number of the cardiac mesoderm population was affected or not by FACS. Although the marker genes for mesoderm were downregulated, the cardiac mesoderm population is not changed, which is indicated by the same percentage of *Flk1* and *PdgfRa* double-positive cells in control and *Jmjd6* knockout D4 EBs (Figure 1.3.10A). Next, I analyzed the expression of CPC marker genes and the CPC population in D5 EBs by RT-qPCR and FACS. A group of genes, including growth factor and transcript factor, which play a crucial role in cardiogenesis, was down-regulated in EBs differentiated from *Jmjd6* KO mESCs (Figure 1.3.10C). Although the CPC marker genes were downregulated in vivo and in vitro, the CPC population increased during the in vitro differentiation measured by the *Nkx2.5*-GFP cell population (Figure 1.3.10B). I reasoned that impaired CPCs were blocked at the cardiac progenitor cell stage due to the downregulation of many critical genes supporting the further differentiation to cardiomyocytes.

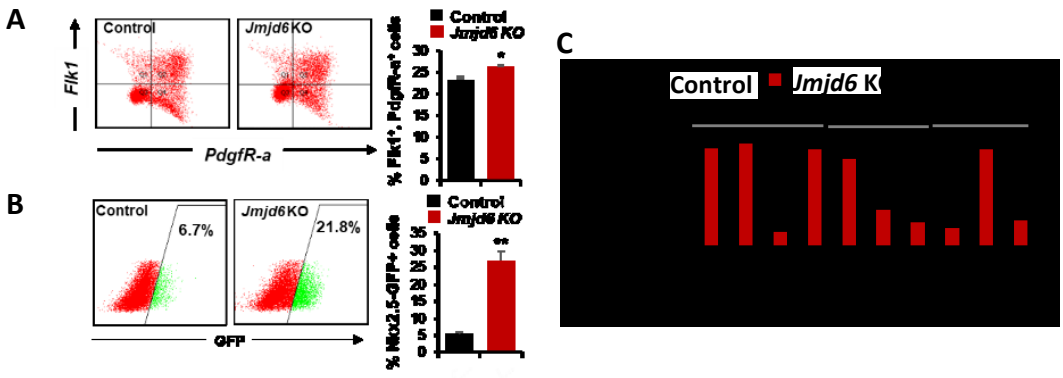

Figure 1.3.10. Loss of *Jmjd6* blocks cardiac progenitor cells from further differentiation. (A) FACS analysis of cardiac mesoderm population in D4 EBs derived from control and *Jmjd6* KO mESCs (left) and quantification of Flk1+,Pdgfra+ cells (right) (n=3). **(B)** FACS analysis of cardiac progenitor population in D4 EBs derived from control and *Jmjd6* KO mESCs (left) and quantification of Nkx2.5-GFP+ cells (right) (n=3). **(C)** CPC marker gene expression in D5 EBs differentiated from control and *Jmjd6* KO mESCs (n=4).

Given that many critical genes for heart development were downregulated in CPCs, I then performed an RNA-seq for CPCs to evaluate transcriptome changes in cardiac CPCs upon *Jmjd6* knockout systemically. CPCs were sorted with FACS on day 5 of ESC differentiation by handing drop method followed by RNA isolation and sequencing. I identified 1428 upregulated genes and 1953 downregulated genes (fold change > 1.5; log2 fold change < -0.58, > 0.58; p-value < 0.05) (Figure 1.3.11A). GO analysis of downregulated genes shows GO terms linked to heart development, cardiac right ventricle formation, and cardiac muscle cell proliferation. In contrast, GO analysis of upregulated genes showed enrichment of GO terms linked to anterior/posterior specification and skeletal system development (Figure 1.3.11B).

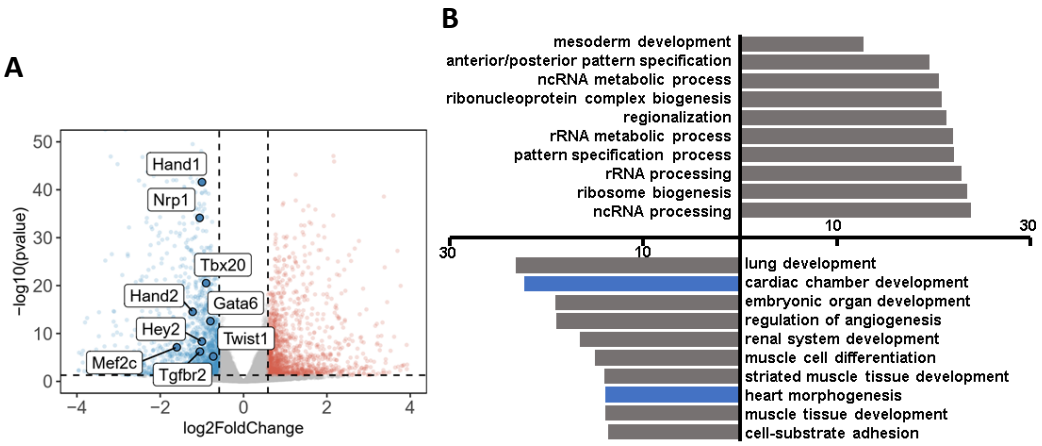

Figure 1.3.11. Loss of *Jmjd6* leads to downregulation of many heart developmental genes in CPCs. (A) Volcano plot of RNA-seq analysis of FACS-sorted Nkx2-5^{+} CPCs derived from control and *Jmjd6* KO mESCs (n=2; fold change > 1.5; log2 fold change < -0.58, > 0.58; *p*-value < 0.05). **(B)** GO term enriched in significant dysregulated genes upon *Jmjd6* knockout in CPC.

1.3.3.2 Cluster analysis showed that the downregulation of heart morphogenesis genes begins at the MES stage but mainly happens at the CPC stage

I next analyzed the expression dynamics between key steps of cardiogenesis: ESC, MES, and CPC stages. Six clusters were observed using K-MEAN clustering (Figure 1.3.12A). From the GO analysis, four clusters were relevant to heart morphogenesis: cluster 1, cluster 2, cluster 3, and cluster 4 (Figure 1.3.12B). All four cluster shows either downregulation in MES or CPC but not in the ESC stage (Figure 1.3.12A). The genes in cluster 2 are downregulated at MES slightly but upregulated again in CPC. Genes in clusters 1, 3, and 4 are significantly downregulated in MES or CPC. Thus, I focused on clusters 1, 3, and 4 for the following study and analysis.

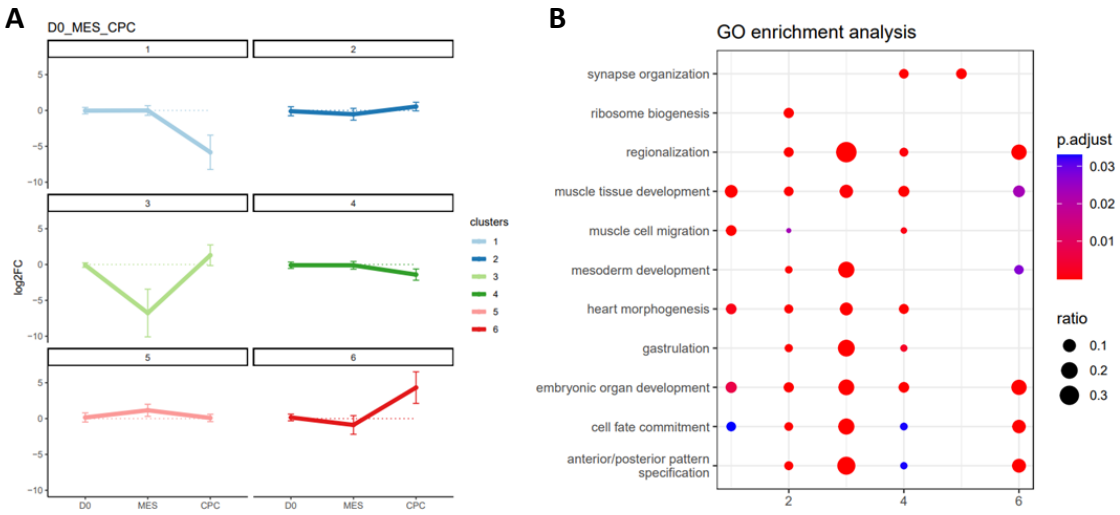

Figure 1.3.12. *Jmjd6* regulates cardiac development. (A) K-MEAN clusters of dysregulated genes in ESC, MES, and CPC. **(B)** Dot-plot of GO terms enriched in each cluster from (A).

Many essential heart development genes are transiently induced in MES or CPC stages. The proper induction of these genes is vital for cardiac development. To understand in better detail the transcription factors alternations in *Jmjd6* KO CPCs, I plotted the RPKM expression of clusters 1 to 4 at all three time points for WT and *Jmjd6* KO cells (Figure 1.3.13). In the WT situation, genes in cluster 1 and cluster 4 are only highly expressed in CPC, and genes in cluster 3 are transiently expressed in MES, consistent with the gastrulation gene expression pattern (Mitiku and Baker 2007). Genes in cluster 2 are highly expressed in mESCs. They showed a decrease at the mesodermal

stage but caught up at the CPC stage. These data indicate that *Jmjd6* impairs the induction of cardiac-specific gene expression in the MES and CPC stage. In cluster 1, I found growth factor receptors like *Acvrl1*, ligands like *Slit2*, *Angpt1*, and extracellular matrix genes like *Flrt2* and *Fat4*. In cluster 3, I found *Mesp1*, *Mesp2*, and *T*, which are essential for cardiac progenitor cell formation. In cluster 4, I found transcript factors like *Hand1*, *Hand2*, *Gata5*, *Gata6*, and *Tbx20*; ligands and receptors such as Bmp2 and Bmpr2; extracellular matrix genes like Col11a1, Col5a1, and Dchs1.

Overall, the data suggest that *Jmjd6* plays a vital role in inducing early cardiac mesodermal and cardiac progenitor gene expression.

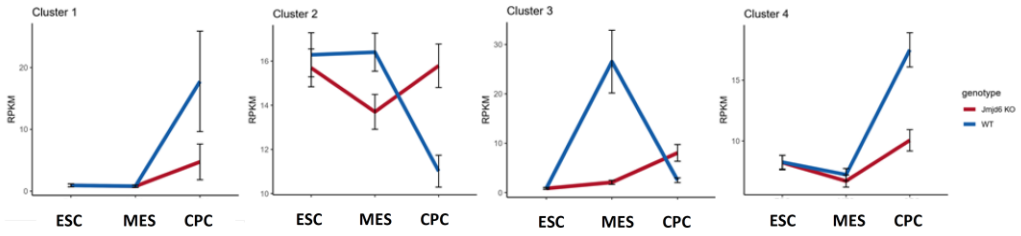

Figure 1.3.13. Average RPKM expression for genes from clusters 1, 2, 3, and 4 at three time points in WT and *Jmjd6* KO cells. Average gene expression of clusters 1, 2, 3, and 4 in WT and *Jmjd6* knockout cells at ESC, MES, and CPC stages were plotted.

1.3.3.3 Loss of *Jmjd6* results in defective cardiomyocyte in vitro

At last, I analyzed the cardiomyocyte formation upon *Jmjd6* knockout in vitro. Compared to the EBs derived from control mESCs in which 80 percent of EBs were beating strongly, the EBs derived from *Jmjd6* KO mESCs showed almost no beating (Figure 1.3.14A). I then analyzed the mRNA expression of essential cardiomyocyte marker genes *Mlc2a*, *Mlc2v*, *Tnnt2,* and *Ttn* in D9 EBs by qPCR. Consistent with barely beating EBs, expression of all four genes was dramatically decreased in EBs derived from *Jmjd6* KO mESCs (Figure 1.3.14B). I also analyzed marker genes for endothelial cells and smooth muscle cells, also derived from cardiac progenitor cells. Consistent with the impaired CPC, the marker genes for those two lineages were also significantly down-regulated (Figure 1.3.14B). I further analyzed the percentage of cardiomyocyte

and endothelial cell population in D10 EBs by FACS. As expected, both cell populations were decreased in D10 EBs (Figure 1.3.14C and D). Immunostaining for MF20 and Troponin I in cardiomyocytes derived from D10 EBs and cardiomyocytes isolated from E15.5 embryo revealed decreased expression of cardiac myosins and less sarcomere structures upon *Jmjd6* knockout (Figure 1.3.14E). In conclusion, knocking out *Jmjd6* restrains CPC from differentiating to cardiomyocyte, endothelial, and smooth muscle cells.

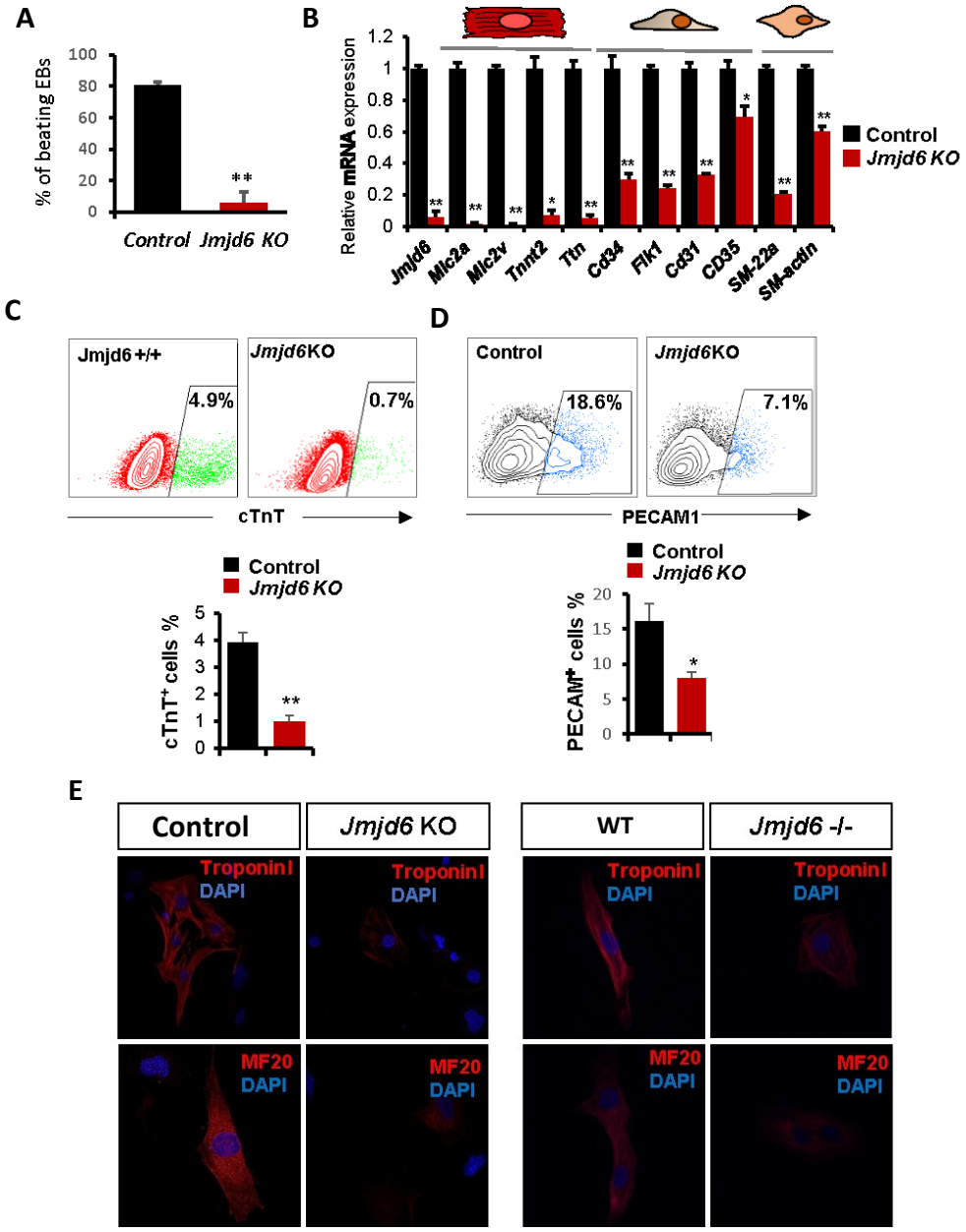

Figure 1.3.14. Ablation of *Jmjd6* results in defects in cardiac progenitor cell and cardiomyocyte differentiation. (A) Percentage of beating EBs in cardiomyocytes derived from control and *Jmjd6* KO mESCs (n=2). **(B)** Relative mRNA expression of cardiac progenitor cell marker genes in D5 EBs differentiated from control and *Jmjd6* KO mESCs (n=4). **(C)** FACS analysis of cTnT expression in D9 EBs differentiated from control and *Jmjd6* KO mESCs(up) and quantification of FACS result (n=3) (down). **(D)** FACS analysis of PECAM1 expression in D9 EBs differentiated from control and *Jmjd6* KO mESCs(up) and quantification of FACS result (n=3) (down). **(E)** Immunostaining for Troponin and MF20 in D10 cardiomyocyte derived from control and *Jmjd6* KO mESCs (left) and isolated E15.5 cardiomyocyte from WT and *Jmjd6*-/- embryos (right).

1.3.4 Loss of *Jmjd6* leads to the imbalance of H3K27me3 and H3K4me3 at the bivalent promoters of heart morphogenesis genes

Similar to the MES stage, many genes that play a role in development were significantly dysregulated in CPCs upon *Jmjd6* knockout. To check whether the bivalent domain marks those genes, I plotted the TSS profile of H3K27me3 and H3K4me3 signals from published data for dysregulated and no changed genes in CPCs upon *Jmjd6* knockout. The accumulation of H3K4me3 on dysregulated genes was significantly high, although a higher level of H3K4me3 was found on no changed genes. There was almost no accumulation of H3K27me3 on the no changed genes, but there was a significantly high level of H3K27me3 deposited on dysregulated genes (Figure 1.3.15A). The dysregulated genes upon *Jmjd6* knockout were marked by bivalent domain, whereas the no changed genes were only marked by H3K4me3, implying *Jmjd6* may regulate gene expression by affecting the resolution of the bivalent domain on those genes. As the downregulated genes were related to heart development, I focused on the downregulated genes in the following analysis.

First, I overlapped the downregulated gene list with the bivalent gene list in the CPC stage. It turns out that 35% of genes were marked by the bivalent domain (Figure 1.3.15B). GO terms enriched in those genes were linked to organ development such as lung, kidney, and heart development (Figure 1.3.15C). Next, I performed ChIP-seq of H3K27me3 and H3K4me3 of CPCs derived from control and *Jmjd6* knockout mESCs. By the volcano plot, I found many peaks with dysregulated H3K27me3 and H3K4me3 upon *Jmjd6* knockout (Figure 1.3.15E). The H3K27me3 signal on the promoter was increased while the H3K4me3 signal on the promoter was decreased genome-wide (Figure 1.3.15F). I also plot H3K4me3 and H3K27me3 signals on the promoter of that 35% downregulated genes, which are marked with the bivalent domain. The active histone maker H3K4me3 was decreased while the repress histone marker H3K27me3 was increased (Figure 1.3.15D). Examples of downregulated heart development genes with dysregulated bivalent domain resolution upon *Jmjd6* knockout are shown (Figure 1.3.16).

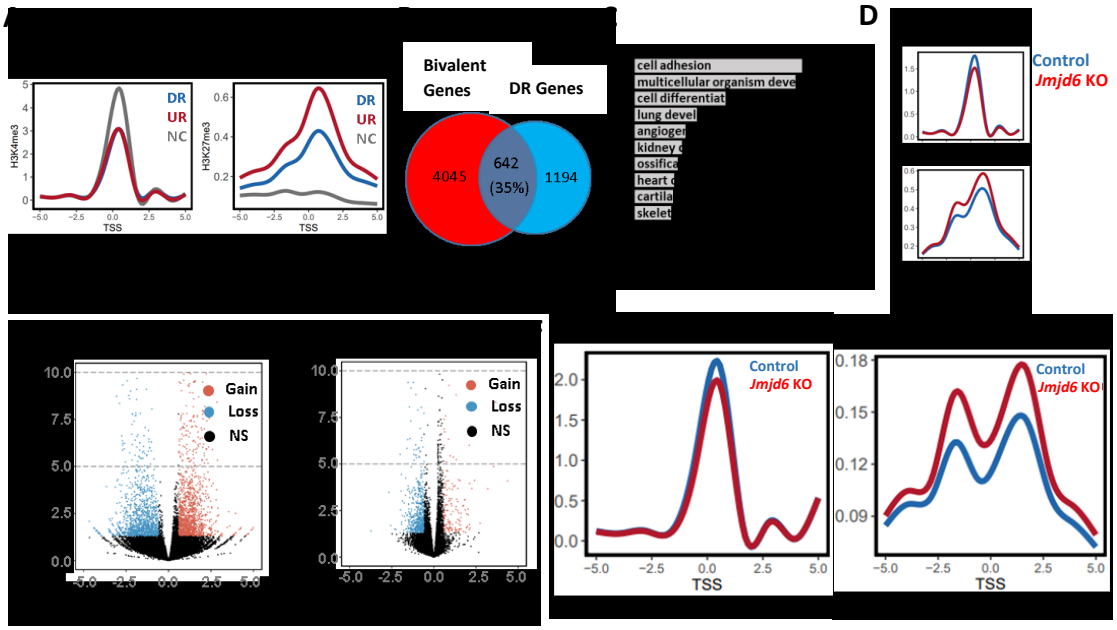

Figure 1.3.15.Loss of *Jmjd6* leads to increased H3K27me3 and decreased H3K4me3 at heart developmental genes. (A) TSS profile plot of H3K4me3 (left) and H3K27me3 (right) for upregulated, downregulated, and non changed genes in *Jmjd6* KO CPCs. **(B)** Overlap between bivalent genes and downregulated genes in *Jmjd6* KO CPCs. **(C)** GO terms enriched in overlapped genes from (C). **(D)** TSS profile plot of H3K4me3 (left) and H3K27me3 (right) for overlapped genes from (C). **(E)** Volcano plot of ChIP-seq for H3K27me3 (left) and H3K4me3 (right) (n=2; fold change > 1.5; log2 fold change < -0.58, > 0.58; *p*-value < 0.05). **(F)** TSS profile plot of H3K27me3 (left) and H3K4me3 (right) genome-wide.

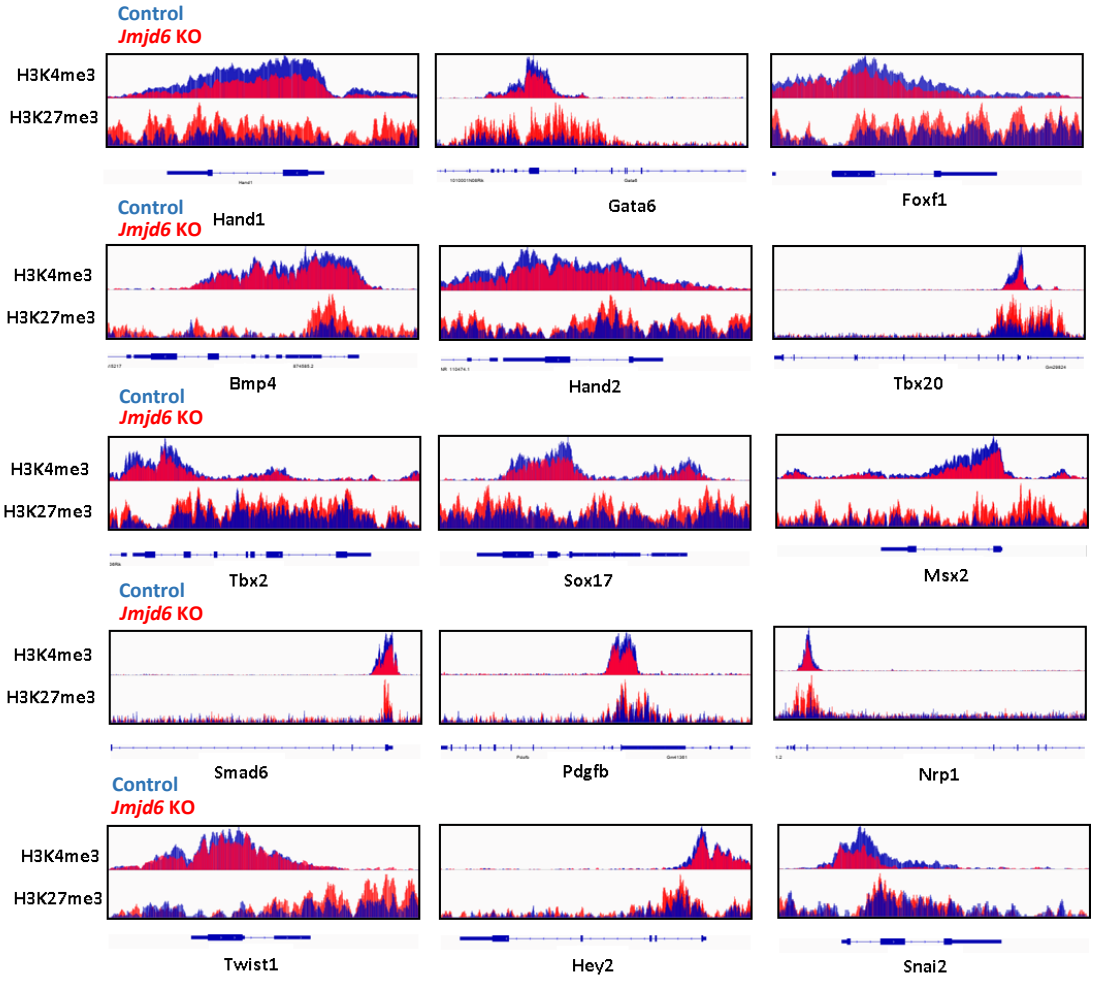

Figure 1.3.16. Examples of genes with dysregulated bivalent domain in *Jmjd6* KO CPC, showing genome tracks of H3K4me3 and H3K27me3 ChIP-Seq.

1.3.5 *Jmjd6* knockout embryos

1.3.5.1 *Jmjd6* knockout embryos showed development arrest and the cardiac defect

To study the function of *Jmjd6* in embryonic development, including heart formation in vivo, a *Jmjd6* knock-out mouse was used, in which a cassette including SV40 polyA was inserted between exon2 and exon3 (Figure 1.3.17A). While the *Jmjd6* heterozygous mutants are healthy and fertile, the homozygous mutants are lethal. *Jmjd6*+/- was then crossed with *Jmjd6* +/- to obtain WT and *Jmjd6*-/- embryos. *Jmjd6*-/- embryos showed development arrest from E9.5 with a significantly smaller size than WT embryos (Figure 1.3.17B). Nevertheless, I did not find any obvious phenotype before E8.5. Interestingly, *Jmjd6*-/- embryos showed wide body size and morphology variation. After E9.5, some embryos showed significantly smaller body sizes and deformed heads; others showed relatively standard body size and normal head morphology. To rule out the possibility of inefficient gene ablation in the *Jmjd6*-/- embryos that showed a less pronounced phenotype, I checked *Jmjd6* mRNA expression with RT-qPCR targeting exon4 and exon5, which should not be expressed in *Jmjd6*-/- embryos. In all *Jmjd6*-/- embryos, no expression of *Jmjd6* mRNA was detected, suggesting that the phenotype variation is not due to inefficient deletion. (Figure 1.3.17C and D). Consistent with the previous study, I also observed that some of the *Jmjd6*-/- embryos showed severe defects in head formation and eye development (Figure 1.3.17B) (Li, Sarkisian et al. 2003, Böse, Gruber et al. 2004, Kunisaki, Masuko et al. 2004). In E15.5 *Jmjd6*-/- embryos, edema was detected on the back of embryos, which is a sign of dysfunctional cardiovascular system. Hematoxylin and eosin (HE) staining of mouse embryos confirmed the edema in the *Jmjd6*-/- embryo (Figure 1.3.17B). Compared to the WT embryo, *Jmjd6*-/- hearts showed ventricular septal defects and decreased expression of cardiomyocyte structural genes (Figure 1.3.17E and F).

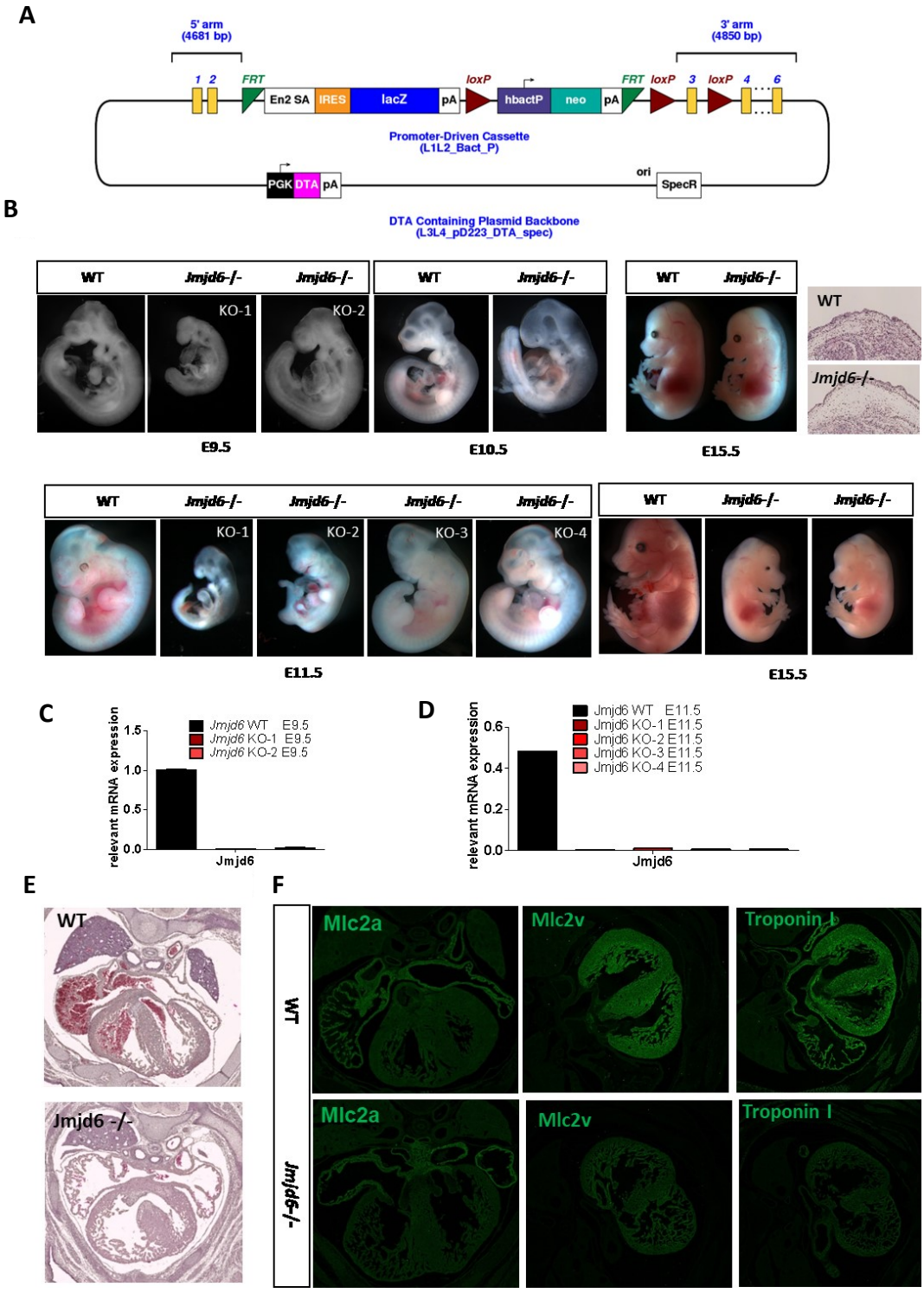

Figure 1.3.17. *Jmjd6* knockout showed development arrest and a cardiac defect. (A) Scheme representation of *Jmjd6* knock-out allele. **(B)** Morphology of WT and *Jmjd6*-/- embryos from E9.5 to E11.5. **(C-D)** Relative mRNA expression of *Jmdj6* in WT and *Jmjd6*-/- embryos at E9.5**(C)** and E11.5 **(D)**. **(E)** HE staining of heart from WT and *Jmjd6*-/- embryos at E15.5 **(F)** Immunostaining of Mlc2a, Mlc2v, and Troponin I in E15.5 embryo heart.

1.3.5.2 *Jmjd6* knockout mouse embryos show defective heart development genes expression

To confirm the function of *Jmjd6* for CPC development in vivo, I then checked cardiac progenitor marker gene expression in embryonic day 10.5 (E10.5) embryo heart. Consistent with what I found in CPC in vitro, cardiac progenitor marker genes were also downregulated in the E10.5 embryo heart (Figure 1.3.18A). To validate our findings, I isolated mRNA from *Jmjd6* +/+ and *Jmjd6* -/- embryos at E8.5 before the onset of phenotype in *Jmjd6*-/- embryos and performed RNA-seq. I found 332 down-regulated and 210 upregulated genes in *Jmjd6* -/- embryos (fold change > 1.5; log2 fold change < -0.58, > 0.58; p-value < 0.05) (Figure 1.3.18B). GO analysis of downregulated genes revealed GO terms linked to heart contraction, cardiac muscle cell differentiation, and cardiac cell development (Figure 1.3.18C).

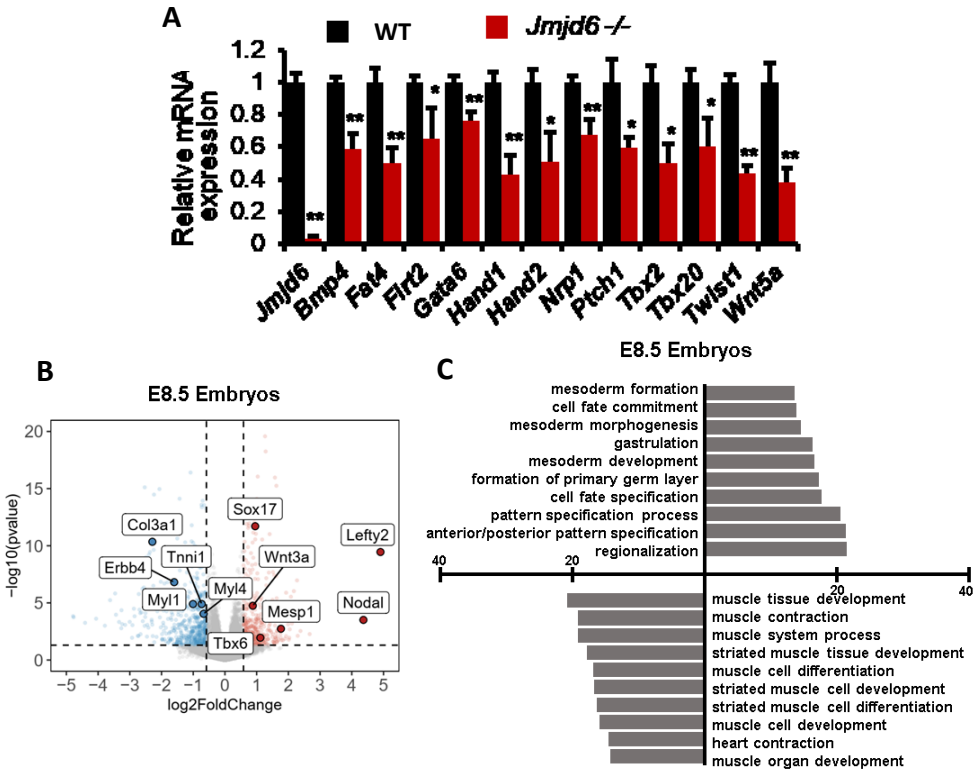

Figure 1.3.18. *Jmjd6* knockout mouse embryos show impaired heart development gene expression. (A) Relative mRNA expression of cardiac progenitor cell marker genes in E10.5 embryonic heart from WT and *Jmjd6*-/- embryos (n=4). **(B)** Volcano plot of RNA-seq from E8.5 embryos (n=3; fold change > 1.5; log2 fold change < -0.58, > 0.58; *p*-value < 0.05). **(C)** GO terms enriched in downregulated genes in E8.5 embryos.

In summary, *Jmjd6* plays a vital role in embryonic development. The loss of *Jmjd6* leads to various morphology defects, including small size and abnormal heart and eye development. In heart development, I found a significant downregulation of many key cardiac development genes and cardiomyocyte marker genes, which all contribute to the VSD of *Jmjd6*-/- embryos.

1.3.6 *Jmjd6* is involved in gene alternative splicing

1.3.6.1 Generation of E14-Nkx2.5-GFP-3XFlag-*Jmjd6* cells knock-in mESC line

There are no commercial antibodies available for *Jmjd6* that work for immune precipitation. Therefore, I knocked in a 3XFlag at the N-terminal of *Jmjd6* in the E14-Nkx2.5-GFP cell line. I designed a single-strand oligo DNA that contains a 3xFlag sequence flanked by the *Jmjd6* genomic sequence as a donor for generating 3XFlag-*Jmjd6* knock-in cells. A gRNA near the ATG site of *Jmjd6* and oligo DNA serving as donor were transfected together into mESc, and 3XFlag-*Jmjd6* knock-in cells were screened by PCR (Figure 1.3.19A).

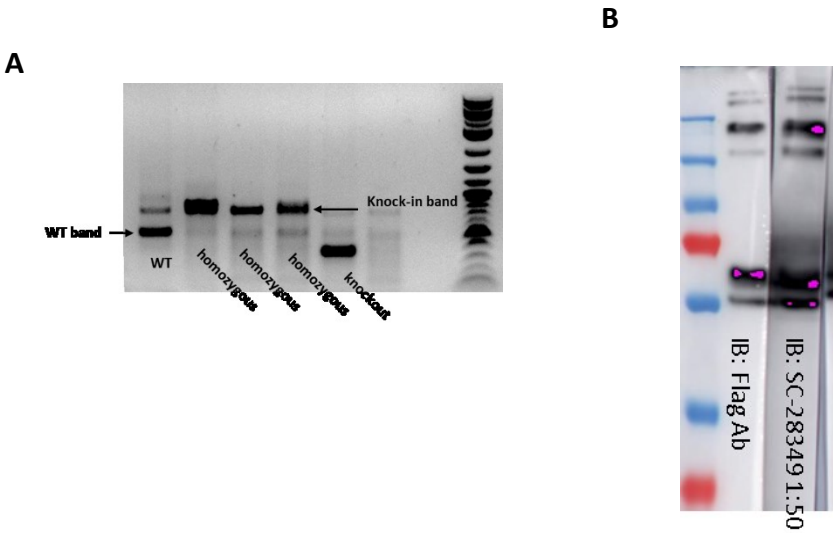

Figure 1.3.19. Generation of E14-Nkx2.5-GFP-3XFlag-*Jmjd6* mESC line. (A) Screen E14-Nkx2.5-GFP-3XFlag-*Jmjd6* mESC line with PCR. **(B)** Western blot of Nkx2.5-GFP-3XFlag-*Jmjd6* and WT mESC with Flag and *Jmjd6* antibody.

I performed WB analysis to validate the expression and the ability to form an oligomer of the 3xFlag-*Jmjd6*. By blotting with M2 antibody for Flag tag and SC-28349 antibody for *Jmjd6,* I showed 3xFlag-*Jmjd6* also form oligomer and shows same bands as WT *Jmjd6* protein (Figure 1.3.19B).

1.3.6.2 *Jmjd6* interacts with splice factors

To gain insight into the functions of *Jmjd6* in development, I performed IP with Flag antibody for WT and 3xFlage-*Jmjd6* knock-in mESCs, coupled with proteomic analysis by mass spectrometry. I identified 129 proteins interacting with *Jmjd6* in mESCs (Figure 1.3.20A). I then run GO analysis for those 129 genes with DAVID (https://david.ncifcrf.gov/summary.jsp). GO term enriched in mRNA processing, cell-cell adhesion, and translation (Figure1.3.20B). I then analyzed the interaction of those proteins and grouped them according to their interaction and similarity by STING (https://string-db.org/). In line with the previous report, two groups of proteins interact with JMJD6: mRNA splicing proteins and ribosome proteins (Figure 1.3.20C). It is also notable that *Jmjd6* is reported to involve in gene alternative splicing by hydroxylating U2AF65(Webby, Wolf et al. 2009). Co-immunoprecipitations (co-IPs) using Flag antibody revealed interaction of endogenous JMJD6 and U2AF65 in mESCs (Figure 1.3.20D). In addition, I also found that cell adhesion proteins bind to *JMJD6*. This interaction may indicate a function of *Jmjd6* in cell migration which may also contribute to embryonic development.

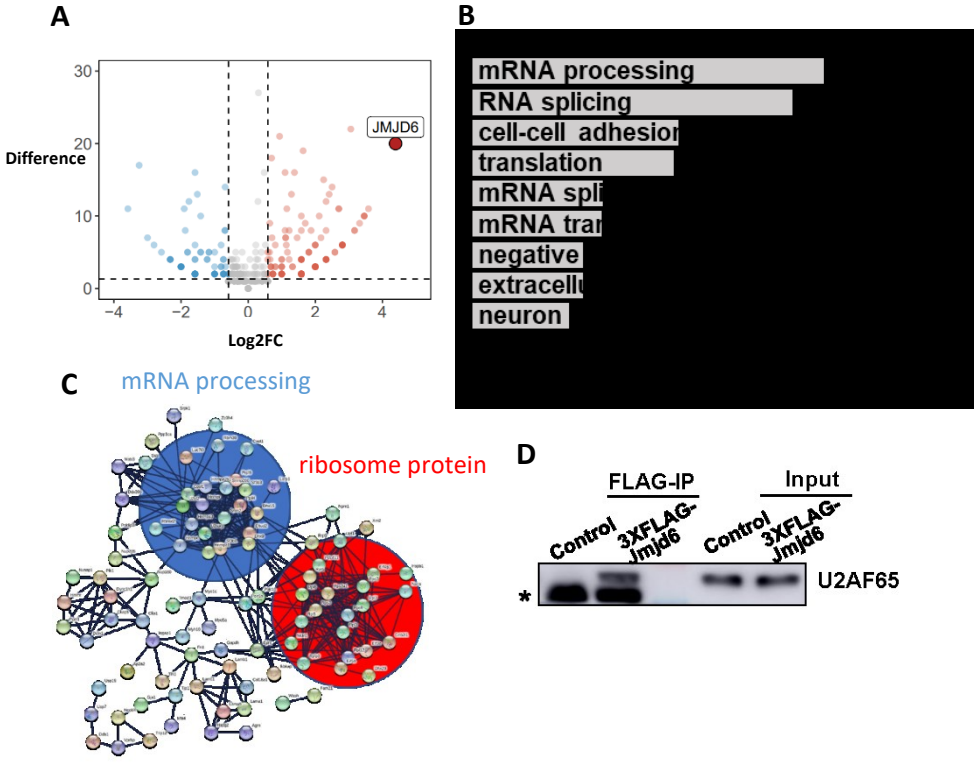

Figure 1.3.20. *JMJD6* interacts with splice factors and ribosome proteins. (A) 129 proteins interact with JMJD6 by the mass spectrometry quantification (difference >= 2; log2 fold change >= 0.58). **(B)** GO terms for proteins that interact with JMJD6. **(C)** Protein-protein interactions of proteins that interact with *Jmjd6* by STRING. **(D)** Co-immunoprecipitation of endogenous JMJD6 and U2AF65 in mESCs using FLAG antibody followed by WB analysis with U2AF65 antibody.

1.3.6.3 Loss of *Jmjd6* leads to alternative splicing change of histone methyltransferase *Prmt6*

Since many proteins involved in alternative splicing were found to interact with *Jmjd6*, I future investigated gene alternative splicing upon *Jmjd6* knockout. To access the possibility that *Jmjd6* regulates gene alternative splicing, which contributes to early lineage choice decisions and heart development, I utilized JunctionSeq (Hartley and Mullikin 2016). Splicing analysis at ESC, MES, CPC, and E8.5 embryos revealed 142, 223, 207, and 260 genes that showed differential expression in at least one exon or intro between WT and *Jmjd6* KO cells. GO analysis of differentially spliced genes revealed that splicing and chromatin modification genes were in the top GO terms. (Figure 1.3.21).

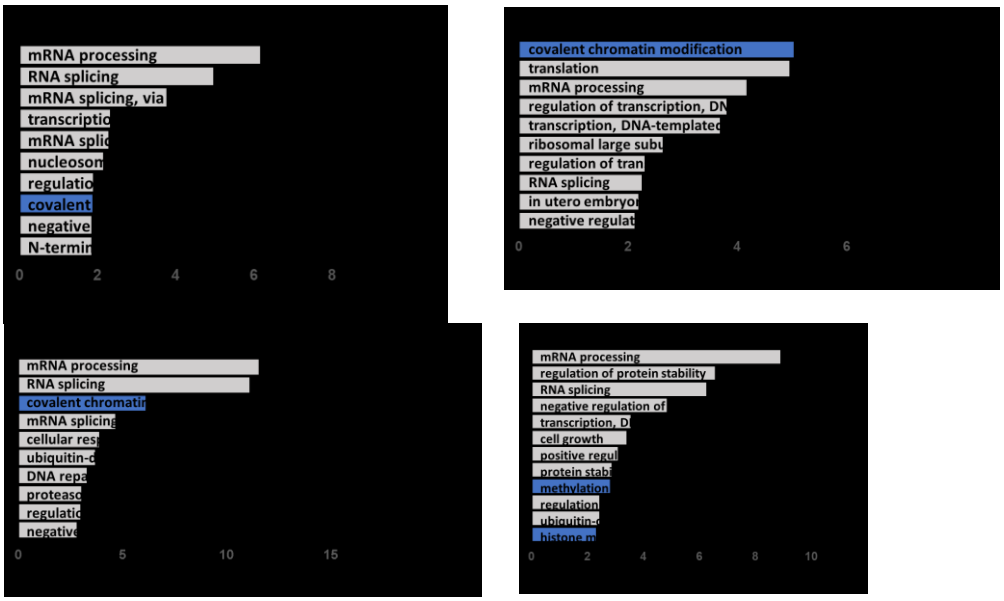

Figure 1.3.21. GO analysis of alternative splicing genes regulated by *Jmjd6*. GO analysis of differential spliced genes in ESC, MES, CPC, and E8.5 embryos.

Among all differential spliced genes, *Prmt6* drew our attention. *Prmt6* functions as a methyltransferase to methylate arginine residues at H3 to form H3R2me2a. Many studies have suggested a negative correlation between H3R2me2a and H3K4me3 (Guccione, Bassi et al. 2007, Hyllus, Stein et al. 2007, Kirmizis, Santos-Rosa et al. 2007, Bouchard, Sahu et al. 2018). I hypothesized that upregulation of *PRMT6* protein promotes H3R2me2a, which prevents H3K4me3 modification at the gene promoter. Two isoforms have been reported for the *Prmt6* gene according to the Refseq annotation database. Compared to the isoform NM_178891.5, which code protein, isoform NR_024139.2, which has a long 3' UTR, was suggested to undergo non-sense mediated degradation (Figure 1.3.22B). I then looked closer at the alternative splicing of *Prmt6* at ESC, MES, CPC, and E8.5 embryos. Except for the ESC stage, I found significant changes in *Prmt6* isoform expression in WT and *Jmjd6* KO cells (Figure 1.3.22A). I designed qPCR primers targeting NMD-*Prmt6* (NR_024139.2) and *Prmt6*-SUTR (NM_178891.5) to check the ratio of *Prmt6*-SUTR/NMD-*Prmt6*. Real-time PCR analysis revealed that during differentiation, *Prmt6*-SUTR/NMD-*Prmt6* was increased in *Jmjd6* KO cells compared to WT cells (Figure 1.3.22D). Importantly, the ratio also increased in the E10.5 mouse embryo heart (Figure 1.3.22D). Loss of *Jmjd6* leads to more *Prmt6*-SUTR, which codes proteins, and less NMD-*Prmt6,* which may undergo NMD. Next, I analyzed PRMT6 protein expression at ESC, MES and CPC stages. As expected, the protein level of PRMT6 was significantly increased in *Jmjd6* KO cells at MES and CPC stage (Figure 1.3.22F). In contrast, the mRNA expression *Prmt6* is not changed during the differentiation (Figure 1.3.22E). Interestingly, NMD-*Prmt6* seems not expressed in mESCs as there are no reads in the 3'UTR region of this isoform in mESCs (Figure 1.3.22C). However, both NMD-*Prmt6* and *Prmt6*-SUTR are expressed in MES and CPC. Adjustment of *Prmt6* isoforms expression during the differentiation may be required to regulate its protein level and activity during the development.

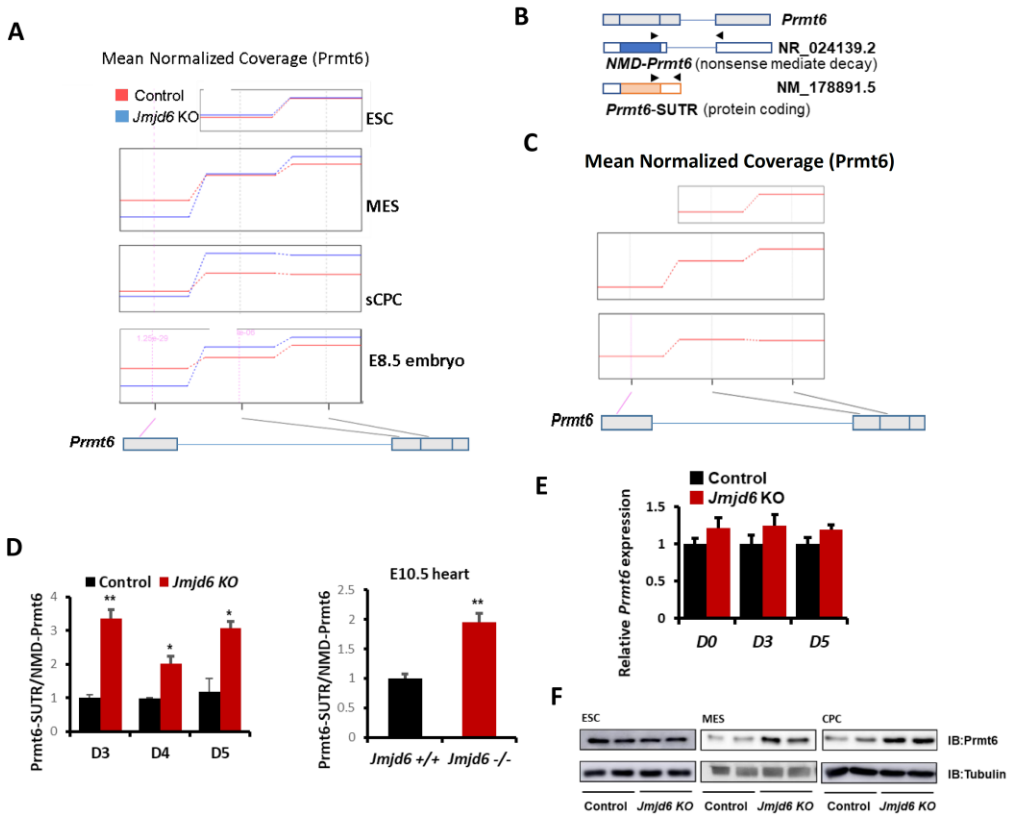

Figure 1.3.22. Altered alternative splicing of *Prmt6* upon *Jmjd6* knock out results in upregulated *PRMT6* protein level. (A) Alternative splicing events of *Prmt6* in ESC, MES, CPC, and E8.5 embryos. **(B)** *Prmt6* mRNA isoforms according to the Refseq annotation. **(C)** Different *Prmt6* isoforms were expressed during differentiation **(D)** Quantification of Prmt6-SUTR/NMD-Prmt6 in D3, D4, D5 EBs, and E10.5 embryos by RT-qPCR (n=4). **(E)** Relative mRNA expression *Prmt6* during the differentiation in WT and *Jmjd6* KO cells (n=4). **(F)** The protein level of *Prmt6* during the differentiation in WT and *Jmjd6* KO cells.

1.3.7 PRMT6 overexpression leads to a decrease of H3K4me3 at the bivalent promoters

1.3.7.1 *Jmjd6* loss of function results in an increase of H3R2me2a and a decrease of H3K4me3

Many studies have indicated a negative correlation between H3R2me2a and H3K4me3 (Guccione, Bassi et al. 2007, Hyllus, Stein et al. 2007, Kirmizis, Santos-Rosa et al. 2007). Thus, I analyzed the enrichment of H3R2me2a at the promoter region of gastrulation like *Cer1*, *Eomes*, *Fgf8* and *T* and heart development genes like *Bmp2*, *Bmp4*, *Hand1*, *Hand2*, and *Tbx20* by ChIP-qPCR. In line with the upregulated PRMT6 level upon *Jmjd6* knockout, H3R2Me2a modifications on those genes promoter were significantly upregulated. (Figure 1.3.23A and B).

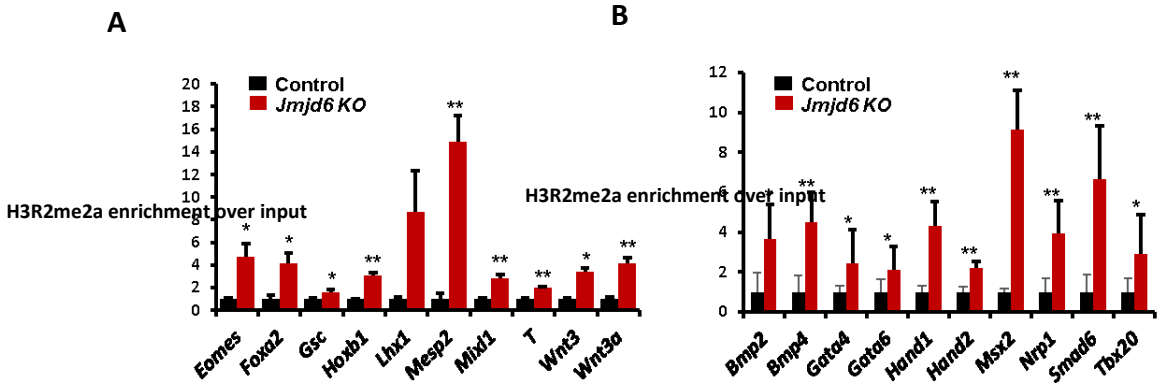

Figure 1.3.23: Loss of *Jmjd6* leads to higher accumulation of H3R2me2a on the promoter region of gastrulation and heart development genes in *Jmjd6* KO cells. (A) ChIP-qPCR result of H3R2me2a enrichment at gastrulation gene promoters in D4 EBs derived from control and *Jmjd6* KO mESCs (n=3). **(B)** ChIP-qPCR result of H3R2me2a enrichment at heart development gene promoters in CPCs derived from control and *Jmjd6* KO mESCs (n=3).

1.3.7.2 *Prmt6* overexpression mimics *Jmjd6* KO phenotype while silencing rescue *Jmjd6* KO phenotype during cardiomyocyte differentiation

To assess whether overexpression of *Prmt6* in WT mESCs mimics the *Jmjd6* KO mESCs

phenotype, I ectopically overexpressed *Prmt6* in WT mESCs and differentiated them into cardiomyocyte with hanging drop. *Prmt6* overexpression decreased key gastrulation and heart development gene expression (Figure 1.3.24A and B). Cardiomyocyte marker gene expression was also dramatically decreased in d9 EBs derived from *Prmt6* overexpression mESCs compared to the WT mESCs (Figure 1.3.24C).

In order to assess whether the up-regulated expression of *Prmt6* is responsible for the failed cardiomyocyte differentiation in *Jmjd6* KO mESCs, I knocked down *Prmt6* in WT or *Jmjd6* KO mESCs with shRNA. Importantly, *Prmt6* knocking down in *Jmjd6* KO mESCs could rescue cardiac differentiation, measured by increased mRNA level of cardiac progenitor marker genes (Figure 1.3.24D).

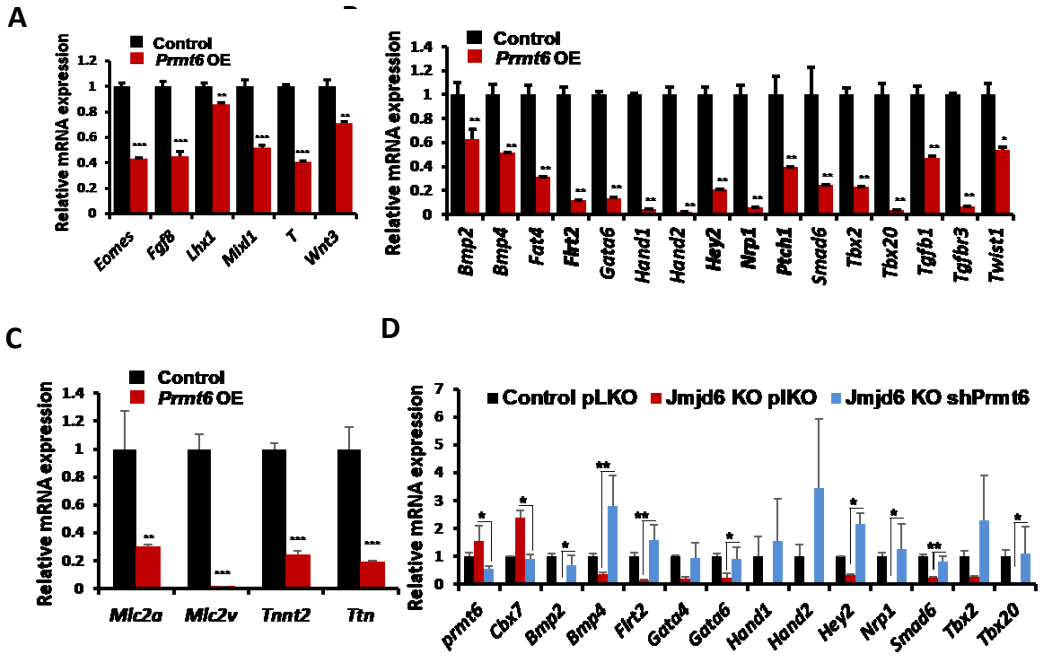

Figure 1.3.24. *Prmt6* overexpression resembles *Jmjd6* loss of function while silencing of *Prmt6* rescues the cardiomyocyte differentiation defect in *Jmjd6* KO. (A) Relative mRNA expression of key gastrulation genes in D4 EBs derived from control and *Prmt6* overexpression mESCs (n=4). **(B)** Relative mRNA expression of key heart development genes in D5 EBs derived from control and *Prmt6* overexpression mESCs (n=4). **(C)** Relative mRNA expression of cardiomyocyte marker genes in D9 EBs derived from control and *Prmt6* overexpression mESCs (n=4). **(D)** Relative mRNA expression of key heart development genes in D5 EBs derived from control infected with pLKO, *Jmjd6* KO infected with pLKO, and *Jmjd6 KO* infected with sh*Prmt6* mESCs (n=4).

Next, I performed ChIP-qPCR to check whether the up-regulated *Prmt6* is responsible for the decreased H3K4me3 on the promoter region of gastrulation and heart development genes. Overexpressing Prmt6 in mESCs indeed led to decreased H3K4me3 on those gene promoter regions (Figure 1.3.25A and B).

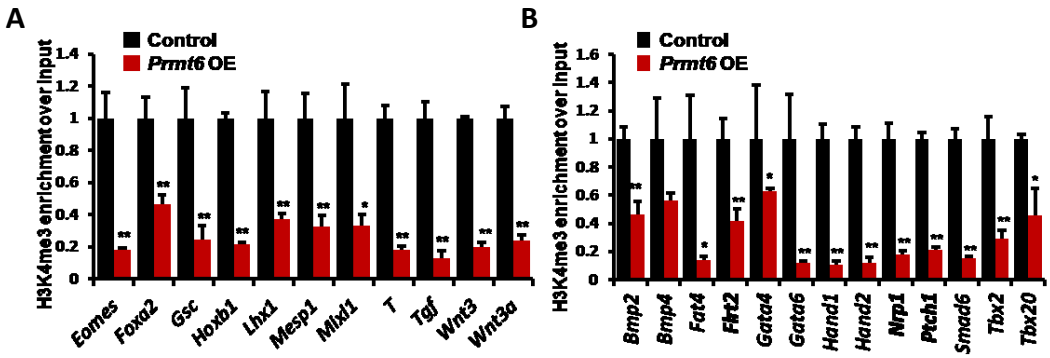

Fi . . ter of gastrulation and heart development genes. (A) ChIP-qPCR result of H3K4me3 enrichment at gastrulation gene promoters in D4 EBs derived from control and *Jmjd6* KO mESCs (n=3). **(B)** ChIP-qPCR result of H3K4me3 enrichment at gastrulation gene promoters in CPCs derived from control and *Jmjd6* KO mESCs (n=3).

Taken together, these data indicate that *Jmjd6* restrain PRMT6 protein level by regulating the *Prmt6* isoform expression ratio. Knocking down or overexpression of *Prmt6* could activate or repress cardiac progenitor marker gene expression, suggesting a repressive role of *Prmt6* in cardiomyocyte differentiation. Restrained *Prmt6* protein level is essential for H3K4me3 accumulation and expression of gastrulation and heart development genes.

1.3.8 *Cbx7* upregulation leads to increased H2AK119ub and H3K27me3 accumulation at the bivalent promoter

1.3.8.1 *Cbx7* is upregulated upon *Jmjd6* loss of function

As H3K27me3 is significantly increased in the promoter region of gastrulation and heart developmental genes, I first analyzed the expression of the core membranes of the PRC1 and PRC2 complex upon *Jmjd6* knockout. Surprisingly, *Cbx7* was highly upregulated in both MES and CPC stages, while most other members showed minor changes or decreased expression. (Figure 1.3.26A).

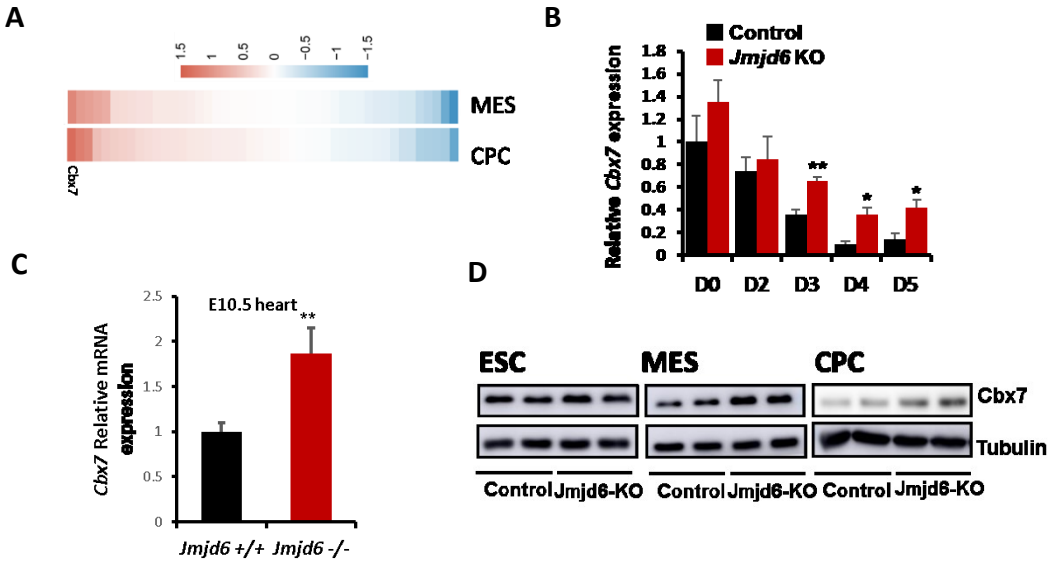

Figure 1.3.26. *Cbx7* was upregulated in *Jmjd6* KO cells at MES and CPC stage. (A) Log2 fold change of PRC1 and PRC2 complexes members in WT and *Jmjd6* KO CPC. **(B)** Relative mRNA expression *Cbx7* from D0 to D5 of hanging drop differentiation in WT and *Jmjd6* KO cells (n=4). **(C)** Relative mRNA expression *Cbx7* in WT and *Jmjd6* -/- E10.5 embryos (n=4). **(D)** The protein level of *Cbx7* during the differentiation in WT and *Jmjd6* KO cells.

I then further validated the upregulation of *Cbx7* during the differentiation in *Jmjd6*KO cells by RT-qPCR analysis. In contrast to the control cells, *Cbx7* was still highly expressed in D3, D4, and D5 but not in D0 and D2 EBs derived from *Jmjd6* KO mESCs (Figure 1.3.26B). During the differentiation, *Cbx7* expression decreases along with the differentiation (Figure 1.3.26B), which is in line with the previous study (Morey,

Pascual et al. 2012, Wamstad, Alexander et al. 2012). This downregulation is required for the activation of differentiation genes due to the repressive nature of *Cbx7* for developmental genes (Morey, Pascual et al. 2012). Moreover, analysis of the E10.5 mouse embryo hearts revealed that *Cbx7* is also upregulated in the *Jmjd6*-/- embryo (Figure 1.3.26C). Western blot further confirmed that the CBX7 protein level is upregulated in *Jmjd6* KO cells (Figure 1.3.26D). Taken together, *Cbx7* is highly upregulated upon *Jmjd6* loss of function during the differentiation.

1.3.8.2 Sustained H3k27ac at the enhancer region of *Cbx7* maintains its expression in *Jmjd6* KO cells

There are five CBX proteins, including *Cbx2*, *Cbx4*, *Cbx6*, *Cbx7* and *Cbx8,* associated with the PRC1. Studies from Morey et al. indicate that *Cbx7* was the primary CBX protein associated with PRC1 in mESC. Importantly, there is a dynamic switch of CBX protein in PRC1 during the differentiation. Specifically, *Cbx7* was down-regulated, and *Cbx2*, *Cbx4* and *Cbx8* were up-regulated in the same time (Morey, Pascual et al. 2012). To find out what drives *Cbx7* down-regulation during mESC differentiation and abnormal expression in *Jmjd6* KO cells. We took the published data in which RNA expression and H3K27ac modification were analyzed in the process of direct cardiomyocyte differentiation (Wamstad, Alexander et al. 2012). Consisted with what we found, *Cbx7* mRNA expression was highly expressed in mESC but dramatically decreased in the later stage (Figure 1.3.27B).

Interestingly, we found two H3K27ac peaks, enhancer histone markers, downregulated during the differentiation (Figure 1.3.27A). The decrease of enhancer marker H3K27ac is consistent with the mRNA expression of *Cbx7* during the direct cardiomyocyte differentiation. It implies that decreased H3k27ac may be responsible for the *Cbx7* mRNA expression reduction during cardiac differentiation.

To test whether H3K27ac is still sustained in the promoter and upstream region of *Cbx7*, we did the H3K27ac ChIP-qPCR in WT and *Jmjd6* KO CPCs. ChIP-qPCR showed

increased H3K27ac modification in *Jmjd6* KO CPCs compared to WT CPCs for those two peaks (Figure 1.3.27C). It has been reported that the H3R2me2a promotes the H3K27ac in the enhancer region(Bouchard, Sahu et al. 2018). To access the possibility that elevated *Prmt6* leads to the upregulation of *Cbx7*. I checked the *Cbx7* expression level in CPC derived from WT and *Prmt6* overexpression mESCs. *Cbx7* expression level indeed is upregulated when overexpressing *Prmt6* (Figure 1.3.27D).

In summary, sustained enhancer marker H3K27ac results in the relatively high expression of *Cbx7* in MES and CPC derived from *Jmjd6* KO mESC.

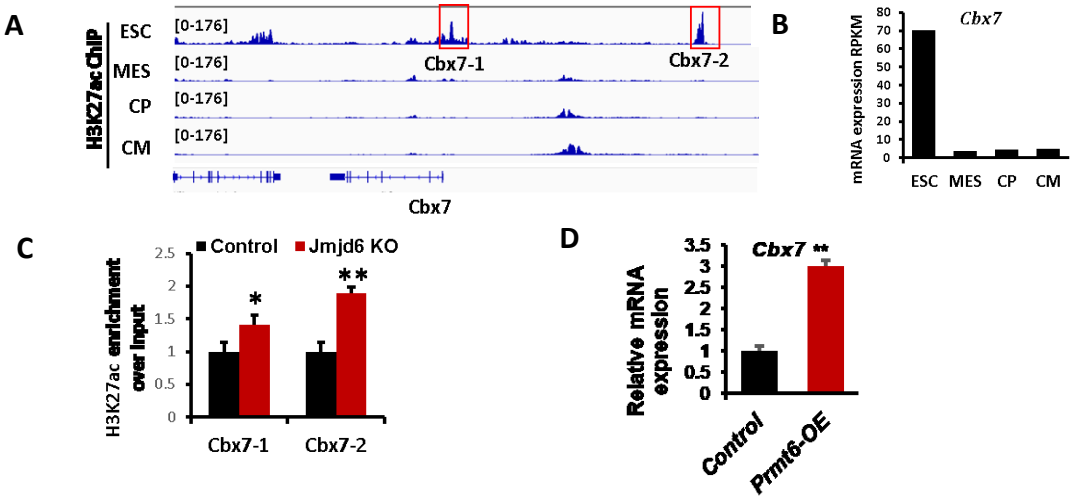

Figure 1.3.27. Sustained H3K27ac promotes *Cbx7* expression in CPC derived from Jmjd6 KO mESCs. (A) Reduced H3K27ac at upstream of *Cbx7* along cardiomyocyte differentiation **(B)** mRNA expression of *Cbx7* during cardiomyocyte differentiation. **(C)** H3K27ac accumulation is upregulated in CPC derived from *Jmjd6* KO mESC by ChIP-qPCR(n=3). **(D)** Relative mRNA expression *Cbx7* of CPC derived from WT and *Jmjd6* KO mESC (n=4).

1.3.8.3 Positive loop of PRC1 and PRC2 complexes increase H3K27me3 accumulation in *Jmjd6* KO cells

As a member of PRC1, *Cbx7* has been shown to recognize H3K27me3 directly (Yap, Li et al. 2010). Moreover, among all the CBX proteins, *Cbx7* is an exception. Its binding to the promoter depends entirely on PCR2 activity in ESCs (Morey, Pascual et al. 2012, Zhen, Tatavosian et al. 2016). As the PRC1 complex contain histone H2A E3 ubiquitin

ligases, the upregulation of *Cbx7* will lead to H2AK119ub accumulation. H2AK119ub further recruits the PRC2 complex containing Ezh1/2, which methylates H3K27 to H3K27me3 (Cooper, Dienstbier et al. 2014). PRC1 complex containing CBX7 and PRC2 complex form a positive loop to maintain repressive marker H3K27me3.

To study whether the PRC2 or PRC1 complex plays an important role in regulating dysregulated genes upon *Jmjd6* knockout, I first analyzed the binding of key members in the PRC1 and PRC2 complex on upregulated, downregulated, and no changed genes upon *Jmjd6* knockout in D4 and D5 EBs ((Ballaré, Lange et al. 2012, Creppe, Palau et al. 2014, Yoo, Oh et al. 2015, Juan, Wang et al. 2016, Mas, Blanco et al. 2018, Zepeda-Martinez, Pribitzer et al. 2020)). I found that dysregulated genes were highly bound by PRC2 complex members EZH2, SUZ12, and EED, while the no changed genes were not or were slightly bound by those members. On the opposite, the binding of Ezh1, which is mainly functional in adult tissue, showed a higher signal on no changed genes compared to dysregulated genes (Figure 1.3.28A and B). Ring1b, which is critical for H2AK119ub as an E3 ubiquitin ligase of the PRC1 complex, and *Cbx7* were highly bound on dysregulated genes but not on the no changed genes. In contrast, *Cbx8*, which was repressed by *Cbx7* to maintain the pluripotency of ES cells, was bound more on no changed genes instead of dysregulated genes. Moreover, the RYBP, which is mutually exclusive to *Cbx7*, binds equally to dysregulated or no changed genes (Figure 1.3.28A and B). The fact that dysregulated genes upon *Jmjd6* KO are highly bound by Ezh2, SUZ12, EED, Ring1b, and *Cbx7* highlights the importance of *Cbx7*-containing PRC1 and Ezh2-containing PRC2 on those genes' expression.

To access the possibility that sustained expression of CBX7 in d4 and D5 EBs leads to H2AK119ub1 accumulation, which further recruits the PCR2 to write H3k27me3 at cardiac-specific gene promoter loci. First, I did the intersection of *Cbx7* target genes (Morey, Aloia et al. 2013) and downregulated genes in d4 and D5 EBs derived from *Jmjd6* KO mESCs. 359 or 313 genes bound by *Cbx7* showed lower mRNA expression in either d4 or D5 EBs derived from *Jmjd6* KO cells. Significantly, GO analysis of those 359 revealed GO terms linked to pattern specification process, regionalization and cell fate commitment (Figure 1.3.28C); and the GO analysis of those 313 genes revealed GO terms linked to outflow tract morphogenesis, ventricular septum morphogenesis, and

heart development (Figure 1.3.28D).

I then analyzed the enrichment of H2AK119ub and the PRC2 catalytic subunit EZH2 at the promoter region of gastrulation and heart development genes by ChIP-qPCR. Importantly, H2AK119ub and Ezh2 also showed increased enrichment at the promoter region of those genes (Figure 1.3.29A, B, C and D). Together, the upregulated CBX7 leads to higher H2AK119ub, which recruits more PCR2 complex at the bivalent promoter of gastrulation and heart development genes and finally results in higher H3K27me3 enrichment in *Jmjd6* KO sCPCs.

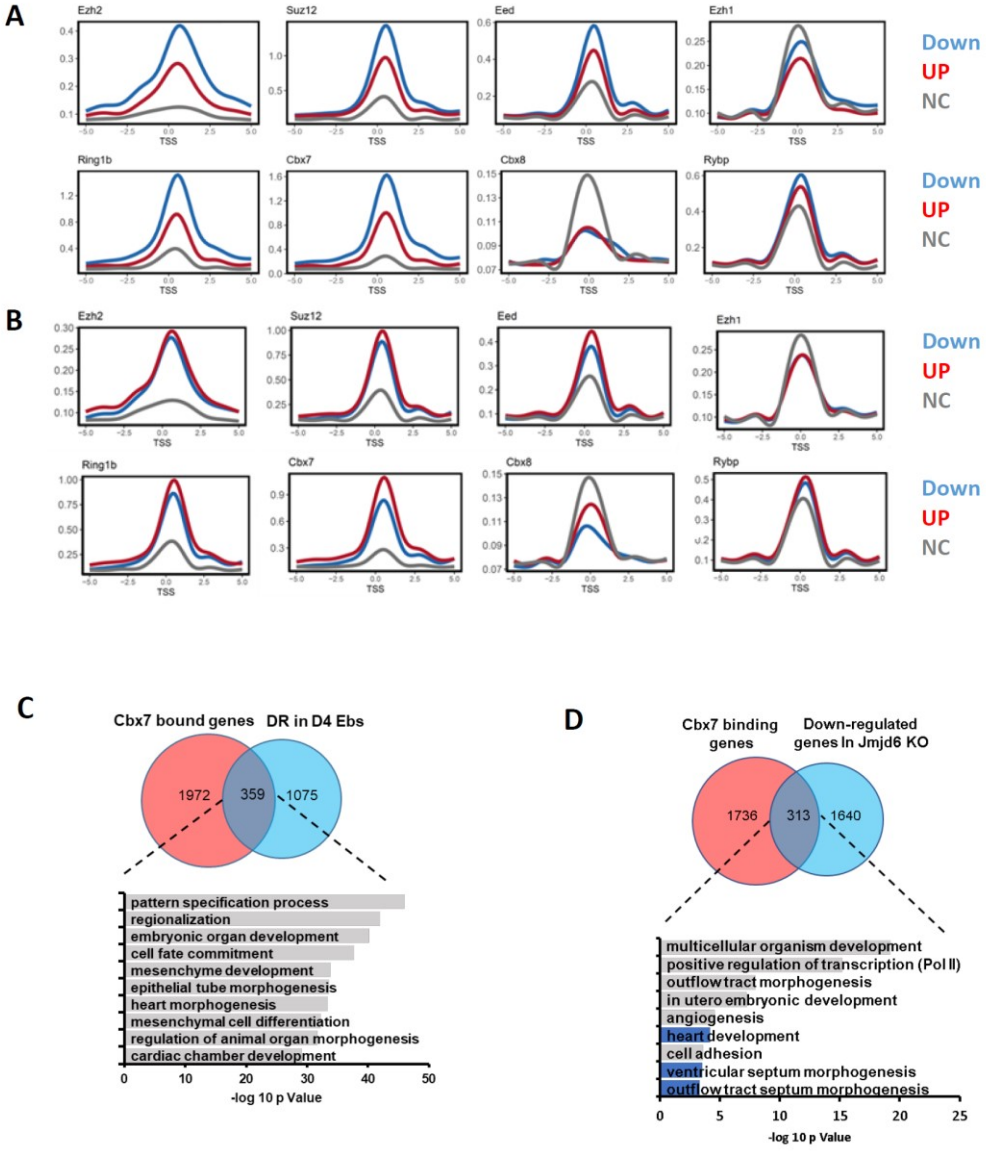

Figure 1.3.28. Dysregulated genes upon *Jmjd6* knockout are marked by PRC1 and PRC2 complex. (A and B) TSS profile plot of PRC1 and PRC2 complex members on upregulated, downregulated, and no changed genes at D4 EBs **(A)** or D5 EBs **(B)** upon *Jmjd6* knockout. **(C)** Overlap between *Cbx7* binding genes and down-regulated genes

in D4 EBs derived from *Jmjd6* KO mESCs (up) and the GO term enriched in overlapped genes (down). **(D)** Overlap between *Cbx7* binding genes and down-regulated genes in D5 EBs derived from *Jmjd6* KO mESCs (up) and the GO term enriched in overlapped genes (down).

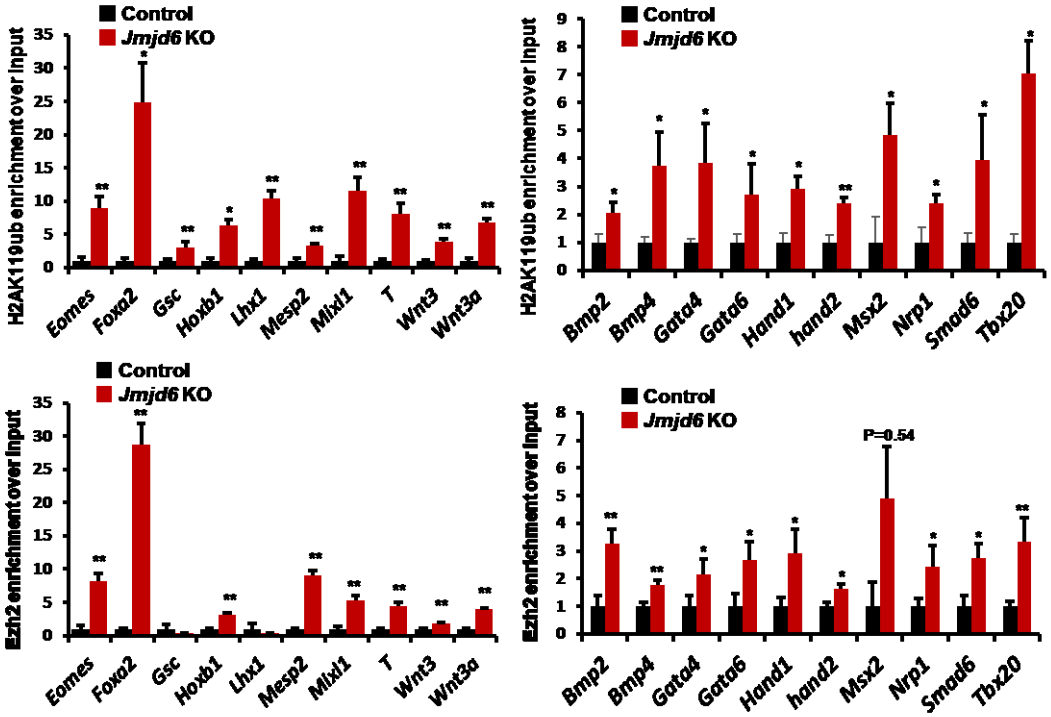

Fi

gastrulation and heart development genes in control and *Jmjd6* KO cells. (A) ChIP-qPCR result of H2AK119ub enrichment at gastrulation gene promoters in D4 EBs derived from control and *Jmjd6* KO mESCs (n=3). **(B)** ChIP-qPCR result of H2AK119ub enrichment at heart development gene promoters in CPCs derived from control and *Jmjd6* KO mESCs (n=3). **(C)** ChIP-qPCR result of Ezh2 enrichment at gastrulation gene promoters in D4 EBs derived from control and *Jmjd6* KO mESCs (n=3). **(D)** ChIP-qPCR result of Ezh2 enrichment at heart development gene promoters in CPCs derived from control and *Jmjd6* KO mESCs (n=3).

1.3.8.4 *Cbx7* overexpression mimics *Jmjd6* KO phenotype while silencing rescue *Jmjd6* KO phenotype

To evaluate whether overexpression of *Cbx7* mimics the phenotype in *Jmjd6* KO cells, I generated E14-Nkx2.5-GFP-*Cbx7*-OE stable cell line and differentiated these cells using the hanging drop method. Forced expression of *Cbx7* also decreased the expression of key gastrulation and heart development genes (Figure 1.3.30A and B). Cardiomyocyte marker gene expression was dramatically decreased in *Cbx7*

overexpression D9 EBs (Figure 1.3.30C). To assess whether the up-regulated expression of *Cbx7* is responsible for the defective cardiomyocyte differentiation in *Jmjd6* KO mESCs, I knocked down *Cbx7* in WT or *Jmjd6* KO mESCs and differentiated those cells into cardiomyocytes. As expected, *Cbx7* slicing in *Jmjd6* KO mESCs could fully rescue cardiac differentiation, as measured by increased mRNA level of cardiac progenitor marker genes (Figure 1.3.30D).

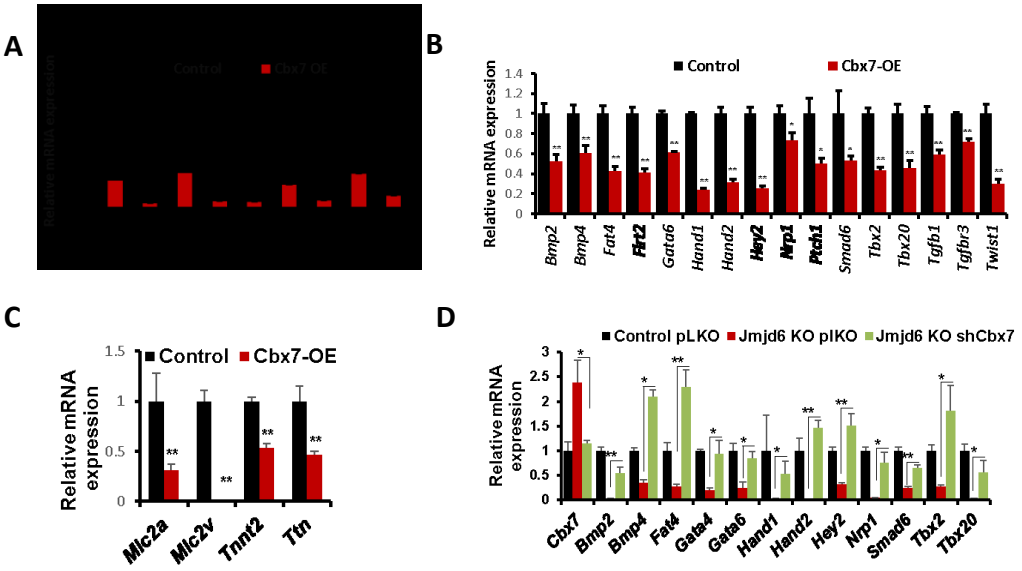

Figure 1.3.30. *Cbx7* overexpression resembles *Jmjd6* loss of function while silencing of *Cbx7* rescues the cardiomyocyte differentiation defect in *Jmjd6* KO. (A) Relative mRNA expression of key gastrulation genes in D4 EBs derived from control and *Cbx7* overexpression mESCs (n=4). **(B)** Relative mRNA expression of key heart development genes in D5 EBs derived from control and *Cbx7* overexpression mESCs (n=4). **(C)** Relative mRNA expression of cardiomyocyte marker genes in D9 EBs derived from control and *Cbx7* overexpression mESCs (n=4). **(D)** Relative mRNA expression of key heart development genes in D5 EBs derived from control infected with pLKO, *Jmjd6* KO infected with pLKO, and *Jmjd6* KO infected with sh*Cbx7* mESCs (n=4).

Next, I performed ChIP-qPCR to check whether the up-regulated *Cbx7* is responsible for the increased H2AK119ub, Ezh2 and H3K27me3 on the promoter region of gastrulation and heart development genes. Overexpressing *Cbx7* in mESCs indeed led to increased H2AK119ub, Ezh2 and H3K27me3 (Figure 1.3.31A, B, C, D, E and F).

In summary, the elevated *Cbx7* led to upregulation of H3K27me3 at the promoter region of gastrulation and heart development genes through the positive loop of PRC1 and PRC2 complex. The higher accumulation of H3K27me3 contributed to the

downregulation of key gastrulation and heart development genes.

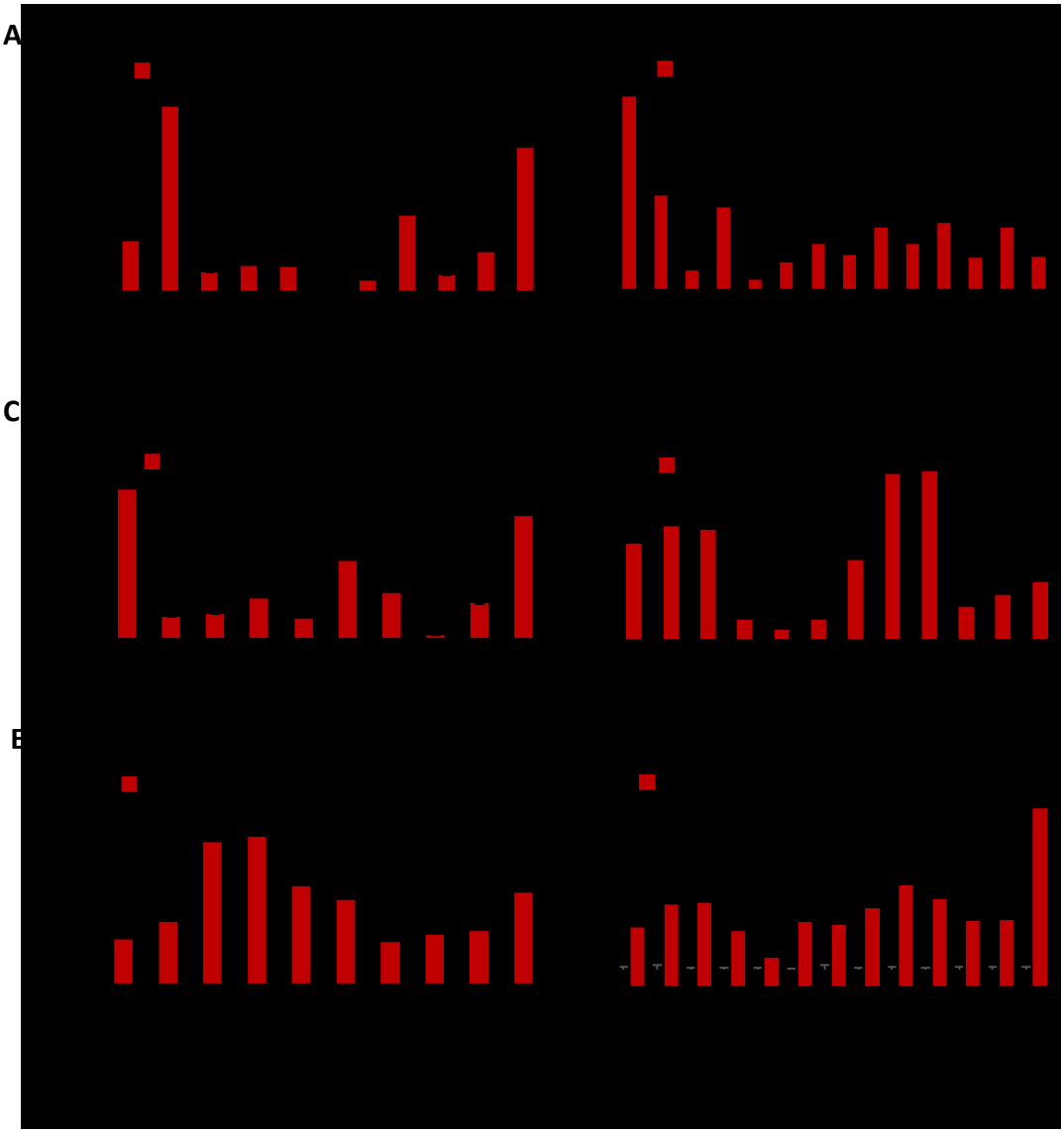

Figure 1.3.31. *Cbx7* overexpression leads to higher accumulation of H2AK119ub1, Ezh2, and H3K27me3 at gastrulation and heart development genes. (A) ChIP-qPCR result of H2AK119ub1 enrichment at gastrulation gene promoters in D4 EBs derived from control and *Cbx7* overexpression mESCs (n=3). **(B)** ChIP-qPCR result of H2AK119ub1 enrichment at gastrulation gene promoters in CPCs derived from control and *Cbx7* overexpression mESCs (n=3). **(C)** ChIP-qPCR result of Ezh2 enrichment at gastrulation gene promoters in CPCs derived from control and *Cbx7* overexpression mESCs (n=3). **(D)** ChIP-qPCR result of Ezh2 enrichment at gastrulation gene promoters in CPCs derived from control and *Cbx7* overexpression mESCs (n=3). **(E)** ChIP-qPCR result of H3K27me3 enrichment at gastrulation gene promoters in CPCs derived from control and *Prmt6* overexpression mESCs (n=3). **(F)** ChIP-qPCR result of H3K27me3 enrichment at gastrulation gene promoters in CPCs derived from control and *Cbx7* overexpression mESCs (n=3).

1.3.9 Working model

In conclusion, these data suggest an essential role of *Jmjd6* in early lineage choice and progenitor cell differentiation. Loss of *Jmjd6* results in abnormal resolution of the bivalent domains at genes that play an important role in those two processes. Mechanismly, on the one hand, I found that *Jmjd6* regulates *Prmt6* splicing, thereby controlling its protein level during stem cell differentiation. Along with the differentiation, isoform NMD-*Prmt6* (NR_024139.2) with long 3'UTR, which undergoes NMD, gradually increases. Without *Jmjd6*, this long 3'UTR is spliced out, leading to a lower expression of NMD-*Prmt6* isoform and a higher expression of *Prmt6*-SUTR in MES and CPC stages. The imbalanced isoform expression ratio results in PRMT6 protein level upregulation.

Furthermore, elevated PRMT6 leads to higher H3R2me2a and lower H3K4me3 accumulation at gastrulation and heart development genes. On the other hand, the sustained CBX7 protein recruits the PRC1 complex to deposit H2AK119ub, which promotes the binding of the PRC2 complex that deposits H3K27me3. Decrease of H3K4me3 caused by elevated Prmt6 and increase of H3K27me3 caused by elevated *Cbx7* both contribute to the repression of early lineage specification and heart development genes.

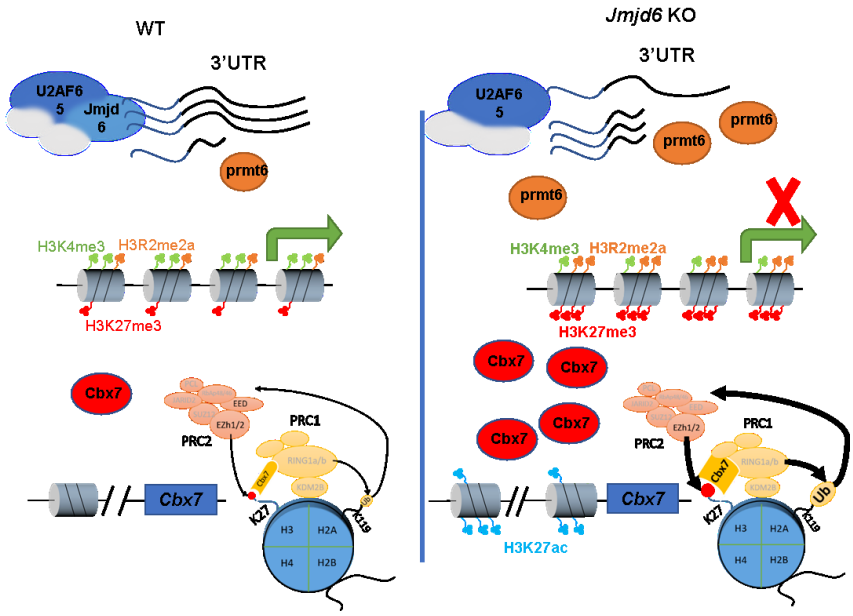

Figure 1.3.32. The working model for how *Jmjd6* regulates early lineage choices and heart development by controlling bivalent domain resolution. *Jmjd6* works together with splicing factor U2AF65 to regulate *Prmt6* alternative splicing. Without *Jmjd6*, *Prmt6* tended to be spliced to isoform with short 3'UTR, which codes the protein. Increased coding isoform and decreased non-coding isoform lead to higher PRMT6 protein, resulting in higher H3R2me2a at gastrulation and the promoter of the heart development gene region. The higher H3R2me2a at the promoter region leads to lower H3K4me3 for those genes but higher H3K27ac at the enhancer region of *Cbx7*. Upregulated *Cbx7* leads to a higher accumulation of H2AK119ub, Ezh2 and H3K27me3, which repress gene expression. Decreased H3K4me3 and increased K3K27me3 lead to the repression of gastrulation and heart development gene expression.

1.4 Discussion

In this work, I showed that loss of *Jmjd6* in mESCs impairs mesoderm and endoderm development but enhances ectoderm. With further differentiation, *Jmjd6* plays a key role in the differentiation of progenitor cells in specialized cell types, as I showed for cardiogenesis. Mechanistically, I showed that JMJD6 interacts with spliceosomal proteins in mESCs and regulates alternative splicing of genes involved in chromatin modification and mRNA processing. Prmt6, an H3R2me2a methyltransferase, was upregulated in protein level in *Jmjd6* knockout cells due to the alternative splicing. Upregulated PRMT6 leads to H3R2me2a accumulation at lineage specification and heart development genes and thus inhibits the deposition of H3K4me3. I further found that the accumulation of H3K27me3, which is the repressive histone modification of the bivalent domain, was increased on lineage specification and heart development genes because of the upregulation of *Cbx7*.

1.4.1 *Jmjd6* plays a key role in germ layer lineage bifurcation choices, progenitor cell differentiation, and organ development.

By in vitro differentiation of control and *Jmjd6* knockout mESCs, I showed that loss of *Jmjd6* impaired mesoderm and endoderm development but favored ectoderm. The imbalanced formation of three germ layers may contribute to the organ development defects as endoderm and mesoderm give rise to organs like lung, kindy, liver, and also heart, while the brain and never system are mainly derived from ectoderm. With further differentiation, whole transcriptome sequencing data for D5 EBs revealed that besides the genes in heart development, many genes involved in the lung, kindy, and vessel development were also downregulated in *Jmjd6* KO cells. Imbalanced germ layer formations and impaired progenitor differentiation upon *Jmjd6* knockout were consistent with the *Jmjd6* knockout mice phenotype reported by other groups and us (Li, Sarkisian et al. 2003, Böse, Gruber et al. 2004, Kunisaki, Masuko et al. 2004). Böse et al. also found that the terminal differentiation of the kidney, intestine, liver, and lung was delayed during embryogenesis (Böse, Gruber et al. 2004). The Head is also

severely deformed in all knockout mice used in previous studies and this study. I observed that *Jmjd6*-/- embryos exhibit growth retarded from E9.5 embryos, which is also true for *Jmjd6*-/- mice generated by Böse et al. and Kunisak et al. (Böse, Gruber et al. 2004, Kunisaki, Masuko et al. 2004). Importantly, those two *Jmjd6*-/- mice also showed cardiovascular defects, including ventricular septal defect and double outlet right ventricle, which is also observed in *Jmjd6*-/- mouse used in this study (Böse, Gruber et al. 2004, Kunisaki, Masuko et al. 2004).

Taken together, those data suggest *Jmjd6* regulates embryonic organ development by balancing the germ layer formation and assuring progenitor cell differentiation.

1.4.2 Loss of *Jmjd6* leads to the imbalanced bivalent domain resolution on gene promoter

In this study, I found that many downregulated genes are developmental genes upon *Jmjd6* loss of function. Epigenetic features like bivalent domains, characterized by active and repressive histone modification such as H3K4me3 and H3K27me3, are essential for key developmental genes silencing in the ES cells while keeping them poised for activation (Bernstein, Mikkelsen et al. 2006). Many marker genes of germ layers like *Eomes*, *Brachyury*, *Mesp1*, *Foxa2*, *Cer1*, *Sox17*, *Sox1*, and *Pax6* are only transiently expressed for a very short time. They are only highly expressed during the hanging drop differentiation for 1-2 days. The bivalent domain on those gene promoter regions is critical for rapid induction and repression in such a short time window. Indeed, most of those genes are marked by H3K4me3 and H3K27me3 at the same time in published ChIP-seq data (Wamstad, Alexander et al. 2012). In addition, our ChIP-seq data also showed high H3K4me3 and H3K27me3 accumulation at those gene promoter regions. A recent study with mouse embryos showed that development genes obtain strong H3K4me3 and H3K27me3 to establish bivalency after embryo implantation (Xiang, Zhang et al. 2020). In addition, I showed that many developmental genes were downregulated due to the imbalanced bivalent domain upon *Jmjd6* knockout.

To sum up, I showed key developmental genes which are critical for gastrulation and heart development are marked by the bivalent domain. Depletion of *Jmjd6* leads to the imbalanced resolution of bivalent domains, resulting in the downregulation of those developmental genes. This study highlights the importance of *Jmjd6* for the proper expression of developmental genes by regulating the bivalent domain.

1.4.3 JMJD6 interacts with splicesome proteins and ribosome proteins

With a 3XFlag-*Jmjd6* knockin mESCs, I identified 129 proteins that interact with JMJD6 by IP coupled with proteomic analysis with mass spectrometry. By clustering those 129 proteins, I found two groups of proteins: splicesome proteins and ribosomal proteins that mainly bind to JMJD6. Consistent with this data, JMJD6 was shown to interact with splicing factors such as U2AF65, Luc7L2, and Luc7L3 (Webby, Wolf et al. 2009, Heim, Grimm et al. 2014) in HEK293 or HeLa cells. In this study, I also identified U2AF65 and LucL3 as partner proteins for *JMJD6* in mESCs. U2AF65 is a subunit of snRNP that binds to the 3' splice site of the pre-mRNA. Luc7L2 and Luc7L3 stabilize the bonding between U2AF and the polypyrimidine tract. In line with the fact that *Jmjd6* interacts with so many spliceosome proteins, *Jmjd6* was reported to be involved in gene alternative splicing during the angiogenesis and E17.5 embryo kidney and brain (Boeckel, Guarani et al. 2011, Yi, Shen et al. 2016). By splicing analysis, I identified about 200 genes with different isoform expressions between WT and *Jmjd6* KO during the hanging drop differentiation and between WT and *Jmjd6*-/- embryos at E8.5.

In vitro incubation of *Jmjd6* and peptides from U2AF65 and Luc7L3 indicated that *Jmjd6* could hydroxylate those proteins (Islam, McDonough et al. 2019). Interestingly, Yi et al. reported that *Jmjd6* could regulate gene alternative splicing in an enzymatic activity-dependent and independent manner (Yi, Shen et al. 2016). Other than hydroxylating splicesome proteins, *Jmjd6* may be functional in a different way that regulates alternative splicing. Given the fact that JMJD6 could bind single-strand RNA, *Jmjd6* could be important for mediating RNA splicing for specific genes which can be recognized and bound by *Jmjd6*.

Another group of proteins that interacts with JMJD6 is ribosome protein. Due to the alternative splicing, *Jmjd6* produces different isoforms that code proteins with a C-terminal difference: the full-length and a truncated protein lacking poly S region. It seems that only truncated JMJD6 lacking poly S region instead of the full-length JMJD6 can bind to ribosome protein. Wolf et al. overexpress GFP fused truncated JMJD6, which lacks poly S region, and full-length JMJD6 in HEK293T. With the GFP pull-down of truncated JMJD6 and MS analysis, they identify 55% (65/118) of those proteins are ribosome proteins (Wolf, Mantri et al. 2013). While the GFP pull-down of full-length JMJD6, only 7% (5/75) of JMJD6 interacted proteins are ribosome proteins. In this study, I knocked in the 3xFlag in the N-terminal of *Jmjd6*. Thus, all *Jmjd6* with or without poly S regions are tagged. So it is not surprising that I detect both groups of proteins interact with *Jmjd6*. It will be interesting to study whether the truncated *Jmjd6,* which seems to bind to ribosome protein specifically, can hydroxylate or demethylate its partner ribosome protein.

In the family of 2-OG-dependent oxygenases, several members, including *Jmjd6*, are relatively small and contain only Jmjc domain. In this sub-family, both NO66 and MIN53 were assigned as demethylase initially but shown to catalyze hydroxylation of ribosomal proteins later. In the following study, MS analysis does not support the demethylase function assigned for those two proteins (Ge, Wolf et al. 2012, Williams, Walport et al. 2014). The assignment of KDM for *Jmjd6* is also controversial. Many studies cannot repeat the demethylase function of *Jmjd6*. Webby et al. found that *Jmjd6* did not produce demethylated arginine histone H4 and H3 fragment peptides. Instead, a hydroxylated product with a clear +16-dalton or +32-dalton was observed (Webby, Wolf et al. 2009). In this study, I did not detect any significant changes in H3K4me3 and H3K27me3 protein levels in *Jmjd6* knockout cells. Considering that JMJD6 binds to a large number of ribosome proteins, JMJD6 could also be a hydroxylase for ribosome proteins.

1.4.4 *Prmt6* are responsible for decreased activate histone marker H3K4me3

In this study, I showed that loss of *Jmjd6* affects gene alternative splicing, especially genes involved in covalent chromatin modification and histone methylation. Among all those genes, I found the arginine methyltransferase *Prmt6* is practically interested. There are two isoforms for *Prmt6*. The difference between those two isoforms is the length of the 3'UTR. According to the annotation of Refseq, the long 3'UTR isoform of *Prmt6* undergoes NMD. I found that the isoform with short 3'UTR of *Prmt6* was significantly increased upon *Jmjd6* knockout. Moreover, the PRMT6 protein level was upregulated in MES and CPC stages upon *Jmjd6* knockout. As I did not find a significant decrease in *Prmt6* mRNA level upon *Jmjd6* knockout, other than that the long 3'UTR isoform of Prmt6 undergoes NMD, it could be that the long 3'UTR isoform is less efficiently translated due to regulation elements on the long 3'UTR.

Interestingly, I observed a gradually decreased expression of the short 3'UTR isoform during the differentiation. The long 3'UTR isoform is not expressed in ES stages but gradually increases during the differentiation. Although the mRNA level of Prmt6 is not changed during the differentiation, the protein level decreases. As only one isoform is expressed in the ES stage, I detect the alternative splicing change for *Prmt6* only in MES and CPC but not in the ES stage. The protein level of PRMT6 is also not changed at the ES stage but increased at later stages like MES and CPC. Considering the repressive character of H3R2m2a, which is produced by PRMT6, decreased protein level of PRMT6 could be required for the differentiation during which many developmental genes start to express.

One way how H3R2me2a represses gene expression is by antagonizing H3K4me3. The methylation of the adjacent arginine residue H3R2 could hamper the methylation of H3K4. Kirmizis et al. reported that H3R2me2a abolish the trimethylation of H3K4 by the Set1 methyltransferase in budding yeast (Kirmizis, Santos-Rosa et al. 2007). At the same time, two independent groups identified *PRMT6* as the major H3 R2 methyltransferase, which leads to H3R2me2a. In addition, they both showed that H3R2me2a prevents methylation of H3K4 as well as the binding of ASH2/WDR5/MLL

family methyltransferase complex (Guccione, Bassi et al. 2007, Hyllus, Stein et al. 2007). With further study of the genome location of *PRMT6*-dependent H3R2me2a, Bouchard showed that *Prmt6* has gene repression function at the promoter region and gene activation function at enhancers. To support the repressive function of *Prmt6*, loss of *Prmt6* in the promoter region leads to enhanced H3K4me3 and upregulated gene expression. Loss of *Prmt6* leads to reduced binding of KMT2D and H3K4me1/H3K27ac deposition with decreased gene expression, indicating activation function of *Prmt6* at enhancers (Bouchard, Sahu et al. 2018).

Indeed, With ChIP-qPCR and ChIP-seq, I showed that H3R2me2a on gastrulation genes and heart development genes are upregulated in MES, and CPCs derived from *Jmjd6* knockout mESCs. In contrast, H3K4me3 was significantly downregulated. Prmt6 overexpressing mESCs mimics the phenotype of *Jmjd6* KO cells during the hanging drop differentiation. I also detected a significant decrease of H3K4me3 on gastrulation genes and heart development genes in *Prmt6* overexpression cells.

1.4.5 *Cbx7* is responsible for the increase of the repressive histone mark H3K27me3

I showed that repressive histone mark H3K27me3 was upregulated on the promoter region of gastrulation and heart development gene in *Jmjd6* knockout cells. PRC2 complex was believed to be responsible for the H3K27me3 modification. However, I did not find any PRC2 complex members whose mRNA expression was dysregulated significantly. Instead, I found that only *Cbx7* from the PRC1 complex was significantly upregulated in MES and CPC stages but not in mESCs. It is reported that a positive loop of PRC1 and PRC2 complex promotes the repressive histone modification H3K27me3 to diminish gene expression (Cooper, Dienstbier et al. 2014, Kalb, Latwiel et al. 2014). *Cbx7* from the PRC1 complex directly recognizes H3K27me3, while the H2AK119ub produced by the PRC1 complex promotes PRC2 complex binding (Cooper, Dienstbier et al. 2014, Kalb, Latwiel et al. 2014). By ChIP-qPCR and ChIP-seq, I showed that the H2AK119ub, mediated by the PRC1 complex, was significantly increased at the promoter region of gastrulation and heart development genes. The higher H2AK119ub accumulation promotes the binding of the PRC2 complex. I then checked Ezh2, which

is the functional enzymatic component of the PRC2 complex. As expected, the binding of Ezh2 at gastrulation and heart development genes was also increased, leading to a higher accumulation of H3K27me3.

That loss of *Cbx7* in mESCs results in downregulation of development, cell differentiation, and cell fate commitment genes, indicates the repressive nature of *Cbx7* for development gene expression (Morey, Pascual et al. 2012). Further analysis of CBX7 ChIP-seq results revealed that CBX7 is bound to genes involved in development processes and mesodermal development in mESCs(Morey, Pascual et al. 2012, Morey, Aloia et al. 2013). This is in line with the compromised mesodermal and progenitor development in *Jmjd6* knockout cells, where the *Cbx7* protein level were significantly elevated in MES and CPC stages. It is reported that *Cbx7* was significantly decreased during the differentiation (Morey, Pascual et al. 2012, Wamstad, Alexander et al. 2012). Other Cbx family members like *Cbx2* and *Cbx4* will replace *Cbx7* in the PRC1 complex, orchestrating the lineage commitment. At the same time, *Cbx7* was repressed to ensure the lineage specification (Morey, Pascual et al. 2012). Consistent with previous reports, I also found that *Cbx7* expression decreased during cardiomyocyte differentiation. *Jmjd6* silencing results in the upregulation of *Cbx7* only in MES and CPC but not in mESCs indicating that *Jmjd6* prevents *Cbx7* repression during the differentiation. The high expressed *Cbx7* maintains the repressive histone marks in MES and CPC stages, leading to compromised lineage commitment. In agreement with this, *Cbx7* overexpression indeed leads to downregulation of gastrulation and heart development genes.

Cbx7 was shown as a direct target of the pluripotency factor *Oct4*, *Nanog* and *Sox2*. At the same time, those three genes were upregulated in *Jmjd6* KO mESCs at MES and CPC stages. The high pluripotency factor expression could also maintain the expression of *Cbx7* during MES and CPC stages.

1.4.6 Conclusion and outlook

In this study, I showed that *Jmjd6* regulates early cell lineage choices and lineage differentiation using both in vitro differentiation and in vivo mouse models. Depletion

of *Jmjd6* results in the downregulation of mesoderm and endoderm marker genes while the ectoderm marker genes are upregulated. During cardiogenesis, *Jmjd6* is important for the expression of the key transcription factor, ligands and receptors, and also extracellular matrix genes. In this study, I first focused on the three germ layer formations. Intersecting our RNA-seq data with single-cell sequencing data from published data, many marker genes of subpopulations during the gastrulation were also dysregulated upon *Jmjd6* knockout. For organ development, I focused on heart development. However, *Jmjd6* knock-out embryos exhibit various phenotypes, including malformation and defects in the heart, lung, spleen, liver, head, and eye. In the following study, single-cell transcriptome in the early embryonic stage can help pinpoint the precise early lineage choices regulated by *Jmjd6* and its potential function for different organs development.

Regarding the mechanism, I identified many splicing factors that interact with *Jmjd6* by IP-MS. Splicing analysis revealed genes involved in chromatin organization and also covalent histone modification to be preferentially altered upon *Jmjd6* loss of function. I showed that *Jmjd6* is important for the bivalent domain balance at lineage choices and heart development genes. I showed that upregulated *PRMT6* protein leads to the higher H3R2me2a, which blocks the H3K4me3 formation in *Jmjd6* knockout cells. Further, I found that *Cbx7* is significantly upregulated, leading to a higher accumulation of H3K27me3. Besides *Prmt6*, It will be helpful to study the alternative splicing of other epigenetic regulations such as *Ktm2b*, *Dnmt3b*, *Trim28*, and *Dnmt1* in detail. The complex phenotype caused by *Jmjd6* loss of function may be further explained. Due to the limitation of second-generation sequencing technology and sequencing depth, many alternative splicing events are challenging to be identified. With advanced technology such as Oxford Nanopore and PacBio, which can sequence very long fragments, I may identify more *Jmjd6*-dependent alternative splicing events, which also help explain the multiple organ development defects of *Jmjd6* knockout mice.

Besides the splicing factors, I also found many ribosome proteins interacting with *Jmjd6.* It seems that only truncated protein lacking poly S region, which is also an isoform of *Jmjd6* due to the alternative splicing, interacts with ribosome protein. It will

be worth making the knock-in cell line to delete the poly S region. By differentiating WT, *Jmjd6* knockout, and this knock-in line, I can identify the unique function of truncated JMJD6 protein lacking poly S region. With Co-IP, specific ribosome protein that interacts with this truncated *Jmjd6* can be identified. With a in vitro incubation of potential peptides from those ribosome proteins and *Jmjd6*, whether *Jmjd6* can hydroxylate or demethylate ribosome protein can be clarified.

Chapter 2. BMP4-p38 MAPK signaling axis controls ISL1 protein stability and activity during cardiogenesis

2.1 Introduction

The heart is the first organ that forms and becomes functional in the vertebrate embryo. It is essential for the circulation of nutrients and removal of waste as soon as the embryos reach a point where diffusion is no longer efficient. In the human population, nearly 1% of newborn children have congenital heart defects and cardiac malformations (Bruneau 2008). Thus, a clear and precise picture of how the heart develops is fundamental for understating the formation of congenital heart disease and paving the road for possible therapy.

2.1.1 Heart development in the mouse embryo

During the gastrulation in embryos at TS 9 or E6.5, cardiac mesoderm cells expressing the earliest cardiac markers *Mesp1* and *Mesp2* start to migrate from the anterior part of the primitive streak and take the anterior-lateral migratory path to form the cardiac crescent at cranial and cranio-lateral parts of the embryo at TS 10 or E7.5 (Figure 2.1.1A and B) (Lawson, Meneses et al. 1991, Tam, Steiner et al. 1997, Saga, Miyagawa-Tomita et al. 1999, Haraguchi, Kitajima et al. 2001, Harvey 2002). In this process, heart mesodermal cells are brought to different niches where they are deployed at different times and in different ways to contribute to the heart. The early differentiating cardiac cells form the cardiac crescent, referred to as the first heart field (FHF), which will fuse at the midline to form the primitive cardiac tube. Cardiac progenitor cells that mainly lie medially and posteriorly to the crescent are referred to as the second heart field (SHF) (Figure 2.1.1B). FHF-derived cardiac tubes, which serve as a scaffold for the subsequent growth of the heart, mainly contribute to the left ventricle.

In contrast, SHF-derived cardiac progenitor mainly contributes to the right ventricle and outflow tract. From E8, the heart tube starts to loop through the addition of

cardiac neural crest cells (cNCC), which migrate from the pharyngeal arches (PA) to the arterial pole (AP) and cells from the proepicardial organ (PEO), which is a transitory mesenchymal structure at the posterior end of the heart tube (Figure 2.1.1C, D and E) (Brand 2003, Vincent and Buckingham 2010). This looped cardiac tube is constituted by the contractile myocardium, which pumps blood in the developing embryo. Within E10.5, cardiac compartments are formed, which include the outflow tract (OFT), right atrium (RA), left atrium (LA), right ventricle (RV), and left ventricle (LV) (Figure 2.1.1F and G).

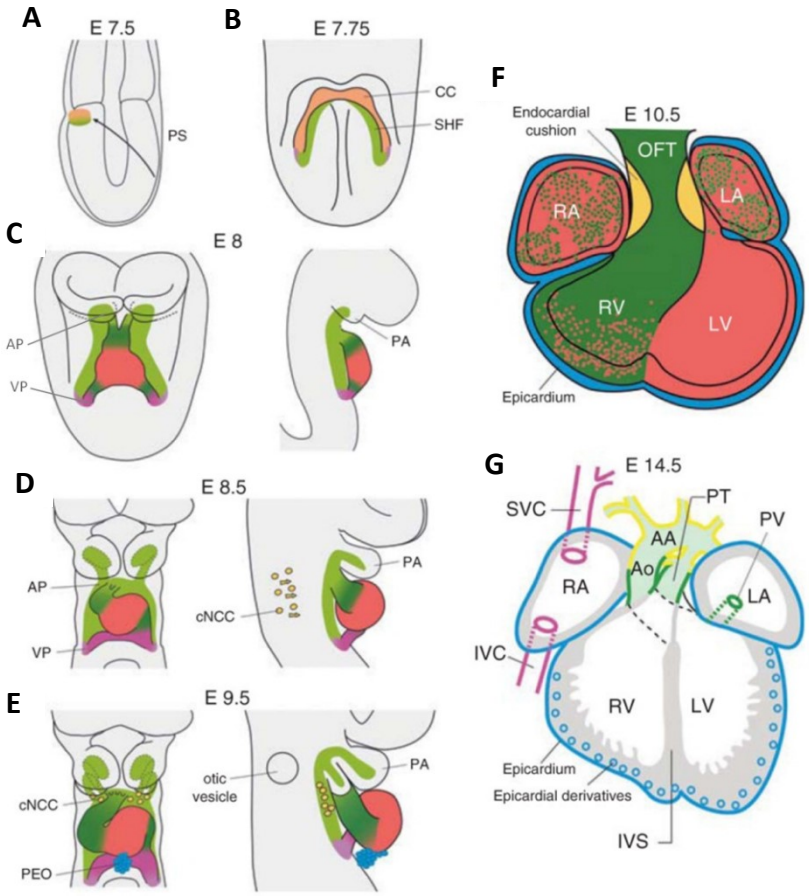

Figure 2.1.1. Schematic representation of key sages in the heart development. (A) Cardiac mesoderm cells migrate from primitive streak (PS). **(B)** Formation of the cardiac crest (CC) and second heart field (SHF) at E7.5. **(C)** Linear heart tube with SHF progenitors in atrial pole (AP) and venous pole (VP) (light green and dark green). **(D-E)** The heart starts looping with the contribution of cells from cardiac neural crest cells (cNCC) and proepicardial organ (PEO). **(F)** Looped heart with outflow tract (OFT), right atrium (RA), left atrium (LA), right ventricle (RV), and left ventricle (LV). **(G)** The mature heart. Interventricular septum (IVS), aortic arch (AA), aorta (AO), pulmonary trunk (PT), pulmonary vein (PV), superior caval vein (SVC), inferior caval vein (IVC), and pharyngeal arches (PA) (modified from (Vincent and Buckingham 2010)).

2.1.2 Important transcription factors in heart development

2.1.2.1 Transcription factors in early cardiac mesoderm cells

One of the earliest maker genes for cardiac progenitor cells is *Mesp1* (Saga, Miyagawa-Tomita et al. 1999). It is expressed in the early mesoderm, giving extraembryonic and cranial-cardiac mesoderm. Meps1 was shown to act as a master regulator for cardiovascular cell fate decisions by directly binding to regulatory DNA sequences located in the promoter of many key genes in the core cardiac transcriptional machinery (Bondue, Lapouge et al. 2008). *Mesp1* knock-out mice showed abnormal heart morphology and cardia bifida (Saga, Miyagawa-Tomita et al. 1999). In addition, the migration of precardiac mesoderm cells from the primitive streak in the anterolateral direction is also dependent on *Mesp1* expression (Saga, Miyagawa-Tomita et al. 1999). During gastrulation, *Mesp1* is directly regulated by T-box transcription factor Brachyury (*T*) and Eomesodermin (*Eomes*) (Costello, Pimeisl et al. 2011, David, Jarsch et al. 2011).

2.1.2.2 Pan cardiac, FHF, and SHF transcription factor

At the initial step of heart development, cardiac progenitor cells of the FHF start differentiating into a contractile myocardium and form a linear heart tube that pumps blood in embryos. Some genes such as *Gata4*, *Hand1,* and *Tbx5,* which are restrictively expressed in FHF and the heart structures derived from FHF, are considered the marker genes for the FHF (Andersen, Tampakakis et al. 2018). The SHF contributes to the outflow tract and most right ventricular myocardium. Genes including *Isl1*, *Tbx1,* and *Hand2* are considered the marker genes for SHF (Black 2007). There are also genes like *Tbx20*, *Nkx2*-5, and *Mef2c* expressed in both FHF and SHF. Those genes are referred to as the pan-cardiac genes (Singh, Christoffels et al. 2005).

One of the transcription factors family which plays an essential role in heart development is the GATA family of zinc-finger. In Vertebrate, *Gata4*, *Gata5,* and *Gata6*

are expressed in the heart (Molkentin 2000). *Gata4*-/- mice die between E8 to E9 because of defects in heart morphogenesis and ventral closure of the foregut. Specifically, *Gata4* null embryos show cardia bifida phenotype due to the ineffective ventral fusion of the lateral aspects of the embryos and the subsequent formation of the foregut (Soudais, Bielinska et al. 1995, Kuo, Morrisey et al. 1997, Narita, Bielinska et al. 1997). In addition, *Gata4* haploinsufficient embryos which lost 70% of *Gata4* die between day 13.5 and 16.5 with atrioventricular canal, double outlet right ventricle, hypoplastic ventricular myocardium (Pu, Ishiwata et al. 2004). *Gata6* null embryos survive until E10.5 with the phenotype of reduced ventricular trabeculation (Zhao, Watt et al. 2005).

The bHLH factors *Hand1* and *Hand2* are members of the twist-family and are broadly expressed throughout development in many tissues: neural crest, cardiac outflow tract, developing limbs, and most significantly, the cardiomyocyte. In mice, *Hand1* expression restricts to the left ventricle and OFT, whereas *Hand2* expression restricts to the right ventricle and OFT (McFadden, Barbosa et al. 2005). *Hand1* null embryos die at E8-8.5 form severe placental and extra-embryonic defects, making it difficult to analyze its function in heart development. Nevertheless, *Hand1* null embryos rescued by aggregation of tetraploid blastomeres show that *Hand1* null embryonic stem cells failed to contribute to the left ventricle of chimeric mouse embryos. These embryos can survive until E10.5 and show abnormal heart looping (Riley, Anaon-Cartwight et al. 1998, Riley, Gertsenstein et al. 2000). McFadden et al. generated conditional knockout embryos for *Hand1* with MHC-Cre or Nkx2-5-Cre. Those embryos showed dysregulated ventricular gene expression but could survive until the perinatal period, when they died from cardiac abnormalities (McFadden, Barbosa et al. 2005). During the cardiogenesis, *Hand2* is expressed in the entire primary heart tube during the early embryonic stages, while as the heart tube loops, it starts to express in the right ventricle and outflow tract. Embryos with systemic *Hand2* deletion die at E9.5 due to hypoplastic right ventricle and OFT vascular defects(Srivastava, Thomas et al. 1997, Yamagishi, Yamagishi et al. 2001).

The T-Box, a highly conversed DNA binding domain, is presented in all T-box family proteins. Members of the T-box family such as *Tbx1*, *Tbx2*, *Tbx3*, *Tbx5*, *Tbx18*, *and*

Tbx20 regulate cardiac development, and many of them have been implicated in human genetic syndromes with congenital cardiac malformations.

Tbx5 is expressed in the cardiac crescent in the early embryonic stage uniformly. When a linear heart tube is formed, *Tbx5* is expressed in a gradient manner with a higher level at the posterior end and a lower level at the anterior end. This graded expression pattern is determined by retinoic acid signaling (Liberatore, Searcy-Schrick et al. 2000, Niederreither, Vermot et al. 2001). In the looped heart, *Tbx5* is mainly expressed in the left ventricle and absent in the right ventricle and outflow tract (Bruneau, Logan et al. 1999). *Tbx5* haploinsufficiency causes cardiac abnormalities, including atrial and ventricular septal defects, hypoplastic left heart, and conduction anomalies. *Tbx5* null embryos show severe hypoplasia of posterior domains in the developing heart (Bruneau, Nemer et al. 2001). In the looped heart tube, *Tbx20* is expressed across the myocardium and strongly in endothelial cells of endocardial cushions (Stennard, Costa et al. 2003, Stennard and Harvey 2005, Takeuchi, Mileikovskaia et al. 2005). Embryos with loss of *Tbx20* show failed cardiac looping, hypoplastic heart, and lack of cardiac chamber differentiation (Stennard, Costa et al. 2003, Brown, Martz et al. 2005, Cai, Zhou et al. 2005, Singh, Christoffels et al. 2005, Takeuchi, Mileikovskaia et al. 2005). The expression of cardiac genes like *Nkx2-5*, *Gata4*, and *Mef2c*, and the cardiac inducers *Bmp2/5*, is downregulated or delayed upon *Tbx20* deletion. In contrast, *Tbx2* is upregulated in *Tbx20* null embryos dramatically. As a transcriptional repressor, *Tbx2* inhibits cell proliferation and chamber differentiation (Cai, Zhou et al. 2005, Singh, Christoffels et al. 2005).

Nkx2-5 is a member of the NK homeobox transcription factor with a DNA-binding domain (Kim and Nirenberg 1989). In the early heart progenitor cells from both the first and second heart field, *Nkx2-5* is highly expressed and continues to be highly expressed in the heart thought adulthood (Komuro and Izumo 1993, Lints, Parsons et al. 1993, Kasahara, Bartunkova et al. 1998, Stanley, Biben et al. 2004). *Nkx2-5* null embryos die around E9-E10 due to the arrested heart looping and growth retardation (Lyons, Parsons et al. 1995, Tanaka, Chen et al. 1999, Biben, Weber et al. 2000). More recently, it was shown that *Nkx2-5* loss of function induces the over-specification of cardiac progenitors at the early stage of heart development. This cardiac progenitor

over-specification was due to the elevation of the bmp2-smad signaling pathway, which controls cardiac specification and progenitor state maintenance. The over-specification of cardiac progenitors further reduces SHF proliferation and OFT truncation (Prall, Menon et al. 2007).

Mef2c is a transcription factor belonging to an evolutionary conserved MADS-box family. There are four *Mef2* genes in mice, including *Mef2a*, *Mef2b*, *Mef2c*, and *Mef2d*. *Mef2c* gene expresses in the cardiac mesoderm that gives rise to the primitive heart tube (Edmondson, Lyons et al. 1994). By E8.5, *Mef2a*, *Mef2c*, and *Mef2d* are all detected in the myocardium. *Mef2c* null embryos show defects in heart looping and loss of right ventricle and die around E9.5 (Lin, Schwarz et al. 1997). However, the conditional knockout *Mef2c* with MHC-Cre shows that myocardial-specific removal of *Mef2c* resulted in viable offspring, which indicates either *Mef2c* is not involved in the formation of the heart after looping morphogenesis or compensation from *Mef2a* and *Mef2d*. (Vong, Ragusa et al. 2005).

2.1.3 p38 MAPK signaling pathway

The mitogen-activated protein kinase (MAPK) pathway plays a key role in bridging extracellular signals to intracellular responses. MAPK signaling pathway is a chain of kinase activation, including MAP4K, MAP3K, MAP2k, MAPK, and MAPK-activated protein kinase (MAPKAPK). There are four major MAPK pathways which are extracellular signal-regulated kinases (ERK) MAPK, the Jun N-terminal kinase (JNK) MAPK, ERK5 MAPK, and p38 MAPK (Guo, Pan et al. 2020).

In the p38 MAPK family, there are four p38 with approx. 60% identical in their amino acid sequence. p38α, p38β, p38γ, and p38δ are encoded by different genes and have tissue-specific expression patterns. The various stimulus can activate the p38 MAPK signaling pathway, such as growth factors, environmental stresses, and inflammatory cytokines. The consequent activation of p38 MAPK is involved in multiple cellular responses, including proliferation, differentiation, and death (Clark, Sarafraz et al. 2007). It has been shown that MKK3, MKK6, and in some cases, MKK4 can activate p38

(Figure 2.1.2). The upstream MAP3Ks such as ASK1 (apoptosis signal-regulating kinase 1), DLK1 (dual-leucine-zipper-bearing kinase 1), TAK 1(TGFβ-activated kinase 1), TAO (thousand-and-one amino acid) 1 and 2, TPL2 (tumor progression loci 2) MLK3 (mixed-lineage kinase 3), MEKK (MAPK/ERK kinase kinase) 3 and MEKK4, and ZAK1 (leucine zipper and sterile-α motif kinase 1) have been shown to activate p38 MAPK signaling pathway (Figure 2.1.2).

p38α is involved in a wide range of signaling pathways that regulate different biological functions (Cuadrado and Nebreda 2010). Growing evidence showed that p38α also plays an important role in mammalian embryonic development, suggesting a physiological role for this isoform (Allen, Svensson et al. 2000). In a healthy heart, among all the p38 MAPK isoforms, p38α is the primary form, whereas p38β, p38γ, and p38δ are expressed at a low level (Lemke, Bloem et al. 2001). Furthermore, the transcription factor Ap-1 has been shown to be the downstream target of p38-signaling to regulate cardiomyocyte differentiation and proliferation. (Eriksson and Leppä 2002). Additionally, p38-signaling plays a role in the early switch between cardiogenesis and neurogenesis (Aouadi, Bost et al. 2006).

At the molecular level, all these signals induce signaling cascades, which converge in the nucleus to regulate the activity of various transcription factors and epigenetic regulators at the transcriptional and post-translational levels. For example, the TAK1/p38 MAPK signaling pathway induced by Bmp signals promotes cardiac differentiation by upregulating the expression of the key cardiac transcription factors Gata4 and Nkx2-5 (Monzen, Shiojima et al. 1999), whereas p38α-dependent Mef2c phosphorylation induces Mef2c translocation in the nucleus (Hernandez-Torres, Martinez-Fernandez et al. 2008).

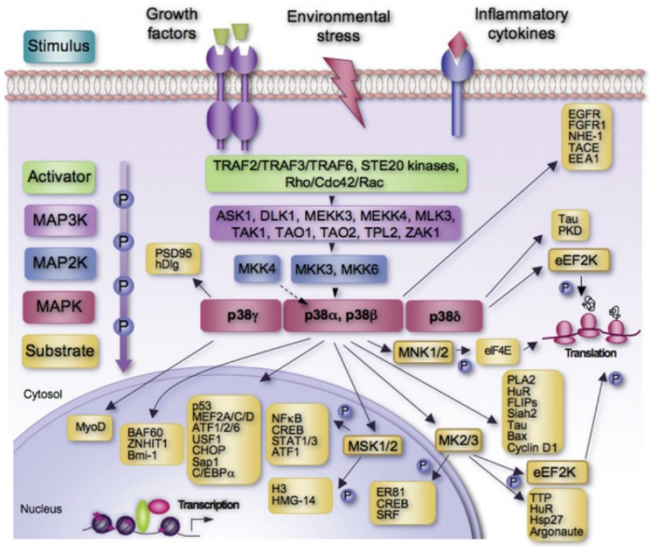

Figure 2.1.2. The p38 MAPK pathway. Various stimuli, including growth factors, inflammatory cytokines, or various environmental stresses, can activate p38 MAPKs. Through the cascade activation, many downstream targets, including protein kinases, cytosolic substrates, transcription factors, and chromatin remodelers, are activated. CHOP, C/EBP-homologous protein; DLK1, dual-leucine-zipper-bearing kinase 1; EEA1, early-endosome antigen 1; eEF2K, eukaryotic elongation factor 2 kinase; eIF4E, eukaryotic initiation factor 4E; HMG-14, high-mobility group 14; NHE-1, Na+/H+ exchanger 1; PLA2, phospholipase A2; PSD95, postsynaptic density 95; Sap1, SRF accessory protein 1; STAT, signal transducer and activator of transcription; TAO, thousand-and-one amino acid; TPL2, tumour progression loci 2; TTP, tristetraprolin; ZAK1, leucine zipper and sterile-α motif kinase 1; ZNHIT1, zinc finger HIT-type 1. (modified from (Cuadrado and Nebreda 2010))

2.1.4 Bmp4 singling pathway in heart development

The bone morphogenetic proteins (BMPs) were initially discovered because they can induce the formation of bone and cartilage in ectopic sites. They belong to the transforming growth factor β superfamily, which comprises a subfamily of more than 20 members. BMP binds to two type I and two type II receptors to form a complex. Next, type II receptor phosphorylate type I receptor, which further phosphorylates SMAD1, SMAD5, or SMAD8. The activated SMAD binds to SMAD4 to form SMAD-complex, which is accumulated in the nucleus and affects gene expression directly or indirectly (Figure 3). As an inhibitory SMADs, SMAD6 preferentially inhibits SMAD signaling initiated by BMP. However, *Madh6* (which encodes the SMAD6 protein) mutation mice have multiple cardiovascular abnormalities, including hyperplasia of cardiac valves and outflow tract septation defects (Galvin, Donovan et al. 2000). Besides this pathway, type II receptors can transmit the signal through Mapk-signaling. For instance, BMP signaling can be mediated by MAP3K7/MAP3K7IP1 (Tak1/Tab1),

which activates p38 MAPK, PI3 kinase (PIK3), RAS, MAPK1 (ERK), and MAPK8 (JNK) (Nohe, Keating et al. 2004).

In mice, *Bmp2*, *Bmp4*, *Bmp5*, and *Bmp7* are expressed in the anterior mesoderm, which gives rise to heart-forming regions (Zhang and Bradley 1996, Dudley and Robertson 1997, Solloway and Robertson 1999). Ectopic delivery of *BMP2* medial but not lateral to the heart forming region leads to expansion of the expression domain of *Nkx2-5*, *Tbx2*, *Gata4*, *Gata5*, *Gata6*, and *smad6* (Schultheiss, Burch et al. 1997, Schlange, Andrée et al. 2000, Yamada, Revelli et al. 2000). The feedback repression of the *Bmp2*/*Smad1* signaling pathway by *Nkx2-5* is critical for SHF proliferation and outflow tract morphology (Prall, Menon et al. 2007). Both *Bmp2* and *Bmp4* regulate *Tbx2* expression, a transcriptional repressor expressed in the AVC and OFT. Cardiac deletion of *Bmp2* with Nkx2.5-Cre results in down-regulation of *Tbx2*, leading to the extension of ventricular formation into the region of the AVC (Ma, Lu et al. 2005). Deletion of Bmp4 in the cardiac lineage with Nkx2-5-Cre results in aberrant septation of the proximal OFT (Liu, Selever et al. 2004). Conditional deletion of Bmp4 with AHF specific Mef2c-Cre results in an insufficient number of cells for developing OFT endocardial cushions, defective cushion remodeling, ventricular septal defects, and abnormal semilunar valve formation (McCulley, Kang et al. 2008).

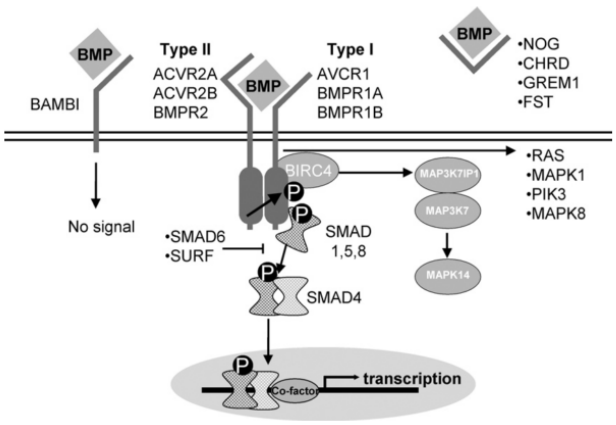

Figure 2.1.3. Bmp signaling pathway. Dimerized Bmp bind to two distinct classes of transmembrane serine-threonine receptor kinases: type I and type II. Type II receptor is constitutively active and phosphorylates type I to form an activated complex. This activated complex further phosphorylates SMAD proteins, which bind to Co-Smads like SMAD4 to form the SMAD complex. This complex will accumulate in nuclear and regulate gene expression directly or indirectly. Besides this transduction pathway, activated type I receptors can also induce p38-, JNK-, or NF-kB-signaling. (modified from (van Wijk, Moorman et al. 2007))

2.1.5 *Isl1* gene, protein, and function in heart development

Islet1(Isl1) was identified first time by screening proteins that can bind to insulin I gene enhancers (Karlsson, Thor et al. 1990). A later study showed that ISL1 is a LIM-homeodomain transcription factor with two LIM domains, one homeodomain (HD) and one LIM homeobox 3 (Lhx3)-binding domain (LBD). Through the homeodomain, ISL1 binds to DNA. The two LIM domains in ISL1 protein, like other members in the LIM-homeodomain transcription factor family, serve for protein interaction. For instance, through the LIM domain, ISL1 binds to the LIM interaction domain (LID) of LDB1 (Caputo, Witzel et al. 2015). The LBD in the c-terminal allows ISL1 to bind to other LIM-HD proteins such as LHX3. In motor neurons, ISL1, LDB1, and LHX3/4 form a ternary complex which is important for motor neuron-specific gene expression.

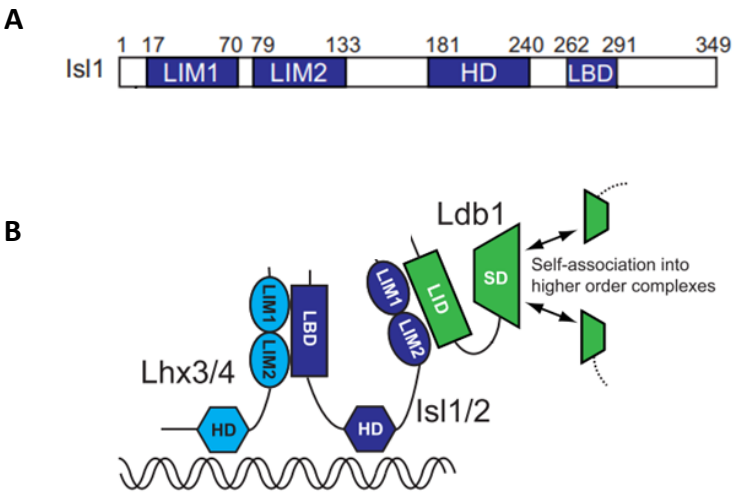

Figure 2.1.4. Multiple domains of ISL1 enable it to bind to different molecules. (A) Schematic representation of ISL1 protein domains. **(B)** ISL1 (blue) binds to DNA by HD; ISL1 binds to /4 (cyan) by LBD; ISL1 binds to LDB1(green) by LIM domain. (Modified from (Gadd, Jacques et al. 2013))

During the embryogenesis, *Isl1* is expressed in multiple cell types, including the pharyngeal/foregut endoderm and the cardiac mesoderm (Ahlgren, Pfaff et al. 1997, Cai, Liang et al. 2003), limb (Yang, Cai et al. 2006), pancreas (Ahlgren, Pfaff et al. 1997), and brain (Pfaff, Mendelsohn et al. 1996). *Isl1* is detected as early as E7.0 in cardiac progenitor cells. At this stage, *Isl1* was found not co-expressed with *Mlc2a* but rather

expressed in cells contiguous with, but medial and dorsal to, *Mlc2a* expressing cells (Figure 2.1.5A) (Cai, Liang et al. 2003). With an *Isl1*-nlacZ knock-in mouse line, Sun et al. demonstrated that *Isl1* is widely expressed in the outflow tract and partially in the right atria and right ventricle at E8.5 (Figure 2.1.5B) (Sun, Liang et al. 2007). As the heart develops, *Isl1* expression decreases in differentiating progenitor cells. Until E14.5, *Isl1* can be found in the outflow tract, aorta, pulmonary artery, right ventricle, venous valves, atrial septum, and sinoatrial (SA) and atrioventricular (AV) node (Figure 2.1.5 C to E). At postnatal day 3, *Isl1* is still expressed but in a very restricted area in the heart, including cardiac ganglia, the region of the sinoatrial node, and at the base of the aorta/pulmonary artery (Figure 2.1.5F) (Sun, Liang et al. 2007).

Importantly, the pivotal role of *Isl1* in heart development was demonstrated by the total loss of SHF-derived heart structure in the *Isl1*-null embryo. Those *Isl1* positive progenitor cells contribute to the multiple cardiovascular cells of distinct lineages, including myocyte, conduction system, endothelial, and smooth muscle lineages allowing heart growth and complex morphogenetic patterning (Cai, Liang et al. 2003). *Isl1* also orchestrates a complex gene regulatory network driving SHF development and cardiac progenitor cell function (Cai, Liang et al. 2003, Caputo, Witzel et al. 2015, Gao, Liang et al. 2019). Consistent with its important function in the SHF, *Isl1*-deficiency results in the loss of all structures derived from the SHF, including the right ventricle (RV), the outflow tract (OFT), and large portions of the atria (Cai, Liang et al. 2003, Laugwitz, Moretti et al. 2005). In addition, growing evidence suggests the association of *Isl1* genetic variations with congenital heart disease (Friedrich, Dilanian et al. 2013, Wang, Song et al. 2019). Despite the important role of *Isl1* in heart development and disease, how its transcriptional activity is regulated is poorly understood.

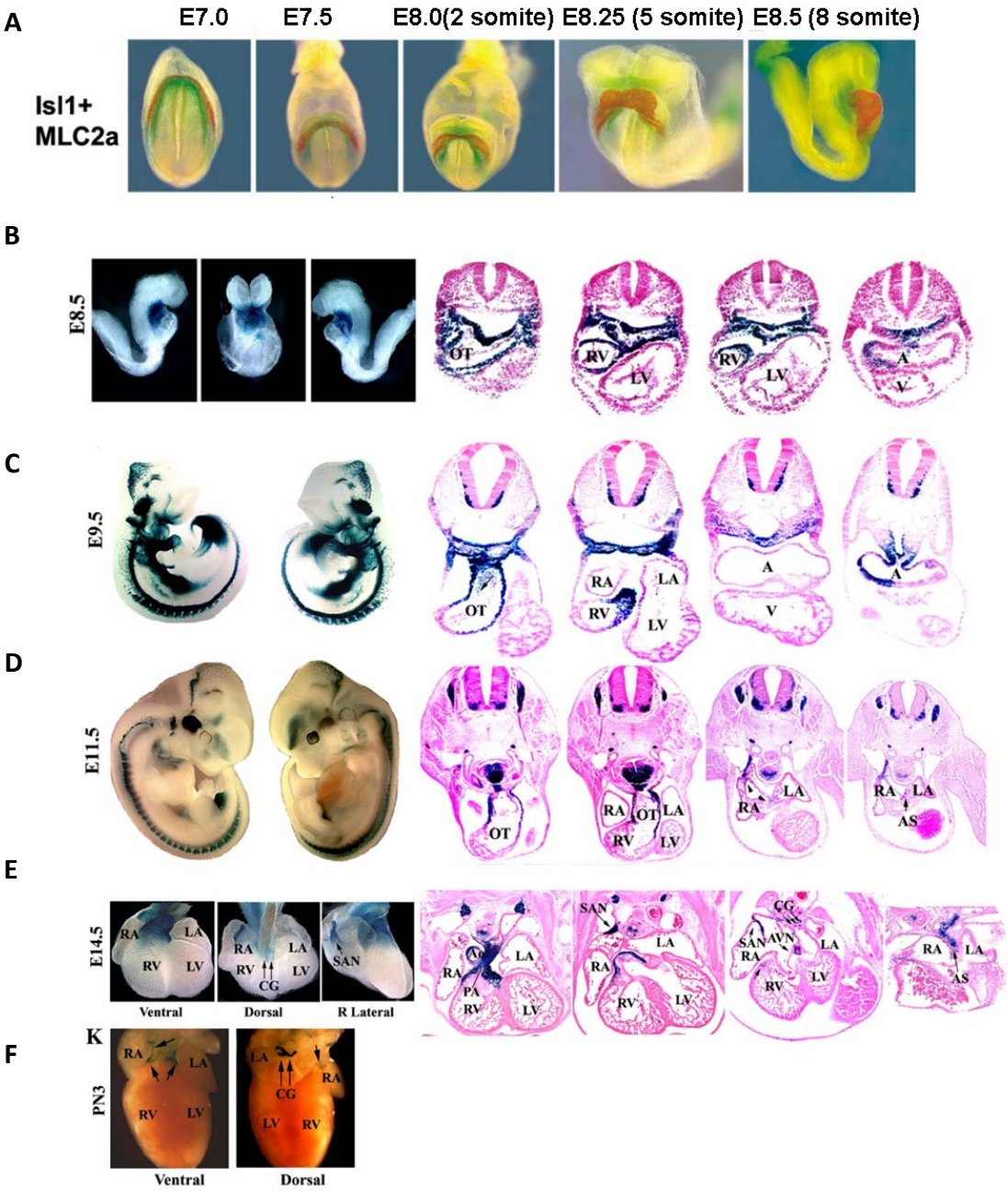

Figure 2.1.5. *Isl1* expression pattern during heart development. **(A)** In-situ hybridization of *Isl1* mRNA (green) and *Mlc2a* mRNA (red) for embryos from E7.0 to E8.5. **(B)** E8.5 *Isl1*-nlacZ knock-in embryos stained with X-gal in left, frontal, and right views revealed active expression of β-gal in foregut endoderm, splanchnic mesoderm (left). Corresponding sections of ED8.5 (10 somites) embryos are shown from anterior to posterior (right). **(C)** E9.5 *Isl1*-nlacZ knock-in embryos stained with X-gal in left and right views (left). Corresponding sections from anterior to posterior revealed *Isl1*-nlacZ expression within the outflow tract, right atria, and right ventricle (right). **(D)** E11.5 Isl1-nlacZ knock-in embryos stained with X-gal in left and right views (left). Corresponding sections from anterior to posterior revealed *Isl1*-nlacZ expression within the outflow tract, atrial septum, and sinoatrial and atrioventricular nodes

(right). **(E)** E14.5 *Isl1*-nlacZ knock-in embryo hearts stained with X-gal in ventral, dorsal, and lateral dorsal views (left). Corresponding sections from ventral to dorsal revealed *Isl1*-nlacZ expression within the outflow tract, aorta, pulmonary artery, atrial septum, venous valves, cardiac ganglia, as well as sinoatrial and atrioventricular nodes (Right). **(F)** At postnatal day 3, *Isl1*-nlacZ expression was observed in cardiac ganglia, the region of the sinoatrial node, and at the base of the aorta/pulmonary artery. A: atria; AS: atria septum; AVN: atrioventricular node; CG: cardiac ganglia; LA: left atria; LV: left ventricle; OT: outflow tract; RA: right atria; SAN: sinoatrial node. (modified from ((Cai, Liang et al. 2003, Sun, Liang et al. 2007))

2.2 objective

Isl1 plays a key role in heart development, especially second heart field development. The total SHF-derived heart structures, including the RV, the OFT, and large portions of the atria, were lost in the *Isl1*-null embryo. Due to the alternative splicing, two Isl1 isoforms code two proteins, ISL1α and ISL1β. ISL1α is the predominant isoform and undergoes phosphorylation (Ando, Shioda et al. 2003). As one of the most important post-translational modifications, phosphorylation plays an essential role in regulating protein stability, activity, and interaction. In this study, we aimed to 1) Identify the kinase responsible for ISL1 phosphorylates and the consequence of this phosphorylation, 2) investigate the effect of this phosphorylation during heart development, and 3) pinpoint the signaling pathway controlling ISL1 phosphorylation.

2.3 Result

2.3.1 ISL1 is phosphorylated by p38 MAPK at serine 269

There are two different isoforms of *Isl1* that exist, ISL1α (predominant) and ISL1β (Ando, Shioda et al. 2003). Due to the recognition of an alternative splicing acceptor site in the fifth exon, ISL1β lacks 23 amino acids in the carboxy-terminal part of the protein. Different from ISL1β, ISL1α is mainly phosphorylated, but the exact mechanism and function of ISL1 phosphorylation are not fully addressed. To identify the ISL1 phosphorylation site, Hagen Witzel mutated all serines and threonines within the 255-279 region, lacking in ISL1β (Figure 2.3.1A), to alanine to prevent phosphorylation. He found that only the S269A mutant protein showed a single band identical to the lower unphosphorylated band of ISL1 and to the wild-type ISL1 protein treated with alkaline phosphatase (Figure 2.3.1B, C). Those data suggest that ISL1 is phosphorylated at S269. On the contrary, mutagenesis of T261A and T263A did not show an altered pattern compared to wild type (typical two-band pattern). To further study ISL1 S269 phosphorylation, a ISL1 phospho-specific antibody recognizing the phosphorylation consensus encompassing S269 was generated. He also observed significant reactivity of the antibody with wild-type ISL1 protein and no reactivity with ISL1 S269A mutant (Figure 2.3.1C). Next, He studied which kinase might induce S269 phosphorylation of ISL1 protein. Computational prediction using NetPhosK 1.0 (http://www.cbs.dtu.dk/services/NetPhosK/) revealed that GSK3 and p38 MAPK might be responsible for ISL1 S269 phosphorylation as putative serine/threonine kinases (Figure 2.3.1D). To determine which was responsible for ISL1 phosphorylation, I treated ISL1 overexpressing HEK293T cells with p38 or GSK3 inhibitor. Importantly, the selective and potent p38 MAPK inhibitor SB202190 significantly inhibited ISL1 S269 phosphorylation, whereas GSK3 inhibition, including bio and CHIR99021, did not inhibit ISL1 S269 phosphorylation (Figure 2.3.1E). Similarly, by in vitro kinase assay using recombinant ISL1 protein and protein extracts treated with DMSO or SB202190, Yanyan Jing revealed that ISL1 phosphorylation was significantly reduced in the

presence of the p38 inhibitor (Figure 2.3.1F). To further study the role of p38 MAPK in ISL1 phosphorylation, She performed co-immunoprecipitation and in vitro kinase assays with purified proteins. p38α was immunoprecipitated together with ISL1, indicating a direct role of p38 on ISL1 phosphorylation (Figure 2.3.1G). Further, She performed in vitro kinase assay using recombinant ISL1 protein and immunopurified kinases and showed that p38α but not its upstream kinase MKK6 or dominant-negative mutant p38α-AF, harboring mutations of the activating phosphorylation sites (kinase-deficient), could phosphorylate ISL1 (Figure 2.3.1H). She further identified that mainly p38α and p38δ were able to phosphorylate ISL1 while p38β and p38γ were not able to (Rose, Force et al. 2010) (Figure 2.3.1I). Taken together, those results indicate that ISL1α is phosphorylated by the p38 MAPK at S269.

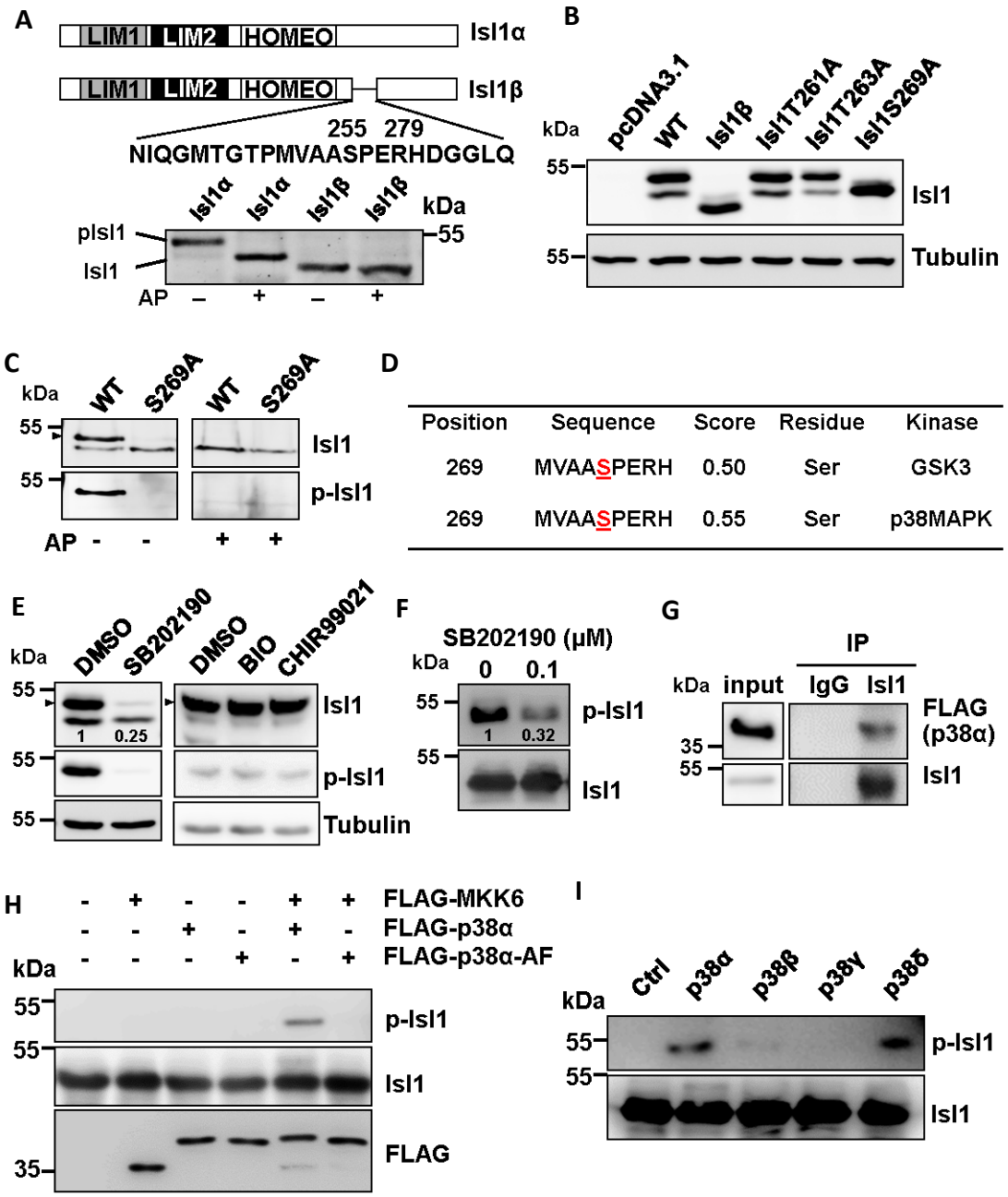

Figure 2.3.1. ISL1 is phosphorylated by p38 on serine 269. (A) Schematic representation of the difference between ISL1α and ISL1β (top panel). Alkaline phosphatase (AP) treatment of lysate from cells expressing either ISL1α or ISL1β, showing that the ISL1β is not phosphorylated. **(B)** Western blot (WB) analysis of lysate of cells expressing ISL1α harboring different mutations in the serine or threonine residues within the 256–278 region. **(C)** AP treatment of lysate from either WT ISL1α or ISL1αS269A overexpressing cells, showing that ISL1αS269A mutant can not be phosphorylated. Phosphorylated ISL1 antibody, raised against synthetic ISL1 phospho-S269-peptide, detected phosphorylated ISL1 only in the lysate of ISL1 overexpressing but not the S269A mutant overexpressing cells. Arrowheads indicate phosphorylated

ISL1 in this and the following figure panels. **(D)** Results of predictions of protein phosphorylation sites and potential kinases using NetPhosK1.0. The potentially modified residues are underlined. **(E)** WB showing ISL1 protein levels in ISL1 overexpressing HEK293T cells treated either with DMSO, 50 mM p38 inhibitor SB202190, or with the GSK3 inhibitors, 2.5 mM BIO and 5 mM CHIR-99021 for 16 h. **(F)** In vitro kinase assay using total protein extracts from cells treated with or without SB202190 incubated with recombinant ISL1. **(G)** Co-immunoprecipitation of cell lysate of HEK293T cells overexpressing ISL1 and FLAG-p38a using ISL1 antibody followed by WB analysis. **(H)** In vitro kinase assay with recombinant ISL1 incubated with different combinations of immunopurified MKK6, p38a, and kinase-deficient p38a (p38a-AF) proteins. FLAG-tagged kinases were overexpressed alone or in combinations and then immunoprecipitated using FLAG antibody. **(I)** In vitro kinase assay with recombinant ISL1 incubated with different p38 MAPK isoforms together with immunopurified MKK6. Experiments for figure 2.3.1 A, B, C and D were done by Hagen Witzel. Experiments for figure 2.3.1 F, G, H and I were done by Yanyan Jing.

2.3.2 Phosphorylation of ISL1 by p38 protects it from proteasomal degradation and preserves its transcription activity

Phosphorylation of proteins often alters their physical and chemical properties, including folding, stability, activity, and function. Thus, next, Yanyan Jing tested whether ISL1 phosphorylation might affect its transcriptional activity. She transfected NIH3T3 with *Isl1* together with a luciferase reporter construct containing the *Mef2c* cardiac-specific enhancer, which is directly bound and activated by Isl1 (Caputo, Witzel et al. 2015). That ISL1 is highly phosphorylated in NIH3T3 cells allows us to study the effect of modulation of ISL1 phosphorylation on its transcriptional activity. She performed luciferase assay in *Isl1*-overexpressing NIH3T3 cells with treatment of DMSO or indicated concentration of SB202190. Importantly, treatment with the p38 inhibitor SB202190 led to a dose-dependent decrease of reporter activity (Figure 2.3.2A). Next, she examined whether p38 inhibition affects ISL1 protein levels and thereby decreases its transcriptional activity. Indeed, she found dramatically lower ISL1 levels in cells treated with SB202190 (Figure 2.3.2B), suggesting that by affecting its protein stability, ISL1 phosphorylation by the p38 pathway regulates ISL1 transcriptional activity. Consistent with these results, I activated p38 signaling by either adding the serum to serum-starved NIH3T3 overexpressing ISL1 or by treating the p38 agonist anisomycin, leading to an increase of ISL1 protein levels and transcriptional activity (Figure 2.3.2C-F).

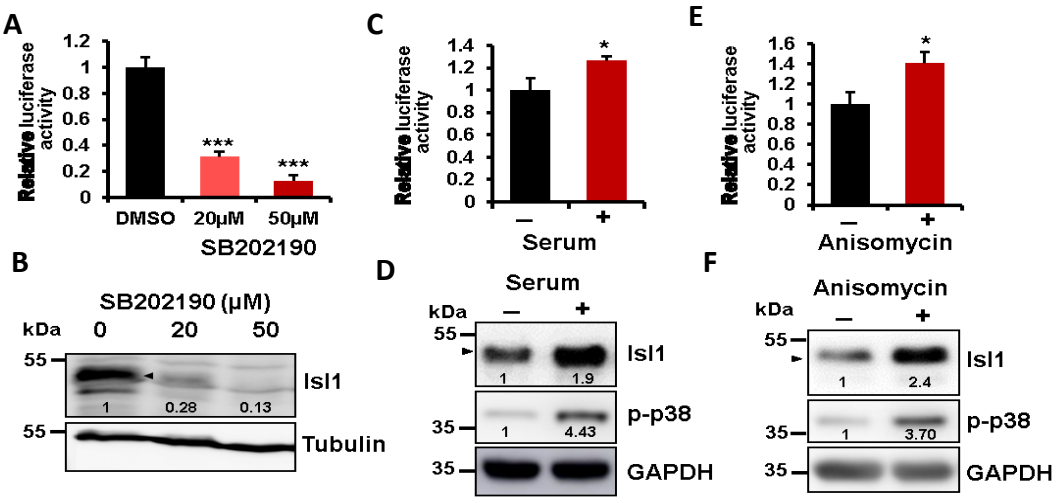

Figure 2.3.2. ISL1 phosphorylation by the p38 affects its transcription activity by preserving ISL1 protein stability. (A and B) Luciferase assay of DMSO or the p38 inhibitor SB202190 treated NIH3T3 cells expressing *Isl1* and a *Mef2c* anterior heart field (AHF) enhancer reporter construct (pGL4-Mef2cPromoter-Luc2-AHF) (n = 3) **(A)** and WB analysis for ISL1 of the cell lysate used in the Luciferase assay **(B)**. **(C–F)** Luciferase assay of Isl1 overexpression NIH3T3 cells transfected with the *Mef2c* reporter construct and treated with or without 10% fetal bovine serum for 1 h (n = 3) **(C)** or with or without 0.01 mM anisomycin for 1 h (n = 3) **(E)**, and WB analysis for ISL1 of the cell lysate used in the Luciferase assay **(D, F)**. Expirment for Figur3 2.3.2 A and B were done by Yanyan Jing.

Our lab has previously reported that ISL1 protein levels are tightly regulated by the proteasome system (Caputo, Witzel et al. 2015). To assess whether p38 inhibition induces ISL1 degradation due to ubiquitination, Yanyan Jing co-expressed HA-tagged ubiquitin and FLAG-tagged *Isl1* in HEK293T cells. Identical amounts of total protein were immunoprecipitated with FLAG M2 antibody and detected with an anti-HA antibody. As expected, cells treated with SB202190 showed an extensive increase in polyubiquitin chains conjugated to ISL1, suggesting that the phosphorylation of ISL1 prevents ISL1 polyubiquitination and proteasomal degradation (Figure 2.3.3A). In addition, treatment with MG132 blocked the degradation of ISL1 induced by p38 inhibition (Figure 2.3.3B). Taken together, those results show that ISL1 phosphorylation by p38 protects it from proteasomal degradation and assures its transcription activity.

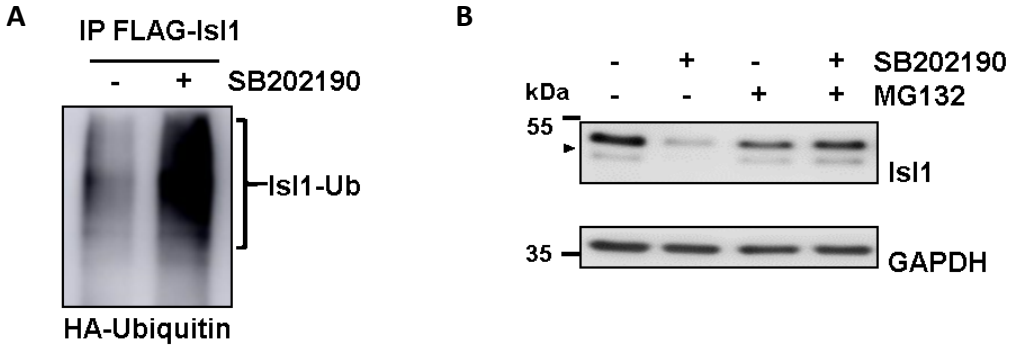

Figure 2.3.3. Phosphorylation of ISL1 by p38 protects it from proteasomal degradation. (A) HEK293T cells, transiently expressed with HA-tagged ubiquitin and FLAG-tagged ISL1, were treated with DMSO or SB202190 together with MG132 for 6 h. Identical amounts of total protein were used for immunoprecipitation with an anti-FLAG antibody and detected with an anti-HA antibody. **(B)** WB analysis for ISL1 of lysate of ISL1 overexpressing NIH3T3 cells treated with DMSO or SB202190 with or without the proteasome inhibitor MG132 for 16 h before harvesting. Experiments for figure 2.3.3 A and B were done by Yanyan Jing.

2.3.3 BMP–p38 MAPK signaling axis regulates ISL1 protein stability during cardiogenesis

Cardiogenesis is a complex morphogenic process coordinated by tight spatiotemporal control of many signaling pathways and their interaction with upstream activators and downstream targets. Interestingly, during the directed cardiac differentiation (Kattman, Witty et al. 2011, Wamstad, Alexander et al. 2012), although the total p38 levels remained no change, activated p38 levels were high only in cardiac progenitor cell (CPC), similar to ISL1 which was exclusively phosphorylated and expressed in 93% of cells at CPC stage, i.e., day 5 of differentiation (Figure 2.3.4A, B, C and E). In agreement with this, Eriksson M et al. showed that p38 is activated from d4 in human cardiomyocyte differentiation with P19 cells (Eriksson and Leppä, 2002). Importantly, treating CPC extracts with alkaline phosphatase indicated that almost all ISL1 proteins are phosphorylated in CPC (Figure 2.3.4F). Many signaling components are transiently and specifically expressed during cardiogenesis and have been shown to play important roles in cardiac commitment, progenitor cell expansion and differentiation,

such as BMP4, Activin A, FGF, etc (Figure 2.3.4D, (Kattman, Witty et al. 2011, Wamstad, Alexander et al. 2012)).

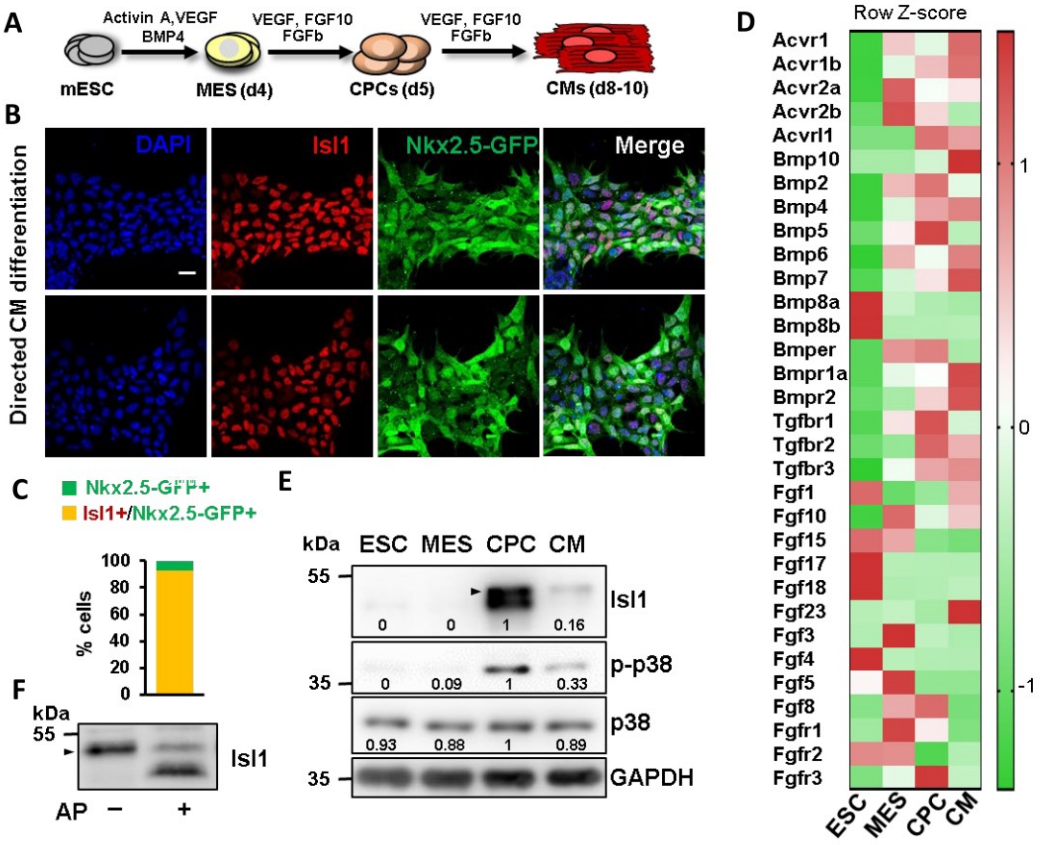

Figure 2.3.4. Isl1 was phosphorylated during the direct cardiac differentiation in vitro. (A) Scheme representation of the distinct stages of directed cardiac differentiation (top). MES, mesoderm; CPCs, cardiac progenitor cells; CMs, cardiomyocytes. **(B)** Immunostaining for ISL1, DAPI (nuclei) and Nkx2.5-GFP in CPCs differentiated from E14-NKX2-5-EmGFP mESCs. Scale bar, 20 µm. **(C)** and quantification of ISL1+/ NKX2.5-GFP+ double-positive cell as well as only NKX2.5-GFP+ cells. **(D)** Heatmap representation of expression data for genes involved in BMP, activin, and FGF signaling during directed cardiac differentiation ((Wamstad, Alexander et al. 2012)). **(E)** WB analysis for ISL1, p38 and activated phospho-p38 at different stages of directed differentiation of mESCs into CMs. **(F)** AP treatment of extracts from CPCs, showing that ISL1 is exclusively phosphorylated. Experiments for Figure 2.3.4 E and F were done by Yanyan Jing.

To study the upstream signals that lead to p38 activation and Isl1 phosphorylation during cardiogenesis, various growth factors were used to treat *Isl1*-/- mouse embryonic stem cells (mESC) and BEAS-2B (B2B) cells overexpressing *Isl1* under a CMV

promoter. The CMV promoter is not affected by growth factor treatments, and therefore, make sure that the ISL1 protein level change is not due to the transcription level difference. Further, the lower levels of activated p-p38 in B2B cells and mESCs allow us to study the timing of p38 and ISL1 phosphorylation. Bmp4 treatment increased activated phospho-p38 and ISL1 phosphorylation, whereas treatment with Activin A and bFGF did not have a significant effect on phospho-p38 and ISL1 levels (Figure 2.3.5C). To exclude the possibility that serum or BMP4 activates *Isl1* on the transcriptional level, I performed qPCR to quantify the *Isl1* mRNA level for all the treated cells. As expected, the *Isl1* mRNA level did not change in all treatments (Figure 2.3.5A and B). Consistent with the high level of p-p38 in CPCs, BMP ligands and their transmembrane receptors, including BMPR-I (*Bmpr1a*, *Acvr1*, *Acvr1b*, *Acvrl1*, *Tgfbr1*)-7) and BMPRII (*Bmpr2*, *Tgfbr2*/3), are expressed after cardiac mesoderm commitment and peak in CPCs, (Figure 2.3.4D). Those data suggest that the BMP–p38 MAPK signaling axis might regulate cardiogenesis by controlling ISL1 protein stability and activity.

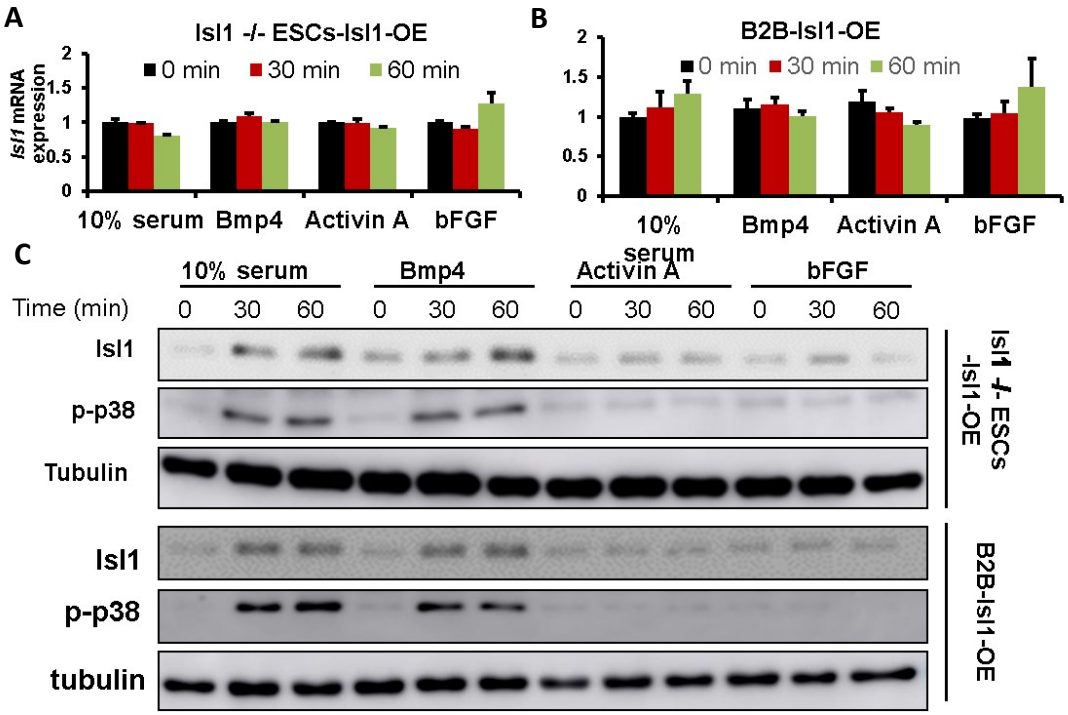

Figure 2.3.5. BMP–p38 MAPK signaling axis regulate ISL1 protein stability. (A) *Isl1* mRNA expression in mESCs overexpressing *Isl1* under CMV promoter treated with BMP4, basic FGF (bFGF), or activin for 30 or 60 min (n=3). **(B)** *Isl1* mRNA expression in

B2B overexpressing *Isl1* under CMV promoter treated with BMP4, basic FGF (bFGF), or activin for 30 or 60 min (n=3). **(C)** WB analysis for ISL1 and activated phospho-p38 MAPK of lysate from *Isl1*-/-mESCs (up panel) or B2B (bottom panel) overexpressing *Isl1* under CMV promoter treated with BMP4, bFGF, or activin for 30 or 60 min.

2.3.4 p38 regulates key cardiogenesis genes in cardiac progenitor and cardiomyocyte by stabilizing ISL1 protein

Isl1 has been shown to play an important role in heart development by shaping the chromatin landscape and setting up a cardiac-specific transcriptional program (Caputo, Witzel et al. 2015, Gao, Liang et al. 2019). To further study how p38 signaling regulates ISL1 activity during cardiac differentiation, Yanyan Jing differentiated mESCs using a directed cardiomyocyte (CM) differentiation protocol (Kattman, Witty et al. 2011, Wamstad, Alexander et al. 2012, Gao, Liang et al. 2019) and treated cardiac mesodermal (MES) precursors (day 4) either with DMSO or SB202190. In a dose-dependent manner, treatment with the p38 inhibitor significantly decreased ISL1 protein levels (Figure 2.3.6A). In contrast, the *Isl1* mRNA level was not decreased (Figure 2.3.6B), indicating that the decrease of ISL1 protein levels is not due to a downregulation of *Isl1* gene expression but rather a protein degradation. A mild increase of *Isl1* mRNA level may be due to the compensation for low ISL1 protein level (Figure 2.3.6B). Next, she analyzed the expression of *Hand2* and *Mef2c,* which are known downstream targets of ISL1. (Caputo, Witzel et al. 2015, Gao, Liang et al. 2019). Importantly, *Hand2* and *Mef2c* were strongly decreased upon p38 inhibition, whereas other progenitor marker genes, such as *Tbx1*, were not decreased (Figure 2.3.6C). Consistent with the direct role of *Isl1* in regulating cardiomyocyte structural and contraction genes (Gao, Liang et al. 2019), p38 inhibition led to a decrease of the cardiomyocyte genes *Mlc2a*, *Myocd*, *Tnnt2,* and *Ttn* expression in a dose-dependent manner. (Figure 2.3.6D). I next analyzed the expression of the different p38 MAPK isoforms during the course of cardiac differentiation and found that p38α is the only isoform highly expressed during cardiogenesis (Figure 2.3.6K). Importantly, similar to p38 inhibition, silencing of *p38α* with shRNA led to decreased ISL1 protein levels without affecting *Isl1* mRNA levels (Figure 2.3.6E, F and L). Q-PCR showed that key ISL1 downstream targets *Hand2* and *Mef2c* were decreased in cardiac progenitor cells

upon *p38α* knocking-down (Figure 2.3.6G). To agree with this, cardiomyocyte marker genes *Mlc2a*, *Myocd*, *Tnnt2*, and *Ttn* were also significantly down-regulated when knocking down *p38α* (Figure 2.3.6H). To better understand how *p38* regulates ISL1 activity in cardiogenesis, I further analyzed cardiac progenitors and cardiomyocyte numbers. FACS analysis for Nkx2-5-GFP found no differences in the number of CPC upon *p38* inhibition and *p38α* silencing, similar to ablation of *Isl1* (Figure 2.3.6I). However, differentiation into cardiomyocytes was severely impaired in loss of function of either p38 MAPKs or *Isl1* (Figure 2.3.6J). Overall, these results show that similar to *Isl1* depletion, p38 silencing or inhibition does not affect ISL1+ CPC specification but rather their differentiation in cardiomyocytes.

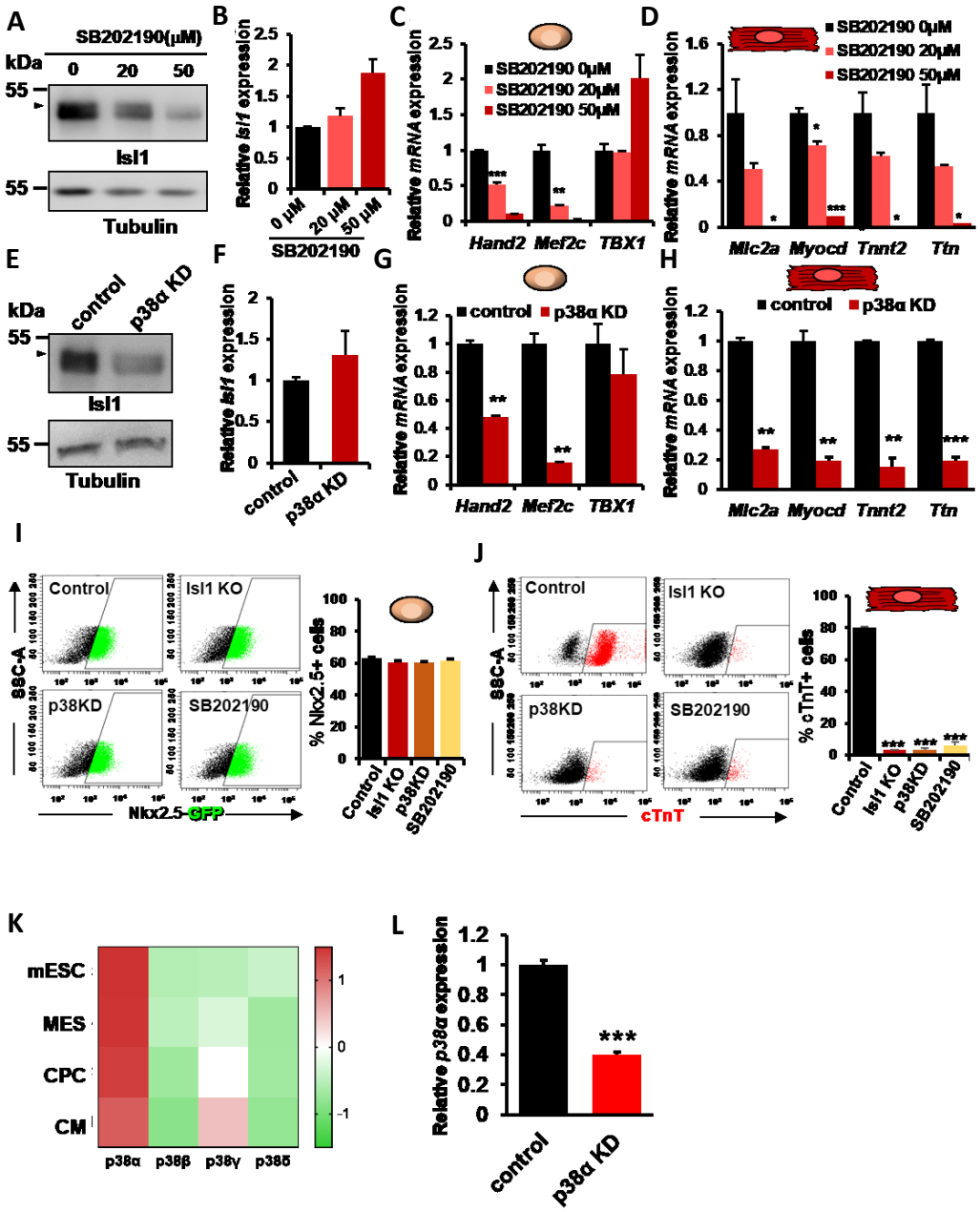

Figure 2.3.6. p38 regulates key cardiogenesis genes by stabilizing ISL1 protein. (A and B) WB analysis of cell lysate **(A)** and *Isl1* qPCR analysis (n = 4) **(B)** of mESC-derived CPCs treated with different concentrations of SB202190 at the MES stage (d4) for 24 h. **(C)** Relative mRNA expression of *Tbx1* and two ISL1 downstream targets (*Hand2* and *Mef2c*) in CPCs (d5) treated with different concentrations of SB202190 at the MES stage for 24 h (n = 4). **(D)** Relative mRNA expression of CM marker genes in CMs (d8) differentiated from cells treated with different concentrations of SB202190 at the cardiac mesoderm stage for 96 h (n = 4). **(E and F)** WB analysis of cell lysate **(E)** and *Isl1* qPCR analysis (n = 4) **(F)** of CPCs (d5) derived from control or *p38α* knockdown meSCs. **(G and H)** Relative mRNA expression of *Tbx1* and two ISL1 downstream targets *Hand2* and *Mef2c* in CPCs (n = 4) **(G)** and of CM marker genes in CMs (n = 4) **(H)** derived from control and *p38α* knockdown mESCs. **(I)** Representative FACS analyses of NKX2.5

+ CPCs derived from *Isl1*-/- and *p38α* knockdown mESCs or mESCs treated at the MES stage with *p38* inhibitor for 24 h (left). Percentage of NKX2.5+ CPCs at d5 measured by FACS analysis (n = 3) (right). **(J)** Representative FACS analyses of cTnT+ CMs at d10 (left) and percentage of cTnT+ CMs at d10 measured by FACS analysis (n = 3) (right). **(K)** Heatmap representation of *p38* isoforms expression data during cardiac differentiation. **(L)** Relative mRNA expression of *p38α* in mESC stably overexpressing control shRNA or shRNA against *p38α*. Experiments for figure 2.3.6 A to H were done by Yanyan Jing.

2.3.5 BMP–p38 MAPK signaling axis regulates cardiogenesis

To further study how the BMP4-p38 MAPK signaling axis functions in cardiogenesis Yanyan Jing treated cardiac mesodermal precursors (day 4) with Noggin, a potent BMP inhibitor that prevents BMPs from binding to their receptors. Consistent with the essential role of BMP signaling in cardiac specification, treatment with Noggin led to a significant decrease of *Isl1* mRNA as well as ISL1 protein levels (Figure 2.3.7A and B) (van Wijk, Moorman et al. 2007). To dissect the role of BMP signaling on the regulation of ISL1 protein levels versus its role in controlling its mRNA expression, she utilized *Isl1*-/- mESC overexpressing CMV-driven *Isl1*. Treatment of cardiac mesodermal precursors (day 4) derived from *Isl1*-/- mESC overexpressing CMV-driven *Isl1* with noggin led to a decrease of activated phospho-p38 and phosphorylated ISL1, although *Isl1* mRNA levels were even slightly elevated upon noggin stimulation (Figure 2.3.7C). The expression of *Hand2* and *Mef2c*, *Isl1* downstream targets, was also decreased in CPCs (Figure 2.3.7D), and she observed a dramatic decrease of genes *Mlc2a*, *Myocd*, *Tnnt2,* and *Ttn* expression in CMs upon noggin treatment (Figure 2.3.6E), similar to *Isl1* ablation, consistent with a role of BMP-p38-Isl1 signaling axis in regulating ISL1 protein stability and activity.

It has been reported that p38 MAPK signaling regulates stem cell differentiation by targeting many regulatory factors that play essential roles during cardiogenesis, such as *Gata4*, *Mef2a/c*, SRF, *Baf60c*, etc (Yokota and Wang 2016). To check the specific effect of *p38* signaling on *Isl1*-dependent transcription, *Isl1*-/- mESCs overexpressing wild-type ISL1, ISL1S269D and ISL1S269E under the EF1α promoter were subjected to directed cardiac differentiation(Figure 2.3.7F). I treated the cells either with DMSO or SB202190 at the cardiac mesoderm stage. ISL1 protein levels were strongly

downregulated upon SB202190 treatment, whereas ISL1S269D and ISL1S269E levels did not change (Figure 2.3.7G). In line with an essential role of *p38* signaling in ISL1 activity regulation during cardiogenesis, p38 inhibition led to a significant downregulation of ISL1 primary downstream targets in CPCs and CM overexpressing wild-type ISL1. In contrast, no significant differences were found in CPCs and CM overexpressing ISL1S269D and ISL1S269E mutants (Figure 2.3.7H and I). In summary, these results indicate a key role of p38 signaling in regulating ISL1 protein stability and activity during cardiac differentiation.

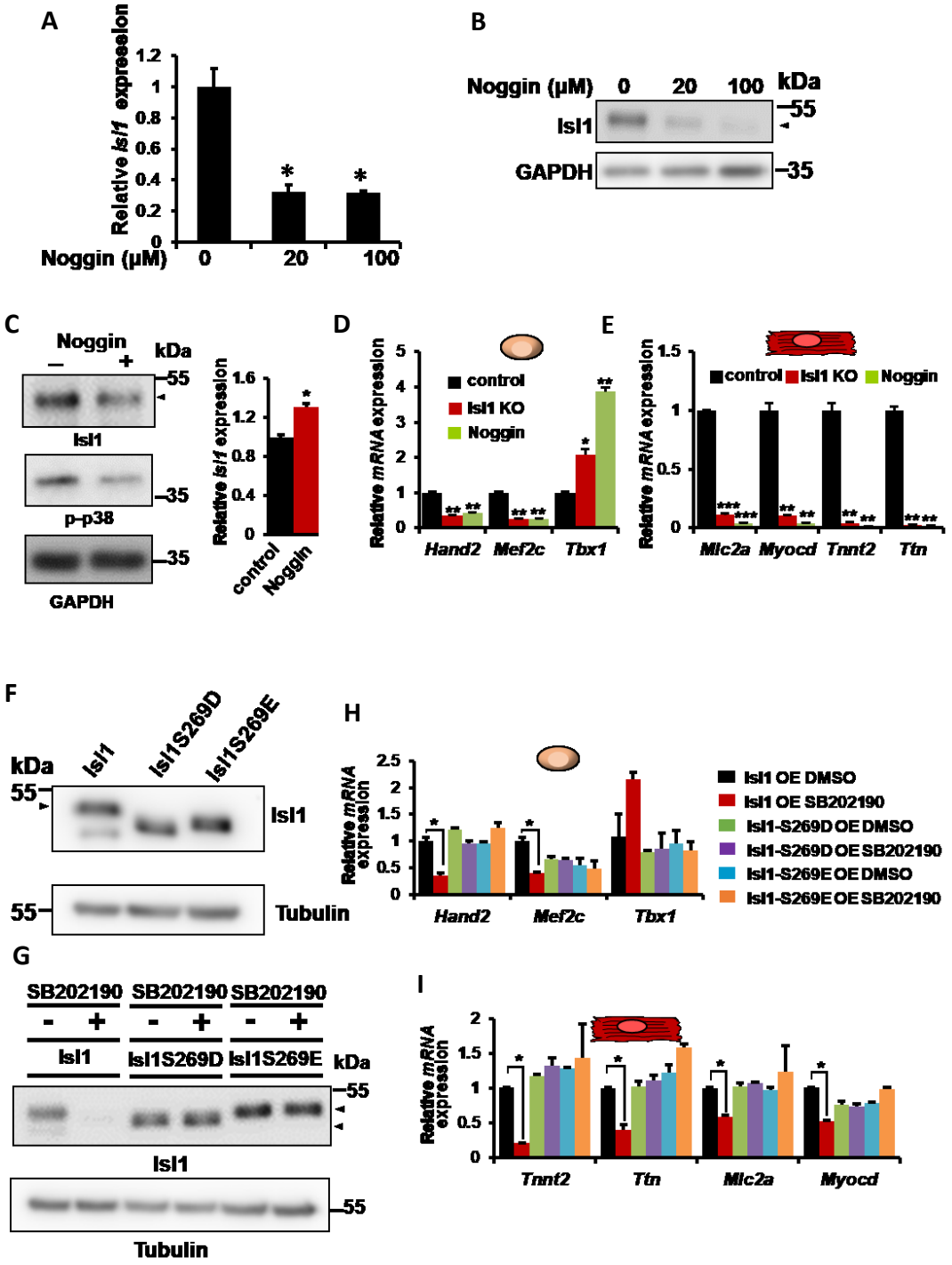

Figure 2.3.7. BMP–p38 MAPK signaling axis regulate Isl1 protein stability. (A) Relative *Isl1* mRNA expression in CPCs (day 5) treated with Noggin at mesodermal stage for 24 hours. **(B)** Western blot analysis of lysate from CPCs (day 5) treated with Noggin at the mesodermal stage for 24 hours. **(C)** WB analysis of cell lysate (left) and *Isl1* qPCR analysis (right) of CPCs derived from *Isl1*-/- mESCs overexpressing CMV-driven *Isl1* treated with Noggin at the MES stage for 24 h. **(D and E)** Relative mRNA expression of Tbx1, Hand2, and Mef2c in CPCs (d5, n = 4) **(D)** and of CM marker genes

in CMs (d8, n = 4) **(E)**, differentiated from cells treated with Noggin from the MES stage. **(F)** Western blot analysis of lysate from *Isl1*-/- mESCs overexpressing EF1α-driven ISL1 or ISL1 carrying phosphomimetic mutations of serine 269 (ISL1S269D, ISL1S269E). **(G)** WB analysis of lysate from CPCs differentiated from *Isl1*-/- mESCs overexpressing ISL1, ISL1S269D or ISL1S269E under EF1, a promoter treated with either DMSO or SB202190 at the MES stage for 24 h. **(H and I)** Relative mRNA expression of *Tbx1*, *Hand2*, and *Mef2c* in CPCs (d5, n = 4) **(H)** and of CM marker genes in CMs (d8, n = 4) **(I)**, derived from *Isl1*-/- mESCs overexpressing ISL1, ISL1S269E, or ISL1S269D treated with either DMSO or SB202190 from the MES stage. Experiments for figure 2.3.7 A, B, C, D and E were done by YanyanJing.

2.3.6 Inhibition of p38 in vivo results in ISL1 degradation and in defects in cardiac morphogenesis and function in zebrafish

To assess whether p38 signaling regulates ISL1 activity in heart development in vivo, I utilize zebrafish and mouse embryos. In zebrafish, three Islet family members (*isl1*, *isl2a,* and *isl2b*) that show high overall homology exist (Witzel, Cheedipudi et al. 2017). Remarkably, the protein phosphorylation domain is conserved within the zebrafish *Isl1* family members as well as in mice and humans (Figure 2.3.8A), and computational prediction pointed to p38 MAPK as a putative kinase for all Islet homologs (Figure2.3.8B). Alkaline phosphatase treatment (Figure 2.3.8C) indicated that all Islet protein members in zebrafish are phosphorylated, implying that interfering with p38 signaling may affect the specific roles of all islet family members within the zebrafish heart.

A

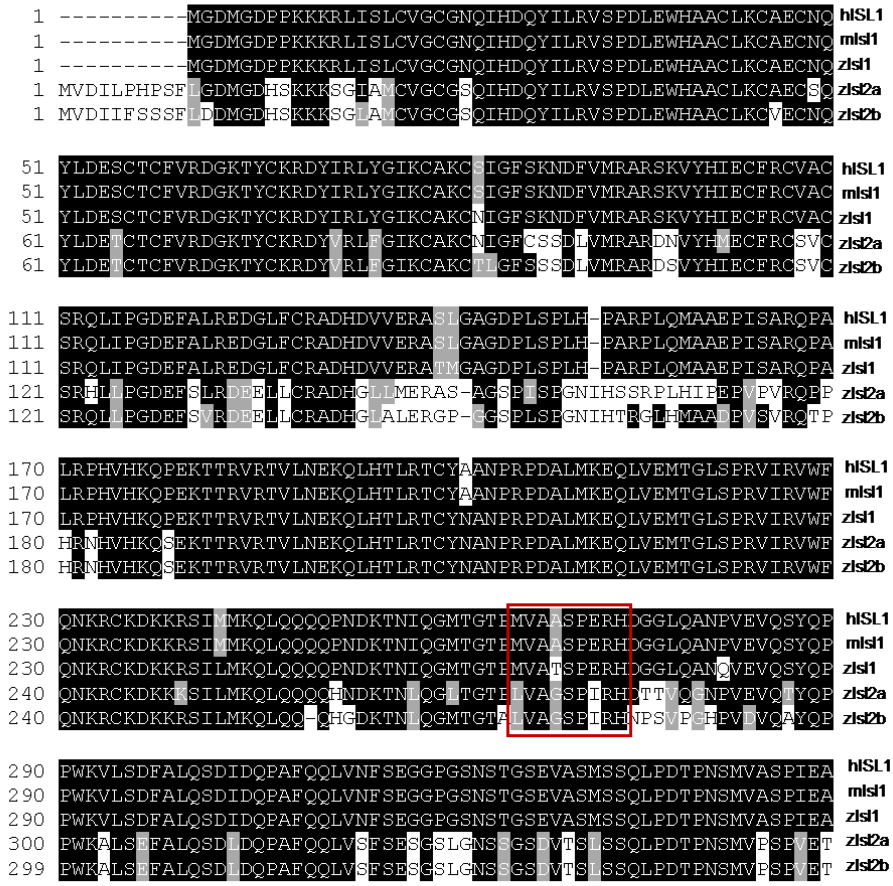

B

	Position	Context	Score	Residue	Kinase
zIsl1	269	MVATSPERH	0.536	Ser	CKI
zIsl1	269	MVATSPERH	0.527	Ser	cdk5
zIsl1	269	MVATSPERH	0.52	Ser	p38MAPK
zIsl1	269	MVATSPERH	0.507	Ser	GSK3
zIsl2a	279	LVAGSPIRH	0.554	Ser	CKI
zIsl2a	279	LVAGSPIRH	0.537	Ser	cdk5
zIsl2a	279	LVAGSPIRH	0.51	Ser	GSK3
zIsl2a	279	LVAGSPIRH	0.472	Ser	p38MAPK
zIsl2b	278	LVAGSPIRH	0.526	Ser	cdc2
zIsl2b	278	LVAGSPIRH	0.506	Ser	p38MAPK
mIsl1	269	MVAASPERH	0.546	Ser	p38MAPK
mIsl1	269	MVAASPERH	0.504	Ser	GSK3
hISL1	269	MVAASPERH	0.546	Ser	p38MAPK
hISL1	269	MVAASPERH	0.504	Ser	GSK3

C

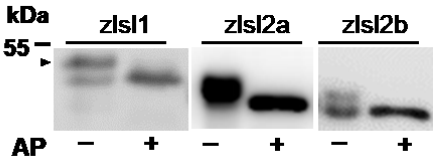

Figure 2.3.8. ISL1 proteins are conserved in humans, mice, and zebrafish. (A) alignment of Human ISL1 (hISL1), mouse ISL1 together with zebrafish ISLET family members zIsl1, zIsl2a, and zIsl2b protein, showing conservation of the protein phosphorylation site in all Islet homologues. **(B)** Results of predictions of kinase-specific protein phosphorylation sites using NetPhosK1.0, revealing p38 MAPK as a

putative kinase for all Islet family members. **(C)** Western blot analysis of lysate from HEK293 cells overexpressing zIsl1, zIsl2a, and zIsl2b not treated or treated with alkaline phosphatase.

To check whether p38 MAPK signaling regulates ISL1 activity in cardiac development in zebrafish, I treated fertilized zebrafish embryos with the p38 inhibitor SB202190 at the 3 somite stage, the time of ISL1 CPC specification (Witzel, Jungblut et al. 2012). I first titrated the dose of SB202190 to avoid toxicity (Figure 2.3.9A and B). *In situ* hybridization at the 10 somite stage revealed that the expression of ISL1 direct downstream targets *Mef2ca* and *Mef2cb* were significantly reduced, while *Isl1* and *Nkx2*-5 mRNA levels were largely unchanged (Figure 2.3.9E). Consistent with our cell culture based studies, ISL1/2 protein levels were strongly reduced upon SB202190 treatment (Figure 2.3.9C).

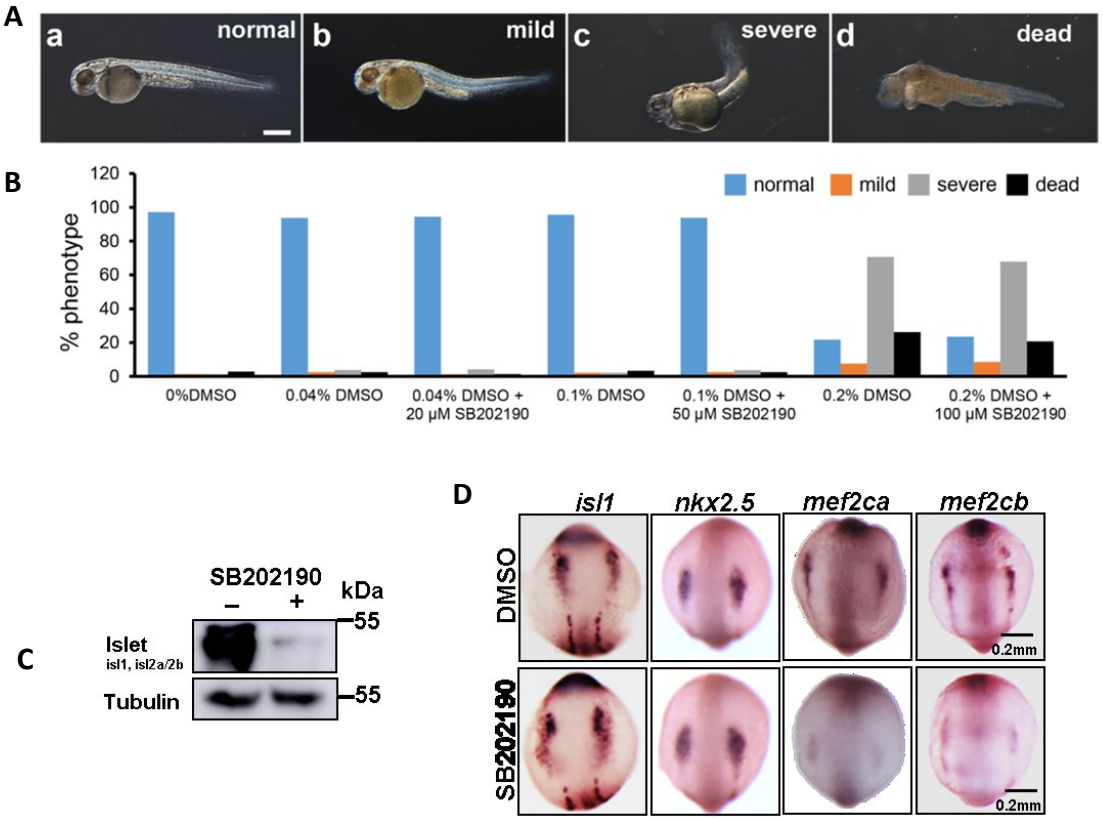

Figure 2.3.9. Inhibition of p38 leads to lower expression of ISL1 direct downstream targets without affecting the embryo morphology. (A) Testing of SB202190 toxicity in zebrafish embryos. Representative images of embryos showing normal development (a), mild phenotype (b), severe phenotype (c), or dead embryos (d).

Lateral view of embryos are presented with anterior to the left. Scale bar, 0.5 mm. **(B)** Precentage of the four different phenotypes after treating with different concerntrations of DMSO and SB202190. No treatment, n=71; 0.04% DMSO, n=82; 0.04% DMSO + 20 µM SB202190, n=73; 0.1% DMSO, n=94; 0.1% DMSO + 50 µM SB202190, n=83; 0.2% DMSO, n=116; 0.2% DMSO + 100 µM SB202190, n=128. **(C)** WB analysis of ISL1/2 protein level in 72 hpf zebrafish embryos treated either with DMSO or p38 inhibitor at 24 hpf (at least 20 embryos per sample). **(D)** In situ hybridization of ten somite stage zebrafish embryos for *isl1*, *mef2ca*, *mef2cb*, and *nkx2*.5 expression. Treatment with DMSO or SB202190 starts from the three somite stage. Scale bar, 0.2 mm.

We have previously shown that *isl1*, *isl2a,* and *isl2b* are expressed in discrete patterns in the developing zebrafish heart and control the formation of distinct regions within the heart (Witzel, Cheedipudi et al. 2017). *Isl2b* controls the development of the arterial pole, and *isl2b*-deficiency leads to pronounced cardiac looping defects, significantly smaller ventricle, and decreased expression of *ltbp3*, which have been shown to identify the anterior SHF in zebrafish (Zhou, Cashman et al. 2011, Witzel, Cheedipudi et al. 2017). In contrast, *isl1* regulates the differentiation of cardiomyocytes at the venous pole where contractions are initiated and *isl1* loss of function results in severe bradycardia and loss of ISL1+ *bmp4*- expressing cells at the sinus venosus (de Pater, Clijsters et al. 2009, Arrenberg, Stainier et al. 2010). Importantly, similar to the *Isl1* deficient fish phenotype, reduced heart rate at 48 hpf and 72 hpf and loss of *bmp4* at the venous pole were observed in zebrafish treated with SB202190 at 24 hpf (Figure2.3.10D and E). Furthermore, the confocal image revealed that zebrafish hearts of SB202190-treated embryos showed pronounced cardiac looping defects, smaller ventricles and a significantly reduced number of ventricular cardiomyocytes at 48 hpf and 72 hpf (Figure 2.3.10A and B), similar to *Isl2b*-deficient zebrafish embryos (Witzel, Cheedipudi et al. 2017), while the overall embryo morphology was not affected (Figure 2.3.10C). In addition, by *in situ* hybridization, I showed that *ltbp3* was strongly decreased upon p38 inhibition, similar to *isl2b*-/- embryos (Figure 2.3.10F). In line with an important function of the Bmp4-p38 signaling axis in SHF development, *p38α*, *bmp4*, and *isl1* are expressed in overlapping patterns in the developing heart (Figure 2.3.10G and (Witzel, Cheedipudi et al. 2017)). Taken together, those data demonstrate that p38 inhibition affects both anterior and posterior SHF development in zebrafish controlled by *isl2b* and *isl1*, both harboring

the evolutionally conserved phosphorylation site.

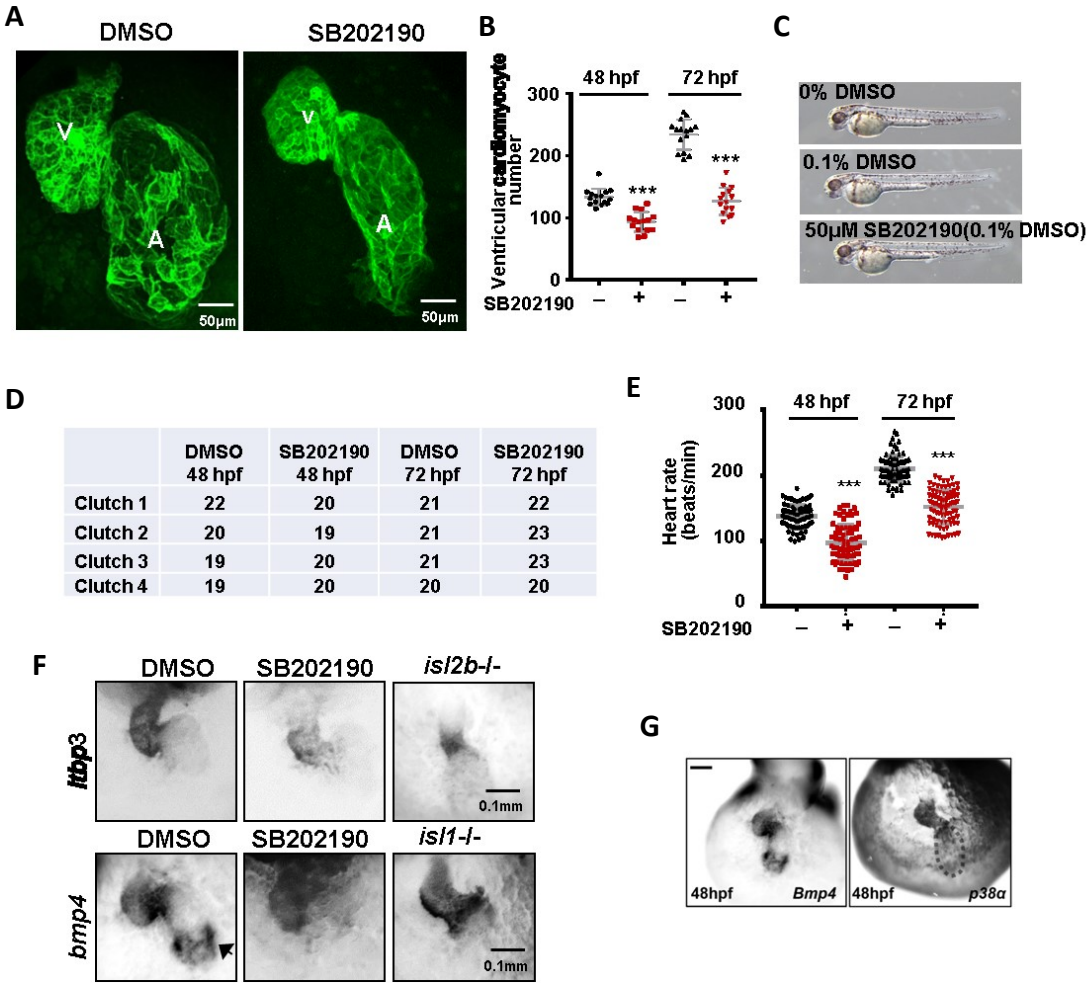

	DMSO 48 hpf	SB202190 48 hpf	DMSO 72 hpf	SB202190 72 hpf
Clutch 1	22	20	21	22
Clutch 2	20	19	21	23
Clutch 3	19	20	21	23
Clutch 4	19	20	20	20

Figure 2.3.10. Inhibition of p38 in vivo results in defects in cardiac morphogenesis and function in zebrafish. (A) Representative confocal images of 72 hpf Tg(myl7:EGFP-HsHRAS)s883 embryos treated with DMSO or p38 inhibitor at 24hpf. Scale bar, 50 µm. **(B)** Quantification of ventricular CM numbers of 48 and 72 hpf zebrafish embryos treated either with DMSO or p38 inhibitor at 24 hpf. DMSO, n = 15; 50 mM SB202190, n = 15, from 3 clutches. **(C)** The gross appearance of zebrafish embryos at 48 hpf treated with either DMSO or 50 µM SB202190 at 24 hpf. Scale bar, 0.5 mm. **(D and E)** Heart beats per minute of 48 and 72 hpf zebrafish embryos treated with either DMSO or p38 inhibitor at 24 hpf. Error bars represent SEM of four clutches (E). The numbers of embryos used per condition (D). **(F)** In situ hybridization for ltbp3 (top) or bmp4 (bottom) of 48 hpf zebrafish embryos treated with either DMSO or p38 inhibitor at 24 hpf as well as of isl2b-/- or isl1-/- embryos. The arrow indicates the bmp4 expression at the venous pole lost upon p38 inhibitor treatment and in isl1-/- embryos. Scale bar, 0.1 mm. **(G)** In situ hybridization for bmp4 and p38α of 48 hpf zebrafish embryos. Scale bar, 0.5 mm.

2.3.7 Inhibition of p38 in vivo results in ISL1 degradation and in defects in cardiac morphogenesis and function in mouse

Next, I studied the role of p38 signaling on ISL1 activity during mouse cardiac development using whole-embryo *ex vivo* culture of mouse embryos (Figure 2.3.11A and B). To avoid the toxicity, I first tritiated the concentration of SB202190. While around 80% of the embryos showed axis rotation in the sagittal plane when treated with DMSO, 20µM and 50µM SB202190, embryos treated with 100µM SB202190 did not turn (Figure 2.3.11C). Inhibition of p38 signaling starting from E8.5 (6 somites stage) for 24 hours by SB202190 led to a massive decrease in ISL1 protein levels, whereas *Isl1* mRNA levels were not significantly changed (Figure 2.3.11D and E). In line with the important role of p38 signaling in regulating Isl1 function, I observed dose-dependent defects in SHF development, including dramatically smaller right ventricle (Figure 2.3.12A and C). Consistent with the important role of ISL1 in cardiomyocyte differentiation and pacemaker development (Liang, Zhang et al. 2015), the heart rate of mouse embryos treated with SB202190 was markedly lower compared to embryos treated with DMSO (Figure 2.3.12B) and the expression of cardiomyocyte marker genes as well as markers of the sinoatrial node (SAN) lineage such as *Hcn4* and *Shox2* was significantly decreased (Figure 2.3.12 D).

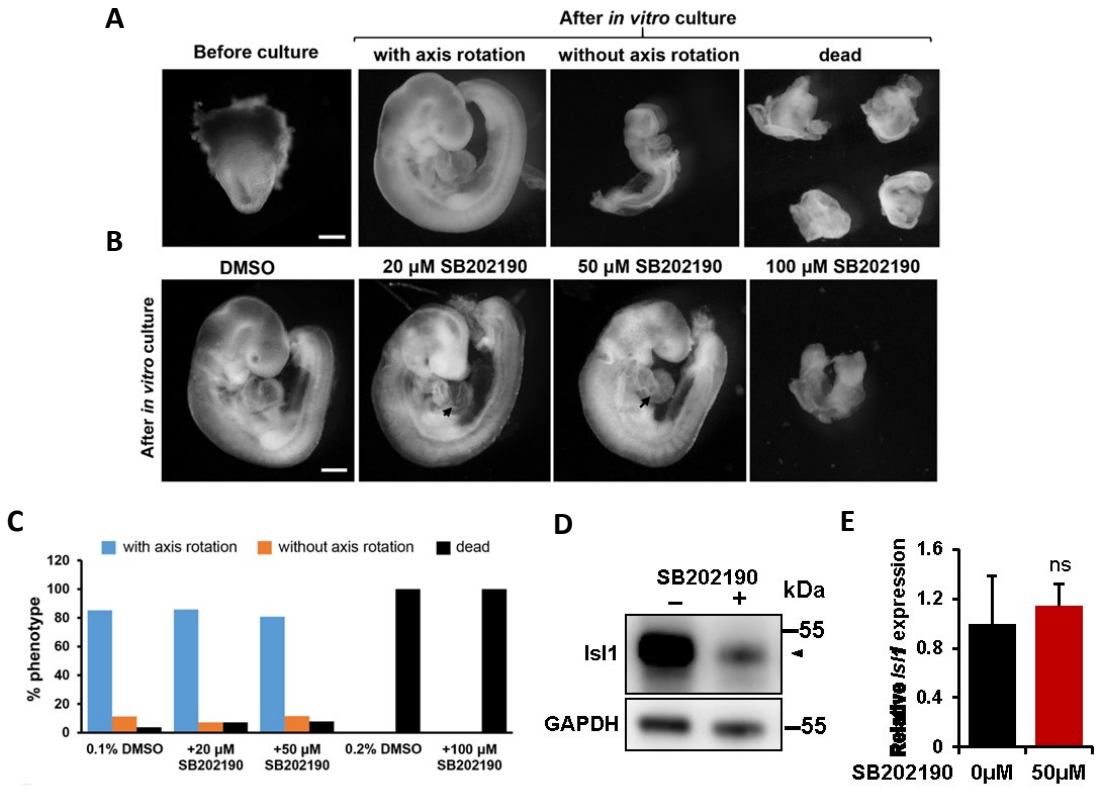

Figure 2.3.11 Treating ex vivo cultured mouse embryos with p38 inhibitor leads to significant downregulation of ISL1 protein without affecting normal development morphology. (A) Embryos at E8.5 (6 somites) before (left panel) and after whole embryo culture. Representative images of embryos after 24 hours of *in vitro* culture, showing axis rotation, no axis rotation, or dead embryos. Scale bar, 0.5 mm. **(B)** Representative images of embryos treated with either DMSO or 20 µM, 50 µM, and 100 µM SB202190 after 24 hours of *in vitro* culture. Scale bar, 0.5 mm. **(C)** Percentage of embryos with and without axis rotation as well as dead embryos after 24 hours of in vitro culture. 0.1% DMSO, n=27; 0.1% DMSO + 20 µM SB202190, n=9; 0.1% DMSO + 50 µM SB202190, n=26; 0.2% DMSO, n=3; 0.2% DMSO + 20 µM SB202190, n=10. **(D)** WB analysis for ISL1 of lysate from E8.5 mouse embryos treated with either DMSO or 50 mM SB202190 for 24 hours in a whole embryo in vitro culture (at least five embryos per sample). **(E)** Relative mRNA expression of *Isl1* in ex-vivo-cultured mouse embryos treated with either DMSO or 50 mM SB202190.

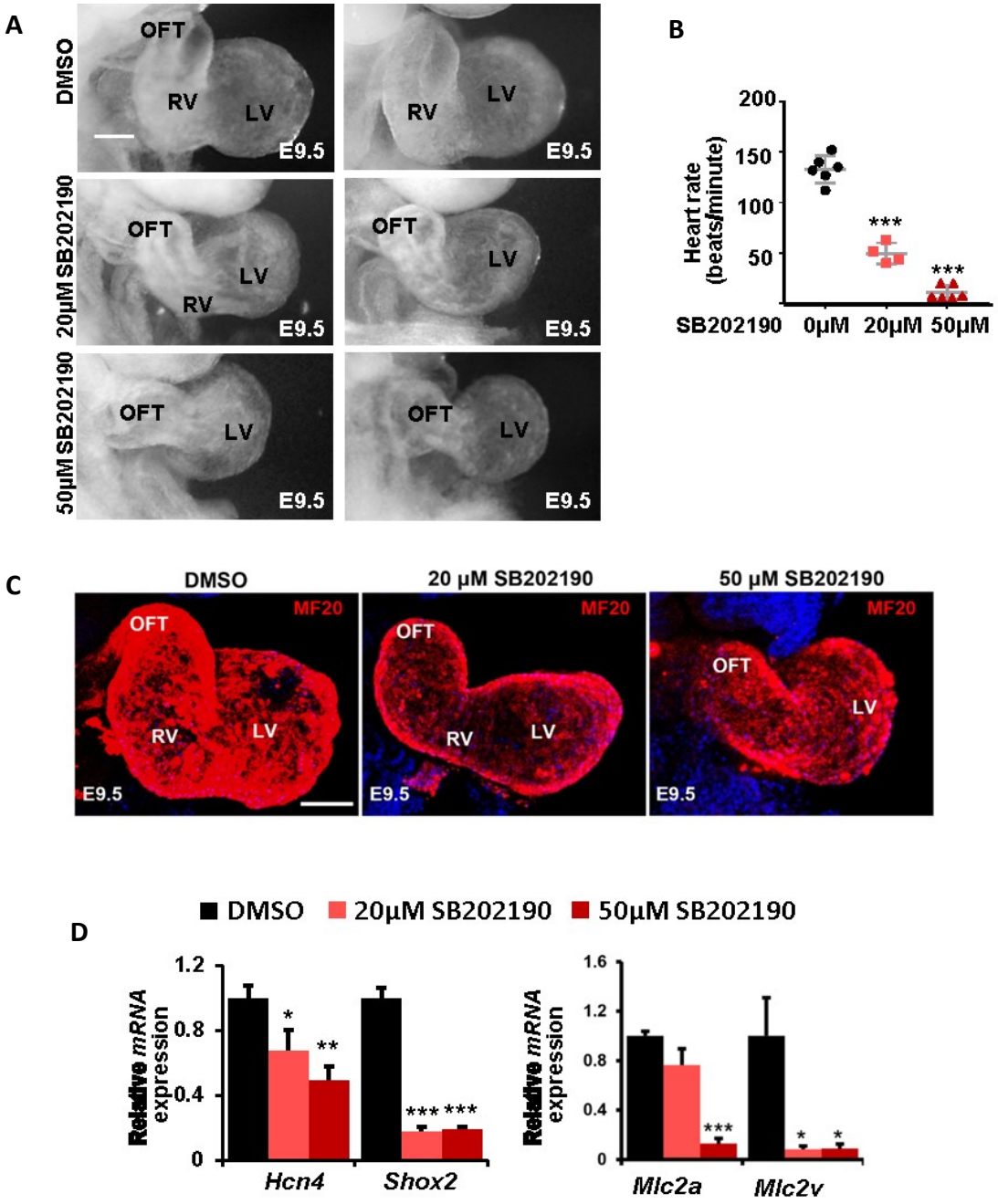

Figure 2.3.12. Inhibition of p38 in vivo results in defects in cardiac morphogenesis and function in mouse. (A) Right lateral views of the hearts of mouse embryos treated with either DMSO (n = 27) or 20 mM (n = 9) and 50 mM SB202190 (n = 26) at E8.5 for 24 h. Scale bar, 0.2 mm. **(B)** Heart beats per minute of ex-vivo-cultured mouse embryos treated either with DMSO or SB202190 (n = 8). **(C)** Representative images of whole-mount immunostaining for MF20 of hearts of mouse embryos treated either with DMSO or with 20 μM and 50 μM SB202190 at E8.5 for 24 hours. Scale bar, 0.2 mm. **(D)** Relative mRNA expression of SAN lineage markers *Hcn4* and *Shox2*, and cardiomyocyte marker genes *Mlc2a* and *Mlc2v* in ex-vivo-cultured mouse embryos treated either with DMSO or 20 and 50 mM SB202190 starting at E8.5 for 24 h (n = 6).

2.3.8. Working model

In conclusion, this study revealed the important role of ISL1 phosphorylation in regulating its protein stability and function during cardiogenesis, and this phosphorylation is mediated by the Bmp4-p38 signaling axis (Figure 2.3.13). In WT CPCs, p38 was activated by BMP signaling. The activated p38 phosphorylates the ISL1 protein at S269, preventing ISL1 degradation and ensuring its transcriptional activity during heart development. Inhibition of the BMP-p38 MAPK signaling axis leads to ubiquitination of ISL1, which is degraded by the proteasome. The decreased ISL1 protein level results in defects in CM differentiation and impaired SHF development during cardiogenesis.

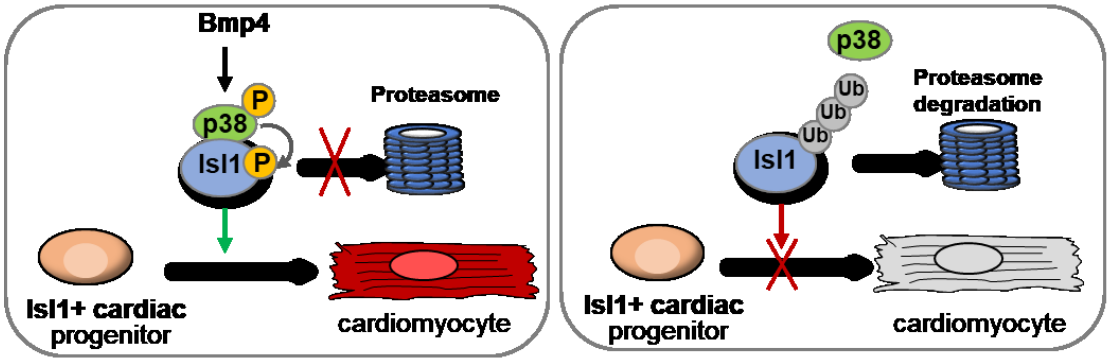

Figure 2.3.13. Working model of the role of BMP-p38 MAPK signaling axis in ISL1-driven cardiogenesis. In WT CPCs, BMP signaling activates p38, which phosphorylate ISL1 at S269. The phosphorylation prevents ISL1 protein from degradation and ensuring its transcriptional activity during the cardiomyocyte formation. Whereas interfering with the BMP-p38 MAPK signaling axis leads to unphosphorylated ISL1 protein, which tend to be depredated by the proteasome. Reduced ISL1 protein level leads to defect cardiomyocyte differentiation and impaired SHF development.

2.4 Discussion

2.4.1 Phosphorylation of ISL1 at serine 269 by p38 MAPK prevents its degradation

Reversible post-translational modification (PTM) is a common way to regulate protein activity. So far, phosphorylation is the best-studied PTM. A recent phosphoproteomic analysis suggests that the majority of proteins in a mammalian cell are phosphorylated at one or more sites (Hunter 2007). This study has shown that the phosphorylation at serine 269 of ISL1 protein prevents it from proteasomal degradation. Previous work from our lab showed that Ldb1 or even the truncated Ldb1 containing the c-terminal LIM-interacting domain (LID) binds to the LIM1 domain of Isl1, preventing it from degradation. As both phosphorylation at S269 and binding to Ldb1 prevent ISL1 from ubiquitination and degradation, it will be interesting to understand whether the phosphorylation and binding to Ldb1 are mutually dependent or not. One possibility is that Ldb1 mediates the interaction between p38 and ISL1. Without interacting with Ldb1, ISL1 will not be bound and phosphorylated by p38, leading to ISL1 degradation. Another possibility is that only phosphorylated ISl1 can bind to Ldb1 and prevent it from degradation.

Interestingly, the ISL1 phosphorylation site S269 is located in the LIM homeobox 3 binding domain (LBD) of ISL1. It has been shown that the LBD domain from Isl1 mimics the LID domain of Ldb1 by X-ray and NMR structures, even though they share low levels of sequence homology (Bhati, Lee et al. 2008). Thus the phosphorylation might also affect its binding to LIM-containing protein and result in alternate protein complexes that can bind to specific genes and thereby regulate cell lineage choice during embryonic development and cardiogenesis.

2.4.2 Bmp4-p38 AMPK axis regulate cardiogenesis.

In vitro differentiation of mESCs and induced pluripotent stem cells in the different cardiovascular lineages has been significantly improved with knowledge accumulated from developmental studies about the signaling pathways regulating the

establishment of the distinct cardiac lineages. However, to overcome the limitations in the use of stem/progenitor cells in regenerative medicine requires a better understanding of the underlying mechanisms of how the stage-specific signaling molecules drive differentiation. Activation of signaling pathways often results in posttranslational protein modifications allowing protein function diversity. This study shows that the phosphorylation of p38 MAPK, activated by BMP signaling, leads to ISL1 phosphorylation at S269, which protects it from degradation and ensures its transcriptional activity during cardiogenesis.

BMP ligands and receptors, expressed in specific patterns in the heart, play distinct and redundant functions during all stages of cardiogenesis (van Wijk, Moorman et al. 2007). Out of 20 different members, Bmp2, Bmp4, Bmp5, and Bmp7 are expressed in the anterior mesoderm, including the heart-forming regions, and are important for heart development. Canonical signaling via SMADs and non-canonical SMAD independent signaling via p38 MAPKare two major pathways activated by binding of Bmp ligands to two type I and two type II receptors (Nohe et al., 2004). Although the critical role of canonical Bmp-SMAD signaling in heart development has been shown by many studies, there is also evidence showing an essential role of noncanonical BMP signaling in cardiogenesis. For instance, the TAK1-MAPK pathway can be activated by BMP to induce in vitro CM differentiation by regulating key cardiac transcription factor gene expression (Monzen et al., 1999). Loss of function of either TAK1 or TAB1, a protein necessary for TAK1 kinase activity, leads to defects in cardiac development (Jadrich, O'Connor et al. 2006). In contrast, overexpression of dominant-negative TAK1 inhibits CM differentiation (Monzen et al., 1999).

This study identifies that a BMP4-p38 MAPK signaling axis controls ISL1 protein stability to regulate ISL1+ CPC differentiation. Disrupting either BMP, p38 MAPKs, or ISL1 leads to major cardiac differentiation and function defects without affecting CPC numbers. In line with the essential role of p38 signaling in maintaining ISL1 stability and activity, blocking p38 signaling in mouse embryos result in major defects in SHF development and heart function due to the dramatically decreased ISL1 protein levels. Similarly, blocking p38 signaling in zebrafish embryos resulted in defects in both arterial and venous pole development, controlled by Isl2b and Isl1, respectively

(Witzel et al., 2017; Zhou et al., 2011), together with a significant decrease if ISL1 protein levels. While our data support a key role of p38-mediated ISL1 phosphorylation in regulating ISL1 stability and SHF development in vivo, additional downstream effectors contribute to the observed phenotype upon p38 inhibition cannot be excluded since p38 induces a wide variety of biological effects.

The expression of the SAN lineage markers, Hcn4 and Tbx3, was decreased by blocking Bmp as well ass p38 signaling and Isl1 depletion, and TAK1 is reported to activate p38 MAPK. It remains to be determined whether the BMP-TAK1-p38-Isl1 axis controls the differentiation towards the SAN lineages. Bmp signaling plays an essential role in cardiac lineage diversification through different receptors and downstream pathways. For instance, Bmp-Smad signaling ensures proper differentiation of myocardial cells by directly suppressing Isl1 expression through miRNA17 and miRNA20a (Wang et al., 2010). The ISL1 protein phosphorylation domain is conserved within the zebrafish Isl1 family members as well as in mice and humans, suggesting that the proposed mechanism is likely an evolutionary conserved way of regulating Islet-1 protein family function during cardiogenesis.

2.4.3 Conclusion and outlook

This study identified that serine 269 of ISL1 protein is phosphorylated by p38. Without the phosphorylation, the ISL1 protein underwent proteasomal degradation. In addition, the decreased ISL1 protein levels impaired cardiac differentiation in vitro and caused defective heart development in vivo. Our study further identified that Bmp4 regulates phosphorylation of p38 during cardiogenesis.

Without the phosphorylation at serine 269, ISL1 protein undergoes proteasomal degradation, but it cannot be excluded that serine 269 needs other modifications like glycosylation to promote protein degradation. A point mutation of endogenous Isl1, which changes serine 269 to alanine to prevent other protein modifications, will help understand whether another protein modification contributes to the degradation by checking the mutated ISL1 protein level. If another modification is needed for the

degradation of ISL1 protein, constant mutated ISL1 protein levels are expected. Mass spectrometry analysis of ISL1 protein from cells treated with p38 inhibitor may also help determine the protein modification that promotes proteasomal degradation.

Due to the alternative splicing, there are two isoforms of Isl1 expressed. Isl1α is predominately expressed, while Isl1β, which lacks the region containing serine 269, is preferentially expressed in murine insulinoma cell lines (Ando, Shioda et al. 2003). Although the ISL1β protein is shorter than ISL1α, its transcriptional activity is even slightly higher than ISl1α lines (Ando, Shioda et al. 2003). It will be interesting to study whether, in some cell types or pathological conditions, Isl1β is the one predominately expressed or not. For instance, are Isl1α and Isl1β expressed differently in the different heart regions. Without tight control between phosphorylation and other modification, Isl1β may work like constitutively active ISL1, resulting in certain disorders such as CHD.

Chapter 3. Materials and methods

3.1 Materials

3.1.1 Chemicals, kits, and equipment used in this study

Chemicals	Source of supply	Reference number
1 kb Plus DNA ladder (0.1-10.0 kb)	NEB	N3200L
Agarose NEEO Ultra	Roth	2267.3
Albumin fraction V (BSA)	Roth	8076.2
Ammonium persulfate (APS)	Sigma	A3678-25G
Ampicillin sodium salt	Sigma	A99518-25G
aqueous 30 % acrylamide and bisacrylamide stock solution (37.5:1)	Carl Roth	3029.1
Bradford reagent, ready-to-use	Fermentas	R1271
Bromophenol Blue	Sigma	B0126
BSA (for ChIP)	NEB	B9000s
Chloroform ($CHCl_3$)	Roth	3313.4
Dimethyl sulfoxide (DMSO)	Sigma	D2438
Dithiothreitol (DTT)	Roth	6908.3
Dry-milk, non fat milk	Cell Signling	#9999
Ethanol	Roth	K928.3
Ethanol	Sigma	459844
Ethidium bromide solution	Sigma	E1510-10ML
ethylene glycol tetraacetic acid (EGTA)	Roth	3054.2
Ethylenediaminetetraacetic acid (EDTA)	Sigma	E5134-250G
Formaldehyde	Sigma	F8775
Gelatin from bovine skin, Type B	Sigma	G9391-100g
Glycerol	Roth	3783,1
Glycine	Sigma	15527
Halt Protease Inhibitor Cocktail (100X) 5 mL	Thermo Fischer	78429
Hexadimethrine bromide (polybrene)	Sigma-Aldrich	#H9268
Isopropanol (C_3H_8O)	Roth	6752,4
Kanamycinsulfate	Roth	T832,1
LB-agar	Roth	X965,2

LB-medium	Roth	X964,2
Lithium chloride (LiCl)	Roth	3739.1
Magnesium chloride ($MgCl_2$)	Sigma	M2393-500G
Magnesium sulfate ($MgSO_4$)	Fischer Scientific	M120,37
Maleic acid ($C_4H_4O_4$)	Roth	K304.1
Methanol (CH_3OH)	Roth	4627.5
Nonidet P-40 (NP-40)	Fluka	74385
PageRuler Plus Prestained Protein Ladder, 10 to 250 kDA	Thermo Fischer	26620
Paraformaldehyde (PFA)	Thermo Fischer	12587010
phosphatase inhibitor cocktail set	Millipore	524632-1SET
Poly(2-hydroxyethylmethacrylate) (PolyHEMA)	Sigma	P3932-10G
Polyethylenimine (PEI)	Sigma-Aldrich	408727-100ML
Potassium chloride (KCl)	Roth	6781.3
Puromycin Dihydrochloride 10x1 mL	Thermo Fischer	A1113803
Sodium dodecyl sulfate (SDS)	Sigma	L4390-100G
Tetramethylethylenediamine (TEMED)	Roth	2367,1
tris(hydroxymethyl)aminomethane (TRIS)	Roth	4855.2
Triton X-100	Sigma	X100-500ML
TRIzol LS Reagent 200 mL	Thermo	10296028
Tween 20	Sigma	T2700-500ML
β-mercaptoethanol (C_2H_6SO)	Sigma	60-24-2

Kits	**Source of supply**	**Reference number**
2x SYBR Green master mix	Applied Biosystems	4367659
Amersham ECL Prime Western Blotting Detection Reagent	GE Healthcare	RPN2232
Bioanalyzer High Sensitivity DNA Analysis	Agilent	5067-4626
ChIP DNAb Clean&Concentrator	Zymo	D5205
GenEluteTM gel extraction kit	Sigma	NA1111
GenEluteTM HP plasmid midiprep kit	Sigma	NA0200
GenEluteTM HP plasmid miniprep kit	Sigma	NA0160
GenEluteTM PCR clean-up kit	Sigma	NA1020
High-Capacity cDNA Reverse Transcription Kit	Applied Biosystems	4368813
NEBNext High-Fidelity 2X PCR Master Mix	NEB	M0541S

NEBNext Ultra II DNA Library Prep Kit with Purification Beads 96 reactions	NEB	E7103L
NEBNext® Multiplex Oligos for Illumina® (96 Index Primers)	NEB	E6609S
NEBNext® Multiplex Oligos for Illumina® (Index Primers Set 1)	NEB	E7335S
Pierce™ BCA Protein Assay Kit	Thermo Scientific	23225
Qubit dsDNA HS Assay Kit-100 assays	Thermo Fisher S	Q32851
RNeasy Plus Universal Mini Kit 50	Qiagen	73404
SuperSignal™ West Femto Maximum Sensitivity Substrate	Thermo Fisher	34094

Equipment	**Source of supply**
Agilent 2100 Bioanalyzer System	Agilent
Bacterial incubator 37°C	Thermo Scientific
Binocular microscope M165FC	Leica
Binocular microscope MZ16FA	Leica
Cell culture incubator	Thermo Scientific
Cell culture safety cabinet	Thermo Scientific
Centrifuge HERAEUS Fresco 17	Thermo Electron Corporation
Centrifuge HERAEUS Multifuge 1S-R	Thermo Electron Corporation
Centrifuge HERAEUS Pico 17	Thermo Electron Corporation
Cold light source KL2500 LCD	Zeiss
Confocal microscope LSM 700	Zeiss
Developing machine	GE Healthcare
Diagenode Bioruptor Homogenizer	Diagenode
Fluorescence microscope DM6000B	Leica
Heating block TH 21	HLC BioTech
Light microscope Wilovert S	Hund Wetzlar
Nanodrop 2000c Spectrophotometer	peQLab
Qubit™ Fluorometer	Thermo Scientific
Real-Time StepOne Plus Real-Time PCR System	Applied Biosystems
Rocking platform 444-0142	VWR
Rotator SB3	Stuart
Scale LC 4800 P	Sartorius
SDS-PAGE apparatus	Bio-Rad
Sonifier Sonopuls GM 2070	Bandelin electronic
Thermal cycler C1000 Touch	BIO-RAD

Thermo block 5436	Eppendorf
Thermo block MHR 23	HLC BioTech
UV light source ebq100	Leistungselektronik Jena
UV light source EL 6000	Leica
UV-Crosslinker	Analytikjena
Vortexer VF2	IKA®-Labortechnik Staufen
Water bath cell culture WMB 22	Memmert
Water bath Julabo U3	Julabo Labortechnik GMBH
Western Blotting Transfer apparatus	Bio-Rad

3.1.2 Materials used for cell culture in this study

Medium/supplements	Source of supply	Reference number
1-Thioglycerol	Sigma	M6145
7.5% BSA	Gibco	15260037
Activin A	R&D systems	338-AC
B27 supplement	Gibco	17504-044
B27 supplement without Vitamin A	Gibco	12587-010
bFGF	R&D systems	233-FB
BMP4	R&D systems	314-BP
DMEM + High glucose	Gibco	10938-025
DMEM + Glutamax	Gibco	61965-026
DMEM/F12	Gibco	21331020
DMSO	Sigma	D2650
DPBS	Gibco	14190-094
FBS	Gibco	10270-106
FGF10	R&D systems	345-FG
gelatin	Sigma	G9391
Ham's F12 Nutrient Mix	Gibco	11765054
IMDM	Gibco	12440053
KnockOut DMEM medium	Gibco	10829-018
KnockOut Serum Replacement	Gibco	10828-028
L-Ascorbic Acid	Sigma	A4403
leukemia inhibitory factor	Millipore	ESG1107
L-Glutamine	Gibco	25030-024
Lipofectamine 2000	Invitrogen	11668019

mitomycin	Sigma	M4287
N2 supplement	Gibco	17502-048
Neurobasal medium	Gibco	1103049
non-essential amino acids	Gibco	11140-035
Penicillin-Streptomycin	Gibco	15140-122
Poly (2-hydroxyethyl methacrylate)	Sigma	P3932
Puromycin	Gibco	A11138-03
sodium pyruvate	Gibco	11360-039
StemPro Accutase	Thermo Fisher	A1110501
StemPro™-34 SFM	Gibco	10639011
Trypsin-EDTA (1x) 0.05%	Gibco	25300-054
VEGF	R&D systems	293-VE-010
X-tremeGENE HP DNA Transfection Reagent	Roche	6366236001
β-mercaptoethanol	Sigma	M3148

Cell culture materials	**Source of supply**	**Reference number**
15ml Centrifuge Tubes	Greiner Bio-One	188271
50ml Centrifuge Tubes	Greiner Bio-One	227261
5ml Plastic pipet	Greiner Bio-One	606180
10ml Plastic pipet	Greiner Bio-One	607180
25ml Plastic pipet	Greiner Bio-One	760180
6-cm dish (cell culture)	Greiner Bio-One	628160
10-cm dish (cell culture)	Greiner Bio-One	664160
15-cm dish (cell culture)	Greiner Bio-One	639160
10-cm petri-dish	Greiner Bio-One	633180
6-well plates (cell culture)	Greiner Bio-One	657160
12-well plates (cell culture)	Greiner Bio-One	665180
24-well plates (cell culture)	Greiner Bio-One	662160
48-well plates (cell culture)	Greiner Bio-One	677180
96-well plate F bottom with lid	Greiner Bio-One	655180
96-well plate V bottom with lid	Greiner Bio-One	651180
Reservior	VWR	89094-664

3.1.3 DNA oligoes used in this study

Oligos	Sequence of oligos
Jmjd6-N-KI-ss-donor	GACGGCGAGCGACTCACGATGGACTACAAAGACC ATGACGGTGATTATAAAGATCATGACATCGACTAT AAGGACGATGATGACAAAAACCACAAGAGCAAGA AGCGCATCCGCGAGGCC
mChIPBmp2F	AAGTTGGGGTTCTCCATGTG
mChIPBmp2R	GGCCTACGCCCCTAACTATT
mChIPBmp4F	ACAGCTCCTGGAGGCAGTTA
mChIPBmp4R	CCACGGCTTTGGTTGATAGT
mChIPGata4F	CGGAGTGGGCACGTAGAC
mChIPGata4R	GCACACCCGCATTCTAGTTC
mChIPGata6F	TCCAGGAAAGAGGGTGAATG
mChIPGata6R	GCCCCACATATCTCTCAAGC
mChIPHand1F	AGTGTTTGCAGGCCTGTTCT
mChIPHand1R	CGCCTGGCTACCAGTTACAT
mChIPHand2F	CCGACGTGAAAGAGGAGAAG
mChIPHand2R	TGCTTTTGAGGAAACCATCC
mChIPMsx2F	TCCCACCCTAAAGCACACTC
mChIPMSX2R	AGCCTGAAATGGGTTGTTTG
mChIPNrp1F	TACCCATCCTCGCCTTTATG
mChIPNrp1R	AGAACGCCTTGGTTGTTCTG
mChIPSmad6F	AGAGCCTTGACGATGGAAGA
mChIPSmad6R	TAGGGAAATCACGCCTAACG
mChIPTbx20F	AGACTTCGAACCAGCAGGAA
mChIPTbx20R	TGCAGAGAGGAGATCCGACT
mChiPMesp1F	ACTCGGGGTCTAGGGTAGG
mChiPMesp1R	ACCTGACCAAGATCGAGACG
mChIPEomes_K27_F	GGTCCCCAAAGCCTCTTAGT
mChIPEomes_K27_R	CAGGAACCTCTGGAAGCTGA
mChIPEomes_K4_F	TCTCCAAAGTCGTGTCCCTT
mChIPEomes_K4_R	GTCACGTAGATCTGCCCTCA
mChIPFoxa2_K4_K27_F	CCCAAAGAGAGCCGGAAAAG
mChIPFoxa2_K4_K27_R	CCTGGGATAGCAACGGAGAT
mChIPGsc_K4_K27_F	GAAAGTTGGTGCCAGGTGAG
mChIPGsc_K4_K27_R	ACAGCTACTTCTACGGGCAG
mChIPHoxb1_K4_K27_F	TGAGAGAACTGACGTGGCTT
mChIPHoxb1_K4_K27_R	CGTTTCATTGAGCTCCAGGG

mChIPLhx1_K4_K27_F	AACTCAGCCTTTCCTCAGCA
mChIPLhx1_K4_K27_R	TGGTCTTGGTTTCTGAGGCT
mChIPMesp2_K27_F	CAGAGGCACGGGATAGACAT
mChIPMesp2_K27_R	GGGAAGTGTGGGAGAGACAA
mChIPMesp2_K4_F	GGCTCAGATGCTTGGTCCTA
mChIPMesp2_K4_R	AGTCAGCGGCTCTTTCTAGG
mChIPMilxl_K4_K27_F	CTGCTGGGACCTTTCAATGG
mChIPMilxl_K4_K27_R	GAGTCCAGGATCCAGGTGAG
mChIPT_K4_K27_F	CGACTTTGTTTCTTCCCGCT
mChIPT_K4_K27_R	GGGACAGCAGAGGGACAAAT
mChIPWnt3_K4_K27_F	CACCATTTTCCCTGCTACCC
mChIPWnt3_K4_K27_R	AATGGAGAAGAGGAGTGGCC
mChIPWnt3a_K4_K27_F	CCCAGGTGAAAAGGAGGCTA
mChIPWnt3a_K4_K27_R	CGGAATTCCTGGGCTCAAGA
qmFlrt2-R	CAGCGGCATACACTAGGGC
qmFoxa2-F	CCCTACGCCAACATGAACTCG
qmFoxa2-R	GTTCTGCCGGTAGAAAGGGA
qmFoxc1-F	CCCCGGACAAGAAGATCACTC
qmFoxc1-R	AGGTTGTGCCGTATGCTGTTC
qmFoxf1-F	ACGCCGTTTACTCCAGCTC
qmFoxf1-R	CGTTGTGACTGTTTTGGTGAAG
qmFzd1-F	CATGCCCAACCTGATGGGTC
qmFzd1-R	GCCACCTGAATTTGAACTGCTC
qmFzd4-F	TGCCAGAACCTCGGCTACA
qmFzd4-R	ATGAGCGGCGTGAAAGTTGT
qmGAPDH_F	AACTTTGGCATTGTGGAAGG
qmGAPDH_R	GGATGCAGGGATGATGTTCT
qmGata4_F	TCTCACTATGGGCACAGCAG
qmGata4_R	GCGATGTCTGAGTGACAGGA
qmGata5-F	ATGAGTTCCGACGTAGCCC
qmGata5-R	CAAGAAGTCAGGTACGAAGCTG
qmGATA6_for	CAAAAGCTTGCTCCGGTAAC
qmGATA6_rev	TGAGGTGGTCGCTTGTGTAG
qmHand1_F	GCGGAAAAGGGAGTTGCCTCAGC
qmHand1_R	GCTCCAGCGCCCAGACTTGC
qmHand2_F	CGGAGAGGCGGAGGCCTTCA
qmHand2_F	CGGAGAGGCGGAGGCCTTCA
qmHand2_R	CAGGGCCCAGACGTGCTGTG
qmHand2_R	CAGGGCCCAGACGTGCTGTG

qmHey2-F	AAGCGCCCTTGTGAGGAAAC
qmHey2-R	GGTAGTTGTCGGTGAATTGGAC
qmIsl1_F	ACGTGCTTTGTTAGGGATGG
qmIsl1_R	CAAGAAGTCGTTCTTGCTGA
qmItga4-F	GATGCTGTTGTTGTACTTCGGG
qmItga4-R	ACCACTGAGGCATTAGAGAGC
qm*Jmjd6*-F	CACCAACTTCCCTGTTGTGTG
qm*Jmjd6*-R	CCTGGAGGTCAACTGCGTC
qmKcnab1-F	GGACTCAGAGTTTCATGCTTGG
qmKcnab1-R	TTGTCATCAGCCGTTCAGCAA
qmLama4-F	ATGAGCTGCAAGGAAAACTATCC
qmLama4-R	CTGTTTCGTTGGCTTCACTGA
qmLhx1-F	CCCATCCTGGACCGTTTCC
qmLhx1-R	CGCTTGGAGAGATGCCCTG
qmMesp1_F	GTTTAAGCCCGGCCGTCTGCA
qmMesp1_R	ATGTCGCTGCTGAAGAGCGGAGA
qmMesp2_F	TAGAAAGAGCCGCTGACTCC
qmMesp2_R	CTAGGCTCTGGGGACATCTG
qmMixl1-F	ACGCAGTGCTTTCCAAACC
qmMixl1-R	CCCGCAAGTGGATGTCTGG
qmMlc2a (Myl7)_F	CCCATCAACTTCACCGTCTT
qmMlc2a (Myl7)_R	CGTGGGTGATGATGTAGCAG
qmMlc2v (Myl2)_F	CTGCCCTAGGACGAGTGAAC
qmMlc2v (Myl2)_R	CCTCTCTGCTTGTGTGGTCA
qmMyocd_F	GCTGAGACTCACCATGACAC
qmMyocd_R	TGGACCTTTCAGTGGCGGTA
qmNanog_F	ACCTGAGCTATAAGCAGGTTAAGA
qmNanog_R	GGGATACTCCACTGGTGCTG
qmNrp1-F	GACAAATGTGGCGGGACCATA
qmNrp1-R	TGGATTAGCCATTCACACTTCTC
qmPdgfra-F	TCCATGCTAGACTCAGAAGTCA
qmPdgfra-R	TCCCGGTGGACACAATTTTTC
qmPkd1l1-F	ATGCCACTCTTGAAGTGAGCA
qmPkd1l1-R	CCAGGCAGTGTATCTTCTTCCA
qm*Prmt6*-AS-F,	TCACCGCTCCAGTCTTCATT
qm*Prmt6*-AS-JC-R	ACACCTCAGGCTTTCATCCA
qm*Prmt6*-AS-R	CAACCCCGGCAGTTAAACAA
qm*Prmt6*-F	ATGTCGCTGAGCAAGAAAAGA
qm*Prmt6*-R	CGGAGTAGCACTCGTAGTACAG

qmPtch1-F	AAAGAACTGCGGCAAGTTTTTG
qmPtch1-R	CTTCTCCTATCTTCTGACGGGT
qmSox2_F	AGAACCCCAAGATGCACAAC
qmSox2_R	TCTCGGTCTCGGACAAAAGT
qmTbx20_F	GCAGCAGAGAACACCATCAA
qmTbx20_for	GCAGCAGAGAACACCATCAA
qmTbx20_R	GTGAGCATCCAGACTCGTCA
qmTbx20_rev	GTGAGCATCCAGACTCGTCA
qmTbx5_F	ATGGTCCGTAACTGGCAAAG
qmTbx5_R	ACAAGTTGTCGCATCCAGTG
qmTek-F	GAGTCAGCTTGCTCCTTTATGG
qmTek-R	AGACACAAGAGGTAGGGAATTGA
qmTgfb1-F	ATGTCACGGTTAGGGGCTC
qmTgfb1-R	GGCTTGCATACTGTGCTGTATAG
qmTgfbr3-F	GGTGTGAACTGTCACCGATCA
qmTgfbr3-R	GTTTAGGATGTGAACCTCCCTTG
qmTie1-F	GGTCACACACACGGTGAACAA
qmTie1-R	TGCCAGTCTAGGGTATTGAAGTA
qmTnnt2_F	ATCCCCGATGGAGAGAGAGT
qmTnnt2_R	CTGTTCTCCTCCTCCTCACG
qmTtn_F	ACCACCCAACTTCAGTCAGC
qmTtn_R	TCCCGGTAGAACTTCACCAC
qmTwist1-F	GGACAAGCTGAGCAAGATTCA
qmTwist1-R	CGGAGAAGGCGTAGCTGAG
qmVegfa-F	CTGCCGTCCGATTGAGACC
qmVegfa-R	CCCCTCCTTGTACCACTGTC
qmWnt3-F	CTCGCTGGCTACCCAATTTG
qmWnt3-R	CTTCACACCTTCTGCTACGCT
qmWnt3a-F	CTCCTCTCGGATACCTCTTAGTG
qmWnt3a-F	GCATGATCTCCACGTAGTTCCTG
qmWnt5a-F	CAACTGGCAGGACTTTCTCAA
qmWnt5a-R	CATCTCCGATGCCGGAACT

3.1.4 Antibodies used in this study

Antibody	Host	Usage and Dilution	Company
Digoxigenin-AP Fab fragments	sheep	*in situ* (1:2000)	Roche, 11 093 274 910

FLAG® M2	mouse	WB (1:2000), CO-IP	Sigma-Aldrich, F1804
Isl1 39.4D5	mouse	WB (1:10), IF (1:10)	Developmental Studies Hybridoma Bank
α-Tubulin	mouse	WB (1:3000)	Sigma-Aldrich, T5168
Anti-mouse Alexa Fluor® 594	goat	IF (1:500)	Invitrogen, A11020
Anti-rabbit Alexa Fluor® 488	donkey	IF (1:500)	Invitrogen, A21206
U2AF65	mouse	IF (1:1000)	Santa Cruz, sc-166695
HA (Y-11)	rabbit	WB (1:150)	Santa Cruz, sc-805
GAPDH	rabbit	WB(1:1000)	Cell signaling technology, 2118
p-p38	rabbit	WB(1:1000)	Cell signaling technology ,4511
p38	rabbit	WB(1:1000)	Cell signaling technology ,9212
p-Isl1	rabbit	WB(1:1000)	Thermo Fisher, generate against peptide TPMVAA(phosS)PERHDG
Jmjd6	mouse	WB (1:100)	Santa Cruz, sc-28349
H3K4me3	rabbit	ChIP	Abcam, ab8580
H3K27me3	rabbit	ChIP	Millipore, 07449
H2AK119ub	mouse	ChIP	Millipore, 05678
H3R2me2a	rat	ChIP	Gift from Prof. Dr. Uta-Maria Bauer
Ezh2	rabbit	ChIP	Cell signaling technology , 5246s

3.1.5 Buffers and medium

Medium/buffer	recipe	usage
ESC medium	DMEM + High glucose, 15% FBS, 2 mM L-Glutamine, 0.07 mM β-mercaptoethanol, 0.1 mM nonessential amino acids, 1 mM sodium pyruvate, 100U/ml Penicillin-Streptomycin	mESC

MEF medium	DMEM + High glucose, 10% FBS, 2 mM L-Glutamine, 0.07 mM β-mercaptoethanol, 0.1 mM nonessential amino acids, 1 mM sodium pyruvate, 100U/ml Penicillin-Streptomycin	MEF, feeder cells
HEK293T medium	DMEM + High glucose, 10% FBS, 2 mM L-Glutamine, 0.1 mM nonessential amino acids, 1 mM sodium pyruvate, 100U/ml Penicillin-Streptomycin	HEK293T, NIH3T3
Neurobasal,DMEM/F12 medium	50% Neurobasal, 50% DMEM-F12, 0.5× N2 supplement, 0.5× B27 supplement, 100U/ml Penicillin-Streptomycin, 2 mML-Glutamine, 0.05% BSA , 0.01% 1.5×104 M monothioglycerol, 10 ng/ml BMP4 , 2,000 U/ml LIF	direct cardiac differentiation
Differentiation medium	75% IMDM , 25% F12 , 0.5× N2, 0.5× B27 supplement without VA, 100U/ml Penicillin-Streptomycin, 1% 50 µg/ml L-Ascorbic acid, 0.04% 4.5×10-4 M monothioglycerol	direct cardiac differentiation
Stempro-34 medium	Stempro-34 medium, 2.6% StemPro supplement, 100U/ml Penicillin-Streptomycin	direct cardiac differentiation
E3 zebrafish medium	5mM NaCl, 0,17mM KCl, 0,33mM CaCl2 0,33mM MgSO4	zebrafish embryos
Co-IP buffer	50mM TRIS-HCl pH=7.5 15mM EGTA 100mM NaCl 0.1% (v/v) Triton X-100	immunoprecipitation

Hybridization solution	50% (v/v) formamide 25% (v/v) 20x SSC solution pH=4.5 35mM SDS 50mg/l (w/v) heparin 50mg/l (w/v) yeast tRNA	in situ
10x MAB	1.5M NaCl 1M maleic acid (pH titrated to 7.5)	in situ
MABT	0.1% (v/v) Tween 20 in MAB	in situ
Solution I	50% (v/v) formamide 25% (v/v) 20x SSC solution pH=4.5 35mM SDS	in situ
5x blocking buffer	10% (w/v) blocking reagent powder in MABT	in situ
20x SSC	3M NaCl 0.3M trisodium citrate dihydrate (pH titrated to 7.0)	in situ
L1 lysis buffer	50 mM Tris pH=8 2mM EDTA pH=8 0.1% (v/v) NP40 10% (v/v) glycerol	ChIP
L2 nuclear resuspension buffer	50mM Tris pH=8 5mM EDTA pH=8 1% (w/v) SDS	ChIP
DB-dilution buffer	200mM NaCl 50mM Tris pH=8 5mM EDTA, 50mM 0.5% NP40	ChIP
NaCl-washing buffer	500mM NaCl 20mM Tris pH=8 2mM EDTA NP40 (v/v) 1% 0.1% (w/v) SDS	ChIP
LiCl-washing buffer	500mM LiCl 20mM Tris pH=8 2mM EDTA 1% (v/v) NP40 0.1% (w/v) SDS	ChIP
EB-extraction buffer	10mM Tris pH=8 1mM EDTA 2% (w/v) SDS	ChIP

TE-buffer	10mM Tris pH=8 1mM EDTA	ChIP

3.1.6 Organisms

Transgenic zebrafish/mouse strain, cell lines, primary cells	Reference	Description
Tg(myl7:EGFP-HsHRAS)s883	Stainier Lab: D'Amico, L. et al., 2007	This construct contains the last 20 C-terminal amino acids of human HRAS fused to the C-terminal end of eGFP.Regulatory regions: Myosin Light Chain 7 (Myl7)
E14 Tg(Nxk2-5-EmGFP)	Hsiao, Yoshinaga et al. 2008	P2A-Emerald GFP were inserted to the open reading frame of the NKX2-5 locus 26 amino acids downstream of the native ATG site in human BAC RP11-88L12 containing the NKX2-5 locus and large flanking regions
HEK293T		R70007, Thermo Fisher
3T3		ATCC number, CRL-1658
B2B		ATCC number, CRL-9609
MEF		primary fibroblast from E13.5 mouse emrbyos
Feeder cells		MEF cells treated with mitomycin

3.2 Methods

3.2.1 Mouse genomic DNA preparation and genotyping

Mice tail or ear tissue was incubated with 500µl of lysis buffer (1% of 10µg/µl proteinase K was freshly added) at 55°C with 500 rpm shaking overnight. Increase the temperature to 95°C for 10 min to inactivate proteinase K the next day. To remove the tissue debris, the sample was centrifuged at 12,000g for 5 min at room temperature (RT). The supernatant was transferred to a new tube and genomic DNA (gDNA) was precipitated by adding the same volume of isopropanol followed by centrifugation with 12,000g for 15min at 4°C. The supernatant was discarded and the gDNA pellet was washed with 70% ethanol followed by centrifugation with 12,000g for 5min at 4°C. gDNA was air-dried for 10 min at RT and then 100µl of ddH_2O was added to the pellet.

PCR reaction was set up as follows,

10µl 2xRedTaq; 0.4 µl *Jmjd6*-5'arm; 0.4 µl *Jmjd6*-3'arm; 0.8 µl *Jmjd6*-LAR3; 1µl gDNA; 7.4µl ddH_2O

3.2.2 Culture of cells

3.2.2.1 Feeder cell generation

E13.5 WT embryos were taken from pregnant mice with sterile forceps and scissors and placed in petri-dish with sterile PBS. Head, limb, and all visceral were removed. The remaining body from all embryos was transferred to a new petri-dish and covered with 1 ml of 0.25% trypsin. Cut the embryo body into small pieces with a sterile knife or scissors. Transfer tissue together with 0.25% trypsin into a 50ml tube and add enough 0.25% trypsin to cover all the tissues. Digest tissue at 37°C for 15min. Pipette up and down the digested tissue a few times. Fill up the tube with a mouse embryonic fibroblast (MEF) medium to stop the digestion. Single cells and small debris were

collected by centrifuging at 1200 rpm for 5 min at RT. Seed the MEF cells as 2 embryos per 15cm dish. MEF cells were incubated at 37 °C with 5% CO_2 for 2-3 days to reach the confluent. MEF cells were then passaged by 1:4 and cultured for another 2-3 days. When MEF cells reach confluent, freeze every 15cm dish cells into 4 tubes.

To prepare feeder cells, thaw one tube of MEF cells into a 15cm dish and split 1:4 when it reaches confluent. Passage for 2-3 generations to get enough cells. Mitomycin C (Sigma, M4287) was dissolved in sterilized ddH_2O and then filtered with a 0.22μM filter to make 1mg/ml stock. Freshly prepared Mitomycin C was added to the confluent MEF cells with a working concentration of 10μg/ml. MEF cells were then incubated at 37°C with 5% CO_2 for 2 hours in the incubator. After the treatment, MEF cells were washed three times with PBS to remove the remaining Mitomycin C. Feeder cells can be digested with trypsin and frozen in liquid nitrogen for long-term storage.

3.2.2.2 Mouse embryonic stem cell lines

E14 Tg(Nxk2-5-EmGFP) ES cells (Hsiao, Yoshinaga et al. 2008) were cultured on feeder cells in a KnockOut medium with 1000U/ml leukemia inhibitory factor (LIF) (Millipore, ESG1107). For stem cell differentiation, virus infection, and plasmid transfection, it can also be cultured on a 0.1% gelatin-coated dish supplied with 2000U/ml LIF.

3.2.2.3 Other cell lines

Other cell lines used in this study were cultured in an appropriate medium (5.1.2) at 37°C with 5% CO2. B2B cells were cultured in Roswell Park Memorial Institute 1640 supplemented with 10% FBS and penicillin/streptomycin/glutamine.

3.2.3 Generation of knockout and Knock-in mESCs with CRISPR/Cas9

3.2.3.1 Generation of gene knockout mESCs

For the generation of *Jmjd6* knockout mESCs by CRISPR/CAS9, a combination of two guide RNAs (gRNAs) were used as follows: gRNA-1: 5'- GAGCAAGAAGCGCATCCGCG -3' and gRNA2: 5'- GTGATGGGACGACACACCGC -3'. pSpCas9(BB)-2A-Puro (PX459) V2.0 (addgene plasmid # 62988) was digested and annealed gRNA was cloned into plasmids pSpCas9(BB)-2A-Puro (PX459) V2.0-gRNA-1 and pSpCas9(BB)-2A-Puro (PX459) V2.0-gRNA-2. To remove the feeder cells, E14-Nkx2.5-EmGFP were digested with 0.05% trypsin and seed on a new plate. After incubating for 45 min in the incubator, undifferentiated mESCs which were not attached to the dish were collected. mESCs were seed on 0.1% gelatin coated 6-well plate with 0.1M cells/well. Both plasmids (in total 3 μg) were transfected into ESCs with Lipofectamine 2000 according to the manual the next day. Positive cells were selected after 24 hours of transfection for 48 h with 4μg/ml puromycin. After puromycin selection, 5000 cells were plated in a 6-cm dish. After 7 days of culture, single clones were picked into 96 well plate with feeder cells. After 2-3 days of culture, split 20% of cells into a new 24-well plate and freeze the rest 80% of cells in -80°C. After 3-5days of culture, gDNA can be purified for genotyping when most of the wells reach confluent. Three primers were used for homozygous and heterozygous *Jmjd6* knock-out cell genotyping (Figure 16A).

For the generation of Isl1 knockout cell lines, a combination of two guide RNAs (gRNAs) was used as follows: gRNA-1: 5'- CCGATTTAAGCCGGCGGAGT -3' and gRNA2: 5'- TCATGAGCGCATCTGGCCGA -3'.

3.2.3.2 Generation of 3xFlag-*Jmjd6* knockin mESCs

For generating 3xFlag-*Jmjd6* knockin, a gRNA and single-strand oligo DNA (ssODNA) which serve as a repair template were used as follows: gRNA-1: 5'- GAGCAAGAAGCGCATCCGCG -3' and *Jmjd6*-N-KI-ssdonor, 5'- GACGGCGAGCGACTCACGATGGACTACAAAGACCATGACGGTGATTATAAAGATCATGAC ATCGACTATAAGGACGATGATGACAAAAACCACAAGAGCAAGAAGCGCATCCGCGAGGCC

-3'. Seed mESCs as 0.1M cells/well on gelatin coated 6-well plate as described in generating knockout cells. 1.5μg of the plasmid carrying gRNA and 1.5 μg ssODNA were co-transfected with Lipofectamine 2000 according to the manual. Positive cell selection with puromycin, picking a single clone, and gDNA preparation are the same as generating knockout cells. Two primers flanking the 3xFlag were used for genotyping.

3.2.4 Generation of stable cell lines

The shRNA used for each gene is from the RNAi consortium (TRC) shRNA library (Sigma-Aldrich). Sequence for shRNA can be found in 5.1.3.

To produce lentivirus, HEK293T cells were seeded on a 6-well plate and were transfected at 50%-80% confluence with 3 μg of plasmids containing 1.5 μg of core plasmid (pLKO served as shRNA control, shRNA plasmid, or gene overexpression plasmid), 975ng of pCMVR8.74, and 525 ng of pMD2.G using X-tremeGENE DNA transfection reagent.

For generating stable mESC lines, the medium was changed with mESC medium (DMEM + High glucose, 15% FBS, 2 mM L-Glutamine, 0.07 mM β-mercaptoethanol, 0.1 mM nonessential amino acids, 1 mM sodium pyruvate, 100U/ml Penicillin-Streptomycin) 24 hours after the transfection. The viral supernatant was collected 72 hours after transfection and filtered with a 0.4 μM filter to remove the cell debris. 2 ml virus together with 1,000 U/ml LIF and 8 μg/ml polybrene (Sigma, TR-1003-G) were used to infect 100.000 ES cells on 5% poly-HEMA (Sigma, P3932) treated plates for overnight. Infected ES cells were plated on feeders on the following day. The next day, stable cells were selected by adding 10 μg/mL puromycin.

For generating other stable cell lines, the medium was changed with fresh HEK293T medium (DMEM + High glucose, 10% FBS, 2 mM L-Glutamine, 0.1 mM nonessential amino acids, 1 mM sodium pyruvate, 100 U/ml Penicillin-Streptomycin). The virus was harvested as described above. 2 ml virus together with 8 μg/ml polybrene (Sigma, TR-1003-G) were used to infect HEK293T, NIH3T3 cells. 48 hours after the infection, HEK293T and NIT3T3 were selected with 5 μg/mL puromycin.

3.2.5 Cardiomyocyte differentiation

3.2.5.1 Handing drop

Remove the feeder from mESC cells as described above. ES cells were then aggregated on the lid of the petri dish as 500 cells in 15ul drops in mESC medium without LIF. A small drop with ES cells inside will be hung on the lid. After 48 hours of culture, embryonic bodies (EBs) were collected in low attachment culture dishes with ES cell growth medium. Cells were then harvested at the indicated time point for further experiment.

3.2.5.2 Direct cardiomyocyte differentiation

Remove the feeder from mESC as described above. mESC were cultured on gelatin coated dish in Neurobasal DMEM/F12 medium (50% Neurobasal, 50% DMEM-F12, 0.5× N2 supplement, 0.5× B27 supplement, 100U/ml Penicillin-Streptomycin, 2 mM L-Glutamine, 0.05% BSA , 0.01% 1.5×104 M monothioglycerol, 10 ng/ml BMP4 , 2,000 U/ml LIF) for two days to expand mESCs. mESCs were then aggregated in low attachment petri dish at 75,000 cells/ml in differentiation medium (75% IMDM , 25% F12 , 0.5× N2, 0.5× B27 supplement without VA, 100U/ml Penicillin-Streptomycin, 1% 50 µg/ml L-Ascorbic acid, 0.04% 4.5×10-4 M monothioglycerol). After 48 hours, EBs were dissociated with accutase (A1110501, Thermo Fisher) and re-aggregated at 150,000 cells/ml in low attachment petri dish with differentiation medium plus 5 ng/ml Activin A (R&D, 338-AC), 5 ng/ml VEGF (R&D, 293-VE-010) and 0.4 ng/ml BMP4 (R&D, 314-BP; Bmp4 concentration vary depending on the lot). EBs were dissociated with accutase 40 hours after the second aggregation and seeded on gelatin coated plates with Stempro-34 medium (Stempro-34 medium, 2.6% StemPro supplement, 100U/ml Penicillin-Streptomycin) plus 5ng/ml VEGF, 10ng/ml bFGF, 25ng/ml FGF10. Change the medium every two days for further culture.

3.2.6 Luciferase assay

For luciferase assays, NIH/3T3 cells were seeded in each well of 24-well plate and transfected 0.25μg pGL4-Mef2c-enhancer-Luc2-AHF reporter plasmid and 0.1μg pRSV-β gal normalization plasmid with lipfeactamine3000 reagent (Thermo Fisher, L3000008) according to the manufacture instructions. 48h after transfection, cells were lysed in 100μl lysis buffer (Promega, E1500). 20μl of lysate was used for luciferase activities measured with Luciferase Assay system (Promega, E1500) by a microplate reader (Tecan Spark). Luciferase values were normalized to β-galactosidase values.

3.2.7 Co-immunoprecipitation, Immunoprecipitation-Mass Spectrometry

3.2.7.1 Co-immunoprecipitation

Cells were harvested by trypsin digestion and resuspended into single-cell. Cells were washed with PBS once and lysed with co-IP buffer (add Protease inhibitor cocktail (539134-1ML, Millipore) and Phosphatase Inhibitor Cocktail (524632-1SET, Millipore) freshly) for 10 mins. The lysate was sonicated in the 30s on 30s off for 3 cycles. Spin down the lysate at 12,000g 5min, 4℃, and then take the supernatant. The first antibody was added to the supernatant overnight at 4℃. Protein G Sepharose(17061801, Cytiva) was added and incubated for 2 hours at 4℃. Beads were then washed with cold co-IP buffer 10min/time three times. The washed beads were resuspended in 20 μl of 2X Laemmli sample buffer and boiled at 95 °C for 5-10 min. The samples were immediately cooled on ice, and analyzed by SDS PAGE and Western blotting.

3.2.7.2 Immunoprecipitation-Mass Spectrometry

Control or 3xFlag-*Jmjd6* knock-in mESCs were harvested by trypsin digestion and resuspended into single-cell. Cells were washed with PBS once and lysed with co-IP

buffer (add Protease inhibitor cocktail (539134-1ML, Millipore) and Phosphatase Inhibitor Cocktail (524632-1SET, Millipore) freshly) for 10 mins. The lysate was sonicated in the 30s on 30s off for 3 cycles. Spin down the lysate at 12,000g 5min, 4℃, and then take the supernatant. ANTI-FLAG® M2 Affinity Gel (A22220, Sigma) was incubated with supernatant overnight. Beads were washed with cold co-IP buffer 10min/time three times.

3.2.8 Immunofluorescence staining

3.2.8.1 Immunofluorescence staining for cells

Cells were washed with PBS once and fixed with 4% PFA for 10mins. Two times of washes with PBS were performed then. Incubate cells with 5% of BSA in PBST (PBS with 0.3% TritonX-100) for 1 hour for permeabilization and blocking at RT. The first antibody was diluted into a blocking buffer (5% of BSA in PBST) and cells were incubated at 4°C overnight. Wash cells with PBST 10 min/time three times the next day. Incubate cells with the second antibody in blocking buffer for 2 hours at RT. Stain nuclear with DAPI for 10 min before washing cells with PBST 10 min/time three times. The cell can be mounted in ProLong™ Gold Antifade Mountant (P10144, Thermo Fisher) for imaging.

3.2.8.2 Immunofluorescence staining for whole-mount zebrafish and mouse embryos

Fix the embryos at 4°C with 4% PFA for 2 hours. Wash embryos with PBS two times. Then treat embryos with PBSTr (PBS with 0.5% Triton X-100) for 20min at RT. Wash embryos with PBSTw (PBS with 0.01% Tween-20) 10min/time for 6 times. Block the embryos with blocking buffer (5% BSA in PBSTw) overnight at 4°C. Dilute primary antibody in blocking buffer and embryos were incubated at 4°C for two days. Wash embryos with PBSTw 10min/time for 6 times. Incubate embryos with diluted second antibody in PBSTw for 2 hours at RT. Wash embryos with PBSTw 10min/time for 6 times. Embryos are ready for imaging.

3.2.9 p38 inhibitor treatment of zebrafish embryos and whole-mount in situ hybridization of zebrafish embryos

3.2.9.1 p38 inhibitor treatment of zebrafish embryos

Embryos and adult zebrafish were raised under standard laboratory conditions at 28 °C. The Tg(myl7:EGFP-HsHRAS)s883 line was used. To treat embryos with p38 inhibitors, 2-somatic embryos were dechorionated with 5 mg/ml stock pronase (Sigma, 10165921001) for 1-3 minutes at 28 ℃ and then cultured in an E3 medium with different concentrations of p38 inhibitors. Heart beating was counted under the microscopy at different time points. For imaging the heart morphology, zebrafish larva were fixed in 4% PFA (pH=7.0) overnight at 4 °C. The next day, zebrafish larva were embedded in 1% low-melting agarose (Roth, 6351). The image was done by Zeiss LSM 710 confocal microscope. Afterward, z-projections of optical sections were performed using ImageJ and cells number were counted.

3.2.9.2 Whole-mount in situ hybridization of zebrafish embryos

Zebrafish embryos were collected at indicated time points and fixed in 4% PFA (pH=7.0) overnight at 4 °C. Afterward, the embryos were dehydrated in 100% methanol and stored at -20°C for further steps. After dehydration or storage, the embryos were rehydrated as flowing at RT: 2x 5min in 70% (v/v) methanol in PTW, 2x 5min in 50% (v/v) methanol in PTW, 2x 5min in 30% (v/v) methanol in PTW, and finally 2x 5min in PTW. To ensure proper probe penetration, a proteinase-K digest was performed for embryos older than 24hpf. Embryos at the 24hpf stage were treated for 3min, 30hpf embryos for 5min, and embryos at 48hpf or older were treated for 20min with proteinase-K solution (1µg/ml in PTW). The embryos were washed once with PTW and incubated for 20min in 4% PFA to stop the digestion. The embryos were washed 2x 5min with PTW. The embryos were then equilibrated in 2x 500µl hybridization solution for 5min before the pre-hybridization. Pre-hybridization was done by incubating embryos in a hybridization solution at 65°C. Dilute the *in situ* probes in hybridization solution to a final concentration of 1µg/ml and denature the probes for 10min at 85°C.

The diluted probes were then incubated for 10min at 65°C and finally added to the pre-hybridized embryos. The hybridization was performed at 65°C in the water bath with shaking overnight. Next, the embryos were washed twice with 50% formamide, 5 x SSC, 1%SDS followed by subsequent washes with 2 × SSC and 0.2 x SSC at 65 °C and finally washed with 1xMABT at RT. Embryos were treated with a 2×blocking reagent (Roche, 11096176001) for 2h at room temperature followed by incubation with alkaline phosphatase-conjugated anti-DIG antibody (Roche, 11093274910) overnight at 4°C. Washing 6x 30min with MABT plus 2mM levamisole was performed to reduce the background staining. A final washing step was done with MABT. For color development, a BM-purple reagent (Roche, 11442074001) was used. Fixation with 4% PFA was used to stop the reaction.

3.2.10 Ex vivo culture of mouse embryos

All solutions were preheated to 37°C, and isolation was performed at this temperature. Embryos at the embryonic stage E8.5 were isolated retaining the connection between embryo and placenta respectively. Embryos were then cultured in DMEM medium (Gibco, 11960-044) supplemented with 50% in-house rat serum overnight with 5% CO2, 20% O2 atmosphere at 37°C (Zeeb, Axnick et al. 2012). p38 inhibitors were added at the indicated concentrations. Before harvesting proteins or RNAs, heart beating was counted under the microscope.

3.2.11 Chromatin immunoprecipitation

Cells from different stages of cardiomyocyte differentiation were harvested as the single-cell suspension. Cells were cross-linked by 1% formaldehyde (Sigma, F8775) for 10 min at RT. Crosslinking was stopped by adding glycine at a final concentration of 125 mM. Cells were then washed with cold PBS 3 x 10min on ice. Nuclei were then isolated by adding L1 lysis buffer (50 mM Tris pH 8.0, 2 mM EDTA pH 8.0, 0.1% NP-40, 10% glycerol) with protease and phosphatase inhibitors and incubated on ice for 10 min. Pellet the nuclei by centrifuging cell lysate at 3,000g for 5 min at 4°C. Isolated

nuclei was stored at -80 ℃ in L2 lysis buffer (50 mM Tris pH 8.0, 5mM EDTA pH 8.0, 1% SDS) for further step. Lysates were sonicated with Bioruptor (Diagenode) to achieve 200-500 bp DNA fragments. Lysates were diluted 1:10 in dilution buffer (50mM Tris pH 8.0, 200mM NaCl, 5mM EDTA pH 8.0, 0.5% NP40) with protease and phosphatase inhibitors and precleared with BSA-coated Protein G Sepharose (GE Healthcare) at 4 ℃ for 2 h. 4 µg anti-H3K4me3 (Abcam #ab8580), 4 µg anti-H3K27me3 (Millipore, #07449), 8 µg anti-H2AK119ub (Millipore, #05678) and 10 µl anti-Ezh2 (Cell Signaling #5246s) antibody were incubated with precleared lysates overnight at 4 ℃ followed by pulldown with BSA-coated protein G sepharose beads. For anti-H3R2me2a immunoprecipitations, 1ml of hybridoma supernatant (gift from Prof. Uta-Maria Bauer[38]) was incubated with BSA-coated protein G sepharose 2 h at 4 ℃. After washing with dilution buffer, antibodies-precoupled beads were incubated with lysates overnight at 4 ℃. Immune complex was washed with NaCl wash buffer (20 mM Tris pH 8.0, 500 mM NaCl, 2mM EDTA pH 8.0, 0.1% SDS, 1% NP40), LiCl wash buffer (20 mM Tris pH 8.0, 500 mM LiCl, 2mM EDTA pH 8.0, 0.1% SDS, 1% NP40) and TE wash buffer (20 mM Tris pH 8.0, 2mM EDTA pH 8.0) 3 x 5 min each. Protein/DNA complexes were extracted in elution buffer (20 mM Tris pH 8.0, 2mM EDTA pH 8.0, 2% SDS) followed by reverse crosslinking at 65 ℃ overnight. Pheno-chloroform was used for DNA purification.

For ChIP-seq, libraries were prepared with NEBNext® Ultra™ II DNA Library Prep Kit for Illumina® (E7645S, NEB)according to the manual.

3.2.12 Bioinformatics analysis

3.2.12.1 RNA-seq analysis

Adaptor sequences were trimmed from raw reads with trimmomatic (Bolger, Lohse et al. 2014) with the default setting. Clean reads were then aligned to mouse mm10 reference genome using STAR (Dobin, Davis et al. 2013) (--outSAMtype BAM SortedByCoordinate) to generate sorted bam files. Duplicated reads were removed

from the sorted bam file with Picard (-REMOVE_DUPLICATES true). The output bam files from Picard are used for generating BigWig files using bamCoverage from deeptools (Ramírez, Ryan et al. 2016). Integrative Genomics Viewer (IGV) (Robinson, Thorvaldsdóttir et al. 2011) was used for viewing BigWig files. The same bam files were also used for quantifying gene expression with featureCounts (Liao, Smyth et al. 2014). Differential gene expression analyses were done by DESeq2 (Love, Huber et al. 2014) R package. PCA plot, heatmap, and also volcano plot were generated in R with a custom script.

3.2.12.2 ChIP-seq analysis

Adaptor trimming, clean reads aligning, and duplicated reads removing are performed in the same way as RAN-seq analysis. A merged bam file for calling peaks was generated by merging all bam files from control or *Jmjd6* knockout samples with samtools. Peaks were called from merged bam with MACS2 (Zhang, Liu et al. 2008). Bed files of the broad peak were used for the following analysis. Peak quantification was done by multicov from The BEDTools (Quinlan and Hall 2010) suite using individual bam files and the bed file of the broad peak from merged bam. Peaks were then annotated with ChIPseeker in R. Differentiation peaks and normalization were done by DESeq2 package in R. Scale factors for each sample were also obtained from DESeq2 for normalization of BigWig files. BamCoverage from deeptools (--normalizeUsing None --scaleFactor) were used for generating BigWig files from the bam files. IGV was used for viewing BigWig files. PCA plot, heatmap, and also volcano plot were generated in R with a custom script. TSS profile plot were done with ngsplot (Shen, Shao et al. 2014).

Chapter 4: Appendix

4.1 Reference

Acloque, H., O. H. Ocaña, A. Matheu, K. Rizzoti, C. Wise, R. Lovell-Badge and M. A. Nieto (2011). "Reciprocal repression between Sox3 and snail transcription factors defines embryonic territories at gastrulation." Developmental cell **21**(3): 546-558.

Ahlgren, U., S. L. Pfaff, T. M. Jessell, T. Edlund and H. Edlund (1997). "Independent requirement for ISL1 in formation of pancreatic mesenchyme and islet cells." Nature **385**(6613): 257-260.

Allen, M., L. Svensson, M. Roach, J. Hambor, J. McNeish and C. A. Gabel (2000). "Deficiency of the stress kinase p38α results in embryonic lethality: characterization of the kinase dependence of stress responses of enzyme-deficient embryonic stem cells." The Journal of experimental medicine **191**(5): 859-870.

Andersen, P., E. Tampakakis, D. V. Jimenez, S. Kannan, M. Miyamoto, H. K. Shin, A. Saberi, S. Murphy, E. Sulistio and S. P. Chelko (2018). "Precardiac organoids form two heart fields via Bmp/Wnt signaling." Nature communications **9**(1): 1-13.

Ando, K., S. Shioda, H. Handa and K. Kataoka (2003). "Isolation and characterization of an alternatively spliced variant of transcription factor Islet-1." Journal of molecular endocrinology **31**(3): 419-425.

Aouadi, M., F. Bost, L. Caron, K. Laurent, Y. Le Marchand Brustel and B. Binétruy (2006). "p38 mitogen‐activated protein kinase activity commits embryonic stem cells to either neurogenesis or cardiomyogenesis." Stem Cells **24**(5): 1399-1406.

Arnold, S. J., G.-J. Huang, A. F. Cheung, T. Era, S.-I. Nishikawa, E. K. Bikoff, Z. Molnár, E. J. Robertson and M. Groszer (2008). "The T-box transcription factor Eomes/Tbr2 regulates neurogenesis in the cortical subventricular zone." Genes & development **22**(18): 2479-2484.

Arnold, S. J. and E. J. Robertson (2009). "Making a commitment: cell lineage allocation and axis patterning in the early mouse embryo." Nature reviews Molecular cell biology **10**(2): 91-103.

Arrenberg, A. B., D. Y. Stainier, H. Baier and J. Huisken (2010). "Optogenetic control of cardiac function." Science **330**(6006): 971-974.

Ballaré, C., M. Lange, A. Lapinaite, G. M. Martin, L. Morey, G. Pascual, R. Liefke, B. Simon, Y. Shi and O. Gozani (2012). "Phf19 links methylated Lys36 of histone H3 to regulation of Polycomb activity." Nature structural & molecular biology **19**(12): 1257-1265.

Bardot, E. S. and A. K. Hadjantonakis (2020). "Mouse gastrulation: Coordination of tissue patterning, specification and diversification of cell fate." Mech Dev **163**: 103617.

Beppu, H., M. Kawabata, T. Hamamoto, A. Chytil, O. Minowa, T. Noda and K. Miyazono (2000). "BMP type II receptor is required for gastrulation and early development of mouse embryos." Developmental biology **221**(1): 249-258.

Bernstein, B. E., T. S. Mikkelsen, X. Xie, M. Kamal, D. J. Huebert, J. Cuff, B. Fry, A. Meissner, M. Wernig and K. Plath (2006). "A bivalent chromatin structure marks key developmental genes in embryonic stem cells." Cell **125**(2): 315-326.

Bhati, M., C. Lee, A. L. Nancarrow, M. Lee, V. J. Craig, I. Bach, J. M. Guss, J. P. Mackay and J. M. Matthews (2008). "Implementing the LIM code: the structural basis for cell type‐specific assembly of LIM‐homeodomain complexes." The EMBO journal **27**(14): 2018-2029.

Biben, C., R. Weber, S. Kesteven, E. Stanley, L. McDonald, D. A. Elliott, L. Barnett, F. Köentgen, L. Robb and M. Feneley (2000). "Cardiac septal and valvular dysmorphogenesis in mice heterozygous for mutations in the homeobox gene Nkx2-5." Circulation research **87**(10): 888-

895.
Black, B. L. (2007). Transcriptional pathways in second heart field development. Seminars in cell & developmental biology, Elsevier.
Black, D. L. (2003). "Mechanisms of alternative pre-messenger RNA splicing." Annual review of biochemistry **72**(1): 291-336.
Blanco, E., M. González-Ramírez, A. Alcaine-Colet, S. Aranda and L. Di Croce (2020). "The bivalent genome: characterization, structure, and regulation." Trends in Genetics **36**(2): 118-131.
Blencowe, B. J. (2006). "Alternative splicing: new insights from global analyses." Cell **126**(1): 37-47.
Boeckel, J. N., V. Guarani, M. Koyanagi, T. Roexe, A. Lengeling, R. T. Schermuly, P. Gellert, T. Braun, A. Zeiher and S. Dimmeler (2011). "Jumonji domain-containing protein 6 (Jmjd6) is required for angiogenic sprouting and regulates splicing of VEGF-receptor 1." Proc Natl Acad Sci U S A **108**(8): 3276-3281.
Bolger, A. M., M. Lohse and B. Usadel (2014). "Trimmomatic: a flexible trimmer for Illumina sequence data." Bioinformatics **30**(15): 2114-2120.
Bondue, A., G. Lapouge, C. Paulissen, C. Semeraro, M. Iacovino, M. Kyba and C. Blanpain (2008). "Mesp1 acts as a master regulator of multipotent cardiovascular progenitor specification." Cell stem cell **3**(1): 69-84.
Böse, J., A. D. Gruber, L. Helming, S. Schiebe, I. Wegener, M. Hafner, M. Beales, F. Köntgen and A. Lengeling (2004). "The phosphatidylserine receptor has essential functions during embryogenesis but not in apoptotic cell removal." Journal of biology **3**(4): 1.
Bouchard, C., P. Sahu, M. Meixner, R. R. Nötzold, M. B. Rust, E. Kremmer, R. Feederle, G. Hart-Smith, F. Finkernagel and M. Bartkuhn (2018). "Genomic Location of PRMT6-Dependent H3R2 Methylation Is Linked to the Transcriptional Outcome of Associated Genes." Cell reports **24**(12): 3339-3352.
Boyer, L. A., K. Plath, J. Zeitlinger, T. Brambrink, L. A. Medeiros, T. I. Lee, S. S. Levine, M. Wernig, A. Tajonar, M. K. Ray, G. W. Bell, A. P. Otte, M. Vidal, D. K. Gifford, R. A. Young and R. Jaenisch (2006). "Polycomb complexes repress developmental regulators in murine embryonic stem cells." Nature **441**(7091): 349-353.
Bracken, A. P., N. Dietrich, D. Pasini, K. H. Hansen and K. Helin (2006). "Genome-wide mapping of Polycomb target genes unravels their roles in cell fate transitions." Genes & development **20**(9): 1123-1136.
Brand, T. (2003). "Heart development: molecular insights into cardiac specification and early morphogenesis." Developmental biology **258**(1): 1-19.
Brown, D. D., S. N. Martz, O. Binder, S. C. Goetz, B. M. Price, J. C. Smith and F. L. Conlon (2005). "Tbx5 and Tbx20 act synergistically to control vertebrate heart morphogenesis." Development **132**(3): 553-563.
Bruneau, B. G. (2008). "The developmental genetics of congenital heart disease." Nature **451**(7181): 943-948.
Bruneau, B. G., M. Logan, N. Davis, T. Levi, C. J. Tabin, J. Seidman and C. E. Seidman (1999). "Chamber-specific cardiac expression of Tbx5 and heart defects in Holt–Oram syndrome." Developmental biology **211**(1): 100-108.
Bruneau, B. G., G. Nemer, J. P. Schmitt, F. Charron, L. Robitaille, S. Caron, D. A. Conner, M. Gessler, M. Nemer and C. E. Seidman (2001). "A murine model of Holt-Oram syndrome defines roles of the T-box transcription factor Tbx5 in cardiogenesis and disease." Cell **106**(6): 709-721.
Cai, C.-L., W. Zhou, L. Yang, L. Bu, Y. Qyang, X. Zhang, X. Li, M. G. Rosenfeld, J. Chen and S. Evans (2005). "T-box genes coordinate regional rates of proliferation and regional specification during cardiogenesis." Development **132**(10): 2475-2487.
Cai, C. L., X. Liang, Y. Shi, P. H. Chu, S. L. Pfaff, J. Chen and S. Evans (2003). "Isl1 identifies a

cardiac progenitor population that proliferates prior to differentiation and contributes a majority of cells to the heart." Dev Cell **5**(6): 877-889.
Caputo, L., H. R. Witzel, P. Kolovos, S. Cheedipudi, M. Looso, A. Mylona, I. W. F. van, K. L. Laugwitz, S. M. Evans, T. Braun, E. Soler, F. Grosveld and G. Dobreva (2015). "The Isl1/Ldb1 Complex Orchestrates Genome-wide Chromatin Organization to Instruct Differentiation of Multipotent Cardiac Progenitors." Cell Stem Cell **17**(3): 287-299.
Carver, E. A., R. Jiang, Y. Lan, K. F. Oram and T. Gridley (2001). "The mouse snail gene encodes a key regulator of the epithelial-mesenchymal transition." Molecular and cellular biology **21**(23): 8184-8188.
Chang, B., Y. Chen, Y. Zhao and R. K. Bruick (2007). "JMJD6 is a histone arginine demethylase." Science **318**(5849): 444-447.
Ciferri, C., G. C. Lander, A. Maiolica, F. Herzog, R. Aebersold and E. Nogales (2012). "Molecular architecture of human polycomb repressive complex 2." elife **1**: e00005.
Cikala, M., O. Alexandrova, C. N. David, M. Pröschel, B. Stiening, P. Cramer and A. Böttger (2004). "The phosphatidylserine receptor from Hydra is a nuclear protein with potential Fe (II) dependent oxygenase activity." BMC cell biology **5**(1): 26.
Ciruna, B. and J. Rossant (2001). "FGF signaling regulates mesoderm cell fate specification and morphogenetic movement at the primitive streak." Developmental cell **1**(1): 37-49.
Ciruna, B. G., L. Schwartz, K. Harpal, T. P. Yamaguchi and J. Rossant (1997). "Chimeric analysis of fibroblast growth factor receptor-1 (Fgfr1) function: a role for FGFR1 in morphogenetic movement through the primitive streak." Development **124**(14): 2829-2841.
Clark, J. E., N. Sarafraz and M. S. Marber (2007). "Potential of p38-MAPK inhibitors in the treatment of ischaemic heart disease." Pharmacology & therapeutics **116**(2): 192-206.
Clissold, P. M. and C. P. Ponting (2001). "JmjC: cupin metalloenzyme-like domains in jumonji, hairless and phospholipase A2β." Trends in biochemical sciences **26**(1): 7-9.
Conway, E. and A. Bracken (2017). Unraveling the Roles of Canonical and Noncanonical PRC1 Complexes. Polycomb Group Proteins, Elsevier**:** 57-80.
Cooper, S., M. Dienstbier, R. Hassan, L. Schermelleh, J. Sharif, N. P. Blackledge, V. De Marco, S. Elderkin, H. Koseki and R. Klose (2014). "Targeting polycomb to pericentric heterochromatin in embryonic stem cells reveals a role for H2AK119u1 in PRC2 recruitment." Cell reports **7**(5): 1456-1470.
Costello, I., I.-M. Pimeisl, S. Dräger, E. K. Bikoff, E. J. Robertson and S. J. Arnold (2011). "The T-box transcription factor Eomesodermin acts upstream of Mesp1 to specify cardiac mesoderm during mouse gastrulation." Nature cell biology **13**(9): 1084-1091.
Creppe, C., A. Palau, R. Malinverni, V. Valero and M. Buschbeck (2014). "A Cbx8-containing polycomb complex facilitates the transition to gene activation during ES cell differentiation." PLoS genetics **10**(12): e1004851.
Cuadrado, A. and A. R. Nebreda (2010). "Mechanisms and functions of p38 MAPK signalling." Biochem J **429**(3): 403-417.
Cui, P., B. Qin, N. Liu, G. Pan and D. Pei (2004). "Nuclear localization of the phosphatidylserine receptor protein via multiple nuclear localization signals." Experimental cell research **293**(1): 154-163.
David, R., V. B. Jarsch, F. Schwarz, P. Nathan, M. Gegg, H. Lickert and W.-M. Franz (2011). "Induction of MesP1 by Brachyury (T) generates the common multipotent cardiovascular stem cell." Cardiovascular research **92**(1): 115-122.
de Pater, E., L. Clijsters, S. R. Marques, Y. F. Lin, Z. V. Garavito-Aguilar, D. Yelon and J. Bakkers (2009). "Distinct phases of cardiomyocyte differentiation regulate growth of the zebrafish heart." Development **136**(10): 1633-1641.
Dobin, A., C. A. Davis, F. Schlesinger, J. Drenkow, C. Zaleski, S. Jha, P. Batut, M. Chaisson and T. R. Gingeras (2013). "STAR: ultrafast universal RNA-seq aligner." Bioinformatics **29**(1): 15-21.
Doetschman, T. C., H. Eistetter, M. Katz, W. Schmidt and R. Kemler (1985). "The in vitro

development of blastocyst-derived embryonic stem cell lines: formation of visceral yolk sac, blood islands and myocardium." Development **87**(1): 27-45.
Dudley, A. T. and E. J. Robertson (1997). "Overlapping expression domains of bone morphogenetic protein family members potentially account for limited tissue defects in BMP7 deficient embryos." Developmental dynamics: an official publication of the American Association of Anatomists **208**(3): 349-362.
Edmondson, D. G., G. E. Lyons, J. F. Martin and E. N. Olson (1994). "Mef2 gene expression marks the cardiac and skeletal muscle lineages during mouse embryogenesis." Development **120**(5): 1251-1263.
Eriksson, M. and S. Leppä (2002). "Mitogen-activated protein kinases and activator protein 1 are required for proliferation and cardiomyocyte differentiation of P19 embryonal carcinoma cells." Journal of Biological Chemistry **277**(18): 15992-16001.
Fadok, V. A., D. L. Bratton, D. M. Rose, A. Pearson, R. A. Ezekewitz and P. M. Henson (2000). "A receptor for phosphatidylserine-specific clearance of apoptotic cells." Nature **405**(6782): 85-90.
Frankel, A., N. Yadav, J. Lee, T. L. Branscombe, S. Clarke and M. T. Bedford (2002). "The novel human protein arginine N-methyltransferase PRMT6 is a nuclear enzyme displaying unique substrate specificity." Journal of Biological Chemistry **277**(5): 3537-3543.
Friedrich, F. W., G. Dilanian, P. Khattar, D. Juhr, L. Gueneau, P. Charron, V. Fressart, J. T. Vilquin, R. Isnard, L. Gouya, P. Richard, N. Hammoudi, M. Komajda, G. Bonne, T. Eschenhagen, O. Dubourg, E. Villard and L. Carrier (2013). "A novel genetic variant in the transcription factor Islet-1 exerts gain of function on myocyte enhancer factor 2C promoter activity." Eur J Heart Fail **15**(3): 267-276.
Gadd, M. S., D. A. Jacques, I. Nisevic, V. J. Craig, A. H. Kwan, J. M. Guss and J. M. Matthews (2013). "A structural basis for the regulation of the LIM-homeodomain protein islet 1 (Isl1) by intra-and intermolecular interactions." Journal of Biological Chemistry **288**(30): 21924-21935.
Galvin, K. M., M. J. Donovan, C. A. Lynch, R. I. Meyer, R. J. Paul, J. N. Lorenz, V. Fairchild-Huntress, K. L. Dixon, J. H. Dunmore and M. A. Gimbrone (2000). "A role for smad6 in development and homeostasis of the cardiovascular system." Nature genetics **24**(2): 171-174.
Gao, R., X. Liang, S. Cheedipudi, J. Cordero, X. Jiang, Q. Zhang, L. Caputo, S. Gunther, C. Kuenne, Y. Ren, S. Bhattacharya, X. Yuan, G. Barreto, Y. Chen, T. Braun, S. M. Evans, Y. Sun and G. Dobreva (2019). "Pioneering function of Isl1 in the epigenetic control of cardiomyocyte cell fate." Cell Res **29**(6): 486-501.
Gao, W. W., R. Q. Xiao, B. L. Peng, H. T. Xu, H. F. Shen, M. F. Huang, T. T. Shi, J. Yi, W. J. Zhang, X. N. Wu, X. Gao, X. Z. Lin, P. C. Dorrestein, M. G. Rosenfeld and W. Liu (2015). "Arginine methylation of HSP70 regulates retinoid acid-mediated RARbeta2 gene activation." Proc Natl Acad Sci U S A **112**(26): E3327-3336.
Gao, Z., J. Zhang, R. Bonasio, F. Strino, A. Sawai, F. Parisi, Y. Kluger and D. Reinberg (2012). "PCGF homologs, CBX proteins, and RYBP define functionally distinct PRC1 family complexes." Molecular cell **45**(3): 344-356.
Gaspar-Maia, A., A. Alajem, F. Polesso, R. Sridharan, M. J. Mason, A. Heidersbach, J. Ramalho-Santos, M. T. McManus, K. Plath and E. Meshorer (2009). "Chd1 regulates open chromatin and pluripotency of embryonic stem cells." Nature **460**(7257): 863-868.
Ge, W., A. Wolf, T. Feng, C.-h. Ho, A. Zayer, N. Granatino, M. E. Cockman, C. Loenarz, N. D. Loik and A. P. Hardy (2012). "Oxygenase-catalyzed ribosome hydroxylation occurs in prokaryotes and humans." Nature chemical biology **8**(12): 960.
Guccione, E., C. Bassi, F. Casadio, F. Martinato, M. Cesaroni, H. Schuchlautz, B. Lüscher and B. Amati (2007). "Methylation of histone H3R2 by PRMT6 and H3K4 by an MLL complex are mutually exclusive." Nature **449**(7164): 933.
Guo, G., M. Huss, G. Q. Tong, C. Wang, L. L. Sun, N. D. Clarke and P. Robson (2010). "Resolution of cell fate decisions revealed by single-cell gene expression analysis from zygote to

blastocyst." Developmental cell **18**(4): 675-685.
Guo, Y. J., W. W. Pan, S. B. Liu, Z. F. Shen, Y. Xu and L. L. Hu (2020). "ERK/MAPK signalling pathway and tumorigenesis." Experimental and Therapeutic Medicine **19**(3): 1997-2007.
Hahn, P., J. Bose, S. Edler and A. Lengeling (2008). "Genomic structure and expression of Jmjd6 and evolutionary analysis in the context of related JmjC domain containing proteins." BMC Genomics **9**: 293.
Hahn, P., I. Wegener, A. Burrells, J. Bose, A. Wolf, C. Erck, D. Butler, C. J. Schofield, A. Bottger and A. Lengeling (2010). "Analysis of Jmjd6 cellular localization and testing for its involvement in histone demethylation." PLoS One **5**(10): e13769.
Han, G., J. Li, Y. Wang, X. Li, H. Mao, Y. Liu and C. D. Chen (2012). "The hydroxylation activity of Jmjd6 is required for its homo‐oligomerization." Journal of cellular biochemistry **113**(5): 1663-1670.
Haraguchi, S., S. Kitajima, A. Takagi, H. Takeda, T. Inoue and Y. Saga (2001). "Transcriptional regulation of Mesp1 and Mesp2 genes: differential usage of enhancers during development." Mechanisms of development **108**(1-2): 59-69.
Hart, A. H., L. Hartley, K. Sourris, E. S. Stadler, R. Li, E. G. Stanley, P. P. Tam, A. G. Elefanty and L. Robb (2002). "Mixl1 is required for axial mesendoderm morphogenesis and patterning in the murine embryo."
Hartley, S. W. and J. C. Mullikin (2016). "Detection and visualization of differential splicing in RNA-Seq data with JunctionSeq." Nucleic acids research **44**(15): e127-e127.
Harvey, R. P. (2002). "Patterning the vertebrate heart." Nature Reviews Genetics **3**(7): 544-556.
Hausinger, R. P. (2004). "Fe (II)/α-ketoglutarate-dependent hydroxylases and related enzymes." Critical reviews in biochemistry and molecular biology **39**(1): 21-68.
Healy, E., M. Mucha, E. Glancy, D. J. Fitzpatrick, E. Conway, H. K. Neikes, C. Monger, G. Van Mierlo, M. P. Baltissen and Y. Koseki (2019). "PRC2. 1 and PRC2. 2 synergize to coordinate H3K27 trimethylation." Molecular cell **76**(3): 437-452. e436.
Heim, A., C. Grimm, U. Muller, S. Haussler, M. M. Mackeen, J. Merl, S. M. Hauck, B. M. Kessler, C. J. Schofield, A. Wolf and A. Bottger (2014). "Jumonji domain containing protein 6 (Jmjd6) modulates splicing and specifically interacts with arginine-serine-rich (RS) domains of SR- and SR-like proteins." Nucleic Acids Res **42**(12): 7833-7850.
Hernandez-Torres, F., S. Martinez-Fernandez, S. Zuluaga, A. Nebreda, A. Porras, A. E. Aranega and F. Navarro (2008). "A role for p38alpha mitogen-activated protein kinase in embryonic cardiac differentiation." FEBS Lett **582**(7): 1025-1031.
Holt, M. V., T. Wang and N. L. Young (2017). "Recent advances in understanding histone modification events." Current Molecular Biology Reports **3**(1): 11-17.
Hong, X., J. Zang, J. White, C. Wang, C. H. Pan, R. Zhao, R. C. Murphy, S. Dai, P. Henson, J. W. Kappler, J. Hagman and G. Zhang (2010). "Interaction of JMJD6 with single-stranded RNA." Proc Natl Acad Sci U S A **107**(33): 14568-14572.
Hsiao, E. C., Y. Yoshinaga, T. D. Nguyen, S. L. Musone, J. E. Kim, P. Swinton, I. Espineda, C. Manalac, P. J. deJong and B. R. Conklin (2008). "Marking embryonic stem cells with a 2A self-cleaving peptide: a NKX2-5 emerald GFP BAC reporter." PloS one **3**(7).
Hunter, T. (2007). "The age of crosstalk: phosphorylation, ubiquitination, and beyond." Molecular cell **28**(5): 730-738.
Hyllus, D., C. Stein, K. Schnabel, E. Schiltz, A. Imhof, Y. Dou, J. Hsieh and U.-M. Bauer (2007). "PRMT6-mediated methylation of R2 in histone H3 antagonizes H3 K4 trimethylation." Genes & development **21**(24): 3369-3380.
Islam, M. S., T. M. Leissing, R. Chowdhury, R. J. Hopkinson and C. J. Schofield (2018). "2-Oxoglutarate-dependent oxygenases." Annual review of biochemistry **87**: 585-620.
Islam, M. S., M. A. McDonough, R. Chowdhury, J. Gault, A. Khan, E. Pires and C. J. Schofield (2019). "Biochemical and structural investigations clarify the substrate selectivity of the 2-

oxoglutarate oxygenase JMJD6." Journal of Biological Chemistry: jbc. RA119. 008693.
Islam, M. S., M. A. McDonough, R. Chowdhury, J. Gault, A. Khan, E. Pires and C. J. Schofield (2019). "Biochemical and structural investigations clarify the substrate selectivity of the 2-oxoglutarate oxygenase JMJD6." Journal of Biological Chemistry **294**(30): 11637-11652.
Jadrich, J. L., M. B. O'Connor and E. Coucouvanis (2006). "The TGF beta activated kinase TAK1 regulates vascular development in vivo." Development **133**(8): 1529-1541.
Juan, A. H., S. Wang, K. D. Ko, H. Zare, P.-F. Tsai, X. Feng, K. O. Vivanco, A. M. Ascoli, G. Gutierrez-Cruz and J. Krebs (2016). "Roles of H3K27me2 and H3K27me3 examined during fate specification of embryonic stem cells." Cell reports **17**(5): 1369-1382.
Kalb, R., S. Latwiel, H. I. Baymaz, P. W. Jansen, C. W. Müller, M. Vermeulen and J. Müller (2014). "Histone H2A monoubiquitination promotes histone H3 methylation in Polycomb repression." Nature structural & molecular biology **21**(6): 569-571.
Kanai-Azuma, M., Y. Kanai, J. M. Gad, Y. Tajima, C. Taya, M. Kurohmaru, Y. Sanai, H. Yonekawa, K. Yazaki and P. P. Tam (2002). "Depletion of definitive gut endoderm in Sox17-null mutant mice."
Karlsson, O., S. Thor, T. Norberg, H. Ohlsson and T. Edlund (1990). "Insulin gene enhancer binding protein Isl-1 is a member of a novel class of proteins containing both a homeo-and a Cys–His domain." Nature **344**(6269): 879-882.
Kasahara, H., S. Bartunkova, M. Schinke, M. Tanaka and S. Izumo (1998). "Cardiac and extracardiac expression of Csx/Nkx2. 5 homeodomain protein." Circulation research **82**(9): 936-946.
Kattman, S. J., A. D. Witty, M. Gagliardi, N. C. Dubois, M. Niapour, A. Hotta, J. Ellis and G. Keller (2011). "Stage-specific optimization of activin/nodal and BMP signaling promotes cardiac differentiation of mouse and human pluripotent stem cell lines." Cell Stem Cell **8**(2): 228-240.
Kemler, R., A. Hierholzer, B. Kanzler, S. Kuppig, K. Hansen, M. M. Taketo, W. N. de Vries, B. B. Knowles and D. Solter (2004). "Stabilization of beta-catenin in the mouse zygote leads to premature epithelial-mesenchymal transition in the epiblast." Development **131**(23): 5817-5824.
Khan, A., C. J. Schofield and T. D. Claridge (2020). "Reducing Agent‐Mediated Nonenzymatic Conversion of 2‐Oxoglutarate to Succinate: Implications for Oxygenase Assays." ChemBioChem **21**(20): 2898-2902.
Kim, Y. and M. Nirenberg (1989). "Drosophila NK-homeobox genes." Proceedings of the National Academy of Sciences **86**(20): 7716-7720.
Kirmizis, A., H. Santos-Rosa, C. J. Penkett, M. A. Singer, M. Vermeulen, M. Mann, J. Bähler, R. D. Green and T. Kouzarides (2007). "Arginine methylation at histone H3R2 controls deposition of H3K4 trimethylation." Nature **449**(7164): 928.
Kojima, Y., O. H. Tam and P. P. Tam (2014). Timing of developmental events in the early mouse embryo. Seminars in cell & developmental biology, Elsevier.
Komuro, I. and S. Izumo (1993). "Csx: a murine homeobox-containing gene specifically expressed in the developing heart." Proceedings of the National Academy of Sciences **90**(17): 8145-8149.
Kunisaki, Y., S. Masuko, M. Noda, A. Inayoshi, T. Sanui, M. Harada, T. Sasazuki and Y. Fukui (2004). "Defective fetal liver erythropoiesis and T lymphopoiesis in mice lacking the phosphatidylserine receptor." Blood **103**(9): 3362-3364.
Kuo, C. T., E. E. Morrisey, R. Anandappa, K. Sigrist, M. M. Lu, M. S. Parmacek, C. Soudais and J. M. Leiden (1997). "GATA4 transcription factor is required for ventral morphogenesis and heart tube formation." Genes & development **11**(8): 1048-1060.
Laible, G., A. Wolf, R. Dorn, G. Reuter, C. Nislow, A. Lebersorger, D. Popkin, L. Pillus and T. Jenuwein (1997). "Mammalian homologues of the Polycomb-group gene Enhancer of zeste mediate gene silencing in Drosophila heterochromatin and at S. cerevisiae telomeres." The EMBO journal **16**(11): 3219-3232.

Laugwitz, K. L., A. Moretti, J. Lam, P. Gruber, Y. Chen, S. Woodard, L. Z. Lin, C. L. Cai, M. M. Lu, M. Reth, O. Platoshyn, J. X. Yuan, S. Evans and K. R. Chien (2005). "Postnatal isl1+ cardioblasts enter fully differentiated cardiomyocyte lineages." Nature **433**(7026): 647-653.
Lawrence, P., J. S. Conderino and E. Rieder (2014). "Redistribution of demethylated RNA helicase A during foot-and-mouth disease virus infection: role of Jumonji C-domain containing protein 6 in RHA demethylation." Virology **452-453**: 1-11.
Lawson, K. A., J. J. Meneses and R. Pedersen (1991). "Clonal analysis of epiblast fate during germ layer formation in the mouse embryo." Development **113**(3): 891-911.
Lee, T. I., R. G. Jenner, L. A. Boyer, M. G. Guenther, S. S. Levine, R. M. Kumar, B. Chevalier, S. E. Johnstone, M. F. Cole, K. Isono, H. Koseki, T. Fuchikami, K. Abe, H. L. Murray, J. P. Zucker, B. Yuan, G. W. Bell, E. Herbolsheimer, N. M. Hannett, K. Sun, D. T. Odom, A. P. Otte, T. L. Volkert, D. P. Bartel, D. A. Melton, D. K. Gifford, R. Jaenisch and R. A. Young (2006). "Control of developmental regulators by Polycomb in human embryonic stem cells." Cell **125**(2): 301-313.
Lee, Y.-H., S. S. Koh, X. Zhang, X. Cheng and M. R. Stallcup (2002). "Synergy among nuclear receptor coactivators: selective requirement for protein methyltransferase and acetyltransferase activities." Molecular and cellular biology **22**(11): 3621-3632.
Lemke, L. E., L. J. Bloem, R. Fouts, M. Esterman, G. Sandusky and C. J. Vlahos (2001). "Decreased p38 MAPK activity in end-stage failing human myocardium: p38 MAPK α is the predominant isoform expressed in human heart." Journal of molecular and cellular cardiology **33**(8): 1527-1540.
Li, G., R. Margueron, M. Ku, P. Chambon, B. E. Bernstein and D. Reinberg (2010). "Jarid2 and PRC2, partners in regulating gene expression." Genes & development **24**(4): 368-380.
Li, M. O., M. R. Sarkisian, W. Z. Mehal, P. Rakic and R. A. Flavell (2003). "Phosphatidylserine receptor is required for clearance of apoptotic cells." Science **302**(5650): 1560-1563.
Liang, X., Q. Zhang, P. Cattaneo, S. Zhuang, X. Gong, N. J. Spann, C. Jiang, X. Cao, X. Zhao, X. Zhang, L. Bu, G. Wang, H. S. Chen, T. Zhuang, J. Yan, P. Geng, L. Luo, I. Banerjee, Y. Chen, C. K. Glass, A. C. Zambon, J. Chen, Y. Sun and S. M. Evans (2015). "Transcription factor ISL1 is essential for pacemaker development and function." J Clin Invest **125**(8): 3256-3268.
Liao, Y., G. K. Smyth and W. Shi (2014). "featureCounts: an efficient general purpose program for assigning sequence reads to genomic features." Bioinformatics **30**(7): 923-930.
Liberatore, C. M., R. D. Searcy-Schrick and K. E. Yutzey (2000). "Ventricular expression of tbx5 inhibits normal heart chamber development." Developmental biology **223**(1): 169-180.
Lin, Q., J. Schwarz, C. Bucana and E. N. Olson (1997). "Control of mouse cardiac morphogenesis and myogenesis by transcription factor MEF2C." Science **276**(5317): 1404-1407.
Lints, T. J., L. M. Parsons, L. Hartley, I. Lyons and R. P. Harvey (1993). "Nkx-2.5: a novel murine homeobox gene expressed in early heart progenitor cells and their myogenic descendants." Development **119**(2): 419-431.
Liu, W., Q. Ma, K. Wong, W. Li, K. Ohgi, J. Zhang, A. K. Aggarwal and M. G. Rosenfeld (2013). "Brd4 and JMJD6-associated anti-pause enhancers in regulation of transcriptional pause release." Cell **155**(7): 1581-1595.
Liu, W., J. Selever, D. Wang, M.-F. Lu, K. A. Moses, R. J. Schwartz and J. F. Martin (2004). "Bmp4 signaling is required for outflow-tract septation and branchial-arch artery remodeling." Proceedings of the National Academy of Sciences **101**(13): 4489-4494.
Loenarz, C. and C. J. Schofield (2008). "Expanding chemical biology of 2-oxoglutarate oxygenases." Nature chemical biology **4**(3): 152-156.
Love, M. I., W. Huber and S. Anders (2014). "Moderated estimation of fold change and dispersion for RNA-seq data with DESeq2." Genome biology **15**(12): 1-21.
Luis, N. M., L. Morey, L. Di Croce and S. A. Benitah (2012). "Polycomb in stem cells: PRC1 branches out." Cell stem cell **11**(1): 16-21.
Lyons, I., L. M. Parsons, L. Hartley, R. Li, J. E. Andrews, L. Robb and R. P. Harvey (1995). "Myogenic and morphogenetic defects in the heart tubes of murine embryos lacking the

homeo box gene Nkx2-5." Genes & development **9**(13): 1654-1666.
Ma, L., M.-F. Lu, R. J. Schwartz and J. F. Martin (2005). "Bmp2 is essential for cardiac cushion epithelial-mesenchymal transition and myocardial patterning." Development **132**(24): 5601-5611.
Maltsev, V. A., J. Rohwedel, J. Hescheler and A. M. Wobus (1993). "Embryonic stem cells differentiate in vitro into cardiomyocytes representing sinusnodal, atrial and ventricular cell types." Mechanisms of development **44**(1): 41-50.
Mantri, M., T. Krojer, E. A. Bagg, C. A. Webby, D. S. Butler, G. Kochan, K. L. Kavanagh, U. Oppermann, M. A. McDonough and C. J. Schofield (2010). "Crystal Structure of the 2-Oxoglutarate- and Fe(II)-Dependent Lysyl Hydroxylase JMJD6." J Mol Biol.
Mantri, M., N. D. Loik, R. B. Hamed, T. D. Claridge, J. S. McCullagh and C. J. Schofield (2011). "The 2-oxoglutarate-dependent oxygenase JMJD6 catalyses oxidation of lysine residues to give 5S-hydroxylysine residues." Chembiochem **12**(4): 531-534.
Mantri, M., C. J. Webby, N. D. Loik, R. B. Hamed, M. L. Nielsen, M. A. McDonough, J. S. McCullagh, A. Böttger, C. J. Schofield and A. Wolf (2012). "Self-hydroxylation of the splicing factor lysyl hydroxylase, JMJD6." MedChemComm **3**(1): 80-85.
Margueron, R., G. Li, K. Sarma, A. Blais, J. Zavadil, C. L. Woodcock, B. D. Dynlacht and D. Reinberg (2008). "Ezh1 and Ezh2 maintain repressive chromatin through different mechanisms." Molecular cell **32**(4): 503-518.
Markolovic, S., T. M. Leissing, R. Chowdhury, S. E. Wilkins, X. Lu and C. J. Schofield (2016). "Structure–function relationships of human JmjC oxygenases—demethylases versus hydroxylases." Current opinion in structural biology **41**: 62-72.
Mas, G., E. Blanco, C. Ballaré, M. Sansó, Y. G. Spill, D. Hu, Y. Aoi, F. Le Dily, A. Shilatifard and M. A. Marti-Renom (2018). "Promoter bivalency favors an open chromatin architecture in embryonic stem cells." Nature Genetics **50**(10): 1452-1462.
McCulley, D. J., J. O. Kang, J. F. Martin and B. L. Black (2008). "BMP4 is required in the anterior heart field and its derivatives for endocardial cushion remodeling, outflow tract septation, and semilunar valve development." Developmental dynamics: an official publication of the American Association of Anatomists **237**(11): 3200-3209.
McFadden, D. G., A. C. Barbosa, J. A. Richardson, M. D. Schneider, D. Srivastava and E. N. Olson (2005). "The Hand1 and Hand2 transcription factors regulate expansion of the embryonic cardiac ventricles in a gene dosage-dependent manner." Development **132**(1): 189-201.
Mikkelsen, T. S., M. Ku, D. B. Jaffe, B. Issac, E. Lieberman, G. Giannoukos, P. Alvarez, W. Brockman, T.-K. Kim and R. P. Koche (2007). "Genome-wide maps of chromatin state in pluripotent and lineage-committed cells." Nature **448**(7153): 553-560.
Milne, T. A., S. D. Briggs, H. W. Brock, M. E. Martin, D. Gibbs, C. D. Allis and J. L. Hess (2002). "MLL targets SET domain methyltransferase activity to Hox gene promoters." Molecular cell **10**(5): 1107-1117.
Mishina, Y., R. Crombie, A. Bradley and R. R. Behringer (1999). "Multiple roles for activin-like kinase-2 signaling during mouse embryogenesis." Developmental biology **213**(2): 314-326.
Mishina, Y., A. Suzuki, N. Ueno and R. R. Behringer (1995). "Bmpr encodes a type I bone morphogenetic protein receptor that is essential for gastrulation during mouse embryogenesis." Genes & development **9**(24): 3027-3037.
Mitchell, J. E., M. Cvetanovic, N. Tibrewal, V. Patel, O. R. Colamonici, M. O. Li, R. A. Flavell, J. S. Levine, R. B. Birge and D. S. Ucker (2006). "The presumptive phosphatidylserine receptor is dispensable for innate anti-inflammatory recognition and clearance of apoptotic cells." Journal of Biological Chemistry **281**(9): 5718-5725.
Mitiku, N. and J. C. Baker (2007). "Genomic analysis of gastrulation and organogenesis in the mouse." Developmental cell **13**(6): 897-907.
Mittnenzweig, M., Y. Mayshar, S. Cheng, R. Ben-Yair, R. Hadas, Y. Rais, E. Chomsky, N. Reines, A. Uzonyi and L. Lumerman (2021). "A single-embryo, single-cell time-resolved model for

mouse gastrulation." Cell **184**(11): 2825-2842. e2822.
Mohn, F., M. Weber, M. Rebhan, T. C. Roloff, J. Richter, M. B. Stadler, M. Bibel and D. Schübeler (2008). "Lineage-specific polycomb targets and de novo DNA methylation define restriction and potential of neuronal progenitors." Molecular cell **30**(6): 755-766.
Molkentin, J. D. (2000). "The zinc finger-containing transcription factors GATA-4,-5, and-6 ubiquitously expressed regulators of tissue-specific gene expression." Journal of Biological Chemistry **275**(50): 38949-38952.
Monzen, K., I. Shiojima, Y. Hiroi, S. Kudoh, T. Oka, E. Takimoto, D. Hayashi, T. Hosoda, A. Habara-Ohkubo, T. Nakaoka, T. Fujita, Y. Yazaki and I. Komuro (1999). "Bone morphogenetic proteins induce cardiomyocyte differentiation through the mitogen-activated protein kinase kinase kinase TAK1 and cardiac transcription factors Csx/Nkx-2.5 and GATA-4." Mol Cell Biol **19**(10): 7096-7105.
Morey, L., L. Aloia, L. Cozzuto, S. A. Benitah and L. Di Croce (2013). "RYBP and Cbx7 define specific biological functions of polycomb complexes in mouse embryonic stem cells." Cell reports **3**(1): 60-69.
Morey, L., G. Pascual, L. Cozzuto, G. Roma, A. Wutz, S. A. Benitah and L. Di Croce (2012). "Nonoverlapping functions of the Polycomb group Cbx family of proteins in embryonic stem cells." Cell stem cell **10**(1): 47-62.
Morgani, S. M. and A. K. Hadjantonakis (2020). "Signaling regulation during gastrulation: Insights from mouse embryos and in vitro systems." Curr Top Dev Biol **137**: 391-431.
Narita, N., M. Bielinska and D. B. Wilson (1997). "Cardiomyocyte differentiation by GATA-4-deficient embryonic stem cells." Development **124**(19): 3755-3764.
Niederreither, K., J. Vermot, N. Messaddeq, B. Schuhbaur, P. Chambon and P. Dollé (2001). "Embryonic retinoic acid synthesis is essential for heart morphogenesis in the mouse." Development **128**(7): 1019-1031.
Nohe, A., E. Keating, P. Knaus and N. O. Petersen (2004). "Signal transduction of bone morphogenetic protein receptors." Cellular signalling **16**(3): 291-299.
Norris, D. P. and E. J. Robertson (1999). "Asymmetric and node-specific nodal expression patterns are controlled by two distinct cis-acting regulatory elements." Genes & development **13**(12): 1575-1588.
O'Loghlen, A., A. M. Muñoz-Cabello, A. Gaspar-Maia, H.-A. Wu, A. Banito, N. Kunowska, T. Racek, H. N. Pemberton, P. Beolchi and F. Lavial (2012). "MicroRNA regulation of Cbx7 mediates a switch of Polycomb orthologs during ESC differentiation." Cell stem cell **10**(1): 33-46.
Oh, S., S. Shin and R. Janknecht (2019). "The small members of the JMJD protein family: Enzymatic jewels or jinxes?" Biochimica et Biophysica Acta (BBA)-Reviews on Cancer.
Pasini, D., P. A. Cloos, J. Walfridsson, L. Olsson, J.-P. Bukowski, J. V. Johansen, M. Bak, N. Tommerup, J. Rappsilber and K. Helin (2010). "JARID2 regulates binding of the Polycomb repressive complex 2 to target genes in ES cells." Nature **464**(7286): 306-310.
Perea-Gomez, A., F. D. Vella, W. Shawlot, M. Oulad-Abdelghani, C. Chazaud, C. Meno, V. Pfister, L. Chen, E. Robertson and H. Hamada (2002). "Nodal antagonists in the anterior visceral endoderm prevent the formation of multiple primitive streaks." Developmental cell **3**(5): 745-756.
Pfaff, S. L., M. Mendelsohn, C. L. Stewart, T. Edlund and T. M. Jessell (1996). "Requirement for LIM homeobox gene Isl1 in motor neuron generation reveals a motor neuron–dependent step in interneuron differentiation." Cell **84**(2): 309-320.
Poulard, C., J. Rambaud, N. Hussein, L. Corbo and M. Le Romancer (2014). "JMJD6 regulates ERα methylation on arginine." PloS one **9**(2): e87982.
Prall, O. W., M. K. Menon, M. J. Solloway, Y. Watanabe, S. Zaffran, F. Bajolle, C. Biben, J. J. McBride, B. R. Robertson and H. Chaulet (2007). "An Nkx2-5/Bmp2/Smad1 negative feedback loop controls heart progenitor specification and proliferation." Cell **128**(5): 947-959.

Pu, W. T., T. Ishiwata, A. L. Juraszek, Q. Ma and S. Izumo (2004). "GATA4 is a dosage-sensitive regulator of cardiac morphogenesis." Developmental biology **275**(1): 235-244.
Quinlan, A. R. and I. M. Hall (2010). "BEDTools: a flexible suite of utilities for comparing genomic features." Bioinformatics **26**(6): 841-842.
Ramírez, F., D. P. Ryan, B. Grüning, V. Bhardwaj, F. Kilpert, A. S. Richter, S. Heyne, F. Dündar and T. Manke (2016). "deepTools2: a next generation web server for deep-sequencing data analysis." Nucleic acids research **44**(W1): W160-W165.
Rashbass, P., L. Cooke, B. Herrmann and R. Beddington (1991). "A cell autonomous function of Brachyury in T/T embryonic stem cell chimaeras." Nature **353**(6342): 348-351.
Riley, P., L. Anaon-Cartwight and J. C. Cross (1998). "The Hand1 bHLH transcription factor is essential for placentation and cardiac morphogenesis." Nature genetics **18**(3): 271-275.
Riley, P. R., M. Gertsenstein, K. Dawson and J. C. Cross (2000). "Early exclusion of hand1-deficient cells from distinct regions of the left ventricular myocardium in chimeric mouse embryos." Developmental biology **227**(1): 156-168.
Robinson, J. T., H. Thorvaldsdóttir, W. Winckler, M. Guttman, E. S. Lander, G. Getz and J. P. Mesirov (2011). "Integrative genomics viewer." Nature biotechnology **29**(1): 24-26.
Rose, B. A., T. Force and Y. Wang (2010). "Mitogen-activated protein kinase signaling in the heart: angels versus demons in a heart-breaking tale." Physiol Rev **90**(4): 1507-1546.
Saga, Y., S. Miyagawa-Tomita, A. Takagi, S. Kitajima, J. Miyazaki and T. Inoue (1999). "MesP1 is expressed in the heart precursor cells and required for the formation of a single heart tube." Development **126**(15): 3437-3447.
Schlange, T., B. Andrée, H.-H. Arnold and T. Brand (2000). "BMP2 is required for early heart development during a distinct time period." Mechanisms of development **91**(1-2): 259-270.
Schneider, J. E., J. Böse, S. D. Bamforth, A. D. Gruber, C. Broadbent, K. Clarke, S. Neubauer, A. Lengeling and S. Bhattacharya (2004). "Identification of cardiac malformations in mice lacking Ptdsr using a novel high-throughput magnetic resonance imaging technique." BMC developmental biology **4**(1): 16.
Schuettengruber, B., H.-M. Bourbon, L. Di Croce and G. Cavalli (2017). "Genome regulation by polycomb and trithorax: 70 years and counting." Cell **171**(1): 34-57.
Schultheiss, T. M., J. Burch and A. B. Lassar (1997). "A role for bone morphogenetic proteins in the induction of cardiac myogenesis." Genes & development **11**(4): 451-462.
Shen, L., N. Shao, X. Liu and E. Nestler (2014). "ngs. plot: Quick mining and visualization of next-generation sequencing data by integrating genomic databases." BMC genomics **15**(1): 1-14.
Simon, J. A. and R. E. Kingston (2009). "Mechanisms of polycomb gene silencing: knowns and unknowns." Nature reviews Molecular cell biology **10**(10): 697-708.
Singh, M. K., V. M. Christoffels, J. M. Dias, M.-O. Trowe, M. Petry, K. Schuster-Gossler, A. Burger, J. Ericson and A. Kispert (2005). "Tbx20 is essential for cardiac chamber differentiation and repression of Tbx2."
Singh, M. K., V. M. Christoffels, J. M. Dias, M.-O. Trowe, M. Petry, K. Schuster-Gossler, A. Bürger, J. Ericson and A. Kispert (2005). "Tbx20 is essential for cardiac chamber differentiation and repression of Tbx2." Development **132**(12): 2697-2707.
Solloway, M. J. and E. J. Robertson (1999). "Early embryonic lethality in Bmp5; Bmp7 double mutant mice suggests functional redundancy within the 60A subgroup." Development **126**(8): 1753-1768.
Soudais, C., M. Bielinska, M. Heikinheimo, C. A. MacArthur, N. Narita, J. E. Saffitz, M. C. Simon, J. M. Leiden and D. B. Wilson (1995). "Targeted mutagenesis of the transcription factor GATA-4 gene in mouse embryonic stem cells disrupts visceral endoderm differentiation in vitro." Development **121**(11): 3877-3888.
Srinivasan, S., K. M. Dorighi and J. W. Tamkun (2008). "Drosophila Kismet regulates histone H3 lysine 27 methylation and early elongation by RNA polymerase II." PLoS Genet **4**(10):

e1000217.
Srivastava, D., T. Thomas, Q. Lin, M. L. Kirby, D. Brown and E. N. Olson (1997). "Regulation of cardiac mesodermal and neural crest development by the bHLH transcription factor, dHAND." Nature genetics **16**(2): 154-160.
Stanley, E. G., C. Biben, A. Elefanty, L. Barnett, F. Koentgen, L. Robb and R. P. Harvey (2004). "Efficient Cre-mediated deletion in cardiac progenitor cells conferred by a 3'UTR-ires-Cre allele of the homeobox gene Nkx2-5." International Journal of Developmental Biology **46**(4): 431-439.
Stennard, F. A., M. W. Costa, D. A. Elliott, S. Rankin, S. J. Haast, D. Lai, L. P. McDonald, K. Niederreither, P. Dolle and B. G. Bruneau (2003). "Cardiac T-box factor Tbx20 directly interacts with Nkx2-5, GATA4, and GATA5 in regulation of gene expression in the developing heart." Developmental biology **262**(2): 206-224.
Stennard, F. A. and R. P. Harvey (2005). "T-box transcription factors and their roles in regulatory hierarchies in the developing heart." Development **132**(22): 4897-4910.
Sun, Y., X. Liang, N. Najafi, M. Cass, L. Lin, C.-L. Cai, J. Chen and S. M. Evans (2007). "Islet 1 is expressed in distinct cardiovascular lineages, including pacemaker and coronary vascular cells." Developmental biology **304**(1): 286-296.
Takeuchi, J. K., M. Mileikovskaia, K. Koshiba-Takeuchi, A. B. Heidt, A. D. Mori, E. P. Arruda, M. Gertsenstein, R. Georges, L. Davidson and R. Mo (2005). "Tbx20 dose-dependently regulates transcription factor networks required for mouse heart and motoneuron development." Development **132**(10): 2463-2474.
Tam, P., K. Steiner, S. Zhou and G. Quinlan (1997). Lineage and functional analyses of the mouse organizer. Cold Spring Harbor symposia on quantitative biology, Cold Spring Harbor Laboratory Press.
Tanaka, M., Z. Chen, S. Bartunkova, N. Yamasaki and S. Izumo (1999). "The cardiac homeobox gene Csx/Nkx2. 5 lies genetically upstream of multiple genes essential for heart development." Development **126**(6): 1269-1280.
Tavares, L., E. Dimitrova, D. Oxley, J. Webster, R. Poot, J. Demmers, K. Bezstarosti, S. Taylor, H. Ura and H. Koide (2012). "RYBP-PRC1 complexes mediate H2A ubiquitylation at polycomb target sites independently of PRC2 and H3K27me3." Cell **148**(4): 664-678.
Tremblay, K. D., P. A. Hoodless, E. K. Bikoff and E. J. Robertson (2000). "Formation of the definitive endoderm in mouse is a Smad2-dependent process." Development **127**(14): 3079-3090.
Unhavaithaya, Y., T. H. Shin, N. Miliaras, J. Lee, T. Oyama and C. C. Mello (2002). "MEP-1 and a homolog of the NURD complex component Mi-2 act together to maintain germline-soma distinctions in C. elegans." Cell **111**(7): 991-1002.
Unoki, M., A. Masuda, N. Dohmae, K. Arita, M. Yoshimatsu, Y. Iwai, Y. Fukui, K. Ueda, R. Hamamoto, M. Shirakawa, H. Sasaki and Y. Nakamura (2013). "Lysyl 5-hydroxylation, a novel histone modification, by Jumonji domain containing 6 (JMJD6)." J Biol Chem **288**(9): 6053-6062.
van Wijk, B., A. F. Moorman and M. J. van den Hoff (2007). "Role of bone morphogenetic proteins in cardiac differentiation." Cardiovasc Res **74**(2): 244-255.
Vincent, S. D. and M. E. Buckingham (2010). How to make a heart: the origin and regulation of cardiac progenitor cells. Current topics in developmental biology, Elsevier. **90:** 1-41.
Vong, L. H., M. J. Ragusa and J. J. Schwarz (2005). "Generation of conditional Mef2cloxP/loxP mice for temporal‐and tissue‐specific analyses." genesis **43**(1): 43-48.
Waldmann, T., A. Izzo, K. Kamieniarz, F. Richter, C. Vogler, B. Sarg, H. Lindner, N. L. Young, G. Mittler and B. A. Garcia (2011). "Methylation of H2AR29 is a novel repressive PRMT6 target." Epigenetics & chromatin **4**(1): 11.
Walport, L. J., R. J. Hopkinson and C. J. Schofield (2012). "Mechanisms of human histone and nucleic acid demethylases." Current opinion in chemical biology **16**(5-6): 525-534.

Wamstad, J. A., J. M. Alexander, R. M. Truty, A. Shrikumar, F. Li, K. E. Eilertson, H. Ding, J. N. Wylie, A. R. Pico, J. A. Capra, G. Erwin, S. J. Kattman, G. M. Keller, D. Srivastava, S. S. Levine, K. S. Pollard, A. K. Holloway, L. A. Boyer and B. G. Bruneau (2012). "Dynamic and coordinated epigenetic regulation of developmental transitions in the cardiac lineage." Cell **151**(1): 206-220.
Wang, E. T., R. Sandberg, S. Luo, I. Khrebtukova, L. Zhang, C. Mayr, S. F. Kingsmore, G. P. Schroth and C. B. Burge (2008). "Alternative isoform regulation in human tissue transcriptomes." Nature **456**(7221): 470-476.
Wang, F., L. He, P. Huangyang, J. Liang, W. Si, R. Yan, X. Han, S. Liu, B. Gui, W. Li, D. Miao, C. Jing, Z. Liu, F. Pei, L. Sun and Y. Shang (2014). "JMJD6 promotes colon carcinogenesis through negative regulation of p53 by hydroxylation." PLoS Biol **12**(3): e1001819.
Wang, Z., H. M. Song, F. Wang, C. M. Zhao, R. T. Huang, S. Xue, R. G. Li, X. B. Qiu, Y. J. Xu, X. Y. Liu and Y. Q. Yang (2019). "A New ISL1 Loss-of-Function Mutation Predisposes to Congenital Double Outlet Right Ventricle." Int Heart J **60**(5): 1113-1122.
Webby, C. J., A. Wolf, N. Gromak, M. Dreger, H. Kramer, B. Kessler, M. L. Nielsen, C. Schmitz, D. S. Butler, J. R. Yates, 3rd, C. M. Delahunty, P. Hahn, A. Lengeling, M. Mann, N. J. Proudfoot, C. J. Schofield and A. Bottger (2009). "Jmjd6 catalyses lysyl-hydroxylation of U2AF65, a protein associated with RNA splicing." Science **325**(5936): 90-93.
Williams, S. T., L. J. Walport, R. J. Hopkinson, S. K. Madden, R. Chowdhury, C. J. Schofield and A. Kawamura (2014). "Studies on the catalytic domains of multiple JmjC oxygenases using peptide substrates." Epigenetics **9**(12): 1596-1603.
Wilson, V., P. Rashbass and R. Beddington (1993). "Chimeric analysis of T (Brachyury) gene function." Development **117**(4): 1321-1331.
Winnier, G., M. Blessing, P. A. Labosky and B. Hogan (1995). "Bone morphogenetic protein-4 is required for mesoderm formation and patterning in the mouse." Genes & development **9**(17): 2105-2116.
Winston, F. and M. Carlson (1992). "Yeast SNF/SWI transcriptional activators and the SPT/SIN chromatin connection." Trends in Genetics **8**(11): 387-391.
Witzel, H. R., S. Cheedipudi, R. Gao, D. Y. Stainier and G. D. Dobreva (2017). "Isl2b regulates anterior second heart field development in zebrafish." Sci Rep **7**: 41043.
Witzel, H. R., B. Jungblut, C. P. Choe, J. G. Crump, T. Braun and G. Dobreva (2012). "The LIM protein Ajuba restricts the second heart field progenitor pool by regulating Isl1 activity." Dev Cell **23**(1): 58-70.
Wobus, A. M., G. Wallukat and J. Hescheler (1991). "Pluripotent mouse embryonic stem cells are able to differentiate into cardiomyocytes expressing chronotropic responses to adrenergic and cholinergic agents and Ca2+ channel blockers." Differentiation **48**(3): 173-182.
Wolf, A., M. Mantri, A. Heim, U. Muller, E. Fichter, M. M. Mackeen, L. Schermelleh, G. Dadie, H. Leonhardt, C. Venien-Bryan, B. M. Kessler, C. J. Schofield and A. Bottger (2013). "The polyserine domain of the lysyl-5 hydroxylase Jmjd6 mediates subnuclear localization." Biochem J **453**(3): 357-370.
Wu, M., P. F. Wang, J. S. Lee, S. Martin-Brown, L. Florens, M. Washburn and A. Shilatifard (2008). "Molecular regulation of H3K4 trimethylation by Wdr82, a component of human Set1/COMPASS." Molecular and cellular biology **28**(24): 7337-7344.
Wu, S. M., Y. Fujiwara, S. M. Cibulsky, D. E. Clapham, C.-l. Lien, T. M. Schultheiss and S. H. Orkin (2006). "Developmental origin of a bipotential myocardial and smooth muscle cell precursor in the mammalian heart." Cell **127**(6): 1137-1150.
Xiang, Y., Y. Zhang, Q. Xu, C. Zhou, B. Liu, Z. Du, K. Zhang, B. Zhang, X. Wang and S. Gayen (2020). "Epigenomic analysis of gastrulation identifies a unique chromatin state for primed pluripotency." Nature genetics **52**(1): 95-105.
Yagi, R., M. J. Kohn, I. Karavanova, K. J. Kaneko, D. Vullhorst, M. L. DePamphilis and A. Buonanno (2007). "Transcription factor TEAD4 specifies the trophectoderm lineage at the

beginning of mammalian development." Development **134**(21): 3827-3836.
Yamada, M., J.-P. Revelli, G. Eichele, M. Barron and R. J. Schwartz (2000). "Expression of chick Tbx-2, Tbx-3, and Tbx-5 genes during early heart development: evidence for BMP2 induction of Tbx2." Developmental biology **228**(1): 95-105.
Yamagishi, H., C. Yamagishi, O. Nakagawa, R. P. Harvey, E. N. Olson and D. Srivastava (2001). "The combinatorial activities of Nkx2. 5 and dHAND are essential for cardiac ventricle formation." Developmental biology **239**(2): 190-203.
Yang, L., C. L. Cai, L. Lin, Y. Qyang, C. Chung, R. M. Monteiro, C. L. Mummery, G. I. Fishman, A. Cogen and S. Evans (2006). "Isl1Cre reveals a common Bmp pathway in heart and limb development." Development **133**(8): 1575-1585.
Yap, K. L., S. Li, A. M. Muñoz-Cabello, S. Raguz, L. Zeng, S. Mujtaba, J. Gil, M. J. Walsh and M.-M. Zhou (2010). "Molecular interplay of the noncoding RNA ANRIL and methylated histone H3 lysine 27 by polycomb CBX7 in transcriptional silencing of INK4a." Molecular cell **38**(5): 662-674.
Yi, J., H. F. Shen, J. S. Qiu, M. F. Huang, W. J. Zhang, J. C. Ding, X. Y. Zhu, Y. Zhou, X. D. Fu and W. Liu (2016). "JMJD6 and U2AF65 co-regulate alternative splicing in both JMJD6 enzymatic activity dependent and independent manner." Nucleic Acids Res.
Yokota, T. and Y. Wang (2016). "p38 MAP kinases in the heart." Gene **575**(2 Pt 2): 369-376.
Yoo, K. H., S. Oh, K. Kang, T. Hensel, G. W. Robinson and L. Hennighausen (2015). "Loss of EZH2 results in precocious mammary gland development and activation of STAT5-dependent genes." Nucleic acids research **43**(18): 8774-8789.
Yoshikawa, Y., T. Fujimori, A. P. McMahon and S. Takada (1997). "Evidence that absence ofWnt-3aSignaling promotes neuralization instead of paraxial mesoderm development in the mouse." Developmental biology **183**(2): 234-242.
Zeeb, M., J. Axnick, L. Planas-Paz, T. Hartmann, B. Strilic and E. Lammert (2012). "Pharmacological manipulation of blood and lymphatic vascularization in ex vivo–cultured mouse embryos." Nature protocols **7**(11): 1970.
Zepeda-Martinez, J., C. Pribitzer, J. Wang, D. Bsteh, S. Golumbeanu, Q. Zhao, T. Burkard, B. Reichholf, S. Rhie and J. Jude (2020). "Parallel PRC2/cPRC1 and vPRC1 pathways silence lineage-specific genes and maintain self-renewal in mouse embryonic stem cells." Science advances **6**(14): eaax5692.
Zhang, H. and A. Bradley (1996). "Mice deficient for BMP2 are nonviable and have defects in amnion/chorion and cardiac development." Development **122**(10): 2977-2986.
Zhang, X., Y. Gao, L. Lu, Z. Zhang, S. Gan, L. Xu, A. Lei and Y. Cao (2015). "JmjC domain-containing protein 6 (Jmjd6) derepresses the transcriptional repressor transcription factor 7-like 1 (Tcf7l1) and is required for body axis patterning during xenopus embryogenesis." Journal of Biological Chemistry **290**(33): 20273-20283.
Zhang, Y., T. Liu, C. A. Meyer, J. Eeckhoute, D. S. Johnson, B. E. Bernstein, C. Nusbaum, R. M. Myers, M. Brown and W. Li (2008). "Model-based analysis of ChIP-Seq (MACS)." Genome biology **9**(9): 1-9.
Zhao, R., A. J. Watt, J. Li, J. Luebke-Wheeler, E. E. Morrisey and S. A. Duncan (2005). "GATA6 is essential for embryonic development of the liver but dispensable for early heart formation." Molecular and cellular biology **25**(7): 2622-2631.
Zhao, X. D., X. Han, J. L. Chew, J. Liu, K. P. Chiu, A. Choo, Y. L. Orlov, W.-K. Sung, A. Shahab and V. A. Kuznetsov (2007). "Whole-genome mapping of histone H3 Lys4 and 27 trimethylations reveals distinct genomic compartments in human embryonic stem cells." Cell stem cell **1**(3): 286-298.
Zhen, C. Y., R. Tatavosian, T. N. Huynh, H. N. Duc, R. Das, M. Kokotovic, J. B. Grimm, L. D. Lavis, J. Lee and F. J. Mejia (2016). "Live-cell single-molecule tracking reveals co-recognition of H3K27me3 and DNA targets polycomb Cbx7-PRC1 to chromatin." Elife **5**: e17667.
Zhou, Y., T. J. Cashman, K. R. Nevis, P. Obregon, S. A. Carney, Y. Liu, A. Gu, C. Mosimann, S.

Sondalle, R. E. Peterson, W. Heideman, C. E. Burns and C. G. Burns (2011). "Latent TGF-beta binding protein 3 identifies a second heart field in zebrafish." Nature **474**(7353): 645-648.

4.2 Acknowledgment

This project would not have been possible without the support of many people. I would like to thank my supervisor Prof.Dr. Gergana Dobreva, as well as Prof.Dr. Thomas Wieland, for their patience, guidance, and support throughout this project.

I would like to express my deepest appreciation to Prof.Dr. Gergana Dobreva for providing me the opportunity of Ph.D. training and much-needed critical advice on experimental design.

Many thanks to Dr.rer.nat. Rui Gao and Dr.rer.nat. Yanhan Jia, who helped me greatly in work and life. Many thanks to Arthur Mathes for all the discussion and support in both science and daily life, especially when I need German language support. Many thanks to Dr. rer.nat. Julio Cordero, Linda Kessler, Arthur Mathes and Adel El Sherbiny for their help in bioinformatics analysis. I would also like to thank all the lab members in our lab for their support and help.

Special thanks to my family and friends who endured this long process with me, always offering support and love. I could not have undertaken this journey without the support of my wife, Dr. Yanyan Jing.

I would like to thank Prof. Dr. Uta-Maria Bauer and Dr. Caroline Bouchard for the help and suggestion regarding *Prmt6* and H3R2me2a.

I would like to thank Stefanie Uhlig in the FlowCore Mannheim of Heidelberg University for the help with the FACS sorting and analysis.